

**Characterization of Epoxy-Amine Systems
and Nylon-11 and PVDF Degradation**

A Thesis

Presented to

The Faculty of the Department of Chemistry

The College of William and Mary in Virginia

In Partial Fulfillment

Of the Requirements for the Degree of

Master of Arts

by

Wendy Raquel Mahler


December 1997

Approval Sheet

This thesis is submitted in partial fulfillment

Of the requirements for the degree of

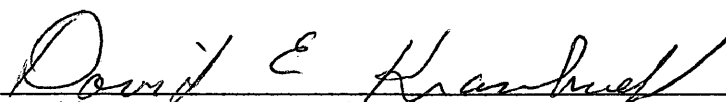
Master of Arts in Chemistry



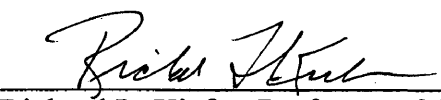
Wendy R. Mahler

Author

Approved, December 1997



David E. Kranbuehl, Professor of Chemistry



Richard L. Kiefer, Professor of Chemistry



Barbara A. Siles, Assistant Professor of Chemistry

Table of Contents

	<u>Page</u>
Acknowledgements	iii
List of Tables	iv
List of Figures	v
Abstract	x
Introduction	1
Chapter I – Techniques and Methodology	
A. FDEMS	3
Polarization	5
Capacitance	7
Dielectric Theory	11
B. DSC	14
C. TMA	16
D. Rheometry	17
E. Mechanical Tensile Testing	20
F. Solution Viscosity Testing	23
G. Mass, Thickness and Hardness	26
Chapter II – Epoxy-Amine Systems	
A. Introduction	31
B. Chemistry	31
C. Results and Discussion	33
Dielectric Measurements	33
Rheology	37
DSC	41
D. Conclusions	43
Chapter III – Degradation of Nylon-11	
A. Introduction	63
B. Mechanism of Nylon-11 Degradation	65
C. Aging Environments	68
D. Results and Discussion	73
E. Conclusions	80
Chapter IV – Poly(vinylidene fluoride) Degradation	
A. Introduction	102
B. Mechanism of Degradation of PVDF	103
C. Aging Environments	105
D. Results and Discussion	105
Phase I	106
Phase II	109
E. Conclusions	113
Conclusions	144
Bibliography	146

Acknowledgements

The author would like to thank Dr. David E. Kranbuehl for his invaluable guidance and understanding during this undergraduate and graduate research. She would also like to thank Dr. Richard Kiefer and Dr. Barbara Siles for their careful reading and criticism of this manuscript. The author would also like to express her gratitude to David Hood and Jeff Rogozinski.

The author would like to express her gratitude to the myriad undergraduates and former undergraduates who assisted with the completion of this research. Of those, Robin Gittleson, James Garrett and Julie Warner are specially recognized. Highest gratitude goes to Andrée Ebersole who has been an immeasurable help through the past three years not only in the laboratory, but as a friend and supporter as well. Special thanks goes to the author's friend and colleague, Jonathan Curley for his tutorial skills, friendship, support and humor over these years.

The author would like to dedicate this work to her family who have provided unending support and strength throughout her undergraduate and graduate years at the College of William & Mary. Warmest thanks go to Kevin Scott Mahler, the author's husband.

List of Tables

<u>Table No.</u>	<u>Description</u>	<u>Page</u>
<u>Chapter II</u>		
2.1	Epoxy-Amine Reactants	32
2.2	Time to Reach τ	34
2.3	Epoxy-Amine System Experiments	35
2.4	m Values for σ and η and the Ratio, x	37
2.5	Data from $\ln \sigma$ vs $\ln \eta$ for 135°C Isotherms—Early in Cure	39
2.6	DSC Data from 135°C Isothermal Cures	42
<u>Chapter III</u>		
3.1	Various Accelerated Aging Environments	69
3.2	Rate Constants for Each Temperature	74
3.3	Ratios of Slope of Molecular Weight versus Day Plots	76
3.4	Characteristics of Amorphous & Crystalline Regions of Nylon-11 And PVDF	78
<u>Chapter IV</u>		
4.1	PVDF Aging Environments	105

List of Figures

<u>Figure No.</u>	<u>Description</u>	<u>Page</u>
<u>Chapter I</u>		
1.1	DekDyne FDEMS Sensor	4
1.2	Ion conduction under applied electric fields	6
1.3	Dipole Moment equation	6
1.4	Total polarization equation	6
1.5	Dipole-polarization equation	7
1.6	Parallel-plate Capacitors and Charge Mobility	7
1.7	Capacitance equation	8
1.8	Surface charge density equation	8
1.9	Gauss's Law equation	8
1.10	Coulomb constant equation	8
1.11	Rearranged equations	8
1.12	Rearranged equations	9
1.13	Net flux equation	9
1.14	Potential difference equation	9
1.15	Capacitance of parallel-plate equation	9
1.16	Complex permittivity equation	10
1.17	ϵ' equation	12
1.18	ϵ'' equation	12
1.19	Ionic and dipolar contribution to ϵ'	12
1.20	Ionic and dipolar contribution to ϵ''	12
1.21	Ionic contribution of ϵ'	12
1.22	Ionic contribution of ϵ''	12
1.23	Conductance, σ	13
1.24	Cole-Davidson function	13
1.25	Dipolar component of ϵ''	13
1.26	DSC Sample Pan Apparatus	14
1.27	An Ideal DSC Scan	15
1.28	Percent Crystallinity	15
1.29	Thermal Mechanic Analyzer	17
1.30	RDA-700 Test Apparatus	18
1.31	Material Deformation for Shear Strain	19
1.32	Strain/Stress Responses for a Sinusoidal Test	19
1.33	Complex Shear Modulus	20
1.34	Shear Storage	20
1.35	Shear Loss	20
1.36	Dynamic viscosity	20
1.37	Viscosity component η'	20
1.38	Viscosity component η''	20
1.39	Tensile Testing Apparatus	21
1.40	Tensile Strength	21
1.41	Percent elongation	21

<u>Figure No.</u>	<u>Description</u>	<u>Page</u>
1.42	Schematic of Tensile Test Sample	22
1.43	Stress-Strain Diagram	23
1.44	Fluid Flow Representation	23
1.45	Capillary Viscometers	24
1.46	Relative Viscosity	25
1.47	Specific Viscosity	25
1.48	Reduced Viscosity	26
1.49	Intrinsic Viscosity	26
1.50	Mark-Houwink Equation	26
1.51	Barcol Hardness Tester	28
 <u>Chapter II</u>		
2.1	Epoxy Group	32
2.2	Epoxy-Amine Reaction	33
2.3	Typical Isothermal Cure with Re-ramp	45
2.4	$\ln \sigma$ versus Time for 4-bpa:dgeba Isotherm	45
2.5	$-\ln \sigma$ versus $1/T$ for 4-bpa:dgeba Pre-cure	46
2.6	$-\ln \sigma$ versus $1/T$ for mcdea:dgeba Pre-cure	46
2.7	$-\ln \sigma$ versus $1/T$ for dgeba only	47
2.8	$-\ln \sigma$ versus $1/T$ for 4-bpa:dgeba Post-cure	47
2.9	$-\ln \sigma$ versus $1/T$ for 3-Cl-2,6-DEA:dgeba Post-cure	48
2.10	$-\ln \sigma$ versus $1/T$ for 2,6-DEA:dgeba Post-cure	48
2.11	$-\ln \sigma$ versus $1/T$ for mcdea:dgeba Post-cure	49
2.12	$-\ln \sigma$ versus $1/T$ for 4-bpa:monoepoxy Post-cure	49
2.13	Arrhenius Relationship	36
2.14	$\log \eta$ versus Time for 4-bpa:dgeba Isotherm	50
2.15	$\log \eta$ versus Time for 4-bpa:dgeba Post-cure ramp	50
2.16	$\ln \eta$ versus $1/T$ for 4-bpa:dgeba Pre-cure	51
2.17	$\ln \eta$ versus $1/T$ for mcdea:dgeba Pre-cure	51
2.18	$\ln \eta$ versus $1/T$ for DGEBA only	52
2.19	$\ln \eta$ versus $1/T$ for 4-bpa:dgeba Post-cure	52
2.20	$\ln \eta$ versus $1/T$ for 2,6-DEA:dgeba Post-cure	53
2.21	$\ln \eta$ versus $1/T$ for mcdea:dgeba Post-cure	53
2.22	$\ln \eta$ versus $1/T$ for 4-bpa:monoepoxy Post-cure	54
2.23	Conductivity – Viscosity Proportionality	38
2.24	$\ln \sigma$ versus $\ln \eta$ for 4-bpa:dgeba Isotherm	55
2.25	$\ln \sigma$ versus $\ln \eta$ for 3-Cl-2,6-dea:dgeba Isotherm	55
2.26	$\ln \sigma$ versus $\ln \eta$ for 2,6-dea:dgeba Isotherm	56
2.27	$\ln \sigma$ versus $\ln \eta$ for mcdea:dgeba Isotherm	56
2.28	$\ln \sigma$ versus $\ln \eta$ for 4-bpa:monoepoxy Isotherm	57

<u>Figure No.</u>	<u>Description</u>	<u>Page</u>
2.29	Ratio of slope of σ to slope of η	39
2.30	Arrhenius relationship of σ and η	39
2.31	Rearrangement of 2.30	40
2.32	$\text{Ln } \eta$ versus α for 4-bpa:dgeba Isotherm	58
2.33	$\text{Ln } \sigma$ versus α for 4-bpa:dgeba Isotherm	58
2.34	$\text{Ln } \eta$ versus α for 3-CI-2,6-DEA:dgeba Isotherm	59
2.35	$\text{Ln } \sigma$ versus α for 3-CI-2,6-DEA:dgeba Isotherm	59
2.36	$\text{Ln } \eta$ versus α for 2,6-DEA:dgeba Isotherm	60
2.37	$\text{Ln } \sigma$ versus α for 2,6-DEA:dgeba Isotherm	60
2.38	$\text{Ln } \eta$ versus α for mcdea:dgeba Isotherm	61
2.39	$\text{Ln } \sigma$ versus α for mcdea:dgeba Isotherm	61
2.40	$\text{Ln } \eta$ versus α for 4-bpa:monoepoxy Isotherm	62
2.41	$\text{Ln } \sigma$ versus α for 4-bpa:monoepoxy Isotherm	62
 <u>Chapter III</u>		
3.1	Amide Group	64
3.2	Poly(imino-1-oxoundecamethylene)	64
3.3	Microcrystalline region of Nylon-6,6	65
3.4	Condensation Polymerization of Nylon-6,6	66
3.5	Mechanism for Acid-Catalyzed Hydrolysis of Polyamids	67
3.6	Accelerated Aging Bath	70
3.7	FDEMS Aging Sensor Apparatus	72
3.8	Tensile Test Sample Mounting Apparatus	73
3.9	Molecular Weight versus Day 70°C	82
3.10	Molecular Weight versus Day 90°C	82
3.11	Molecular Weight versus Day 105°C	83
3.12	Molecular Weight versus Day 120°C	83
3.13	Ln Molecular Weight versus Day 70°C	84
3.14	Ln Molecular Weight versus Day 90°C	84
3.15	Ln Molecular Weight versus Day 105°C	85
3.16	Ln Molecular Weight versus Day 120°C	85
3.17	Activation Energy Equation	74
3.18	$\text{Ln } k$ versus $1/T$	86
3.19	Ln Molecular Weight versus Day for Percent Water	86
3.20	Ln Molecular Weight versus Day for 105°C Buffer Environments	87
3.21	Ln Molecular Weight versus Day for 120°C Buffer Environments	87
3.22	Extrapolated $k(120 \rightarrow 105)$ and Experimental versus pH	88
3.23	105°C slopes versus pH	88
3.24	Relationship of Activation Energies	76
3.25	95% Oil Pot Sensor Data at 105°C; $\text{Log } \epsilon'$ versus Day	89
3.26	95% Oil Pot Sensor Data at 105°C; $\text{Log } \epsilon''^* \omega$ versus Day	89

<u>Figure No.</u>	<u>Description</u>	<u>Page</u>
3.27	95% Oil Pot Sensor Data at 90°C; Log $\epsilon^{**}\omega$ versus Day	90
3.28	95% Oil Pot Sensor Data at 90°C; Log ϵ' versus Day	90
3.29	5% Oil Pot Sensor Data at 90°C; Log $\epsilon^{**}\omega$ versus Day	91
3.30	5% Oil Pot Sensor Data at 90°C; Log ϵ' versus Day	91
3.31	100% Buffer Sensor Data at 90°C; Log $\epsilon^{**}\omega$ versus Day	92
3.32	100% Buffer Sensor Data at 90°C; Log ϵ' versus Day	92
3.33	95% Oil Sensor Data at 70°C; Log ϵ' versus Day	93
3.34	95% Oil Sensor Data at 70°C; Log $\epsilon^{**}\omega$ versus Day	93
3.35	95% Oil Sensor Correlation of MW to $\epsilon^{**}\omega$ at 105°C	94
3.36	95% Oil Sensor Correlation of MW to $\epsilon^{**}\omega$ at 90°C	95
3.37	5% Oil Sensor Correlation of MW to $\epsilon^{**}\omega$ at 90°C	95
3.38	100% Buffer Sensor Correlation of MW to $\epsilon^{**}\omega$ at 90°C	96
3.39	Enthalpy versus Day for 105°C	97
3.40	Melting Temperature versus Day for 105°C	97
3.41	Correlation of Load at Break to $\epsilon^{**}\omega$	98
3.42	Correlation of Load at Break to ϵ'	99
3.43	Correlation of Percent Extension at Break to ϵ'	99
3.44	Correlation of Percent Extension at Break to $\epsilon^{**}\omega$	100
3.45	Percent Elongation versus Day at 105°C	101
 <u>Chapter IV</u>		
4.1	PVDF equation	102
4.2	Mechanism for Degradation of PVDF	104
4.3	WS 95% Oil Sensor Data; $\epsilon^{**}\omega$ versus Day	115
4.4	WS 100% Aniline Sensor Data; $\epsilon^{**}\omega$ versus Day	115
4.5	Coflexip 100% Aniline Sensor Data; $\epsilon^{**}\omega$ versus Day	116
4.6	Melting Temp versus Day Coflexip Aniline & Oil	117
4.7	Melting Temp versus Day Coflexip	117
4.8	Melting Temp versus Day WS Aniline & Oil	118
4.9	Melting Temp versus Day WS	118
4.10	Enthalpy Change versus Day Coflexip Aniline & Oil	119
4.11	Enthalpy Change versus Day Coflexip	119
4.12	Enthalpy Change versus Day WS Aniline & Oil	120
4.13	Enthalpy Change versus Day WS	120
4.14	Melting Temp versus Day in Water & Oil	121
4.15	Enthalpy Change versus Day in Water & Oil	121
4.16	Molecular Weight versus Day Coflexip Aniline & Oil	122
4.17	Molecular Weight versus Day WS Aniline & Oil	122
4.18	Molecular Weight versus Day Coflexip	123
4.19	Molecular Weight versus Day WS	123
4.20	Molecular Weight versus Day; WS and Coflexip	124

<u>Figure No.</u>	<u>Description</u>	<u>Page</u>
4.21	Load versus Day Coflexip in 95% Oil	124
4.22	Load versus Day Coflexip in 100% Aniline	125
4.23	Percent Elongation versus Day Coflexip in 95% Oil	125
4.24	Percent Elongation versus Day Coflexip in 100% Aniline	126
4.25	Percent Change in Mass Coflexip Aniline & Oil	126
4.26	Percent Change in Mass Coflexip	127
4.27	Percent Change in Mass WS Aniline & Oil	127
4.28	Percent Change in Mass WS	128
4.29	Percent Change in Thickness Coflexip Aniline & Oil	128
4.30	Percent Change in Thickness Coflexip	129
4.31	Percent Change in Thickness WS Aniline & Oil	129
4.32	Percent Change in Thickness WS	130
4.33	Percent Change in Hardness Coflexip Aniline & Oil	130
4.34	Percent Change in Hardness Coflexip	131
4.35	Percent Change in Mass Phase II Non-Plasticized Air Oven	132
4.36	Percent Change in Mass Phase II Plasticized Air Oven	132
4.37	Percent Change in Mass Phase II Plasticized Oil Pot	133
4.38	Percent Change in Mass Phase II Non-Plasticized Oil Pot	133
4.39	Percent Change in Thickness Phase II Plasticized Air Oven	134
4.40	Percent Change in Thickness Phase II Non-plasticized Air Oven	134
4.41	Percent Change in Thickness Phase II Plasticized Oil Pot	135
4.42	Percent Change in Thickness Phase II Non-plasticized Oil Pot	135
4.43	Hardness Phase II Plasticized Air Oven	136
4.44	Hardness Phase II Non-Plasticized Air Oven	136
4.45	Hardness Phase II Plasticized Oil Pot	137
4.46	Hardness Phase II Non-plasticized Oil Pot	137
4.47	Melting Temperature Phase II Plasticized Air Oven	138
4.48	Melting Temperature Phase II Non-plasticized Air Oven	138
4.49	Melting Temperature Phase II Plasticized Oil Pot	139
4.50	Melting Temperature Phase II Non-plasticized Oil Pot	139
4.51	Enthalpy Phase II Plasticized Air Oven	140
4.52	Enthalpy Phase II Non-plasticized Air Oven	140
4.53	Enthalpy Phase II Plasticized Oil Pot	141
4.54	Enthalpy Phase II Non-plasticized Oil Pot	141
4.55	Percent Elongation Phase II WS Oil Pot	142
4.56	Percent Elongation Phase II Coflexip Oil Pot	142
4.57	Percent Elongation Phase II 60512 Oil Pot	143

Abstract

This work investigates the changing environment of polymers both during cure and during aging. Several different epoxy-amine systems were monitored throughout cure. These systems were analyzed and compared to one another. The aging of polymers was examined by monitoring both nylon-11 and poly(vinylidene fluoride) [PVDF]. It was determined that although PVDF is tougher and more resilient than nylon-11, it is nonetheless susceptible to extremely harsh conditions.

**Characterization of Epoxy-Amine Systems
And Nylon-11 and PVDF Degradation**

Introduction

The development and implementation of *in situ* frequency dependent electromagnetic sensing (FDEMS) techniques is instrumental in monitoring polymeric phenomena. This technique is sensitive, convenient and can be automated allowing the real time observation of molecular behavior of polymeric systems. FDEMS data can be correlated with macroscopic properties of a curing or aging polymer. This allows immediate information on the current state of the polymeric system.

Until relatively recently, little information could be obtained on the changing state of a polymeric material during cure or during the aging process. FDEMS testing allows a system to be monitored *in situ*. With this technique an entire polymerization process may be monitored and adjustments made as the reaction is continuing. Information can be obtained on the viscosity of the system, the degree of cure, position of the resin, and change in modulus during exposure to the reaction environment.

The cure of epoxy resins was investigated using FDEMS testing. The FDEMS data were correlated with properties such as the viscosity and degree of cure of the system. As model compounds, both a monoepoxy and a diepoxy were reacted with several different amines. This allowed determination of different aspects of the cures by correlation of the conductivity from FDEMS testing to macroscopic properties. As a result, distinct phases of the reaction process were observed.

Degradation of nylon-11 and poly(vinylidene fluoride) (PVDF) in accelerated aging environments were continuously monitored through FDEMS testing. These data were correlated to properties such as the viscosity average molecular weight, degree of crystallinity, melting temperature, modulus, mass, thickness and hardness. Analysis of these correlations allows service life prediction of the polymers in the various aging environments. These environments simulate accelerated field conditions for polymers used in offshore oil drilling pipes.

Chapter I

Techniques and Methodology

For investigating the properties of polymers several different methods of analysis were chosen. Frequency dependent electromagnetic sensing, FDEMS, was used to detect changes in ionic and dipolar mobility on a microscopic level. Macroscopic physical properties were further tested using differential scanning calorimetry (DSC), thermo-mechanical analysis (TMA), rheometry, mechanical tensile testing, viscosity testing, mass, thickness and hardness testing. Each of these methods measures a different aspect of the physical properties of the material and allows correlation between the macroscopic and microscopic properties.

A. FDEMS

The macroscopic changes of a material are detectable on a microscopic level long before the effect of such changes are observable in its functional properties. By the time these characteristics indicate near failure of the material it may be too late to prevent a catastrophe. Frequency dependent electromagnetic sensing, FDEMS, allows the user to monitor changes in the material as they occur. Traditional methods of studying polymers require post-polymerization analysis of the physical properties. Analysis of a small sample of a polymerizing substance as a polymerization reaction is occurring can be done, but this causes a lag in information about the state of the polymer

at the time of interest. The reaction continues while the sample is being analyzed, hence the degree of polymerization (or degradation) has changed by the time the sample has been analyzed. FDEMS views dielectric properties of a material *in situ* as the material is aging or reacting. Dielectric studies require determination of the electrical polarization and conduction properties of a sample subjected to a time-varying electric field. This technique is nondestructive and has high reproducibility and sensitivity¹. The physical state of the polymer can be continuously monitored from an immediate or remote location and the situation may be evaluated and adjusted accordingly.

FDEMS uses impedance measurements involving frequencies from the hertz to megahertz range. The measurements indicate changes in the displacement or motion of charged and dipolar moieties on a molecular level using an applied electric field as the force. The sensor itself was patented by Kranbuehl, Figure [1.1], and consists of two finely interdigitated comb electrodes composed of noble metals and high temperature ceramics laid on either glass or kapton.

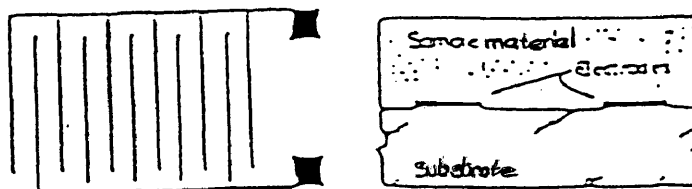


Figure [1.1] DekDyne FDEMS Sensor

The interdigitated combs represent a parallel plate capacitor. When a dielectric material is applied to one of these impedance sensors, there is an increase in the amount of charge on the plates at constant voltage. This is caused by polarization of the dielectric material. The materials studied herein are polar molecules, therefore the molecules and any small ions within the sample will be affected by the charged plates of the capacitor. Polarization, capacitance and dielectric theory must be considered for a thorough understanding of FDEMS testing.

Polarization

Atoms and molecules often exist in an electrically neutral state, meaning they have the same number of electrons and protons. A dipole moment exists in many molecules due to the spatial distribution of electrical charge. Applied electric fields can affect this distribution. The response of atoms or molecules to the electrical field, E_A , can be accurately measured². FDEMS testing is based on this type of measurement.

When molecules are exposed to an electric field as described above, there is a spatial separation of unlike charges³. Once a material is placed on a sensor and voltage is applied, the sample becomes polarized. Figure [1.2]⁴ is an example of ion conduction under an applied electric field.

First, consider an uncharged species such as an atom. An atom has a negatively charged electron cloud which surrounds a positively charged

nucleus. Upon application of the electric field, F , the electrons migrate toward the positive source and the nucleus is drawn toward the negative

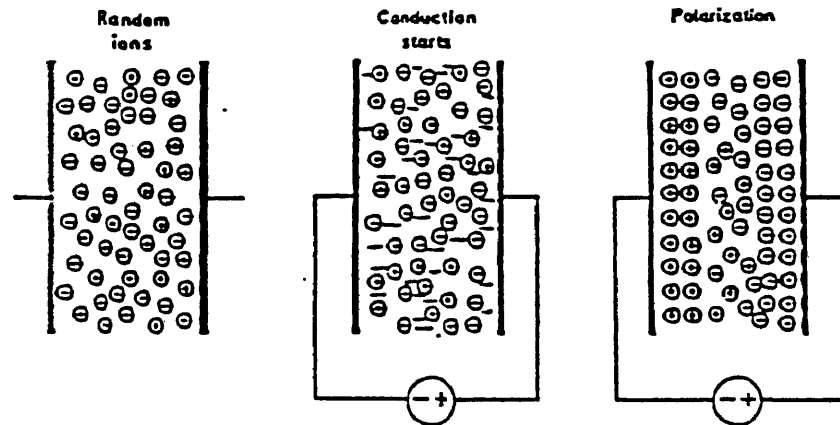


Figure [1.2] Ion conduction under applied electric fields

source [1.2]. This is called polarizability α_t . The polarizability relates to an average total polarized dipole moment, μ_t , by⁵

$$\mu_t = \alpha_t F \quad [1.3]$$

The polarization has three major contributing components: electronic polarization, P_e , due to the distortion of the electron cloud with respect to the nucleus; atomic polarization, P_a , due to the shift of atomic nuclei with respect to the molecule; and a dipolar orientation polarization, P_d , due to dipoles aligning with F . The total polarization, P_t , is the summation of these components and is represented by [1.4].

$$P_t = P_e + P_a + P_d \quad [1.4]$$

A material with N molecules per unit volume has a polarized dipole moment per unit volume of $N\mu_t$. This leads to a relationship with the total polarization substituted into equation [1.3] yielding

$$P_t = N\alpha_t F \quad [1.5]$$

The internal electric field, F , acting on the molecule determines the magnitude of P_t . Each component of P_t will respond differently to varying frequencies of the electric field. Frequency dependence will be discussed further in the section on dielectric theory. At this point it is necessary to understand capacitance.

Capacitance

The ability of a material to store a given charge for a given potential difference is called capacitance. A good illustration of this concept is the

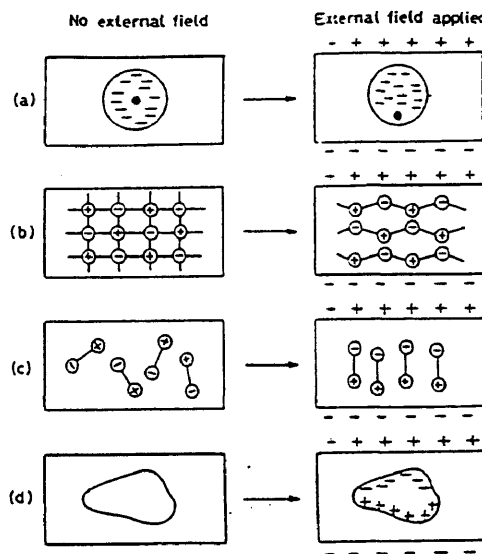


Figure [1.6] Parallel-plate Capacitors and Charge Mobility

parallel-plate capacitor. A parallel-plate capacitor has two geometrically identical plates set a fixed distance apart. A voltage, V , is applied to the plates allowing charge, $+Q$ and $-Q$, to build on the plates (Figure [1.6]⁷).

The capacitance, C , can be defined as the ratio of the potential difference between the plates, V , and the magnitude of the charge on the plate, Q .

$$C = Q/V \quad [1.7]$$

Any point chosen between the plates would behave as if next to an infinite plane of charge if the plates are sufficiently close to one another. The surface charge density, σ , can therefore be defined as the charge per unit area.

$$\sigma = Q/A \quad [1.8]$$

Gauss's law indicates the net flux (E_n) through any surface (S) is equal to $4\pi k$ times the total charge within the surface⁸:

$$\phi = \int SE_n \, dA = 4\pi k Q_{\text{inside}} \quad [1.9]$$

This is often written using the Coulomb constant k in terms of the permittivity of free space ϵ_0 :

$$k = 1/(4\pi\epsilon_0) \quad [1.10]$$

Substituting into equation [1.9] yields

$$\phi = \int SE_n \, dA = (1/\epsilon_0) Q_{\text{inside}} \quad [1.11]$$

Rearranging equations [1.8] and [1.11] (accounting for flux through both sides of the surface), the following is derived:

$$2E_n A = (1/\epsilon_0) \sigma A \quad [1.12]$$

Solving for E_n in equation [1.12] and multiplying by two for the number of plates yields:

$$E = \sigma/\epsilon_0 \quad [1.13]$$

The potential difference, V , in this parallel-plate capacitor would equal the applied electric field multiplied by the distance between the plates.

Substituting equations [1.13] and [1.8] yields:

$$V = Ed = (\sigma/\epsilon_0)d = (Qd/\epsilon_0 A) \quad [1.14]$$

Relating this back to equation [1.7], the capacitance of the parallel-plate is derived as:

$$C = Q/V = (\epsilon_0 A)/d \quad [1.15]$$

where ϵ_0 equals 8.85×10^{-12} Farads per meter.

Various polarization mechanisms take place as the electric field is applied. Consider the behavior of dipoles within the material. If the direction of the field is reversed 180° , the dipole will attempt to reorient, realigning with the new field taking some finite amount of time. As the frequency of the field reversal increases, there is a certain frequency above which the dipole cannot keep up with the alteration of direction. This frequency is referred to as the relaxation frequency. Above this frequency the loss of polarization from the dipole diminishes the effective dielectric constant of the material.

The relaxation frequency of interfacial polarization is relatively low (approximately 1 kilohertz) since the large body of ionic charge must move

through a matrix of fairly resistive dielectric material. Interfacial polarization refers to the point at which ionic motions cannot keep up with the alternating current.

Dipole orientation of small polar groups in fluid media has relaxation frequencies that are above the radio frequency region, generally in the microwave regions. Atoms have much less inertia and tend to vibrate with thermal energy, corresponding to relaxation frequencies around the infrared region. Using frequencies within the hertz to megahertz range both ionic (from interfacial polarization) and dipolar components in viscous media are examined. Because atoms and electrons do not relax at such low frequencies they only contribute to the background of the complex permittivity.

Ions are distributed randomly throughout the samples studied. In the case of epoxy resins these are due to impurities in the reactants, such as Na^+ and Cl^- , and various small catalysts. These are present when the materials are received from the manufacturer and remain constant throughout the cure. For the degradation studies of Nylon-11 and PVDF, ions are also present along with plasticizers. As the sensors are introduced to various aqueous environments other ions infiltrate the polymers. As shown in Figure [1.6] when an electric field is applied to the sensors the positive ions move toward the negative electrode and negative ions toward the positive electrode. They ultimately accumulate at the electrodes. This produces charged layers at both electrodes called electrode polarization. The ionic component tends to dominate at low frequencies, low viscosities and high temperatures. The

dipolar component arises from rotational diffusion of bound charge of molecular dipole moments. It generally dominates the impedance signal at high frequencies in highly viscous media.

Contributions to the overall dielectric polarization come from the polar groups on chain segments whose relaxation times are compared to the time scale of the applied signal. This allows one to distinguish between various polarization mechanisms on the basis of different frequency dependencies. The dipolar contribution is generally observed at frequencies from the kilohertz to megahertz range in viscous media. Both ionic translational mobility, σ , and rotational mobility of the dipole, τ , are observable in the hertz to megahertz range. The physical state of the material and the extent of reaction determine the magnitude of these two parameters.

Dielectric Theory

FDEMS sensing measures the material's dielectric impedance, yielding capacitance, C , and conductance, G . These values are geometry dependent yet can be used to calculate the intensive geometry independent complex permittivity, ϵ^* . The complex permittivity is related to the dielectric permittivity, ϵ' , and the dielectric loss factor, ϵ'' :

$$\epsilon^* = \epsilon' - i\epsilon'' \quad [1.16]$$

where i is an imaginary component. The equations for calculating ϵ' and ϵ'' are as follows:

$$\epsilon' = C_{\text{material}}/C_0 \quad [1.17]$$

$$\epsilon'' = G_{\text{material}}/(C_0\omega) \quad [1.18]$$

where C_0 is air filled capacitance of the sensor and ω is $2\pi f$ where f is the frequency in hertz. There are ionic and dipolar components of both the real, ϵ' , and the imaginary, ϵ'' , components of the complex permittivity. The sum of the ionic and dipolar contribution of each yields the total contribution¹⁰.

$$\epsilon' = \epsilon'_i + \epsilon'_d \quad [1.19]$$

$$\epsilon'' = \epsilon''_i + \epsilon''_d \quad [1.20]$$

The ionic component results from the translational diffusion of charge. This can give rise to localized layers of charge near the electrodes. The ionic contribution of ϵ' and ϵ'' can be described by the following equations:

$$\epsilon'_i = \epsilon'_d + C_0 Z_0 \sin(n\pi/2) \omega^{-(n+1)} (\sigma/\epsilon_0)^2 \quad [1.21]$$

$$\epsilon''_i = \epsilon''_d + (\sigma/\epsilon_0 \omega) - C_0 Z_0 \cos(n\pi/2) \omega^{-(n+1)} (\sigma/\epsilon_0)^2 \quad [1.22]$$

where σ is the specific conductivity, $Z = Z_0 (i\omega)^{-n}$ is the electrode impedance induced by the ions and n is a parameter between 0 and 1¹¹. Equation [1.22] has three terms. The first term is a dipolar contribution. It can be neglected if the ionic component dominates the signal at low viscosities, low frequencies and high temperatures. The second term describes the conductance, σ , of ions translating through the system. The third term results from electrode polarization. It is difficult to interpret and occurs at very low frequencies (below 10 hertz). If the first and third terms are small the ionic conductivity directly relates to the loss factor by

$$\sigma = \epsilon_0 \omega \epsilon''_i \quad [1.23]$$

Dipolar rotations and rotational diffusions of bound charges result in the dipolar contribution to the loss factor. This is shown by the Cole-Davidson function,

$$\epsilon^*_d = (\epsilon_r - \epsilon_u)/(1 - i2\pi fG\tau)^\beta + \epsilon_u \quad [1.24]$$

where τ is a characteristic relaxation time, ϵ_r and ϵ_u are the limiting low and high frequency values of ϵ_d . β is the Cole-Davidson distribution parameter ranging from 0 to 1 and measuring the distribution of relaxation times. This dipolar component dominates in highly viscous media at high frequencies.

The dipolar component of the loss factor can now be determined by subtracting the ionic component from [1.23] from the complex permittivity [1.16], yielding

$$\epsilon''_d = \epsilon^* - \sigma/(\epsilon_0 \omega) \quad [1.25]$$

The two properties of ϵ' and ϵ'' are at the center of the FDEMS research. In this research the dominant contribution to ϵ^* is the ionic component.

Monitoring ionic components of the complex permittivity allows for identifying quantitative relationships between the molecular mobility and the other physical properties discussed herein. This technique is paramount in understanding and correlating the behavior of polymers on both the microscopic and macroscopic levels.

B. Differential Scanning Calorimetry

Several important physical characteristics of polymers can be examined by use of a differential scanning calorimeter, DSC. This technique requires heating a small sample of the polymer to examine the enthalpies of the transition processes. Physical constants such as glass transition temperature, T_g , melting point, T_m , degree of cure, α , and degree of crystallinity can be determined.

The device is designed to determine the enthalpies of various processes by measuring the differential heat flow required to maintain a material sample and an unreactive reference at the same temperature¹². Heat is either absorbed by the material or given off as the sample goes through a transition. This change in the flow of current at the transition can be easily monitored to a precise degree. Sensors are placed in the cells which regulate the current flow into the reference and sample pans. Individual electric heaters are monitored by sensors to adjust the input of heat.¹³

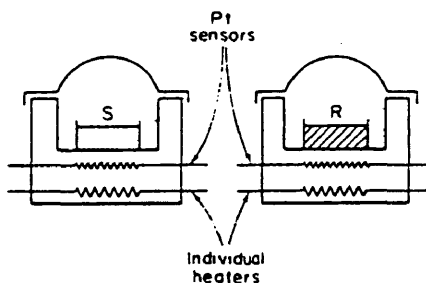


Figure [1.26] DSC Sample Pan Apparatus

Below in figure [1.27] is an ideal DSC scan indicating T_g , a second-order transition, and T_m , a first-order transition:¹⁴

For this study we used a Perkin-Elmer DSC-7 instrument. The samples were crimped inside aluminum pans with a mass of 5 to 15 milligrams depending on the density of the sample. A small sample size is used to help reduce thermal resistance to minimize heating lag of the sample cell compared to the reference cell.

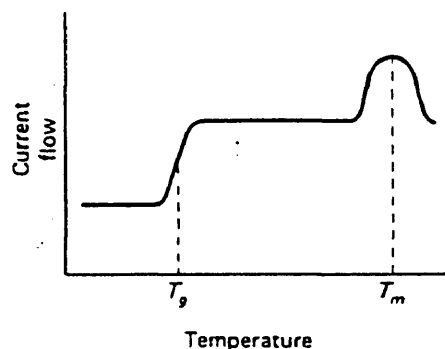


Figure [1.27] An Ideal DSC Scan

After the instrument runs through a programmed temperature ramp or timed isotherm the enthalpy ΔH_{melt} can be calculated by integration of the total peak area. To determine the degree (or percent by multiplying by 100) of crystallinity of a sample the value calculated is compared to the enthalpy of a sample that is purely crystalline, $\Delta H^{\circ}_{\text{melt}}$:

$$\% \text{ Crystallinity} = \left(\Delta H_{\text{melt}} / \Delta H^{\circ}_{\text{melt}} \right) \times 100 \quad [1.28]$$

The $\Delta H^{\circ}_{\text{melt}}$ of nylon-11 is 54.1 cal/g (226 J/g), while the $\Delta H^{\circ}_{\text{melt}}$ of PVDF is 92.9 J/mol.^{15,16}

The advancement of the polymerization process can also be examined after a DSC scan. Generally polymerization is an exothermic process, therefore the peak seen in figure [1.27] would be in the opposing direction. This peak can be integrated representing the heat of reaction as polymerization occurs. The degree of cure, α , can be determined at any point by simply comparing the heat of reaction at that time to the total heat of reaction. For the epoxy systems the heat of reaction was determined for each epoxy group rather than for the mass of the entire sample. This allowed comparison of several different epoxy systems. The theoretical heat of reaction of an epoxy group is 105 kJ/mol.¹⁷

C. Thermal Mechanical Analysis

The effects of a polymeric material undergoing a mechanical deformation under compressive or tensile load at various temperatures can be studied using a Thermal Mechanical Analyzer (TMA). The technique employs a vertical sample probe resting on a relatively flat surface of the sample. The linear displacement of the probe by a change in sample dimension is detected by the instrument and translated into an electrical signal. This is done by displacement of the core of a linear variable differential transformer (LVDT) and is recorded as a function of temperature or time. This signal is read for our experiments as the actual displacement in micrometers, but can also be read as the percentage of the initial known length or thickness of the sample. The TMA has several different modes with

changeable probes to measure penetration, expansion, and elongation. A schematic of the instrument is given in figure [1.29]^{18,19}.

The coefficient of linear thermal expansion, glass transition temperature and melting temperature can be determined by TMA. For this study we primarily use TMA for the determination of glass transition temperature.

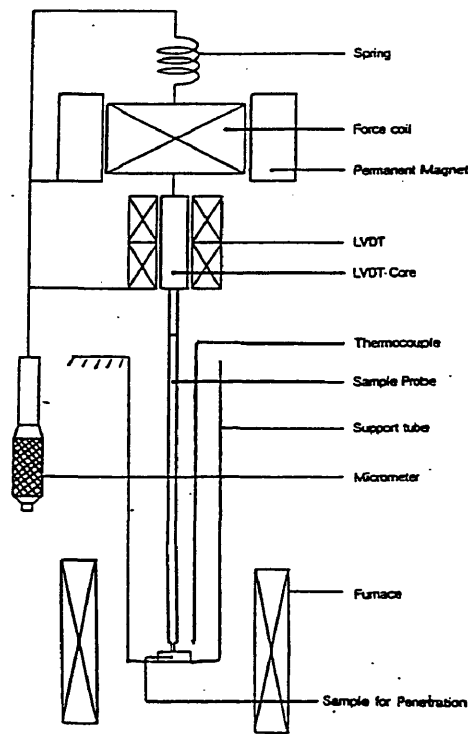


Figure [1.29] Thermal Mechanical Analyzer

D. Rheological Analysis

Rheology is defined as the study of the deformation and flow of matter²⁰. Each of the epoxy systems was rheologically measured on a

Rheometrics RDA-700 apparatus. Figure [1.30] illustrates the experimental testing apparatus²¹

The epoxy resin samples were placed between two parallel plates. The sample thickness was approximately 0.6 millimeters due to the low viscosity of the uncured resins. The servo-motor applies a tangentially deformational

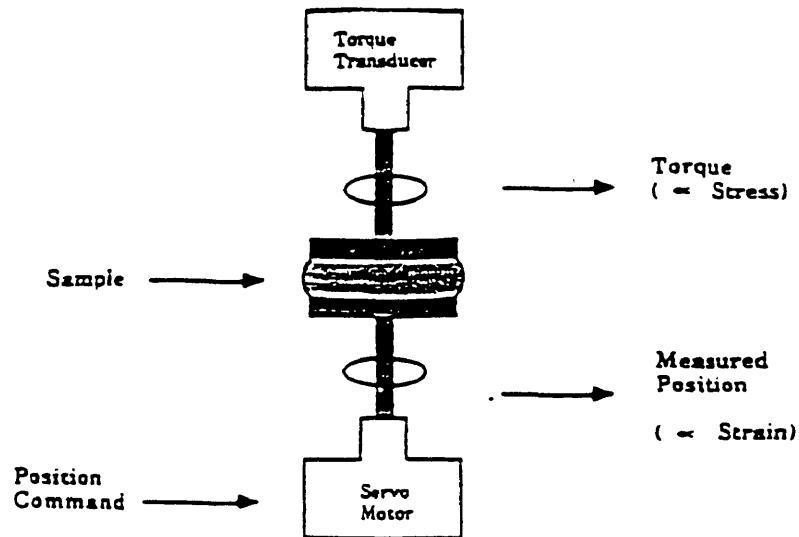


Figure [1.30] RDA-700 Test Apparatus

force to the sample during the experiment. This force acts as a shearing force on the sample. A displacement, x , in the sample may occur as a result of this applied force, Figure [1.31]. The measurement is initiated by displacing the material and creating a change in dimension per unit dimension, meaning a strain is applied to the resin. The torque transducer measures the resulting applied stress in the material with dimensions of force per unit area. Two possible extremes are possible from the torque transducer. First, if the material is ideally elastic there is no displacement; the torque transducer moves equally with the servo-motor. The other extreme is that the material is totally displaced. In this case the torque transducer does not move at all,

meaning the material is ideally fluid. The materials studied herein exhibit behavior somewhere in between the two extremes. Figure [1.31] is a schematic of material deformation.

The RDA-700 subjects resins to a sinusoidal strain in the parallel plate experiment. Figure [1.32] is an example of a hypothetical sinusoidal shear strain experiment²². The material responds with a sinusoidal stress upon

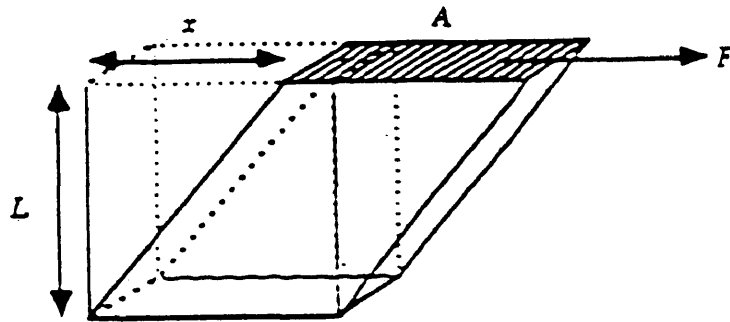


Figure [1.31] Material Deformation from Shear Strain

application of a sinusoidal strain. The difference in the maxima of these two sinusoidal measurements is the phase shift angle, δ .

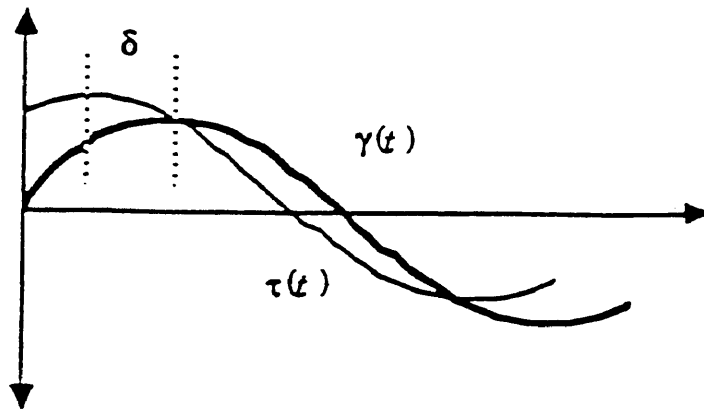


Figure [1.32] Strain/Stress Responses for a Sinusoidal Test

The complex shear modulus, G^* , is determined during the parallel plate experiment. It is represented mathematically by [1.33]:

$$G^* = G' + iG'' \quad [1.33]$$

where G' is the shear storage modulus and G'' is the shear loss modulus.

Mathematical formulae for G' and G'' are:

$$G' = (\sigma/\gamma) \cos \delta \quad [1.34]$$

$$G'' = (\sigma/\gamma) \sin \delta \quad [1.35]$$

The dynamic viscosity, η^* , is measured in poise, grams seconds⁻¹ centimeters⁻¹, and is related to G^* by

$$\eta^* = G^*/\omega \quad [1.36]$$

where ω is $2\pi f$. Solving for both η' and η'' yields

$$\eta' = G''/\omega \quad [1.37]$$

$$\eta'' = G'/\omega \quad [1.38]$$

E. Mechanical Tensile Testing

If a solid object is at equilibrium, such as nylon-11 or PVDF, but is subjected to external forces that stretch, shear or compress it, the shape of the object will change. Tensile stress is the ratio of the force, F , to the cross-sectional area, A , of the sample being tested²³. Mechanical tensile tests were initially performed on nylon-11 using a United SFM-10 tensile test apparatus at NASA Langley. In 1996 the College of William & Mary acquired a

Material Testing Systems tensile test apparatus allowing further tests on nylon-11 and also tests on PVDF to be conducted in house.

The procedure for testing the tensile stress on a material required gripping the sample in place as shown in Figure [1.39]²⁴. As the sample is pulled at a constant rate, the gage length (L) increases as the gage width (a) decreases as shown in Figure [1.42]. The tensile strength of the specimen seen in the figure is equal to the load divided by the cross sectional area

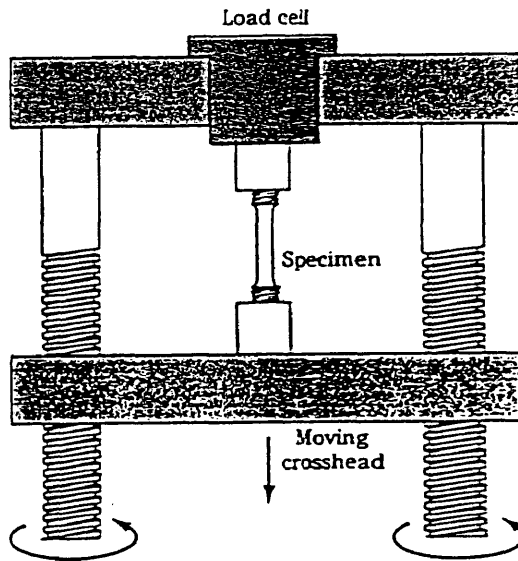


Figure [1.39] Tensile Testing Aparatus

being tested, or

$$\epsilon = F / (a \times b) \quad [1.40]$$

while the percent elongation is calculated as

$$\% \text{ elongation} = (L2 - L1) / L1 \times 100 \quad [1.41]$$

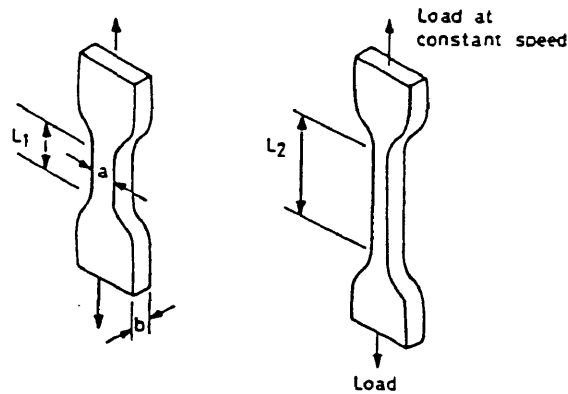


Figure [1.42] Schematic of Tensile Test Sample²⁵

Plotting the stress (tensile strength) versus the strain (elongation) yields a plot similar to Figure [1.43]. The line drawn to the origin before curvature begins is the region of elastic strain. This indicates the polymer can stretch and return to its original dimensions as long as the stress applied does not exceed the point where deviation from linearity occurs. The slope is the elastic modulus. Plastic deformation is an irreversible change in the dimensions of the sample. This occurs at the linear deviation point. Generally the exact point where the elastic region ends and the plastic region begins is not clear, therefore it is standard in American engineering tests to set the yield strength as the tensile strength at 0.2 percent offset (elongation). Figure [1.43] indicates a 0.2 percent offset yield strength of approximately 78,000 psi derived by drawing a line parallel to the linear portion of the curve from 0.002 in/in strain to the intersection with the upper portion of the curve. This diagram also allows determination of the load at break and percent extension at break of the material.

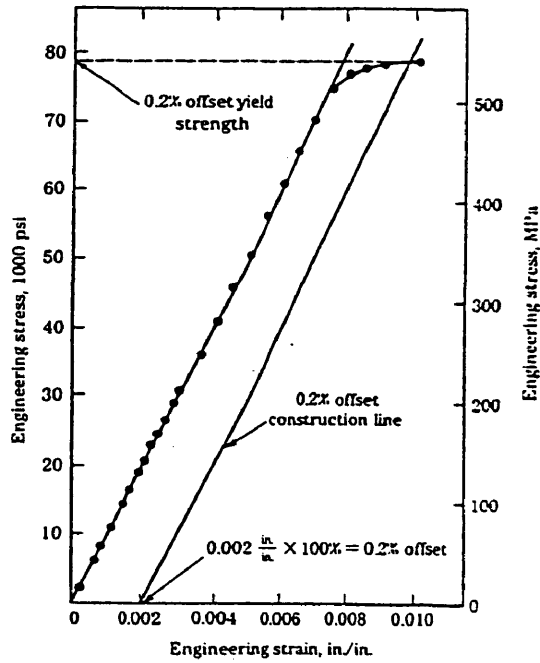


Figure [1.43] Stress-Strain Diagram²⁶

F. Solution Viscosity Testing

The viscosity of a fluid can be defined as the resistance to flow between parallel layers within a stationary fluid when a shearing force is applied:²⁷

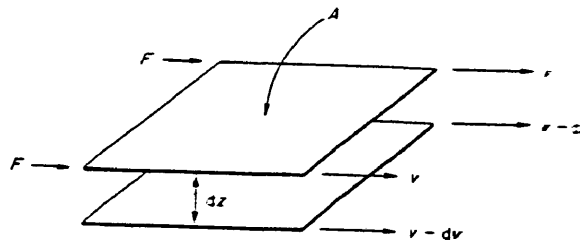
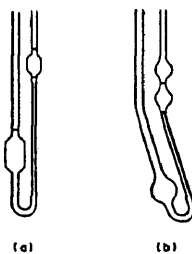


Figure [1.44] Fluid Flow Representation

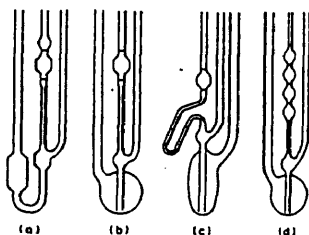
The viscosity, η , is the proportionality constant relating to laminar flow and shear stress.

A solution becomes more viscous after dissolution of a polymer due to the large difference in size between the polymer and the solvent molecules. The relative size of the polymer can be determined by comparing the ratio of the dynamic viscosity between the pure solvent and the dilute polymer. Hence, the molecular weight can then be estimated. Solution viscometry is a quick and inexpensive way to characterize the polymer in solution, although it is not absolute.

The device used to measure the solution viscosity is called a capillary viscometer. Several types of viscometers are shown below.²⁸



U-tube viscometers: (a) Ostwald, (b) Cannon-Fenske



Suspended level viscometers: (a) Ubbelohde; (b) modified Ubbelohde; (c) Desreux-Bischoff type; and (d) Schurz-Immergut type

Figure [1.45] Capillary Viscometers

The most commonly used types are the Ostwald and Ubbelohde. The suspended level viscometers have an advantage over the U-tube variation in that the volume of liquid originally introduced does not affect the driving force for the flow of the fluid through the capillary tube. This removes a large percentage of experimental error. Therefore, Ubbelohde viscometers are used in this study.

The viscometers are kept in a constant temperature bath of 25°C with observed fluctuations of less than 0.1°C. This is necessary because a change in temperature of only one degree from 20°C represents a viscosity change of 1 to 2%. A Fisher lab timer was used to measure the time required for a sample to run from a top mark to the bottom mark on the viscometer. It is this time that is used to calculate the viscosity average molecular weight, M_v .

Relative viscosity, η_r , is defined as the relationship between the measured flow time for a sample with the pure solvent flow time.²⁹

$$\eta_r = \eta/\eta_0 = t/t_0 \quad [1.46]$$

This simplified method neglects minor effects of kinetic energy corrections.³⁰

The specific viscosity measures the relative increase in viscosity from the solvent normalized by the solvent. It is defined as,

$$\eta_{sp} = \eta_r - 1 = (t - t_0)/t_0 \quad [1.47]$$

Both of these values are concentration dependent. As the concentration of the solution increases both of the viscosity terms increase. This dependence is

also seen in the reduced viscosity, which introduces the concentration into the equation:

$$\eta_{\text{red}} = \eta_{\text{sp}}/c \quad [1.48]$$

where c = concentration. This equation can be used to generate the intrinsic viscosity, $[\eta]$ which is the limit of the reduced viscosity as the concentration approaches zero.³¹

$$[\eta] = \lim_{c \rightarrow 0} (\eta_{\text{sp}}/c) = \lim_{c \rightarrow 0} (\eta_{\text{red}}) \quad [1.49]$$

The Mark-Houwink equation allows the correlation of the intrinsic viscosity to the molecular weight of the polymer for a given solvent and temperature:

$$[\eta] = KM_v^a \quad [1.50]$$

where K and a are constants obtained from calibration plots. These are easily obtained in the literature.

G. Mass, Thickness and Hardness Measurements

The final physical measurements which were taken on samples were the mass, thickness and hardness measurements. These are simple, nondestructive methods of examining physical properties of the material. Primarily these studies were done on aging PVDF.

Mass

In this study it was important to monitor the amount of plasticizer in the materials being tested. Plasticizers are used to soften the materials for

easy processing. The polymers become more flexible when plasticizer is added because the small molecules tend to break up crystallinity within the material. This allows the polymer chains to undergo reptation with more ease and therefore it becomes more tractible.

The initial mass of a polymer sample was measured on a Denver Instruments balance. The sample was then put into an aging environment. At various intervals the samples were removed and dried thoroughly in an aqueous environment. The sample was reweighed on the same balance to allow calculation of the weight change of the sample in that environment. Weight loss would indicate loss of plasticizer, while weight gain would show infiltration of the polymer by other small molecules within the aging environment.

Thickness

The thickness of each PVDF sample was measured prior to introduction to its environment. We used a micrometer for these studies. The micrometer we used had a built in mechanism to prevent the experimenter from applying excessive force to the sample. The thickness, as with the mass, was taken periodically throughout the study. This was important for determining if there was dimensional change in the sample due to interaction with different chemical environments.

Hardness

The most common method for testing the hardness of a plastic is to examine its resistance to indentation. Brinell, Vickers, Knoop, Rockwell, Barcol, and Durometer hardness tests each use this method. For this study we examined Barcol hardness using a Barber Coleman impressor (Model GYZJ-935). The hand-held unit is simple to operate. A schematic is shown in Figure [1.51].³² A hardness number can be read off the dial while supporting the back leg of the device on a hard, flat surface and firmly pressing the spring-loaded indenter onto the material. The tester is held in place for 10 seconds prior to reading the measurement. This is necessary due to the amount of creep present in most plastics. The hardness number has no units.

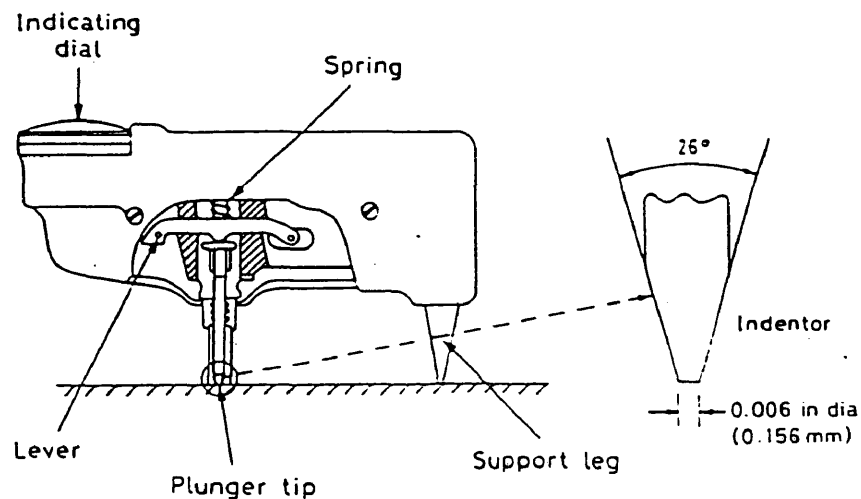


Figure [1.51] Barcol Hardness Tester

It is simply compared to other test numbers from Barcol and other similar hardness testers. The variations in the surface texture and properties generate considerable variation in these measurements, often $\pm 10\%$ is about the average.

References for Chapter I

- ¹ Kranbuehl, D., D. Hood, L. McCullough, H. Aandahl, N. Haralampus and W. Newby. "Frequency Dependent Electromagnetic Sensing (FDEMS) for Life Monitoring of Polymers in Structural Composites During Use." 1995, in press.
- ² Hood, D.K., "Monitoring and Modeling of Infiltration, Polymerization and Degradation Phenomena in Polymeric Systems." Ph.D. Dissertation, College of William & Mary, 1996, p.6.
- ³ Chanda, Manas and Salil, R.K., Plastics Technology Handbook, 2nd edition. New York: Marcel Dekker, Inc. 1993, p.317.
- ⁴ Senturia, S.D., Read, B.E., Williams, G. "Dielectric Analysis of Thermoset Cure." Advances in Polymer Science, Springer-Verlag Publishers, Berlin, Germany, 1986, Vol. 80.
- ⁵ Hood, p.6.
- ⁶ Hood, p.8.
- ⁷ Tipler, Paul A., Physics. New York: Worth Publishers. 1991, p.691.
- ⁸ Tipler, p.623-630.
- ⁹ Mark, H. *et al.*, Encyclopedia of Polymer Science and Engineering, New York: John Wiley & Sons, 1986, Vol. 5, p.26.
- ¹⁰ Kranbuehl, David E., "Cure Monitoring," Encyclopedia of Composites. New York: VCH Publishers, 1990.
- ¹¹ Kranbuehl, "Cure Monitoring".
- ¹² McNaughton, J.L. and C.T. Mortimer. Differential Scanning Calorimetry. Reprint from "IRS; Physical Chemistry Series 2." London: Butterworths. 1975, Vol. 10, p.2.
- ¹³ McNaughton, p.3.
- ¹⁴ Allcock, Harry R. and F.W. Lampe. Contemporary Polymer Chemistry. Englewood Cliffs: Prentice-Hall, Inc. 1990, p.393.

-
- ¹⁵ Inoue, M. "Studies on Crystallization of High Polymers by Differential Thermal Analysis." Journal of Polymer Science. New York: John Wiley & Sons, Inc., 1963, Part A, p.2700.
- ¹⁶ Welch, Gordon, and Robert Miller. Journal of Polymer Science, Polymer Physics Edition. Vol. 14, p.1683.
- ¹⁷ Girard-Reydet, E., *et al.* "Epoxy-Aromatic Diamine Kinetics. 1. Modeling and Influence of Diamine Structure." Macromolecules, 1995, Vol. 28, p.7599-7607.
- ¹⁸ Kranbuehl, "Frequency Dependent Electromagnetic Sensing (FDEMS)..."
- ¹⁹ Tipler, p.691.
- ²⁰ Sperling, L.H. Introduction to Physical Polymer Science. 2nd ed. New York: John Wiley & Sons, 1992, p.487-495.
- ²¹ Argiriadi, M.A. "Characterization and Modeling of Amine Epoxide Resins," Masters Thesis, College of William & Mary, 1994.
- ²² Argiriadi, M.A.
- ²³ Tipler, p.334.
- ²⁴ Smith, William F. Foundations of Materials Science and Engineering, 2nd ed. New York: McGraw-Hill, Inc., 1993, p.201.
- ²⁵ Chanda, p.339.
- ²⁶ Smith, p.205.
- ²⁷ Lovell, Peter A. "Dilute Solution Viscometry." Comprehensive Polymer Science, New York: Pergamon Press. 1989, Vol. 1, p.174.
- ²⁸ Lovell, p.175.
- ²⁹ Allcock, p.383.
- ³⁰ Lovell, p.177.
- ³¹ Sperling, p.102.
- ³² Chanda, p.287.

Chapter II

Epoxy – Amine Systems

A. Introduction

The first epoxy thermoset crosslinking polymer resins, were synthesized in 1936. A diglycidyl ether of bisphenol-A (DGEBA) was produced based on a reaction of DGEBA and epichlorohydrin. A hard, crosslinked thermoset material was produced by reacting the epoxy resin with phthalic anhydride (PHA).¹ Coatings were created from the products and other implications of epoxy compounds were soon discovered.

The epoxy resins are versatile with numerous applications such as adhesives, solders, caulks, and protective coatings. These diverse applications are due to the general physical properties exhibited by epoxy resins. Some of these properties include low viscosity, low shrinkage, high adhesive strength, strong mechanical properties, good chemical resistance and a large range of cure temperatures. The chemistry of epoxy resins is quite flexible and is therefore able to be tailored for desired properties and applications.¹

B. Chemistry

Epoxy resins are composed of molecules with one or more epoxy groups. These groups are also known as epoxide or oxirane groups. Epoxy groups are composed of an oxygen atom bonded to two adjacent carbon atoms forming a strained three-membered ring (Figure [2.1]).

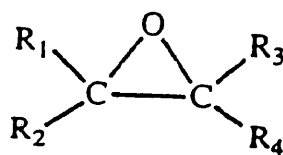


Figure [2.1] Epoxy Group

Epoxy groups are highly reactive due to the polarity and strained nature of the ring. The epoxy group can be converted into a thermoset material by reaction with curing agents such as amines, amides, alcohols, acids and anhydrides.

This study focuses on the difunctional molecule DGEBA.

Reactants used in this study with their masses and melting temperatures are shown below:

Monomers	Formulae	Company	Mass (g/mol)	Melting Temp (°C)
DGEBA(Diglycidyl ether of bisphenol A) i = 0.03 Di-epoxy		Dow Chemical	348	20
4-bpa (4-biphenyl amine) Difxl	-----	Aldrich	169	53
3-Cl-2,6-DEA (3-chloro-[2,6-diethyl-aniline]) Difxl		Aldrich	184	Boiling Point (°C) 138
2,6-DEA (2,6-diethylaniline) Difxl		Aldrich	149	Boiling Point (°C) 243
Monoepoxy (1,2-epoxy-3-phenoxy propane)	-----	Aldrich	150	4.0
MCDEA (4,4'-methylene bis(3-chloro-2,6-diethylaniline) Tetrafxl		Lonza	380	92

Table 2.1 Reactants

The DGEBA is reacted with various amine curing agents. Amines are coreactive curing agents.² Coreactive curing agents act as bridges

connecting epoxy oligomers. Addition of a coreactive curing agent such as an aromatic amine results in nucleophilic attack on the epoxy ring. Regions of low electron density on the epoxy ring are attacked by the donated electron pairs of the Lewis base catalysts. This causes opening of the epoxy ring resulting in the formation of a salt or zwitterionic intermediate. Chain propagation then continues anionically. This process is shown in Figure [2.2].²

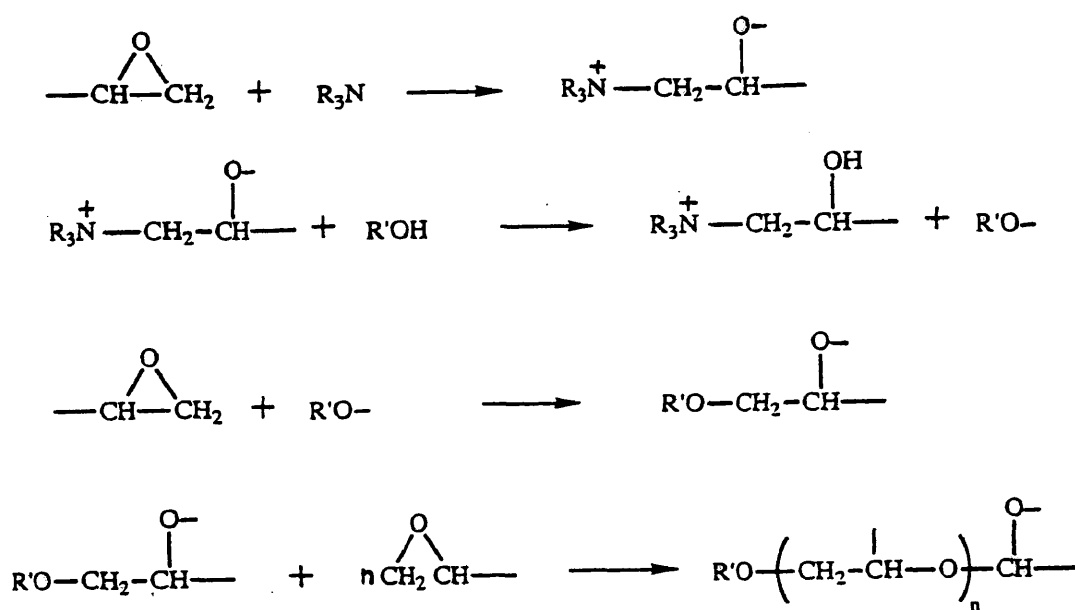


Figure [2.2] Epoxy – Amine Reaction

C. Results and Discussion

Dielectric Measurements

Isothermal cure of each of the five systems was studied at 135°C. This FDEMS data (example in Figure [2.3]) can be used to determine the ionic conductivity of the system, and to determine the characteristic dipolar relaxation time, τ . Dipolar groups in a curing resin, or in a fully cured system, are embedded in a viscous medium and are hindered by

attachment to a growing network. The orientation process has a characteristic time τ . There is a loss of energy associated with the orientation because of the hindering mechanism.

The mean relaxation rate $1/\tau$ of the dipolar rotational movement corresponds to the local maximum at ϵ'' at a given frequency. For isothermal runs this value is the characteristic dipolar relaxation time at that frequency. The mean relaxation time τ is given by $1/(2\pi f)$. The evolution of relaxation time during cure is a reflection of the differences in the molecular size, shape and charge distribution in different types of molecules and of the consequent differences in their reaction kinetics. Table [2.2] indicates the time to reach τ of 3 μs (corresponding to 50 kilohertz) for each of the four DGEBA systems during the isothermal cure. This value is corrected for the time it took the system to reach 135°C.

System	Approximate Time (min) to Reach τ ($1/2\pi(50 \text{ kHz})$)
1:1 molar 4-bpa:DGEBA	45
1:1 molar mcdea:DGEBA	270
1:1 molar 3-CI-2,6-dea:DGEBA	850
1:1 molar 2,6-dea:DGEBA	280

Table [2.2] Time to Reach τ

The value of τ is a measure of the relative rate of reaction of each of the systems and the buildup of the equivalent T_g .

It is generally agreed that the cure of epoxy resins does not generate ions; the ions are primarily due to impurities in the reactants.

Therefore, the ion concentration does not change significantly during cure.³ For an isothermal cure with a fixed number of ions, ionic conductivity is proportional to the mobility of the ions. The ionic mobility factor is highly temperature dependent and is a function of the size of the ion and the mobility of the polymer chain segments.

Ionic conductivity, σ , can be determined from the early portion of the dielectric loss curve by multiplying the loss by the field frequency with the permittivity of free space ($\sigma = \omega \epsilon_0 \epsilon''$). Calculation of σ was done for each system at 125 Hz. This was the lowest frequency in the smooth overlapping region of $2\pi f \epsilon''$. Figure [2.4] is an example of the conductivity versus time for cure of the 4-bpa:DGEBA system. Correlations of mechanical properties such as viscosity with the dielectric data will be explained in the next section.

Several different runs were done on each of the systems: a 135°C isothermal cure, a pre-cure temperature ramp and a post-cure temperature ramp. Table [2.3] indicates which systems underwent each of the runs.

System	135°C Isotherm	Pre-Cure Ramp	Post-Cure Ramp
DGEBA			
4-bpa:DGEBA	X	X	X
3-CI-2,6-DEA:DGEBA	X		X
2,6-DEA:DGEBA	X		X
Mcdea:DGEBA	X	X	X
Monoepoxy			
4-bpa:monoepoxy	X		X
Monomer			
DGEBA		X	

Table [2.3] Epoxy-Amine System Experiments

On occasion there was instrumental difficulty or problems with measuring the properties of that amine and data were not available. The 2,6-dea compounds for example are of extremely low viscosity. Therefore pre-cure data were unavailable because it is not possible to seal the sample inside all of the instruments.

Pre- and post-cure temperature ramps were done dielectrically and rheometrically for most of the systems. These temperature ramps were used to monitor the temperature dependent behavior of the systems during pre-cure as small molecules and during post-cure as large polymers. Plots of the negative natural log of the conductivity, σ , versus reciprocal temperature are shown in Figures [2.5] – [2.12]. The slopes of these plots divided by R are proportional to the activation energy, E_a . The activation energy, E_a , can be calculated from the slope of the plot of $\ln q$ versus $1/T$ using the following equation where q is either the conductivity, σ , or the viscosity, η .

$$\ln(q) = -\frac{E_a}{RT} + \ln A$$

Equation 2.13 Arrhenius Relationship

The values of the slopes are in Table [2.4].

Pre-Cure Systems	$E_a(\sigma)/R$	$E_a(\eta)/R$	X = Ratio of $\frac{E_a(\sigma)/R}{E_a(\eta)/R}$
DGEBA			
4-bpa:DGEBA – difxl	7,500	6,800	1.10
Mcdea:DGEBA – tetrafxl	9,000	7,100	1.30
Monomer			
DGEBA	5,800	8,600	0.68
Post-Cure Systems			
DGEBA			
4-bpa:DGEBA – difxl	14,800	10,570	1.40
3-CI-2,6-DEA:DGEBA – difxl	11,200	N/A	N/A
2,6-DEA:DGEBA – difxl	8,800	9,100	0.97
Mcdea:DGEBA – tetrafxl	16,400	560	29.2
Monoepoxy			
4-bpa:monoepoxy	11,400	11,100	1.00

Table [2.4] m values for σ and η and the Ratio, x

Rheology

For each system mentioned above the viscosity, η , was measured using rheology for isothermal cures as well as pre- and post-cure ramps. Viscosity measures the macroscopic polymeric property characterized by polymer chain segment mobility. Figures [2.14] – [2.15] are example plots of the viscosity of the 4-bpa:DGEBA system during the isothermal cure and during a post-cure ramp respectively. This mechanical property measures the response of polymer chain segments to an applied stress, while ionic conductivity measures the mobility of ions in response to an applied electric potential. The natural log of the viscosity for temperature ramps can be plotted against the reciprocal temperature to give an Arrhenius relationship. This is similar to earlier plots of $\ln \sigma$ versus reciprocal temperature, and therefore proportional to the energy of activation (Figures [2.16] – [2.22]).

Several studies have reported an inverse relationship between experimental ionic conductivity and viscosity well prior to gel.^{4,5,6} Based on the assumption that ion concentration does not change during cure, the conductivity, σ , is proportional to the reciprocal of the viscosity as seen below:

$$\sigma \propto \eta^{-x} \quad [2.23]$$

Correlation plots of natural log σ versus natural log η were created for the different epoxy-amine systems at constant temperature (135°C). The plots are represented in Figures [2.24] – [2.28]. The slope of each of the systems in the early stages of cure is near -1 (+/- 0.2) except for the mcdea:DGEBA system. The mcdea:DGEBA system is the combination of the di-epoxy with a tetrafunctional amine. This system is quite different from the other systems as crosslinking is involved from early in the reaction process. The values obtained for this system are in agreement with values obtained by other researchers.⁷ The slope of the other systems is near one indicating that the conductivity and the reciprocal of the viscosity have similar dependencies on polymer growth and segment mobility. Table [2.5] is a listing of the slopes and intercepts of each isothermal curing system where “difxl” indicates the amine has two functional hydrogens, and “tetrafxl” means the amine has four functional hydrogens.

System	x(slope)	Intercept
DGEBA		
4-bpa:DGEBA – difxl	0.956	13.1
3-CI-2,6-DEA:DGEBA – difxl	0.933	7.95
2,6-DEA:DGEBA – difxl	1.109	6.88
Mcdea:DGEBA – tetrafxl	0.648	15.6
Monoepoxy		
4-bpa.monoepoxy – difxl	1.161	7.07

Data from $\ln \sigma$ vs $\ln \eta$ for 135°C Isotherms – Early in Cure
Table [2.5]

Plots of negative $\ln \sigma$ versus $1/T$ and $\ln \eta$ versus $1/T$ were created for the pre- and post-cure ramps as mentioned earlier. The negative of the $\ln \sigma$ was used simply for easier correlation between σ and η values. The ratio of the slope of the σ plot to the slope of the η plot is indicated in Equation [2.29].

$$\frac{\text{slope}(\sigma)}{\text{slope}(\eta)} = x$$

Equation [2.29]

The behavior of the conductivity and the viscosity as a function of temperature and degree of cure are known to approximately obey a modified Arrhenius equation. Equations [2.30] and [2.31] show the relationships:

$$\rho = \frac{1}{\sigma} = Ae^{\frac{Ea(\sigma)}{RT} + \beta\alpha}$$

Equation [2.30]

$$\eta = Ae^{\frac{E_a(\eta)}{RT} + \beta \cdot \alpha}$$

Equation [2.31]

If the value of α is held constant, the equation is simplified and can be used to determine the activation energy as a simple Arrhenius relationship. Then by comparing the slopes or the activation energies the X in Equation [2.29] is the same ratio X of the activation energies in Table [2.4]. A listing of the X values for the ramped systems during pre- and post-cure is found in Table [2.4].

For the pre-cure, monomer and monoepoxy:4-bpa systems the X value, which is the ratio of the slopes, stays near the value of one. This correlates to the value X in the isotherms mentioned above. This indicates that the monomers during all the stages of growth change in similar ways (Table [2.5]). That is, σ tracks the change in $1/\eta$.

As a system cures further it can be seen from Table [2.4] that the energy of activation changes for both σ and η , but the relationship between σ and η during the cure for the linear (or difxl) systems, does not change or only changes slightly. This is seen in the 4-bpa:DGEBA system which has an increase in the value of X by approximately 25%, but the tetrafunctional amine system shows change in the X value at post-cure. For the tetrafunctional epoxy the isothermal relationship of σ to η changes significantly. This result occurs because η has a strong dependence on branching and crosslinking while σ does not. Thus it is

the strongly changing parameter of $\beta'(\eta)$ and a high order of dependence on α for η rather than differences in the activation energies for η and σ that causes rapid changes in the relationship $\sigma \propto \eta^{-x}$ for tetrafunctional, branching systems.

DSC

Next degree of conversion, α , was analyzed. This was done using the DSC. A particular unreacted system was run on the DSC at a constant temperature of 135°C. After the isothermal run was finished a ramp was done on the same sample to determine any residual heat of reaction. Our enthalpy values for the isothermal cures and for DSC ramps fall short of the theoretical values. Full reaction of the epoxy groups gives a theoretical heat of 105kJ/mol.⁸ Table [2.6] gives the values of the experimental DSC runs in comparison to the theoretical values for that system. The degree of conversion based on the theoretical value was then correlated to the conductivity and viscosity of the isothermal cures to give plots of σ versus α and η versus α respectively. Plots of these data are in Figures [2.32] – [2.41]. This is valuable information which is essential for the application of FDEMS as an on-line cure monitor. This would allow the user to monitor the exact degree of cure based on the dielectric measurements made *in situ*.

System	Exp'tl dH (J/g _{epoxy}) Isotherm	Exp'tl dH (J/g _{epoxy}) Ramp	Theo. dH (J/g _{epoxy})	% Reaction based on Theo Isotherm	% Reaction based on Theo Ramp
DGEBA					
4-bpa:DGEBA	-1,224	-2,086	-2,442	50	85
3-CI-2,6- DEA:DGEBA	-2,540	-2,019	-2,442	104	83
2,6-DEA:DGEBA	-1,118	-2,178	-2,442	46	89
Mcdea:DGEBA	-1,431	-2,072	-2,442	59	85
Monoepoxy					
4-bpa:monoepoxy	-1,226	-2,375	-2,442	51	97

Table [2.6] DSC Data from 135°C Isothermal Cures

Further studies are being done currently to measure the degree of cure using gel permeation chromatography. This would allow verification of the previous DSC data and another method of observing viscosity of the systems over time. Preliminary results indicate that the epoxy-amine systems never reach the full theoretical reaction value. This is reasonable because not every epoxy group is expected to react. This would only be possible if one continuous chain was created. This does not happen in practical experimentation. The epoxy groups will be unreacted at the ends of the oligomeric chains produced during the cure. Since low molecular weight chains are formed, a significant number of epoxy groups remain unreacted.

Analysis of the plots of σ and η versus α show that in later stages of cure for the tetrafunctional systems η is changing rapidly with small changes in α . The value of σ , however, is changing at a fairly constant rate throughout the cure. This information verifies the relationships

investigated earlier. At the point when significant crosslinking is involved, usually just before gel as for the mdea:DGEBA system, there is a rapid increase in the η for small changes in α while σ continues to change steadily as before.

D. Conclusions

Conductivity and viscosity data indicate that the isothermal cures of each of the systems do follow trends. Early during the isothermal cure changes in both σ and η are coupled: as the viscosity increases, the conductivity decreases. The five systems studied maintain a slope on the σ versus η plots of approximately -1 (± 0.2). This relationship holds true during all the stages of cure for linear systems studied but the tetrafunctional amine system experiences a stronger increase in η than in σ just before gel.

The systems were studied at constant α , both prior to and after the cure of the system. Data from these experiments indicate that prior to cure the systems tend to follow the same trend observed for the isothermal cures. The conductivity and viscosity are coupled. Post-cure data indicates that the tetrafunctional systems become decoupled. The constant value of α and X for the linear systems but not the tetrafunctional branched systems demonstrates that branching and gelation cause the variation on the behavior of σ versus η and not the increase in chain length.

References to Chapter II

- ¹ Lee, H.; Neville, K. Handbook of Epoxy Resins. New York: McGraw-Hill, 1967.
- ² Mark, H.F.; Kroschqwitz, J.I. "Epoxy Resins," Encyclopedia of Polymer Science and Engineering. New York: John Wiley & Sons, 1986.
- ³ Senturia, S.D. and Sheppard, N.F. "Dielectric Analysis of Thermoset Cure", Advances in Polymer Science, Springer-Verlag Publishers, Berlin, Germany, 1986, Vol. 80.
- ⁴Kranbuehl, D., *et al*, Polymer Eng Sci. 1989, Vol. 29, p. 285.
- ⁵ Sanford, W.M. and McCullough, R.L. Polymer Science, Polymer Physics. 1990, Vol. 28, p.973.
- ⁶ Wang, Y., *et al*, Polymer Mater. Sci. and Eng. 1993, Vol. 70, p. 279.
- ⁷ Eloundou, J.P., *et al*. "Microdielectric Study of Epoxy-Amine Systems: Relationships between Kinetics, Dielectric, and Rheological Parameters." Preprint in *J. of Polymer Sci.*, 1997.
- ⁸ Girard-Reydet, E., *et al*. "Epoxy-Aromatic Diamine Kinetics. 1. Modeling and Influence of Diamine Structure." Macromolecules. 1995, Vol.28, p. 7599-7607.

Data file: wm052997.a *Post-Cure*
 Probe: 1 dgeba:4-bpa 1:1:mdan 135°C Isotherm/Ramp

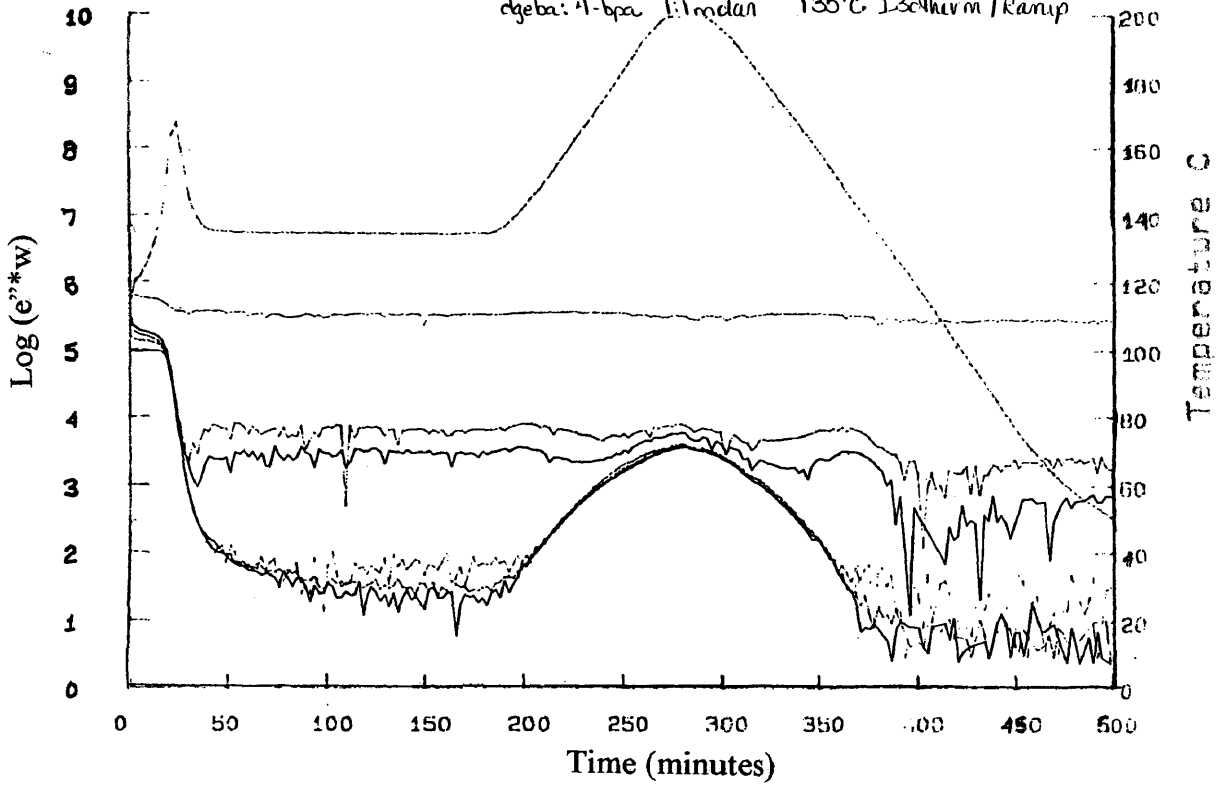


Figure [2.3]

4-bpa:dgeba 135C Isotherm
 Ln Conductivity vs Time

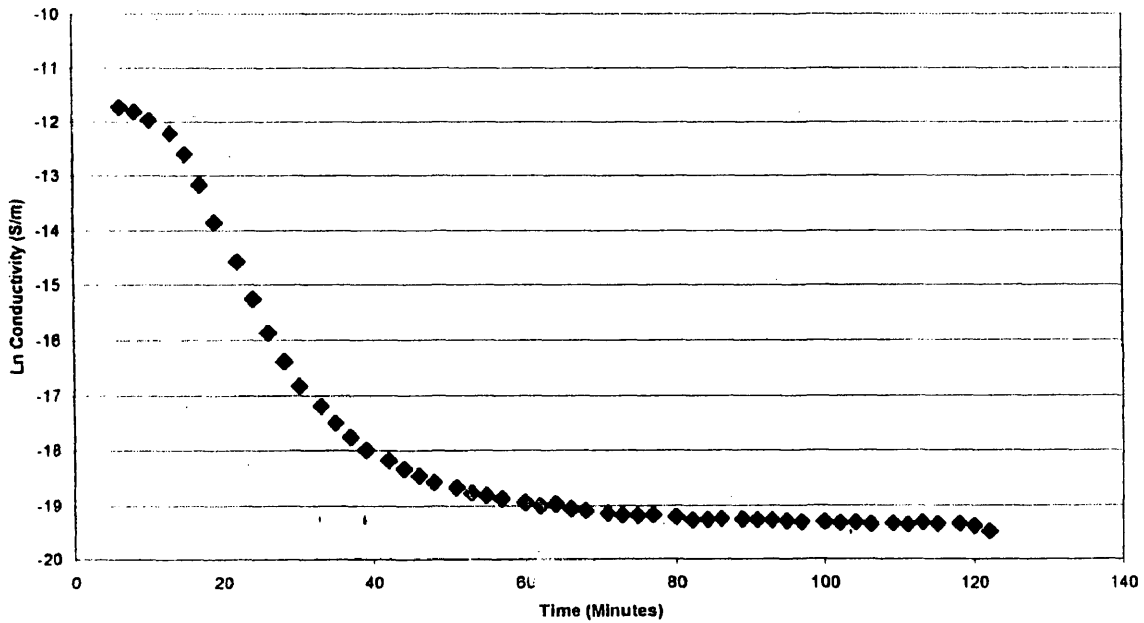


Figure [2.4]

4-bpa:dgeba 1:1 molar Pre-cure - Ln Conductivity vs 1/T

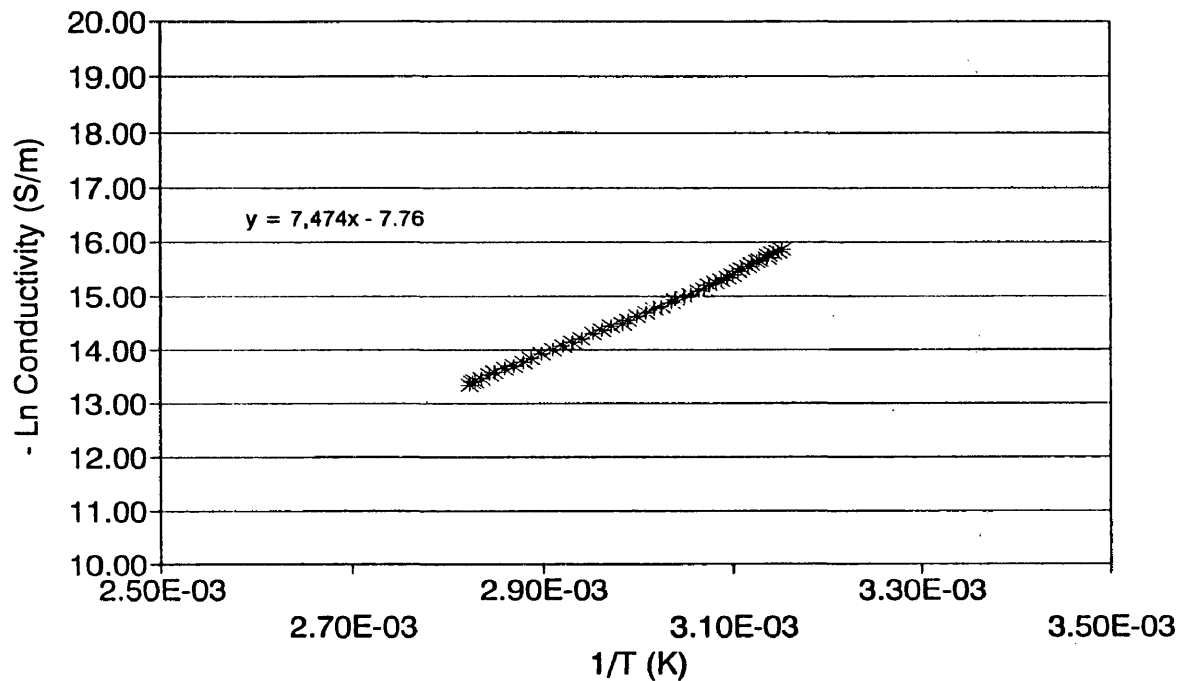


Figure [2.5]

dgeba:mcdea 1:0.5 molar pre-cure ramp - Ln Conductivity vs 1/T(K)

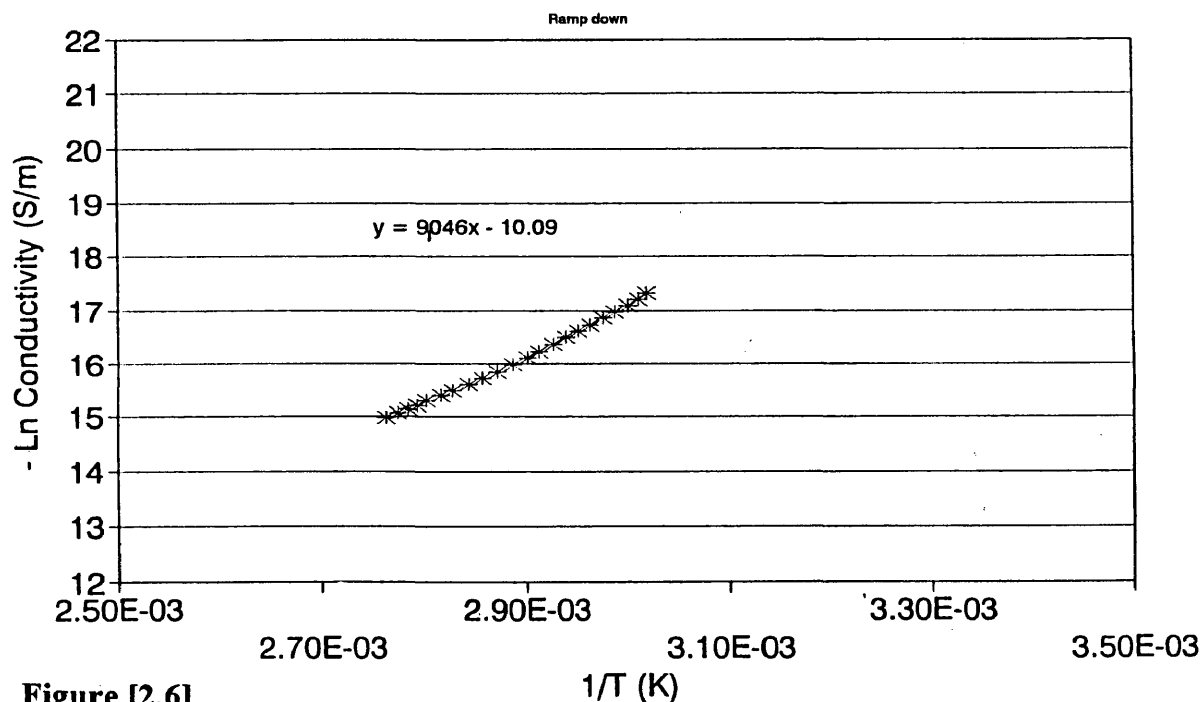


Figure [2.6]

DGEBA Only Ramp
-Ln Conductivity vs 1/T

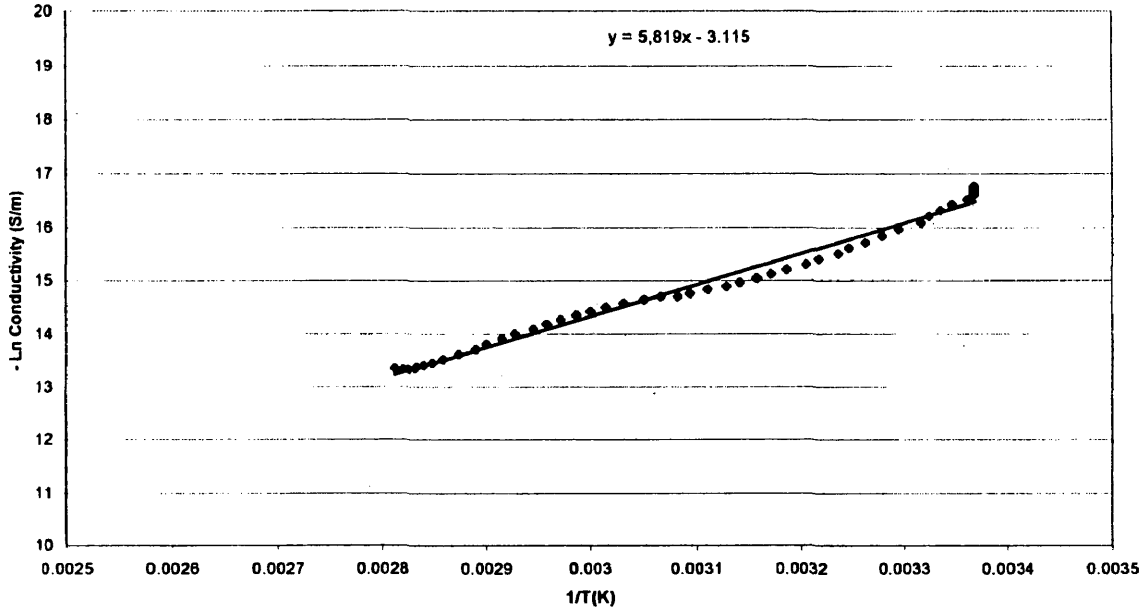


Figure [2.7]

4-bpa:dgeba 1:1 molar Ramp Down
-Ln Conductivity vs. 1/T

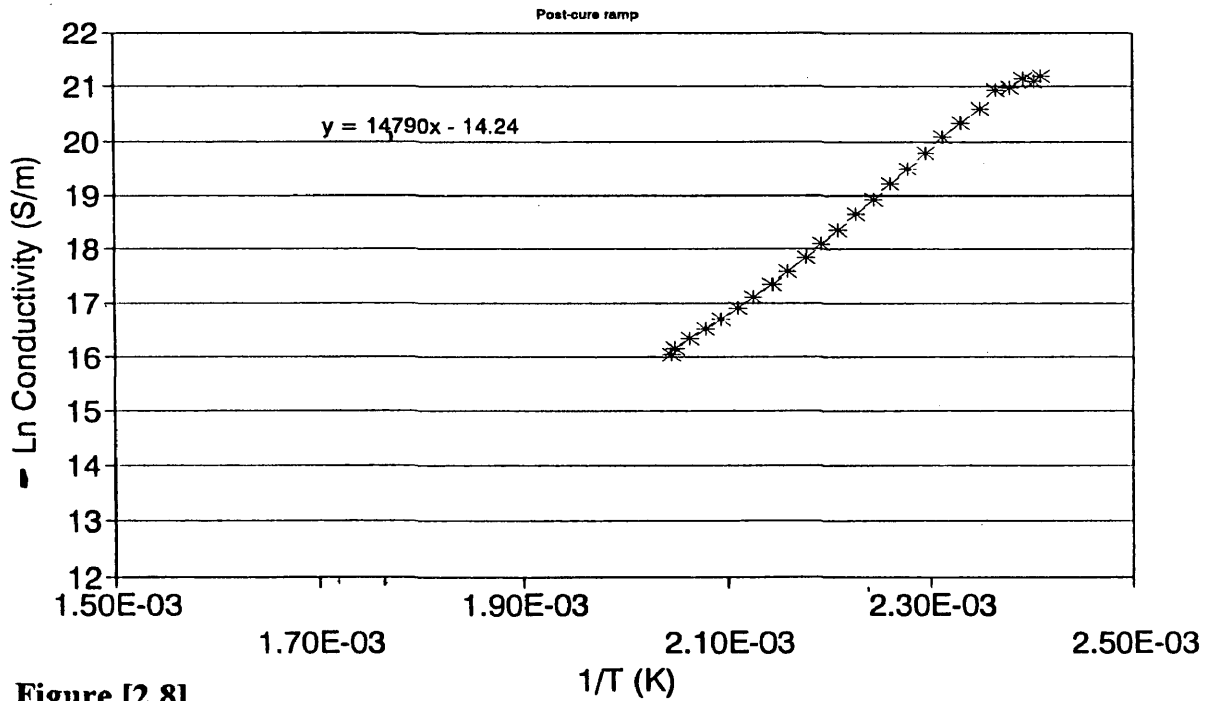


Figure [2.8]

3-CI-2,6-DEA:dgeba 1:1 molar Post-Cure Ramp
-Ln Conductivity vs 1/T

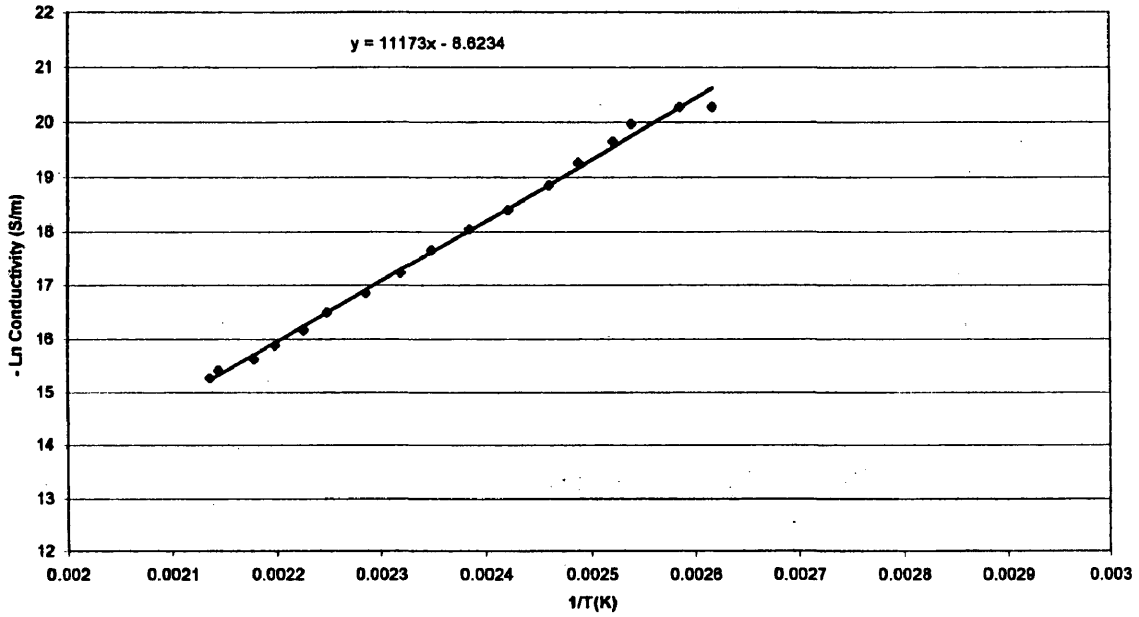


Figure [2.9]

WM081097 Chart 1

2,6-dea:dgeba 1:1 molar Post Cure
-Ln Conductivity vs 1/T

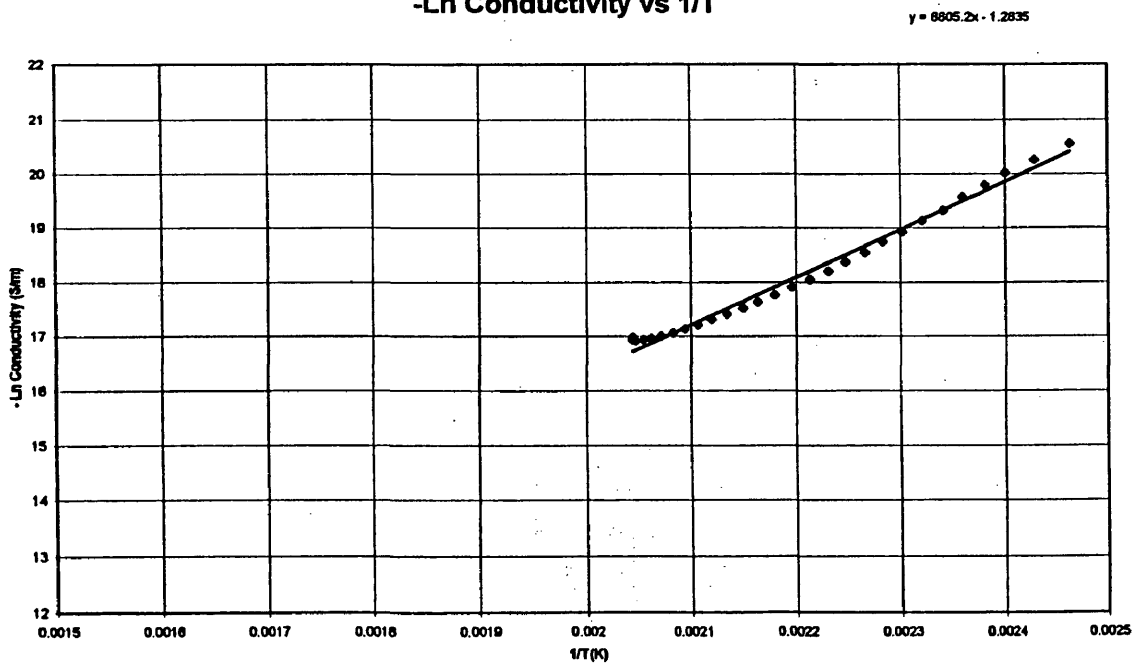


Figure [2.10]

mcdea:dgeba 0.5:1 molar Ramp
Post Cure Ramp Down

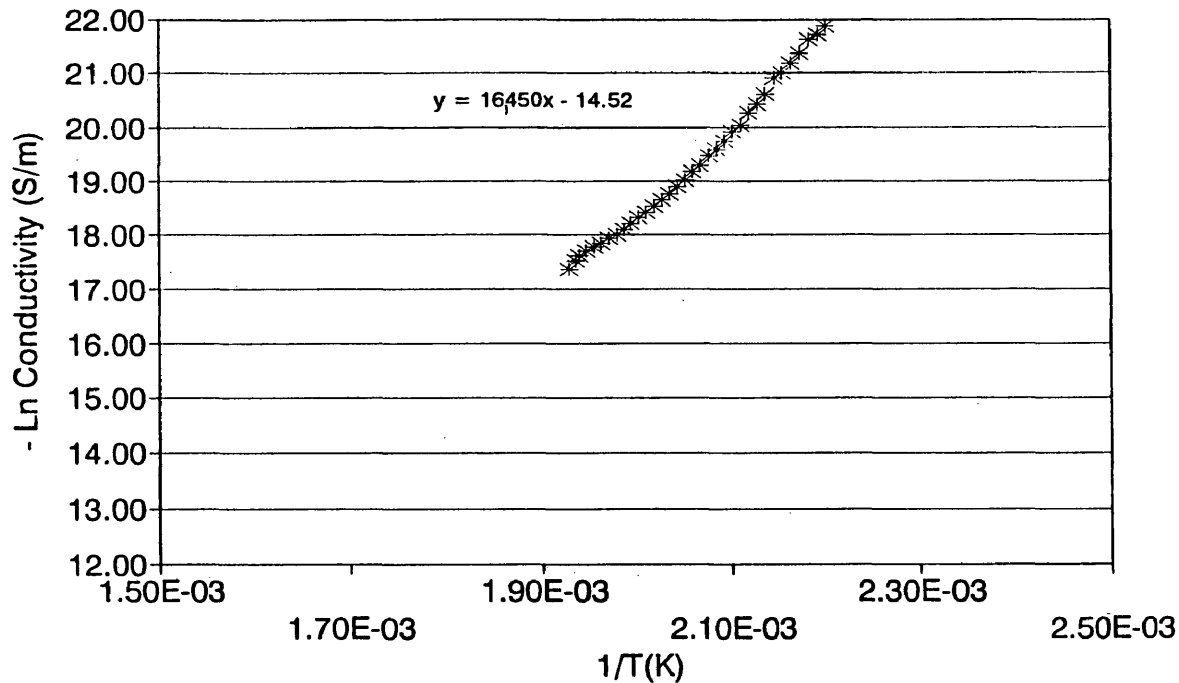


Figure [2.11]

Monoepoxy:4BPA 1:1 molar Post Cure
- Ln Conductivity vs. 1/T

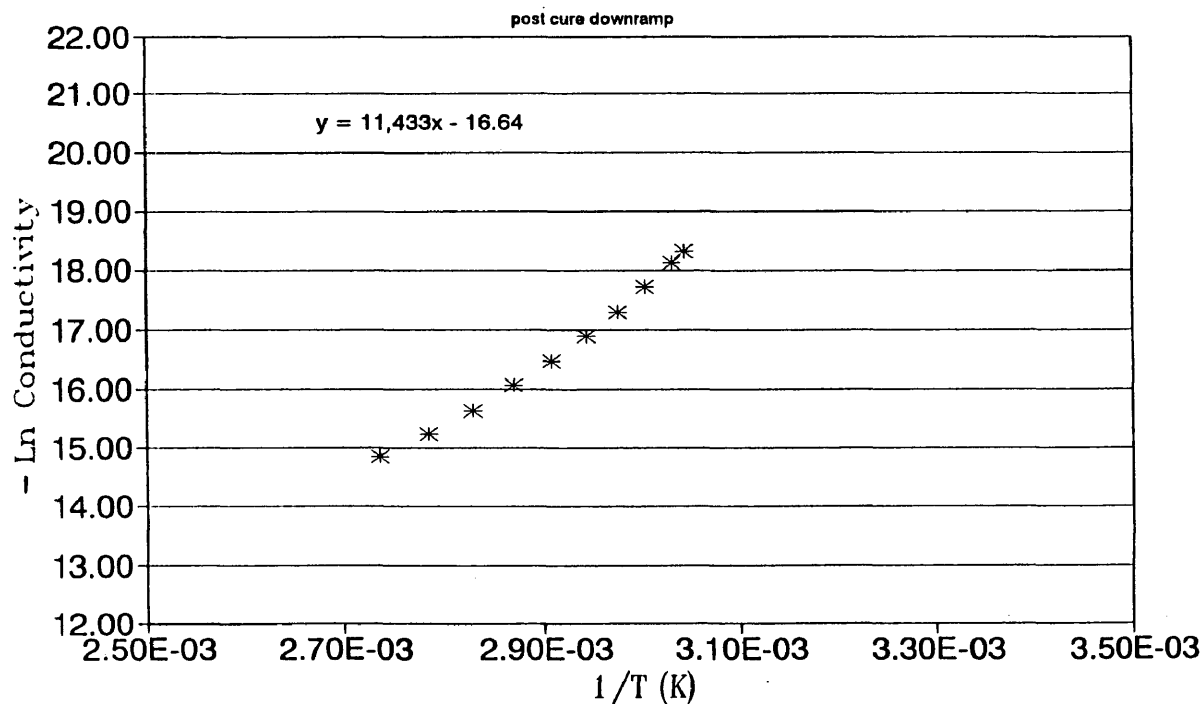


Figure [2.12]

4-bpa:dgeba 1:1 molar 135C Isotherm Log Viscosity vs. Time

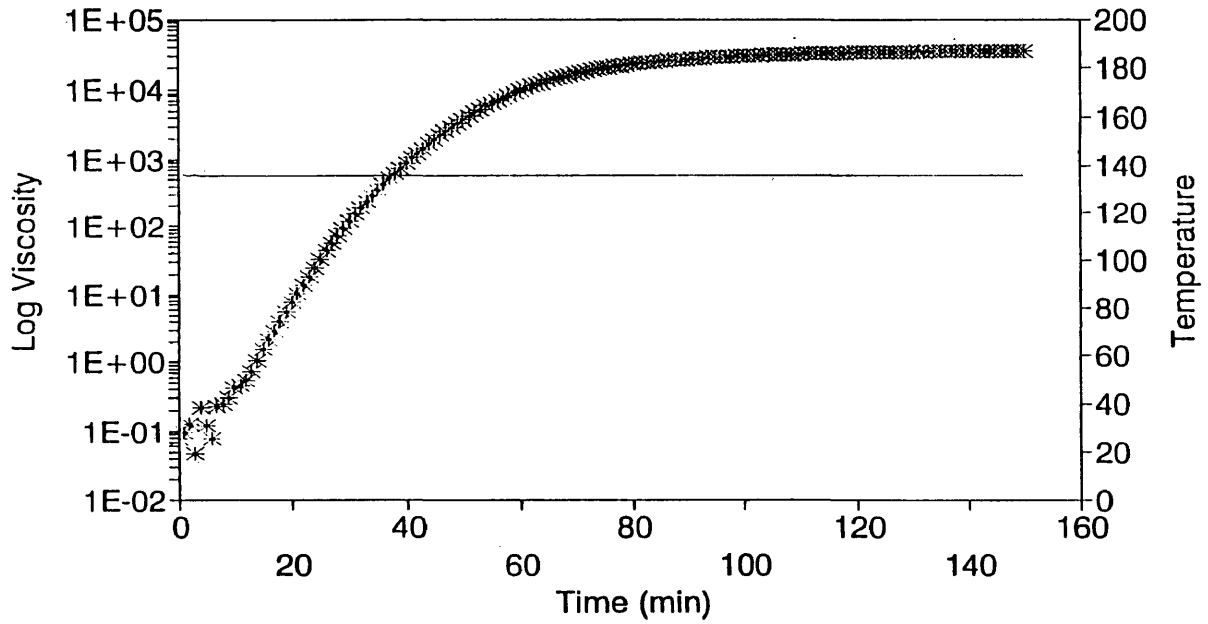


Figure [2.14]

4-bpa:dgeba 1:1 molar Ramp Log Viscosity vs. Time

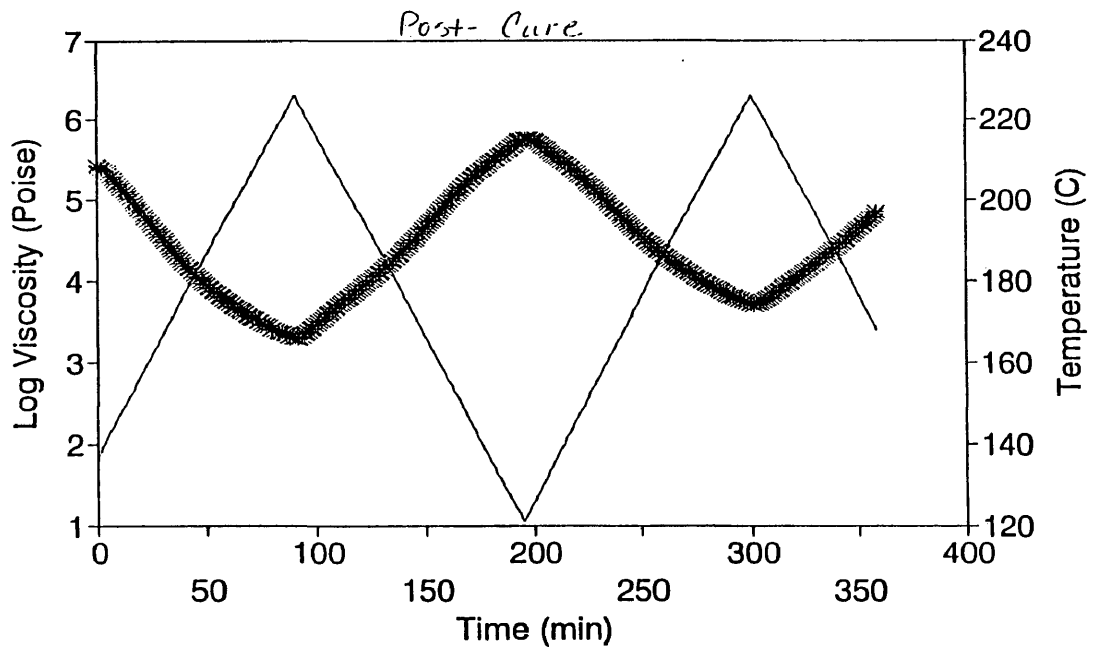


Figure [2.15]

4-bpa:dgeba 1:1 molar Prior to Cure

Ln Viscosity vs 1/T

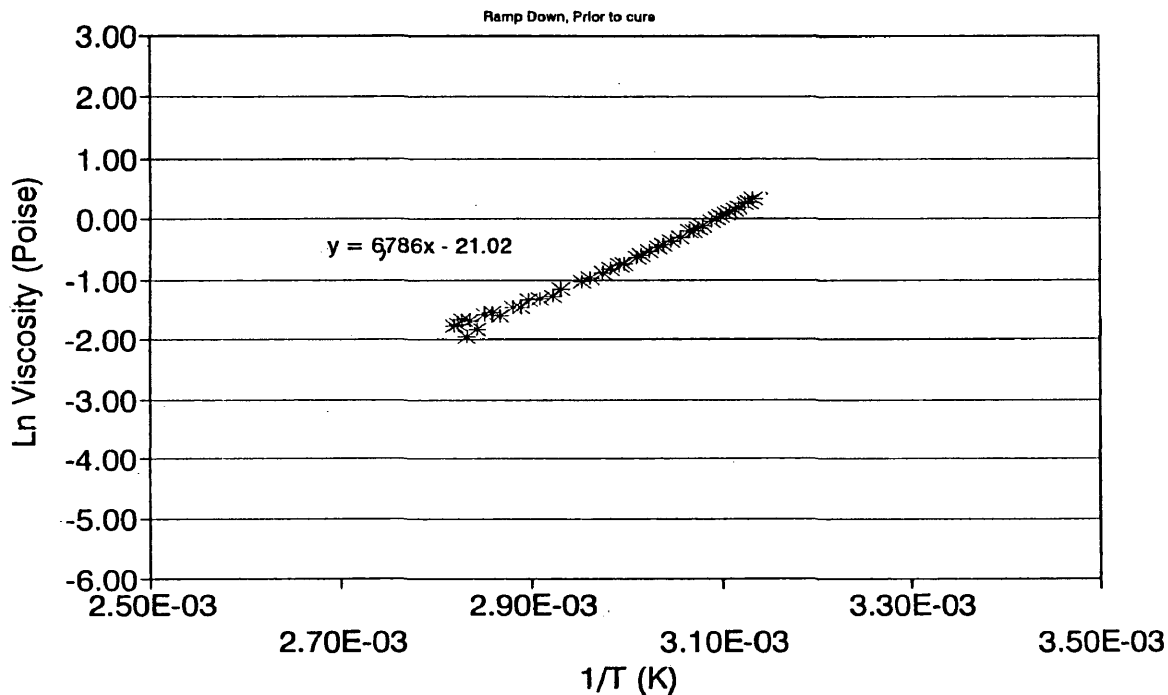


Figure [2.16]

dgeba:mcdea 1:0.5 molar pre-cure ramp

Ln Viscosity vs 1/T(K)

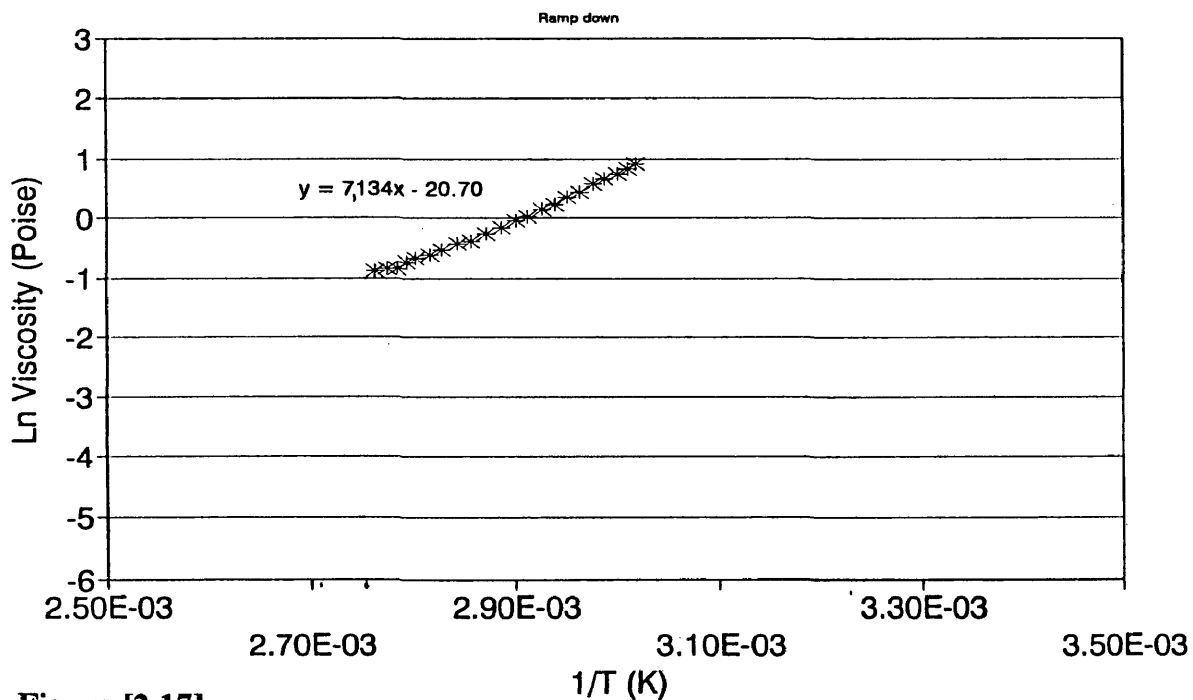


Figure [2.17]

DGEBA Only Ramp
Ln Viscosity vs 1/T

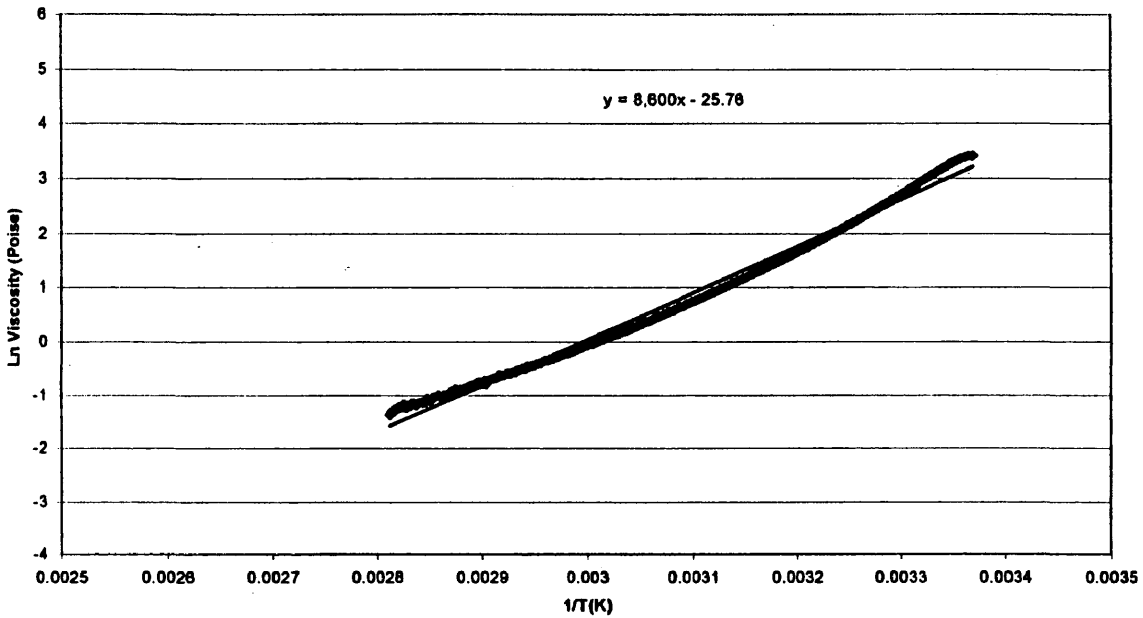


Figure [2.18]

4-bpa:dgeba 1:1 molar Ramp Down
Ln Viscosity vs. 1/T

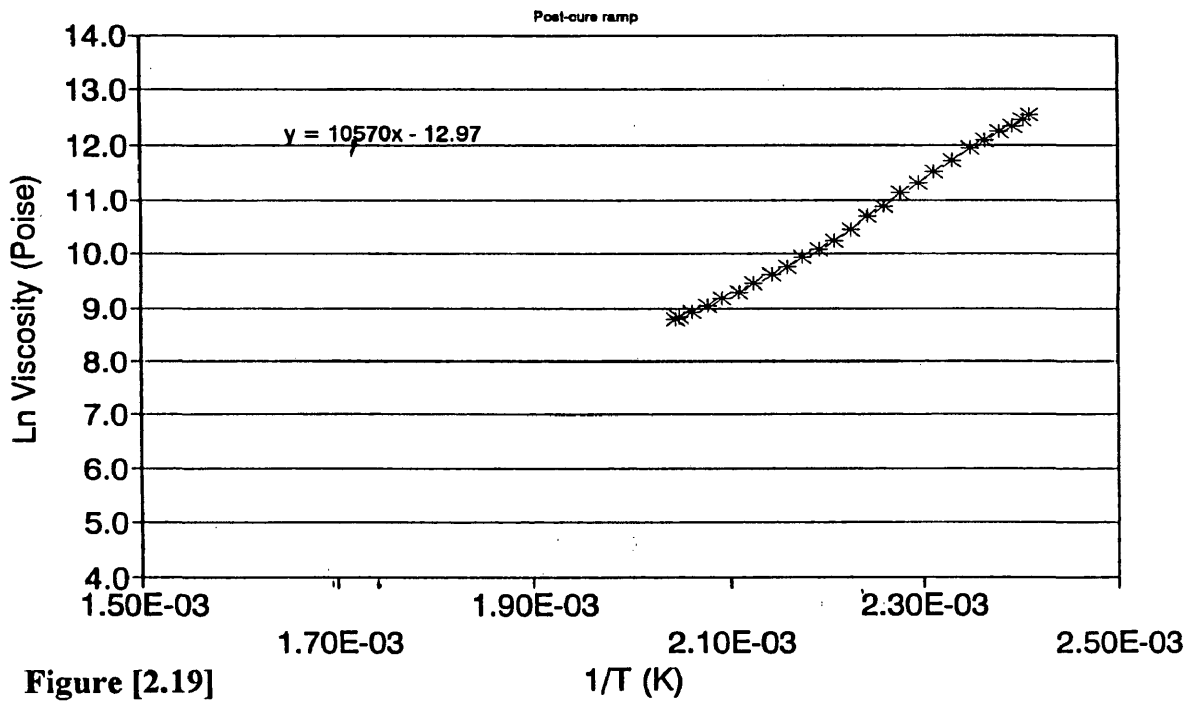


Figure [2.19]

2,6-dea:dgeba 1:1 molar Post-cure
Ln Viscosity vs 1/T

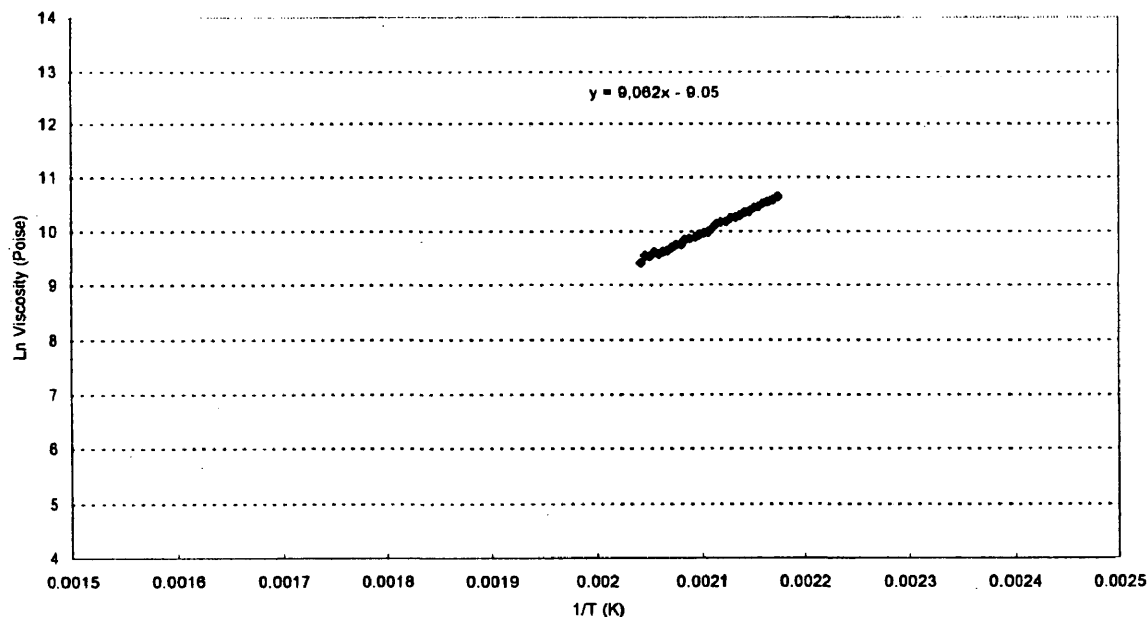


Figure [2.20]

mcdea:dgeba 0.5:1 molar Ramp
Post Cure Ramp Down

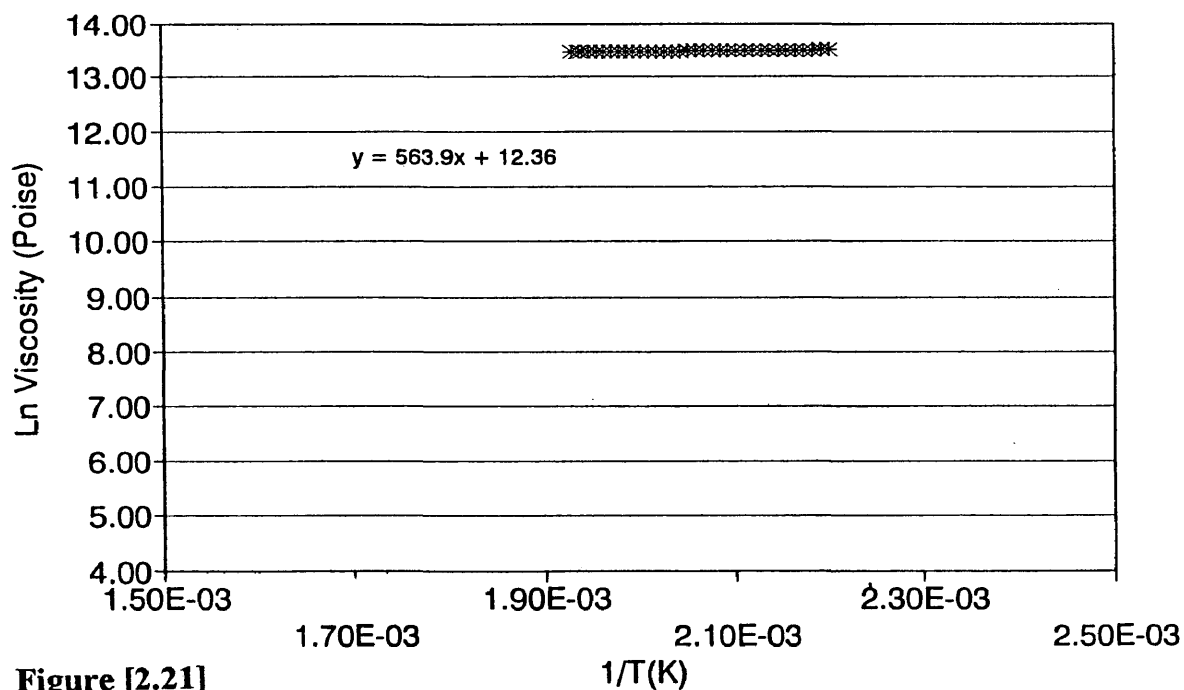


Figure [2.21]

Monoepoxy:4BPA 1:1 molar Post Cure

Ln Viscosity vs. 1/T

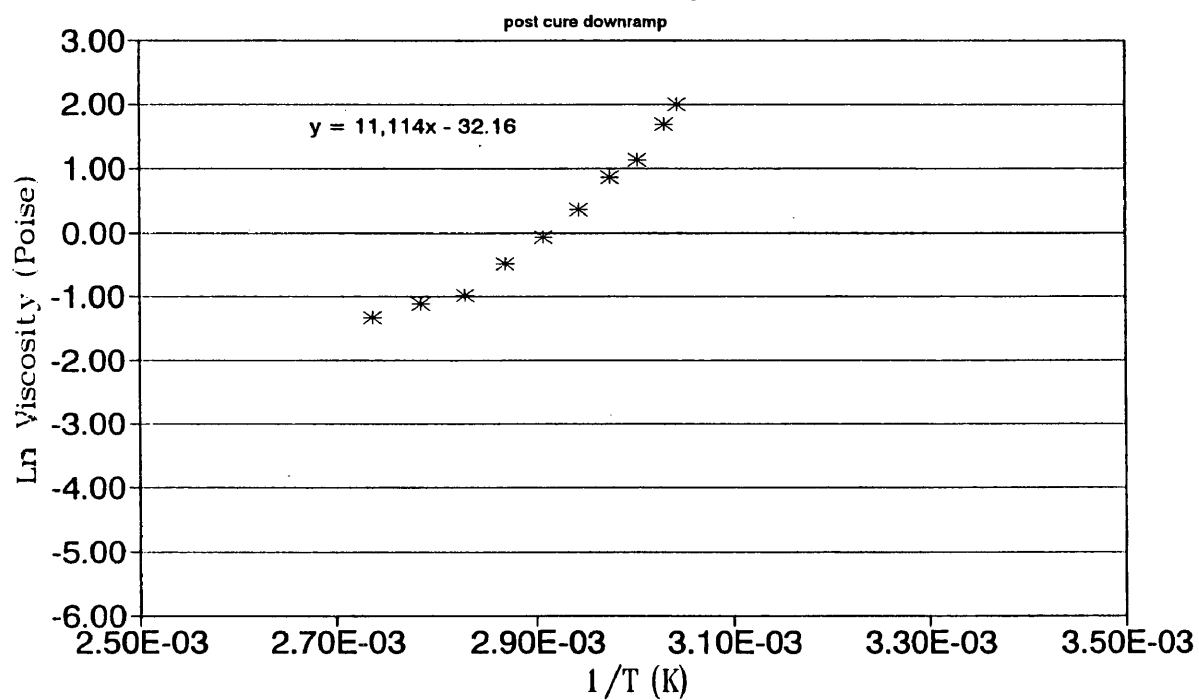


Figure [2.22]

**4-bpa:dgeba 135C Isotherm
Ln Cond vs Ln Visc**

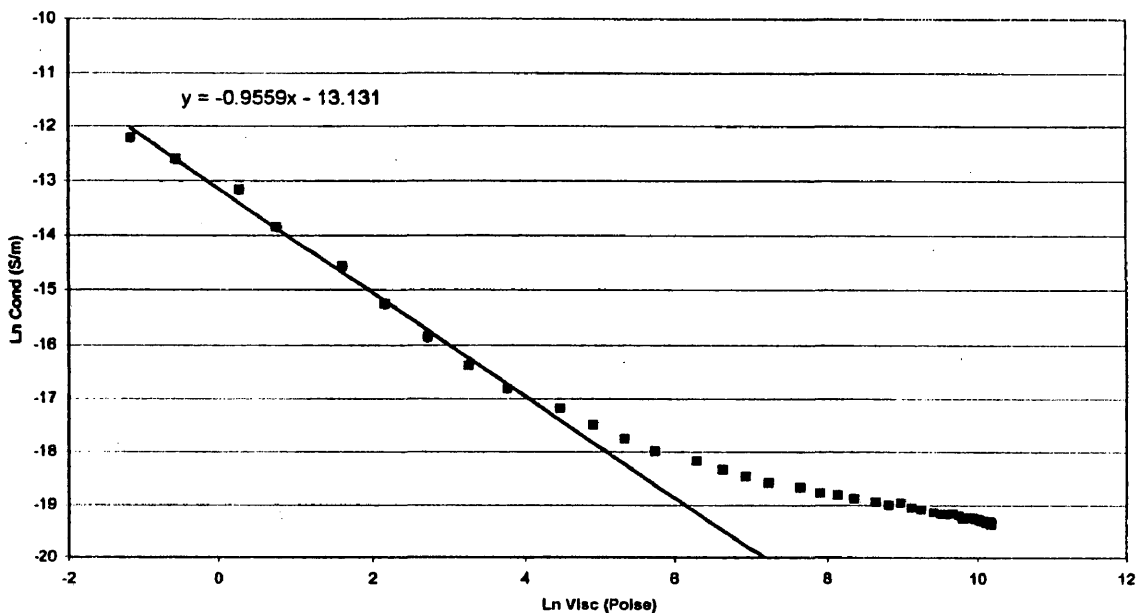


Figure [2.24]

**3-CI-2,6-DEA:dgeba 135C Isotherm
Ln Cond vs Ln Visc
After 600 min at 135C; ie last thirld of run**

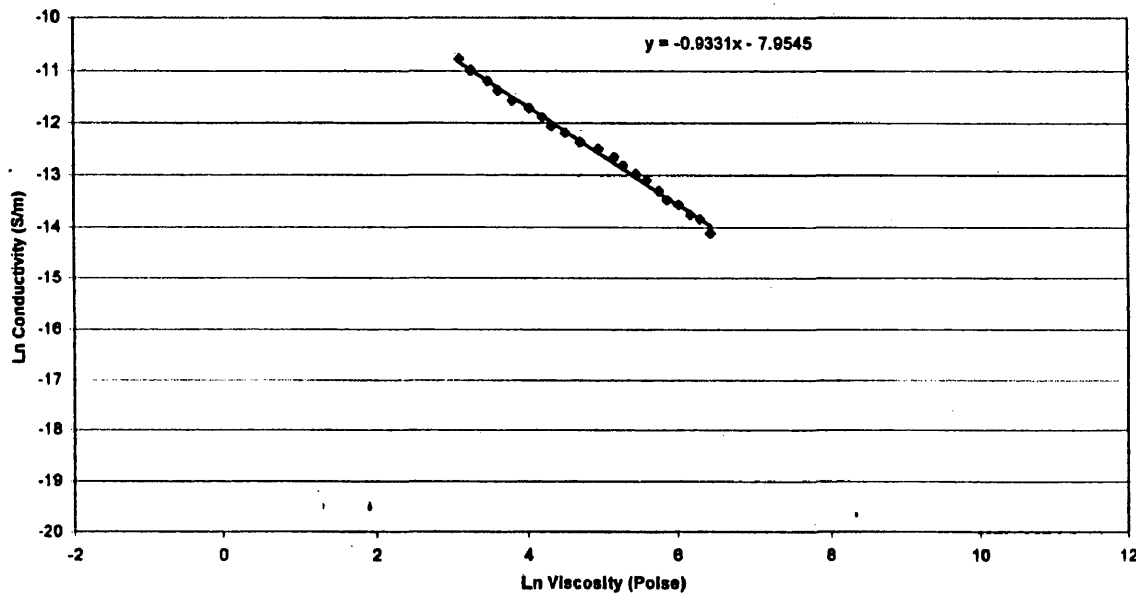


Figure [2.25]

DGEBA:2,6DEA 1:1 molar 135C Isotherm After 160 min isotherm at 135C

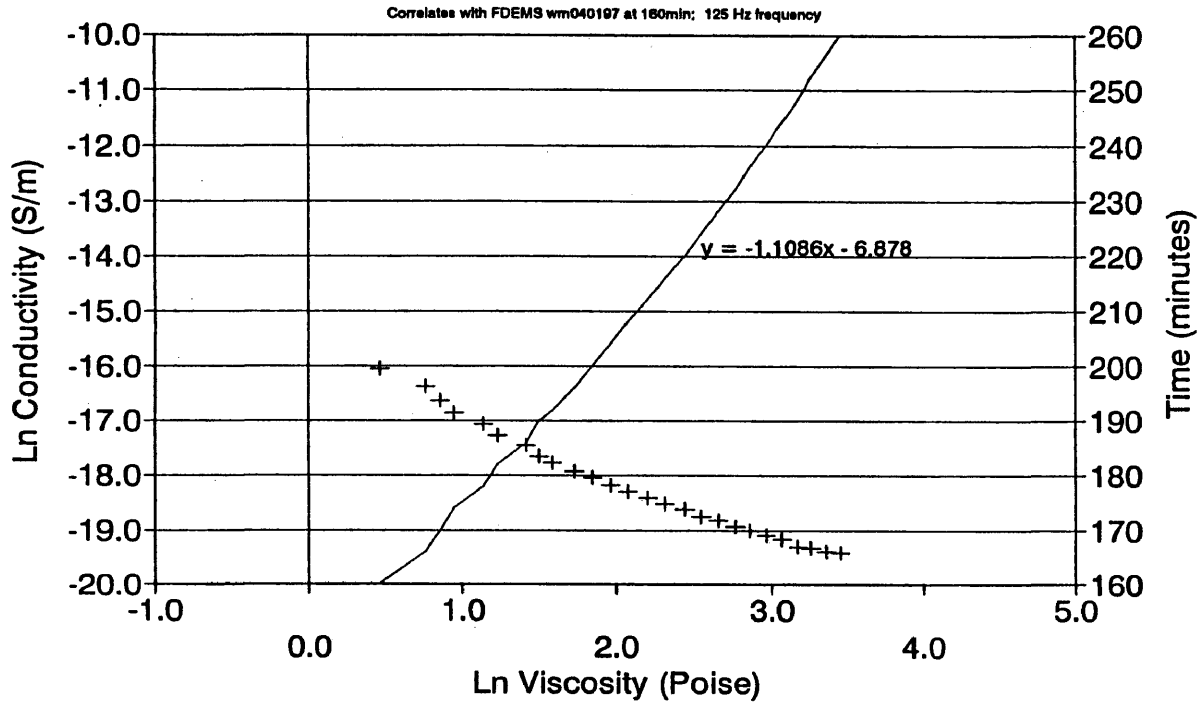


Figure [2.26]

using Aldrich and 2,6-DEA from France (AE)
da# 16; 26dea1_2.wq1; 4/4/97 Rev 7/97

mcdea:dgeba 135C Isotherm Ln Conductivity vs Ln Viscosity

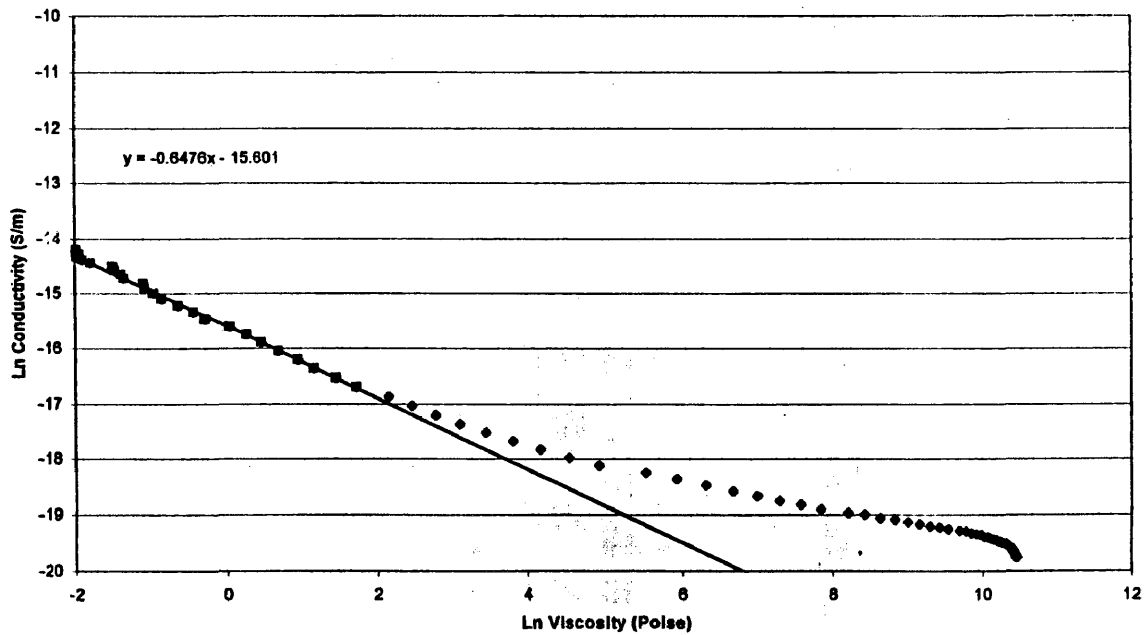


Figure [2.27]

Monoepoxy:4-bpa 135C Isotherm
Ln Conductivity vs Ln Viscosity
Correlated to 80 min on Visc plot (where visc began to increase)

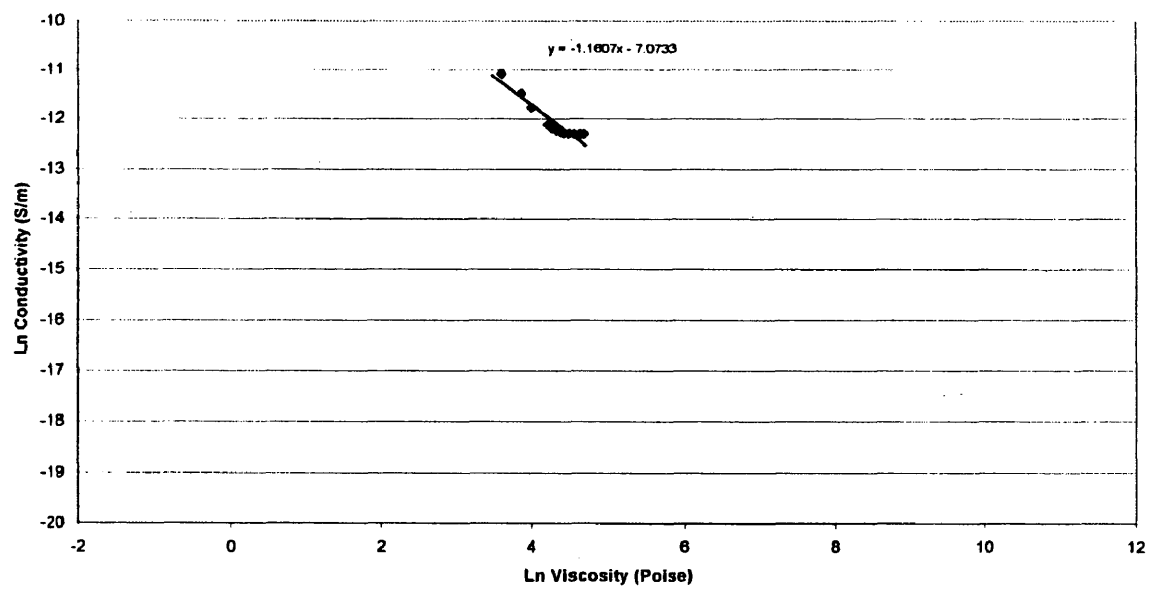


Figure [2.28]

DGEBA:4-bpa 1:1 molar 135C Isotherm

Theoretical Residual Heat = 203 J/g

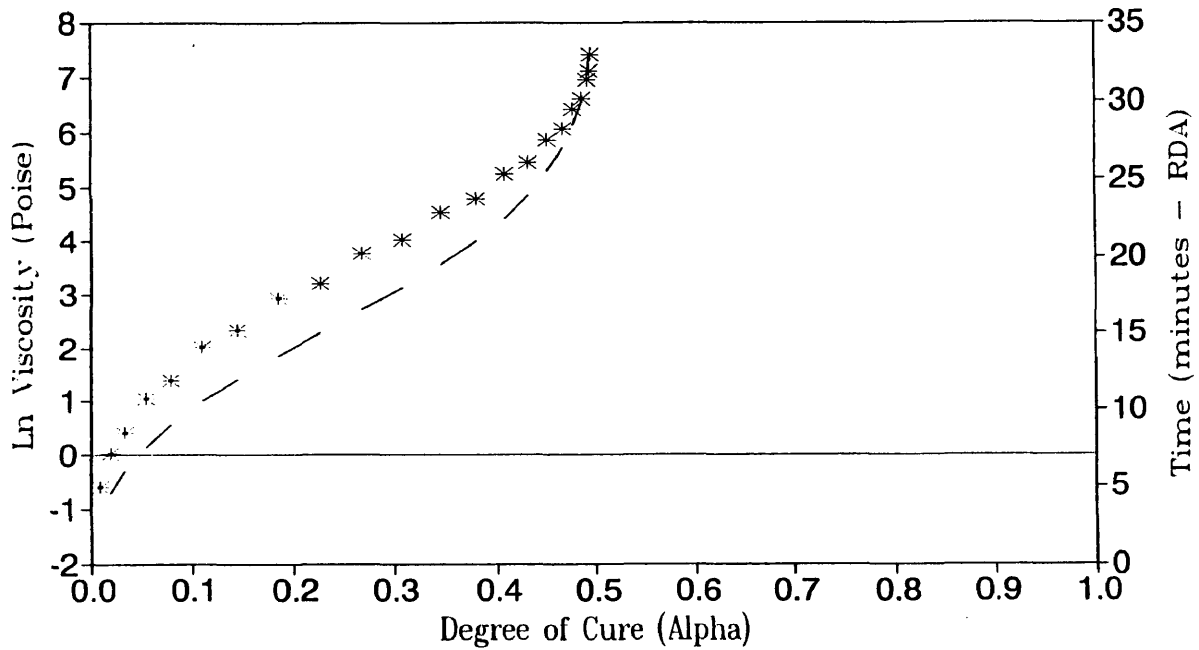


Figure [2.32]

DGEBA:4-bpa 1:1 molar 135C Isotherm

Theoretical Residual Heat = 203 J/g

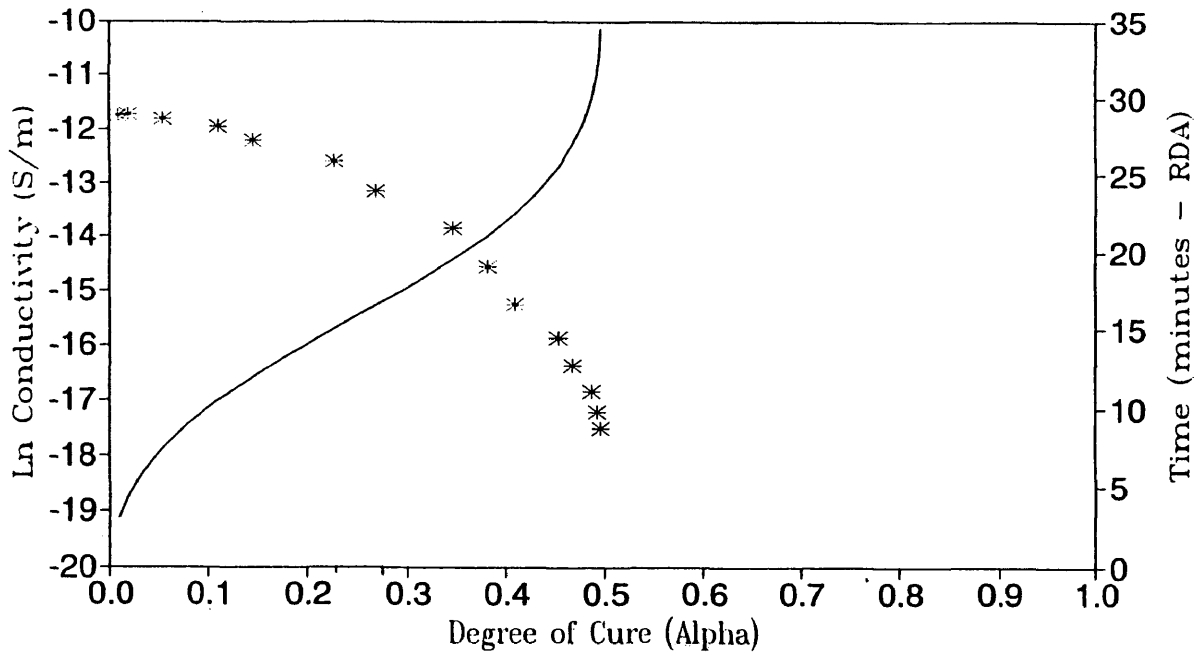


Figure [2.33]

DGEBA:3-CI-2,6-DEA 135C Isotherm

Ln Viscosity vs. Degree Conversion

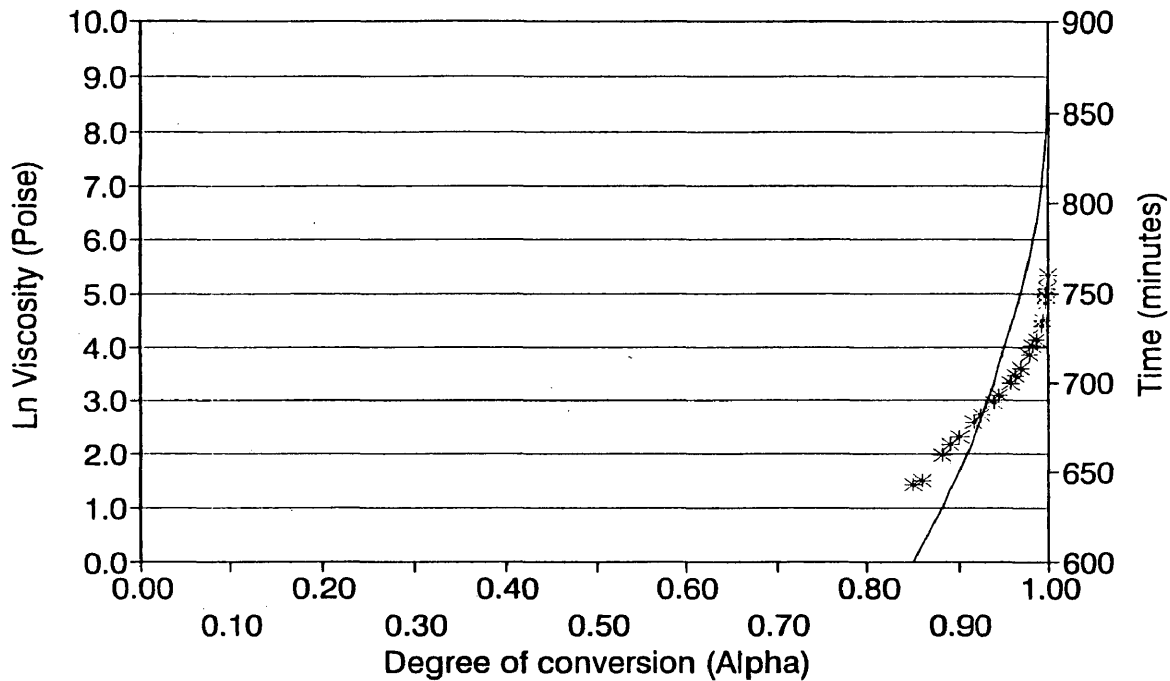


Figure [2.34]

DGEBA:3-CI-2,6-DEA 135C Isotherm

Ln Conductivity vs. Degree Conversion

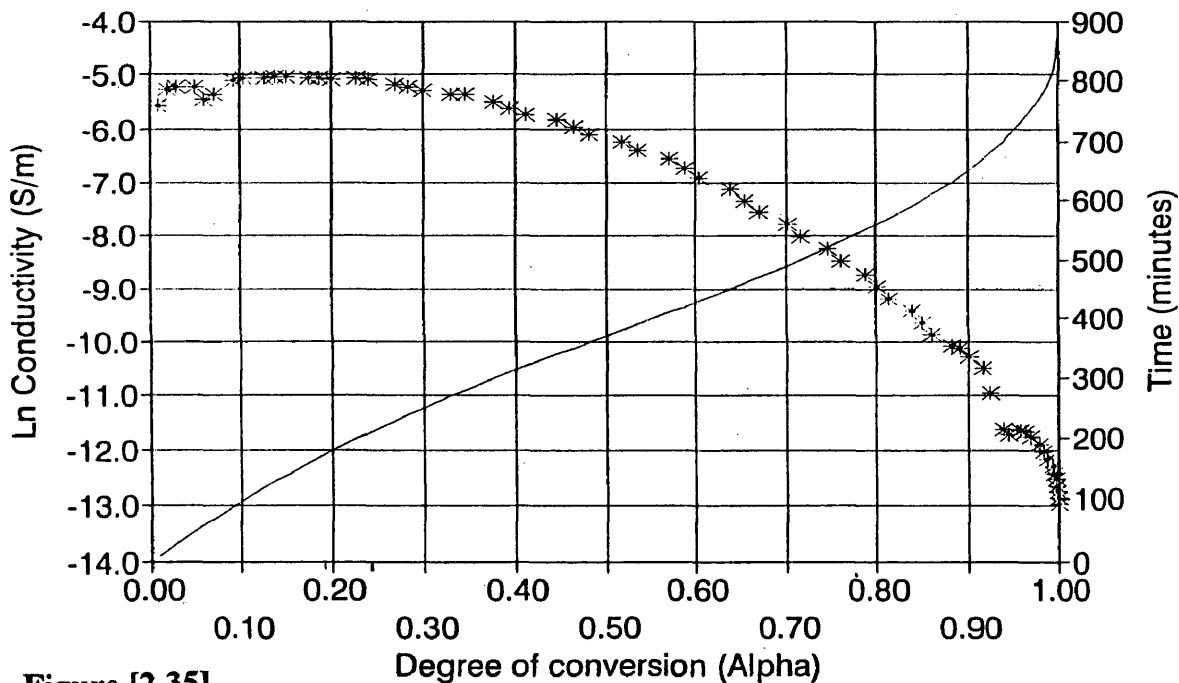
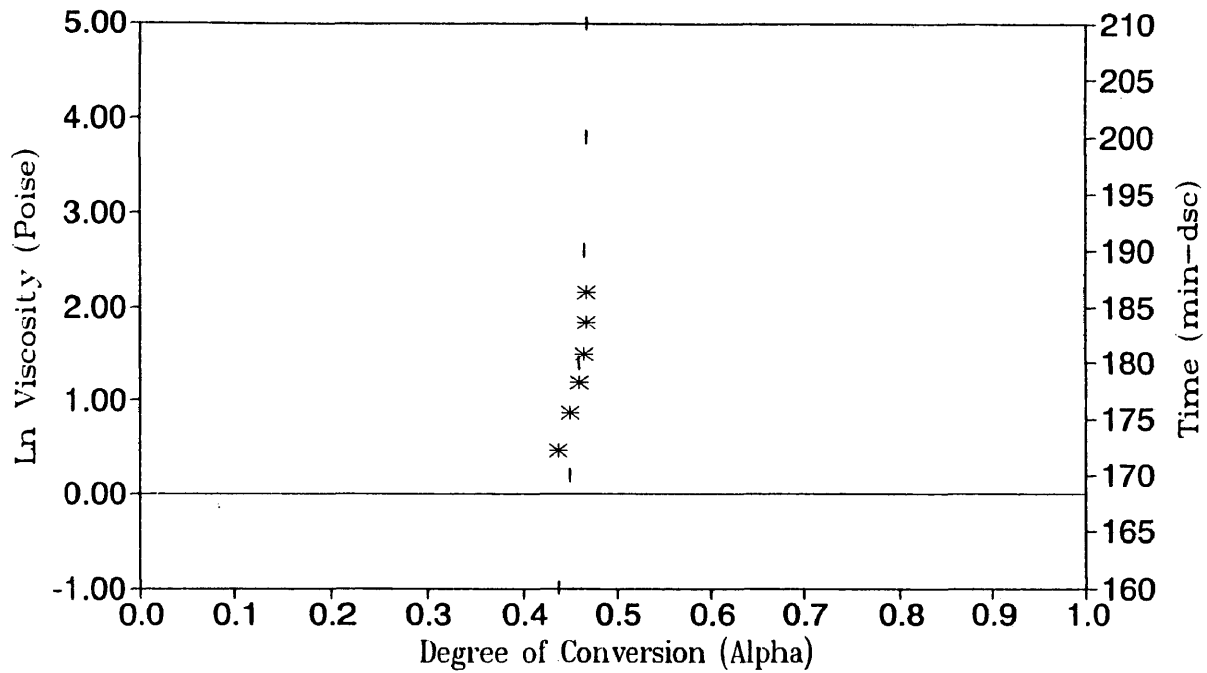


Figure [2.35]

DGEBA:2,6-DEA 1:1 molar 135C isotherm
Theoretical Residual Heat=228J/g



Viscosity tested after run under pressure for 160 min.

Figure [2.36]

DGEBA:2,6-DEA 1:1 molar 135C isotherm
Theoretical Residual Heat=228J/g

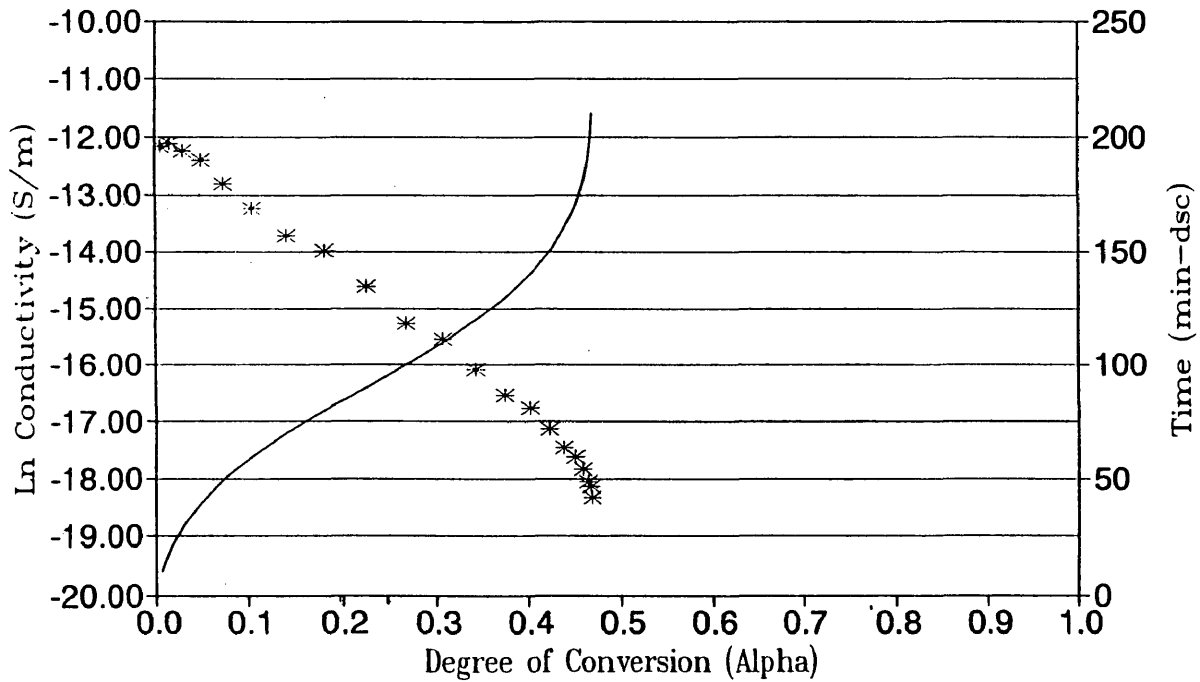


Figure [2.37]

offset by 70 minutes on FDEMS file(wm091996)

DGEBA:MCDEA 1:1 molar 135C Isotherm

Theoretical Residual Heat = 118J/g

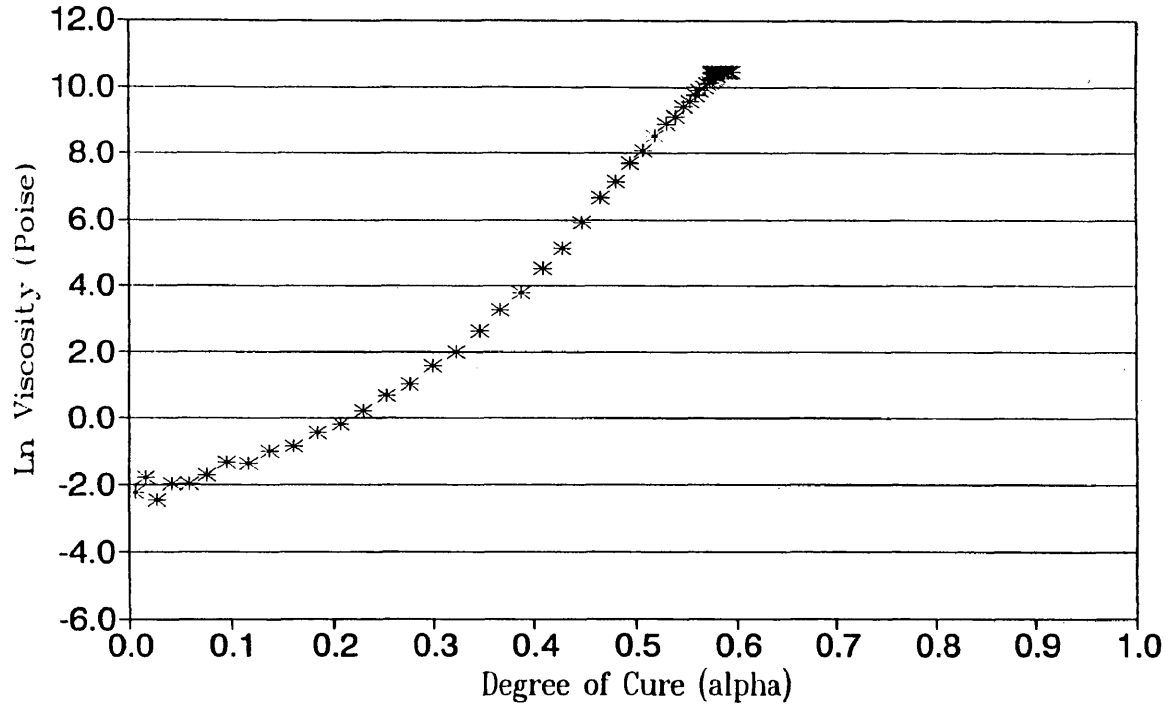


Figure [2.38]

DGEBA:MCDEA 1:1 molar 135C Isotherm

Theoretical Residual Heat = 118J/g

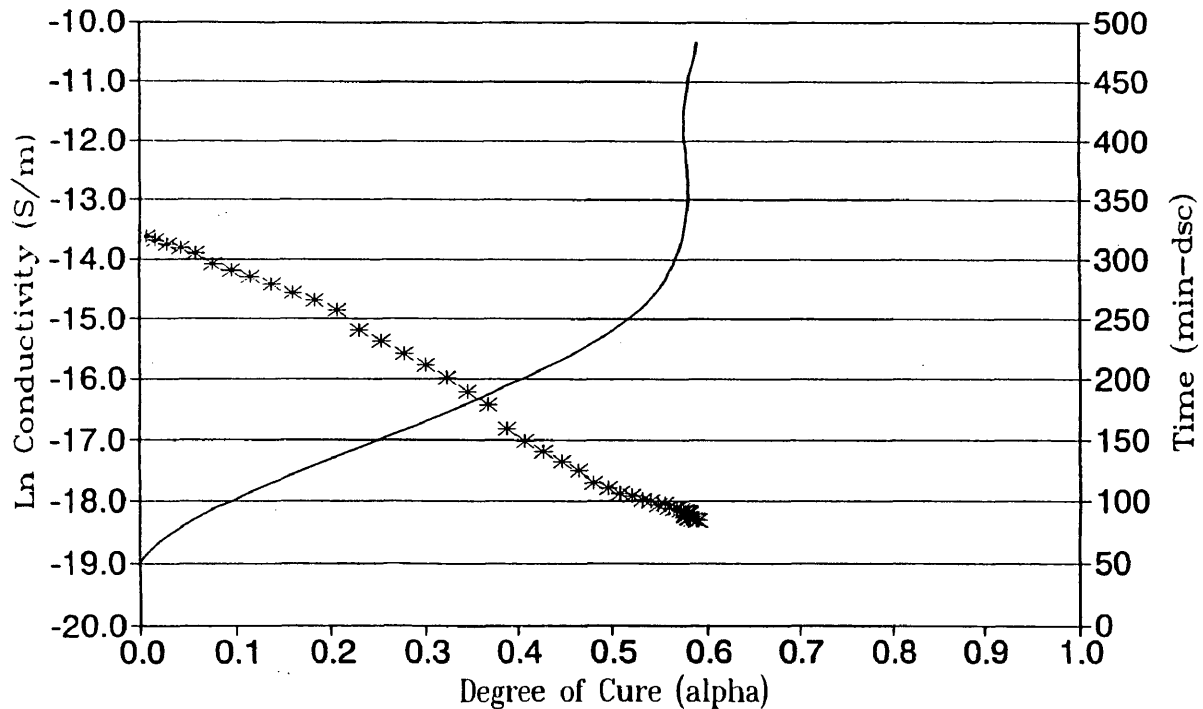


Figure [2.39]

Monoepoxy:4-bpa 1:1 molar 135 iso
Theoretical Residual Heat=165J/g
Correlated to 80 min on Visc plot (where visc began to increase)

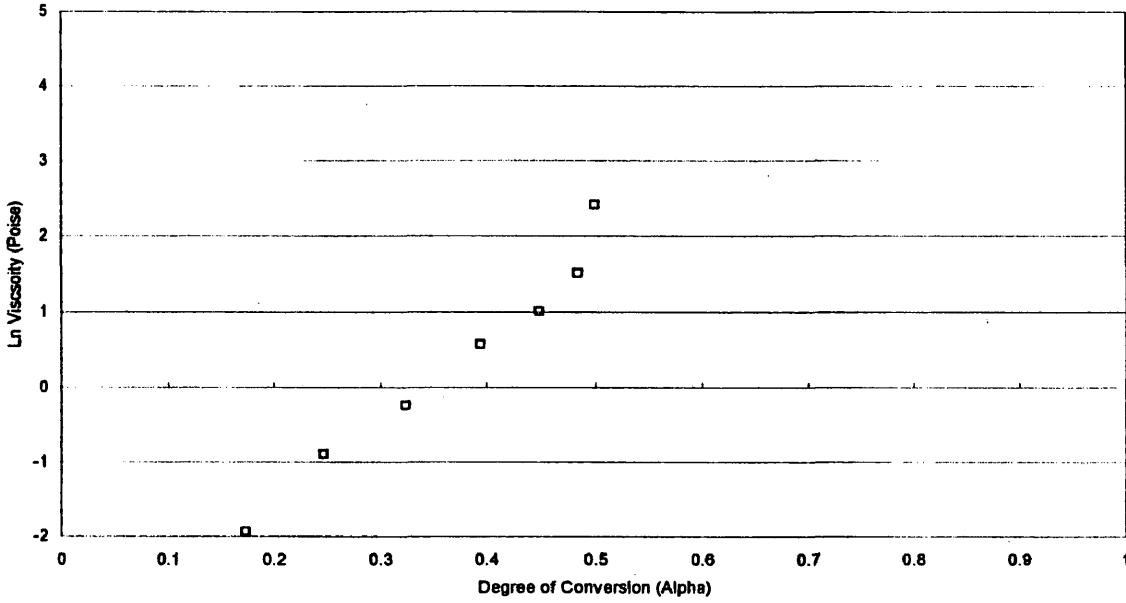


Figure [2.40]

Monoepoxy:4-bpa 1:1 molar 135 iso
Theoretical Residual Heat=165J/g

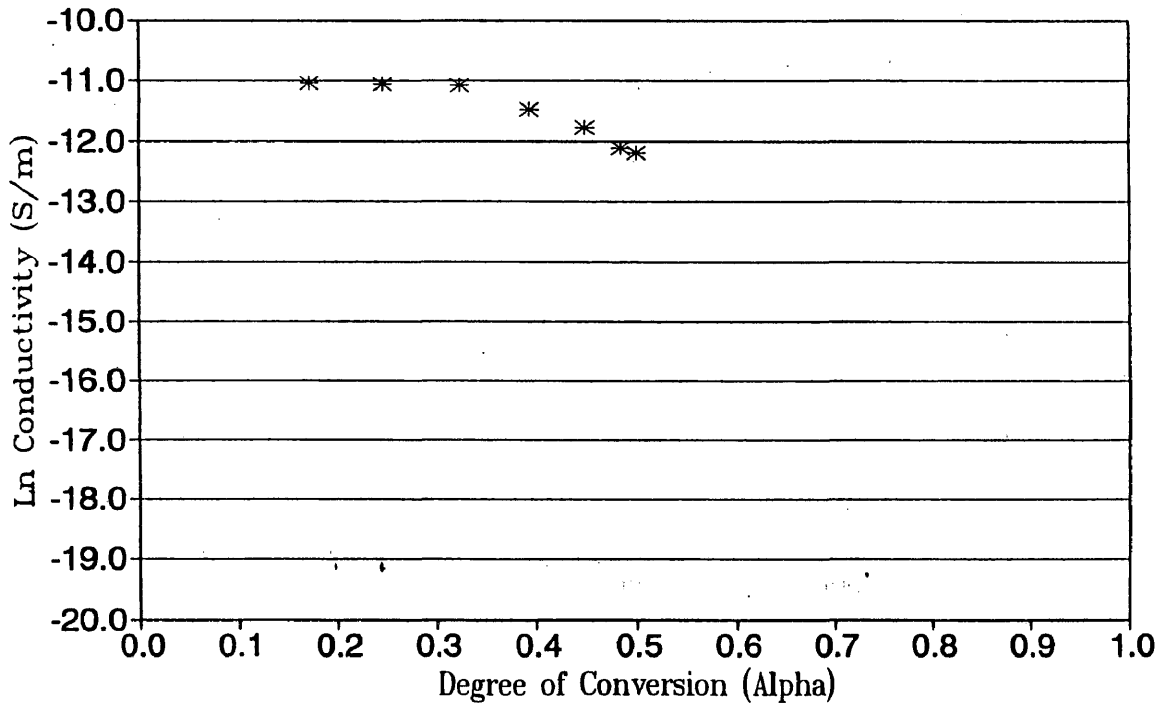


Figure [2.41]

Chapter III

Degradation of Nylon-11

A. Introduction

In 1935 Wallace H. Carothers of the DuPont Company pioneered step polymerization studies eventually leading to the discovery of nylon-6,6. Nylon-6,6 was the first high molecular weight polyamide plastic to be synthesized and is now commonly used in textiles and coatings. The reaction of nylon-6,6 was based on the condensation reaction of hexamethylenediamine and adipic acid. After this discovery the thermoplastic linear polymer chain market soared. Thermoplastics were found to be versatile and there was seemingly no end to possible applications. Polyamides offer characteristics such as high tensile strength, high impact strength, excellent fatigue resistance, and a good protection from a broad range of chemicals. Nylon-6 and nylon-6,6 account for approximately 90% of the total polyamide output in the world. Other polyamides, including nylon-4,6, nylon-6,10, nylon-9, nylon-11 and nylon-12, are tougher and are used for more rigorous environments.¹

The center of polyamide polymers is the amide group linkage itself. The polymers are composed of linear aliphatic, cycloaliphatic, or aromatic carbon chains connected by these amide linkages. An amide group is composed of a single carbonyl group bonded to a secondary amino group. The structure is represented in Figure [3.1].

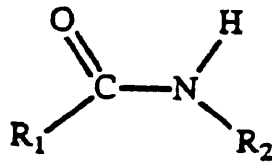


Figure [3.1] Amide Group

The amide group is planar due to the large resonance stabilization offered by the O=C–N bonding. This gives a relative stiffness to the bond, enhancing the ability of the polymer to align to form crystalline regions and intermolecular hydrogen bonds.

The focus of this study is on nylon-11, or poly(imino-1-oxoundecamethylene):



Nylon-11 is produced by a self-condensation polymerization reaction of ω -aminoundecanoic acid (obtained from castor oil). The reaction takes place at approximately 220°C under high pressure. During condensation reactions water is produced. The water is continuously removed during the polymerization to force the polymer to rapid completion. Very little isomerism occurs yielding a generally linear polymer.

Nylons are typically semi-crystalline polymers. This indicates the polymer has some crystalline regions and some amorphous regions that are more random in orientation. The zones of crystallites are present due to the strong polarity of the amide linkages. The regularity of the linear chains allows close

packing of the polymer giving microcrystalline regions. Figure [3.3] represents such microcrystallinity for nylon-6,6.²

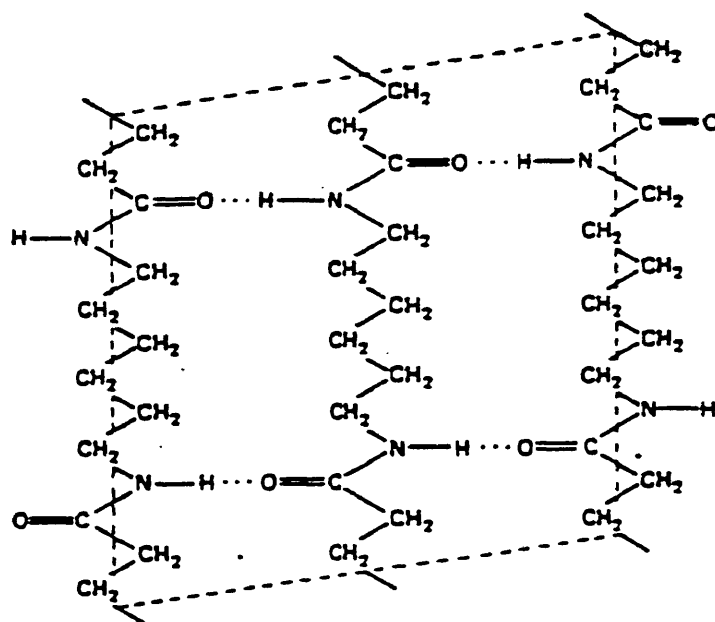


Figure [3.3] Microcrystalline region of Nylon-6,6

This crystalline structure contributes to the usefulness of nylon for a crude oil pipe liner. It is difficult for the hydrocarbon gas or fluid to traverse the crystalline maze. Therefore, the transmission rate of such hydrocarbons across the nylon barrier is exceptionally low.³ Nylon-11 is particularly well suited because it has fewer amide linkages, since there are eleven methylene groups between each, yet retains significant crystallinity.

B. Mechanism of Nylon-11 Degradation

This chapter discusses the degradation of nylon-11 in various aging environments. Degradation is interpreted as irreversible deterioration of the physical properties of the polymer during exposure to a specific environment.

Polyamides have strong resistance to hydrocarbons, glycols, and weak bases. They are susceptible to attack by acids and water molecules. The degradation process is essentially the reverse of the condensation polymerization process as shown in Figure [3.4]. Water is added across the amide bond resulting in chain scission. Chain scission markedly reduces the molecular weight of the polymer.

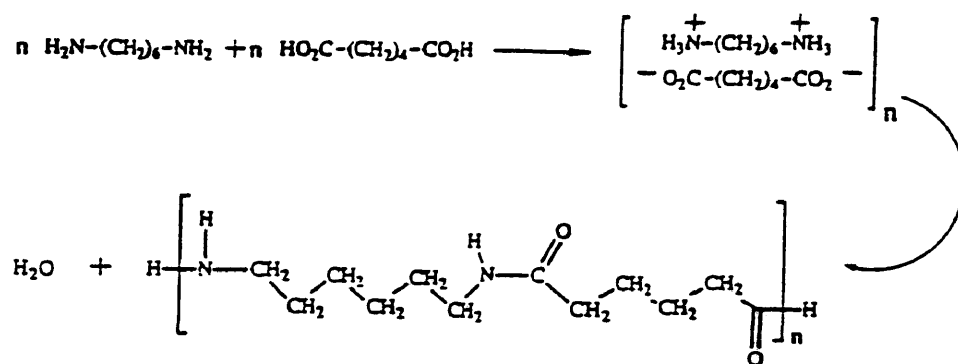


Figure [3.4] Condensation Polymerization of Nylon-6,6

This change in molecular weight is detectable using various methods such as light scattering, gel permeation chromatography and solution viscosity.

Acids and bases catalyze the hydrolysis of the polymer.^{4,5} Hydrolysis is the cleavage of covalent bonds by reaction with water. Acid-catalyzed hydrolysis involves a six step process (Figure [3.5]). Initially the carbonyl oxygen atom is protonated. Next water nucleophilically attacks the carbonyl carbon atom resulting in the formation of an oxonium ion. Third, deprotonation of the oxonium ion yields the neutral diol form of the intermediate. In the fourth step, protonation of the amino nitrogen results in an ammonium ion. Then the

ammonium ion dissociates to form an amine. Finally, the deprotonated acid yields the carboxylic acid.⁶

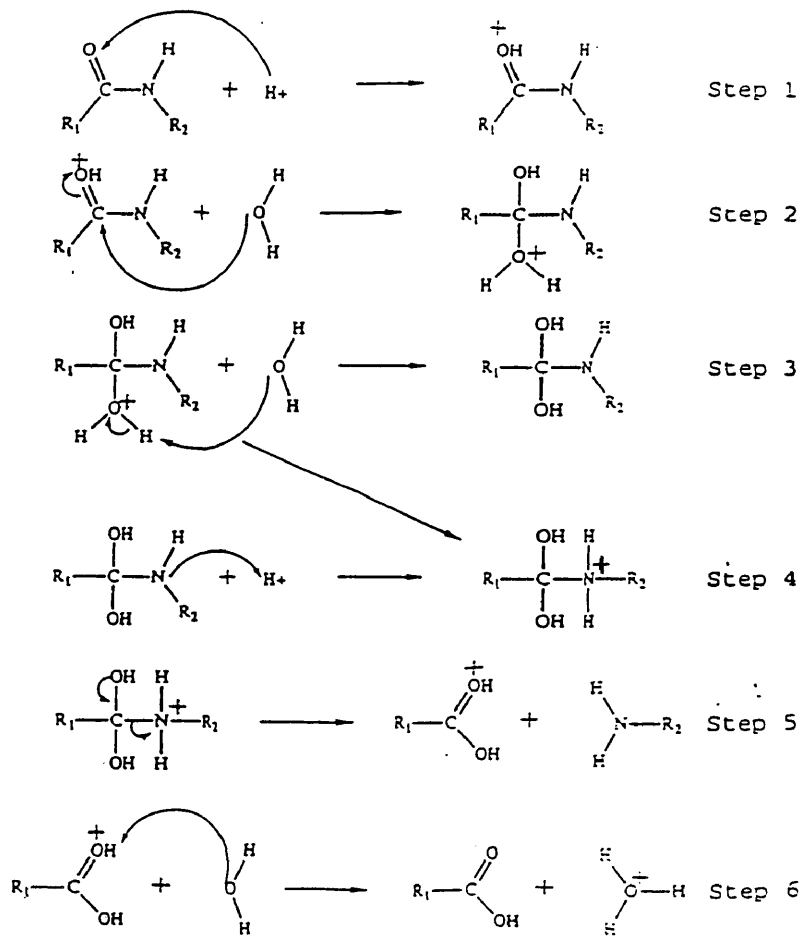


Figure [3.5] Mechanism for Acid-Catalyzed Hydrolysis of Polyamids

Nylon-11 is more useful in aqueous conditions than other types of nylon with more amide linkages, such as nylon-6 and nylon-6,6. This is due to less amide linkages, therefore a lower ratio of water-susceptible polar amide groups. The amorphous region of the semi-crystalline polymer is more vulnerable to hydrolysis. This hydrolysis, i.e. chain scission, results in an increase in the

overall crystallinity of the polymer. Higher crystallinity causes the material to become embrittled, losing flexibility and tensile strength. As the polymer becomes more crystalline, however, the rate of hydrolysis decreases as there is less amorphous area to attack. This explains why the initial stages of polymeric degradation tend to yield the greatest change in the physical properties such as molecular weight.

C. Aging Environments

Laboratory testing of nylon-11 consisted of several different aging environments. The environments can be divided up into several different categories. These environments separated by aging temperature are listed in Table [3.1]. There were two main types of oil used in these environments. ASTM oil refers to both ASTM oil #3 and IRM oil #903. Crude oil refers to unprocessed oil taken directly out of the Balmoral pipeline.

Initial studies focused on the temperature dependence of nylon degradation in the various environments. Of primary importance was the change in the rate of degradation based on the water content of the environment. We focused on 100% oil, 95% oil with 5% water and 5% oil with 95% water. After time it became apparent that the rate of degradation of nylon-11 may be pH dependent. Therefore the material was introduced to several different pH environments and tested for viscosity average molecular weight. Those environments listed with a pH from 4.5 to 6.0 are due to the environment being

Temp °C	Environment	pH	Sensors
130	5%ASTM/95%Water	4.5-6.0	
120	95%ASTM Oil/5% Water	4.5-6.0	
120	95%ASTM Oil/5%pH 6.0 Buffer	6.0	
120	100% Water	7.0	
105	100% Crude Oil	N/A	FDEMS
105	100% Dry Crude Oil	N/A	
105	99% Dry Crude Oil/1% Water	N/A	
105	99.99%ASTM Oil/0.01% Water	N/A	
105	99.9% ASTM Oil/0.1% Water	N/A	
105	99% ASTM Oil/1.0% Water	N/A	
105	97.5%ASTM Oil/2.5% Water	N/A	
105	95% Crude Oil/5% Water	4.5-6.0	
105	95%ASTM Oil/5% Water	4.5-6.0	FDEMS
105	95%ASTM Oil/5% pH6 Buffer	6.0	
105	5%ASTM Oil/95% Water	4.5-6.0	FDEMS
105	50% Methanol/50% Water	N/A	
105	100% Water	7.0	
105	100% pH 6.0 Buffer	6.0	
105	100% Water with CO2	4.5-6.0	
90	95%ASTM Oil/5% Water	4.5-6.0	FDEMS
90	95%ASTM Oil/5%pH 6.0 Buffer	6.0	
90	5%ASTM Oil/95% Water	4.5-6.0	FDEMS
90	100% pH 6.0 Buffer	6.0	FDEMS
90	100% Water	7.0	
70	95%ASTM Oil/5% Water	4.5-6.0	FDEMS
70	95%ASTM Oil/5% pH 6.0 Buffer	6.0	
70	5%ASTM Oil/95% Water	4.5-6.0	FDEMS
70	100% Water	7.0	

Table [3.1]

Various Accelerated Aging Environments

charged with carbon dioxide gas causing the pH to drop to approximately 4.5, slowly rising as the gas escaped the system.

Some of the environments were inside a pressurizable aging bath as illustrated below in Figure [3.6]. Three different types of environment were used in these studies: 100% Crude Oil, 95% ASTM oil with 5% water and 5% ASTM oil with 95% water. We imbedded the FDEMS dielectric sensors in nylon-11 to view the microscopic changes in the material. We also aged separate mechanical samples for study of macroscopic properties of the material after aging. We aged small flattened strips of nylon-11 to use solely for molecular weight analysis. Samples were removed from the aging environments at various exposure times for testing and examination.



Figure [3.6] Accelerated Aging Bath

The type of environment in Figure [3.6] was used to submerge both dielectric sensors and mechanical pieces to view their properties over time. These properties included FDEMS sensing, solution viscosity measurements, DSC

measurements, and tensile measurements. Sealed test tube environments were used to strictly study the changes in molecular weight of small samples. In Table [3.1] those environments with dielectric sensors are labeled FDEMS in the right hand column.

The environments which were strictly ASTM oil and water were slightly acidic. The acidity of the environments was determined by American Society for Testing and Materials (ASTM) method D974-92. Acid numbers near two were observed for the 95% ASTM Oil/H₂O and 5%ASTM Oil/H₂O baths. For the 100% Crude Oil bath the acid number was near one. Subsequent testing of the aqueous layer revealed a pH of approximately 5.5.

There has been testing done in an operational oil field flexible pipe. The samples are referred to as “field aged” and their results resemble those of the simulated aging environments.

FDEMS sensors were embedded in nylon-11. Several different methods were employed over the years of this study. The most frequently used method was to embed two or three sensors between two ¼ inch (”) slabs of nylon-11. The polymer with sensors in between was placed on a heated hydraulic press. The nylon-11 was brought just to the melting point and the two plates melded together with the sensors securely inside. Leads to the FDEMS sensors were coated with Teflon for greater resistance to the environmental conditions. The ¼” thick sensor panels were bolted between two stainless steel (SS) plates, 3” x 3” by 1/8” to minimize flexing of the polymer. Holes or slits had been previously drilled through the SS plate covering the active side of the sensor to enable the diffusion

process to occur. This promoted diffusion in and out of the polymer from primarily one side. An illustration of the apparatus just prior to bolting the SS plates together is presented in Figure [3.7].⁷

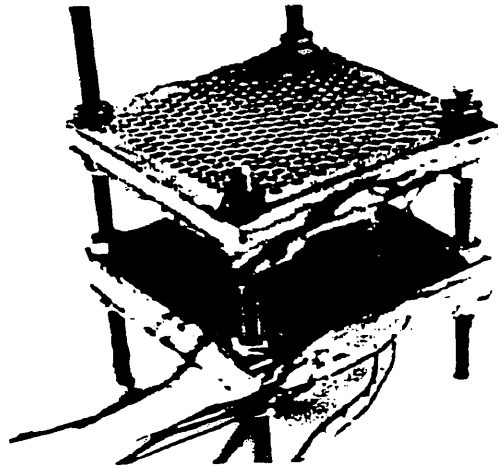


Figure [3.7] FDEMS Aging Sensor Apparatus

Once constructed the sensors were submerged into their fluid aging environments. The leads from the sensors were inserted through the lid of the aging bath. This allowed the bath to remain sealed while FDEMS sensing measurements were taken.

Mechanical samples were placed in the aging environments to be taken out periodically for tensile testing. These pieces were placed between two 6.5" x 6.5" x 1/8" SS plates. Again holes were previously drilled into one of the plates to allow diffusion into the polymer. An illustration of this apparatus is in Figure [3.8].⁸

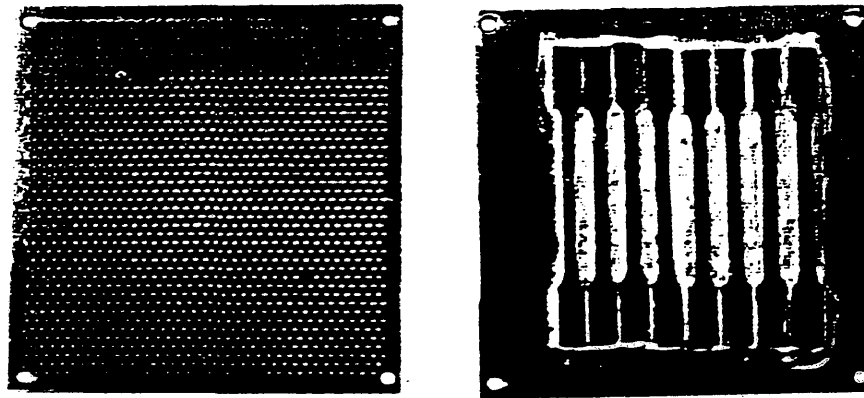


Figure [3.8] Tensile Test Sample Mounting Apparatus

D. Results and Discussion

The most indicative test of the degradation of nylon-11 was to determine the viscosity average molecular weight of the sample. Figures [3.9] – [3.12] indicate the molecular weight of the samples in their respective temperature environments. The natural log of the molecular weight was also plotted against the day in figures [3.13] – [3.16]. The natural log of the viscosity average molecular weight for each environment shows a decrease over time. There is an obvious temperature correlation: as the temperature increases, the rate of the degradation process is also increased. Degradation is directly correlated to the decrease in molecular weight. Nylon-11 aged at higher temperatures degrades faster than those samples aged at a lower temperature.

Plotting the natural log of the molecular weight versus time results in a slope equal to the rate constant k if first order kinetic decay is assumed. This rate constant for each temperature is listed below in Table [3.2].

Temperature in °C	Rate Constant in Days ⁻¹
70	-0.00194
90	-0.00501
105	-0.00940
120	-0.02050

Table [3.2]

The energy of activation, E_a , can be calculated from the rate constant values using the following equation:

$$\ln k = -E_a/RT + \ln A \quad [3.17]$$

where R is the gas constant, 8.314 J/K, T is the temperature in Kelvin, and A is the Arrhenius constant. The value of E_a calculated from the plot of $\ln k$ versus $1/T$ from Figure [3.18] is 59.8 kJ/mol, and A is $\ln 14.5 \text{ days}^{-1}$. This E_a is reasonable when compared to the value of 84 kJ/mol for small molecule amide systems of caprolactam in sulfuric acid.⁹

Hydrolysis of the polymer is the fundamental cause of its degradation. For this reason we studied the concentration of water necessary for a higher rate of degradation. It has been determined through earlier studies that the rate of degradation between the 95% water and 5% water with ASTM oil was virtually the same. Therefore, a threshold concentration of water must be necessary to increase the rate of degradation in comparison to the 100% oil environments. The natural log of the molecular weight versus time at 105°C is shown in Figure [3.19]. It can be seen that the rate of degradation only begins to slow slightly for the environments with 0.01% and 0.1% water with ASTM oil. The 1.0% water environment is slower, but very close to the rate of the higher water concentration

environments. Therefore, it is preliminarily hypothesized that there need be only a concentration of approximately 1.0% water to significantly increase the rate of nylon-11 degradation.

Similar plots were done in attempt to determine any pH dependence at 105°C and 120°C. To date little information is available for the rate of nylon-11 degradation in various acidic solutions at temperatures below 120°C.¹⁰ Some information is available on the molar mass and weight changes, but no molecular weight data is available. From the studies on molar mass and weight changes it was determined that two stages of aging occur. First water is physically absorbed into the polymer until equilibrium is established. Second, polymer hydrolysis begins. The rate of polymer hydrolysis increases with temperature and solution acidity. This rate decreases with thickness of the sample, however, indicating degradation is diffusion controlled. In the thicker samples, embrittlement and cracking only occur on the surface of the polymer. In this study we observe changes in the molecular weight of nylon-11 samples which are approximately ¼ inch thick. The natural log of the molecular weight at varied pH versus time can be found in Figures [3.20] – [3.21]. These environments consist of 100% buffered solution at the temperature indicated. Table [3.3] shows the ratio of slopes of ln molecular weight versus time at a particular pH. The fact that the ratio of these numbers is very close indicates that the kinetics are very similar for the two temperatures. If the energies of activation are consistent, Equation [3.24] should hold true. The B value is the activation energy taken from the slope of the

PH	105 Slope	120 Slope	Ratio of 105 to 120 slopes
2.0	-0.027	-0.066	0.409
3.0	-0.061	-0.116	0.525
4.0	-0.031	-0.059	0.525
4.6	-0.034	-0.083	0.405
7.0	-0.009	-0.020	0.477

Table [3.3] Ratios of Slope of Molecular Weight vs. Day Plots

natural log of the molecular weights versus temperature above. From this equation, using experimental data from the 120°C pH environments, a rate can be back calculated for the 105°C pH environments. Figure [3.22] indicates each of the experimental values in comparison to values extrapolated from 120°C to 105°C in this manner. The values are very close, indicating this relationship appears to hold true. Figure [3.23] is a similar plot excluding data at pH of 2.0. The rate of degradation at pH 2.0 does not follow the previously observed trend, and the reason behind this is presently unknown.

$$\frac{k(120)}{k(105)} = e^{-B\left(\frac{1}{T(120)} - \frac{1}{T(105)}\right)}$$

Equation [3.24]

Study of the dielectric changes of nylon-11 at 105°C has been ongoing in this laboratory for several years. An example of the data for ϵ' and $\epsilon''*\omega$ in the 95%ASTM Oil with 5% water pot is shown in Figures [3.25] and [3.26] respectively. Data from the newer FDEMS measurements at 90°C and 70°C are in Figures [3.27] – [3.34] for temperatures of 90°C and 70°C. There is an initial increase in the ϵ' and $\epsilon''*\omega$ values in the first few days of the study. This is due to the absorption of water and small molecules by the nylon-11. There is an

eventual leveling off of the sensor readings before any degradation can be detected. As the temperature of the aging environment decreases the time it takes for the small molecules to infiltrate the polymer increases. Each of the temperatures shows an eventual decrease in ionic mobility (see $\epsilon''^*\omega$ plots) due to a decrease in molecular weight of the polymer and a corresponding increase in the crystallinity. This is a result of the hydrolytic degradation mentioned previously. As chain scission occurs and the molecular weight decreases, there are more small molecules to line up in an orderly fashion, thereby increasing the crystallinity.

Sensors in the 105°C environments show a gradual decrease in ionic mobility as the polymer degrades. The 70°C and 90°C environments do not have as rapid a decrease in ionic mobility. They show a more gradual decrease. Correlation plots of the data for the sensor output of dielectric data to the aging polymer's molecular weight were created. First the dielectric data had to be normalized. This was done by dividing the ϵ' or $\epsilon''^*\omega$ data by the value at the time of equilibration with the environment. This is considered to be an early day with a high ionic mobility. The time it takes for the polymer to become saturated with the small ions in its environment is temperature dependent. At the higher temperatures equilibration occurs quickly while at the lower temperatures it takes more time. Plots of the normalized data for each temperature and environment were correlated with the molecular weight for the corresponding days. This yields a plot of the molecular weight versus the normalized values of ϵ' or $\epsilon''^*\omega$. Plots of normalized $\epsilon''^*\omega$ versus molecular weight are exhibited in Figures [3.35] for 105°C (from earlier studies) and [3.36] – [3.38] for 90°C. It will be shown

that this technique allows direct correlation of the microscopic and macroscopic properties of the aging polymer.

The DSC was used to determine the percent crystallinity and the melting temperature of the polymer. The results of these data for environments at 105°C are found in Figures [3.39] – [3.40]. It is expected that the crystallinity will increase as degradation progresses. Initially the crystallinity increases significantly for each of the environments. This may be due to annealing of the polymer. Annealing, which is alignment of the molecules into a higher crystalline structure, occurs due to the aging temperature lying between nylon’s glass transition temperature and melting temperature. Table [3.4] lists characteristics of both nylon-11 and PVDF that will be discussed later.

	T_g	T_m	ΔH_{melt}	M_v^\diamond
Nylon-11	57°C	194°C	226 J/g	49,000 g/mol
PVDF	-61°C	210°C	6,700 J/mol	520,000 g/mol

Table [3.4] Characteristics of Amorphous and Crystalline Regions of Nylon-11 and PVDF¹¹

Mechanical tensile testing has been done on nylon-11 samples as well. The initial studies were done in three different environments at 105°C: 100% Crude Oil, 95% ASTM Oil with 5% water, and 5%ASTM Oil with 95% water. These tests were performed on tensile testing apparatus at NASA-Langley in

[♦] These are approximate viscosity average molecular weight values obtained through these studies.

Hampton, Virginia, during an earlier study¹². The data from the tensile tests was correlated with the normalized ϵ' and ϵ''/ω data as well. This allowed another look at the mechanical versus microscopic properties. Correlation plots are exhibited in Figures [3.41] – [3.44].

More recently samples were aged in 95% Crude Oil with 5% pH 4.63 buffer. Testing of these samples was performed at the College of William & Mary. The results of these more recent tests conducted during this study are in Figure [3.45] with percent elongation on the primary y-axis and the force per unit area (Pa) on the secondary y-axis.

The most significant difference between this aging environment and that from the previous part of the study was the introduction of the 5% pH 4.63 buffer, lowering the pH. It is difficult to believe this change in environment caused the drastic change in the polymer degradation rate shown herein. The cause was more likely attributable to a smaller sample size. The approximate sample gage area used in the previous study was 63.5mm x 6.17mm x 5.82mm, while samples used in this study were 12.7mm x 4.76mm x 3.18mm. This smaller size gage area caused the mechanical samples to age much faster than expected. The infiltration of water into the polymer, hence hydrolytic degradation, is a diffusion controlled process as mentioned previously. A smaller sample would therefore be exposed to a higher ratio of water molecules sooner, causing faster degradation. This suggests a geometry effect on the aging of the polymer. New samples with varied dimensions have been introduced into the same environment to be tested at a later date.

E. Conclusions

Several conclusions can be drawn regarding the degradation of nylon-11. It has been shown that the rate of polymeric degradation is dependent on temperature, concentration of water and pH. As temperature increases the rate of polymeric degradation increases. As the concentration of water increases, the rate of degradation also increases. From the temperature data an Arrhenius relationship was established giving activation energy. The rate of degradation is size dependent and initially diffusion controlled.

FDEMS testing was correlated to macroscopic properties such as the viscosity average molecular weight and tensile strength testing. From correlation plots of FDEMS molecular mobility to mechanical properties one can determine by *in situ* testing of a material what the physical properties of the material are at that instant. This will allow intelligent monitoring of the material in use and accurate service life prediction of the polymer.

References for Chapter III

- ¹ Hall, Christopher. Polymer Materials. 2nd ed. New York: John Wiley & Sons, 1989. p.216.
- ² Allcock, H.R. and Lampe, F.W. Contemporary Polymer Chemistry. Englewood Cliffs, New Jersey: Prentice Hall, 1990.
- ³ Gruenwald, G. Plastics. New York: Hanser Publishers, 1993. p.131.
- ⁴ Anton, A. *Journal of Analytical Chemistry*, 1968, Vol 40, p.1116.
- ⁵ Mori, S., Furusawa, M., and Takeuchi, T. *Journal of Analytical Chemistry*, 1970, Vol. 42, p.138.
- ⁶ Carey, F.A. Organic Chemistry. New York: McGraw-Hill Company, 1987.
- ⁷ Hood, D.K. "Monitoring and Modeling of Infiltration, Polymerization and Degradation Phenomena in Polymeric Systems," Ph.D. Dissertation, College of William & Mary, 1996, p.214.
- ⁸ Hood, p.218.
- ⁹ Kohan, M.I. Nylon Plastics Handbook. New York: Hanser/Gardner Publishers, Inc., 1995, p.49.
- ¹⁰ Chaupart, G.S. and Verdu, J. "Ageing of polyamide 11 in acidic solutions." *Polymer*, 1997, Vol. 38, No. 8, p.1011.
- ¹¹ Mark, H.F., *et al.* Encyclopedia of Polymer Science; 2nd Ed.; Wiley & Sons, Inc.: New York, 1985, Vol.16, p.773.
- ¹² Hood, p.100.

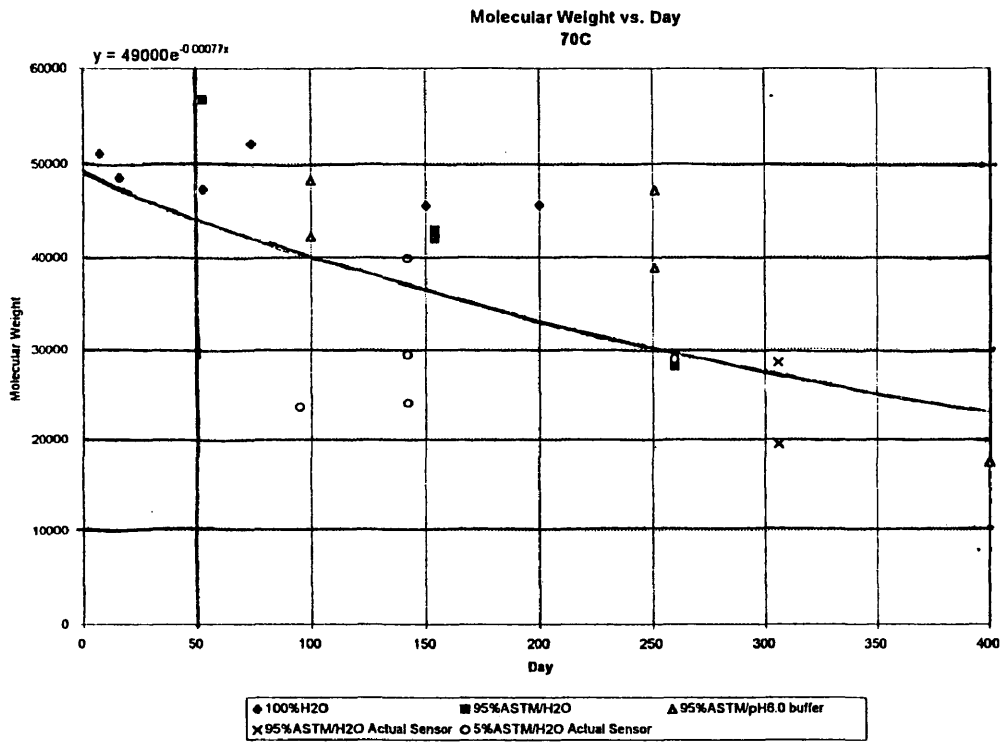


Figure [3.9]

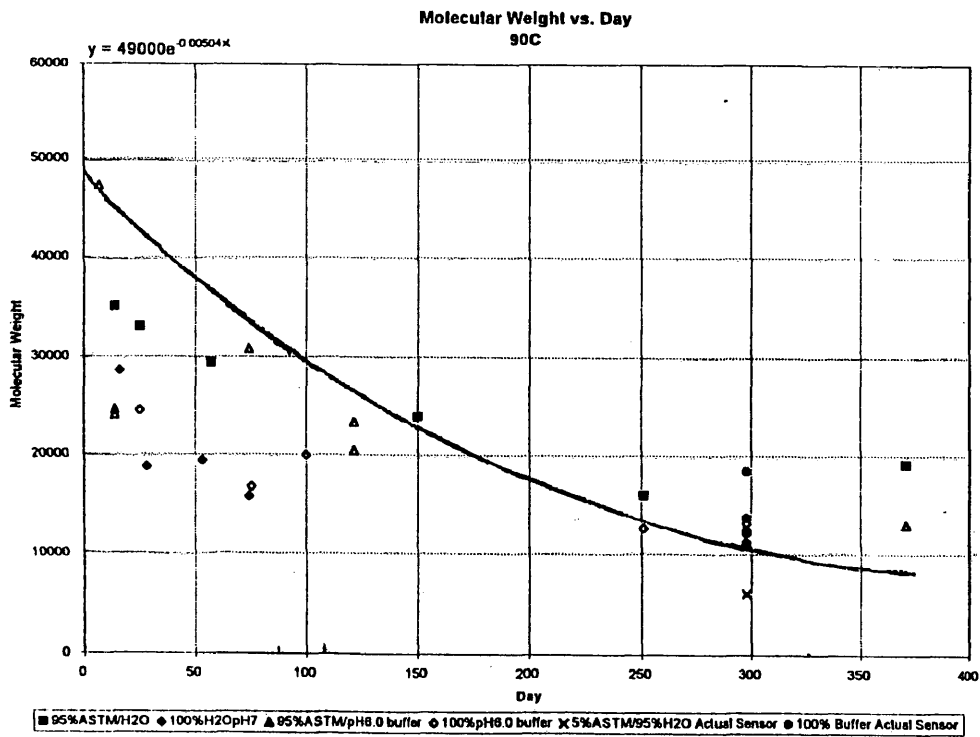


Figure [3.10]

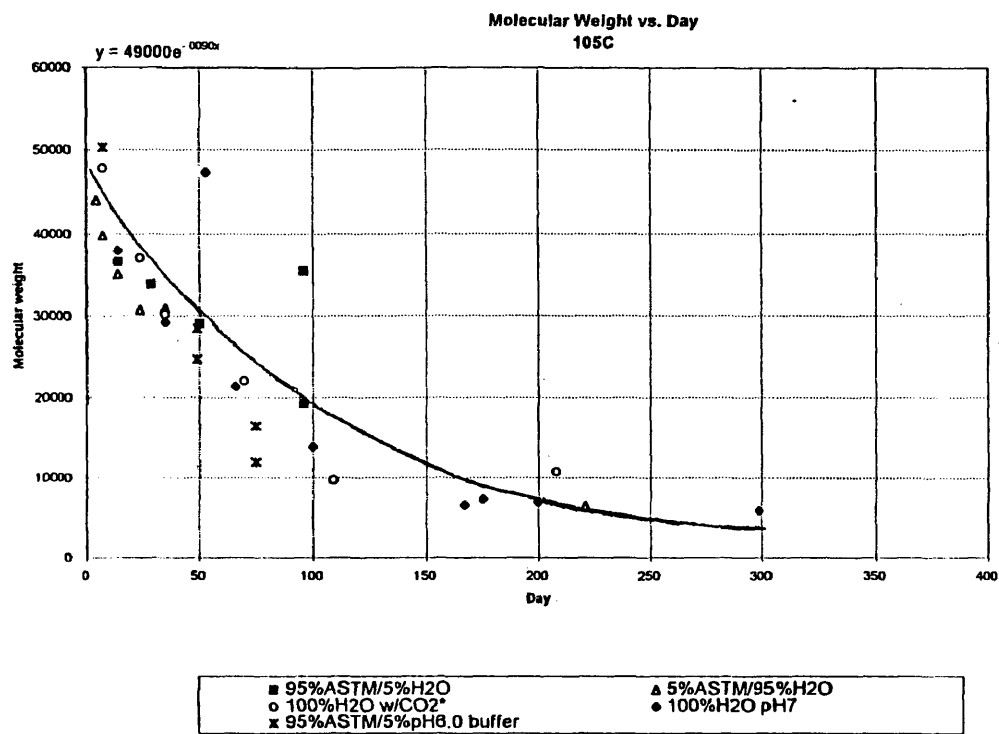


Figure [3.11]

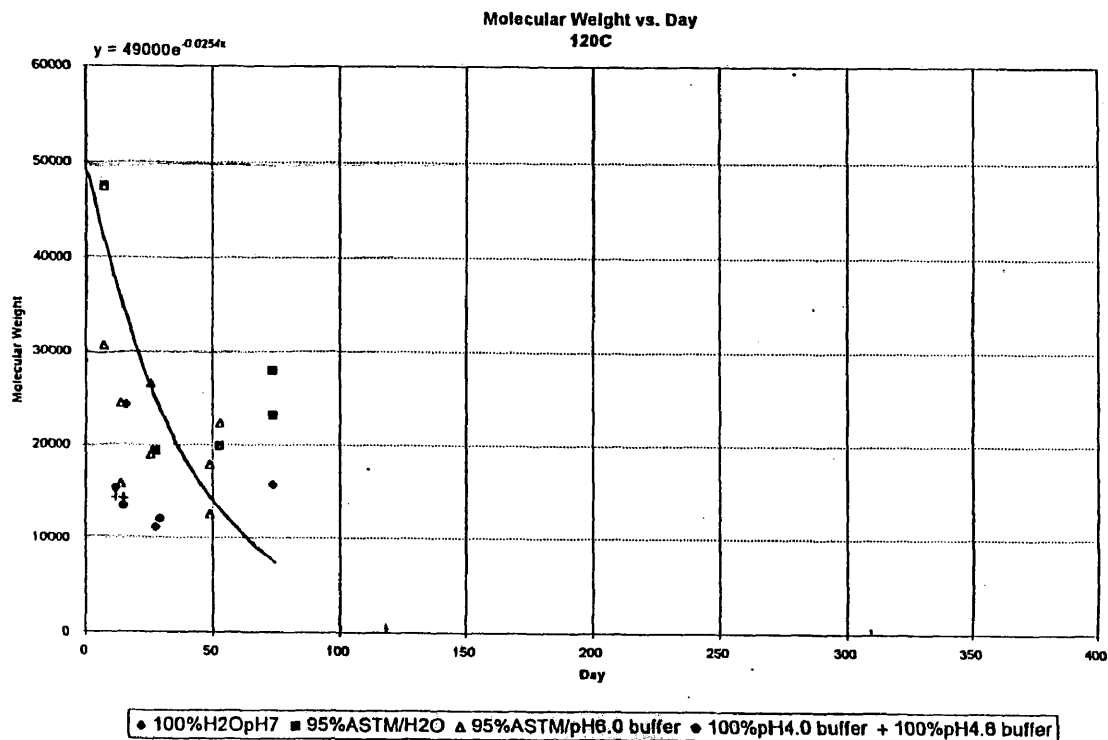


Figure [3.12]

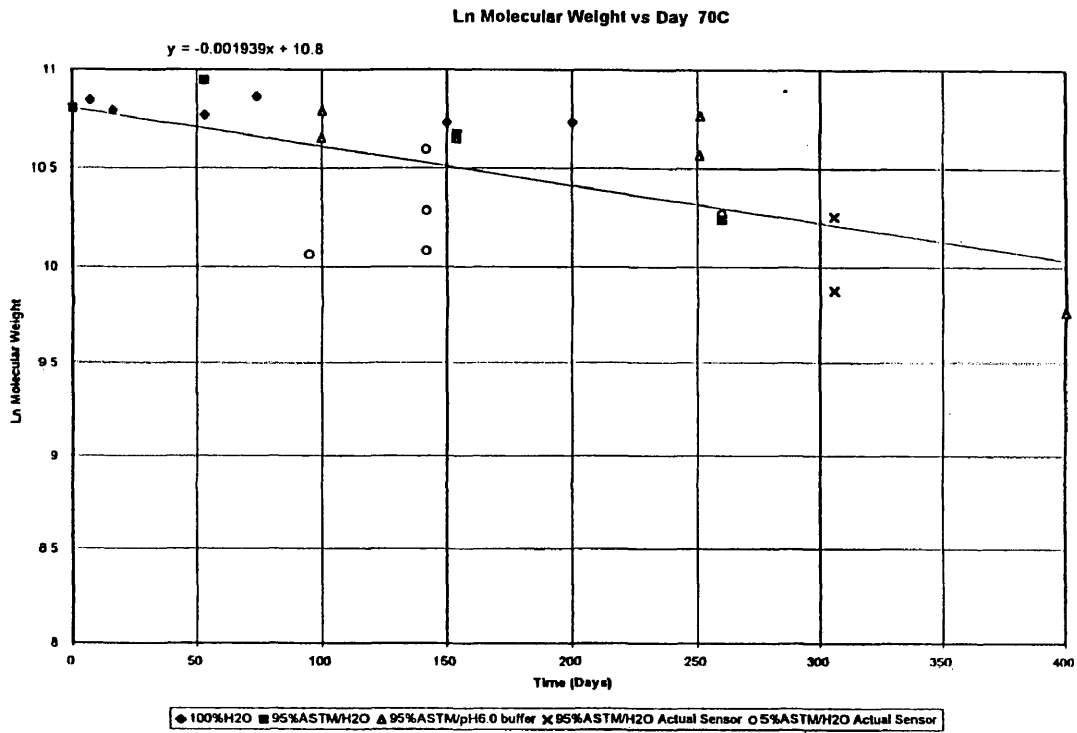


Figure [3.13]

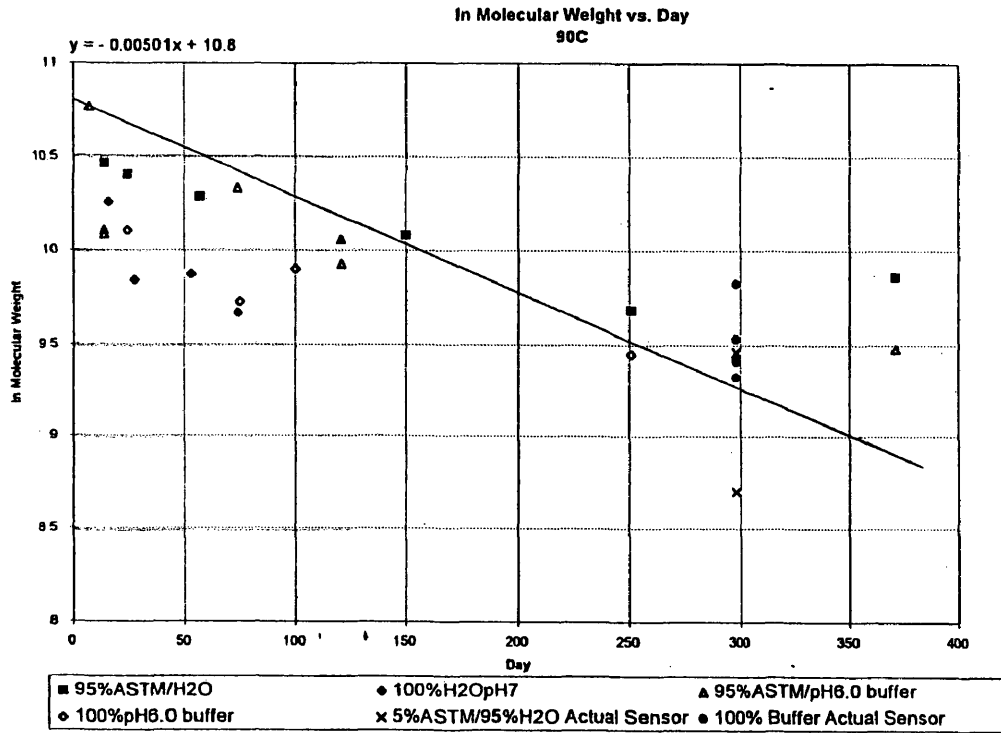


Figure [3.14]

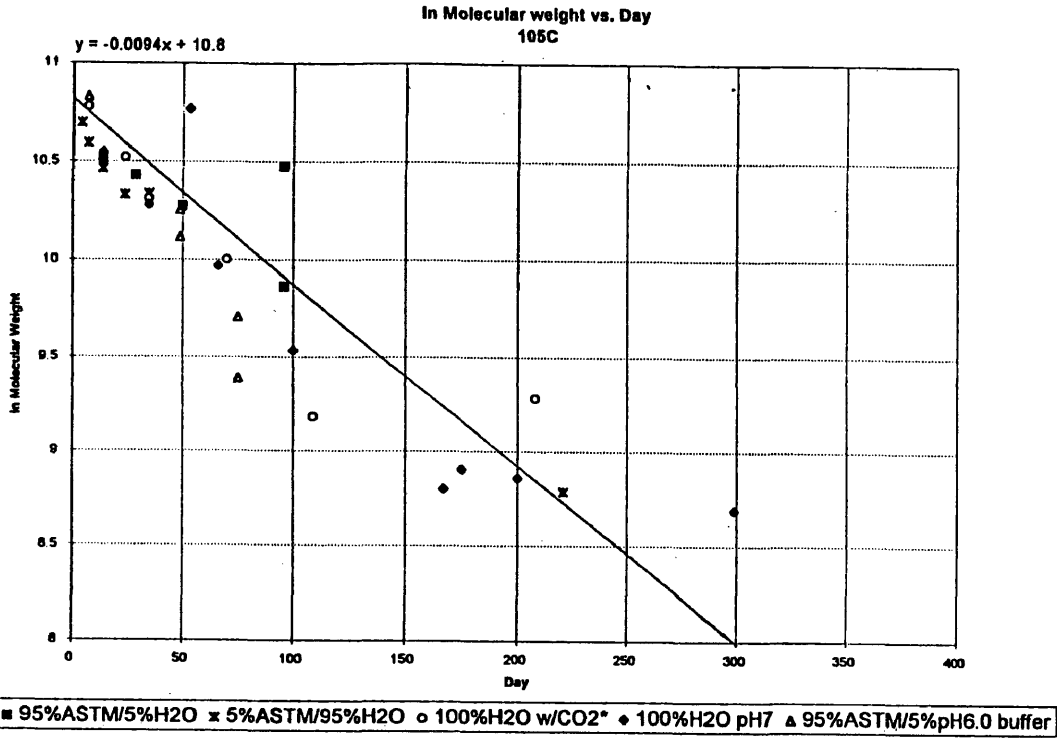


Figure [3.15]

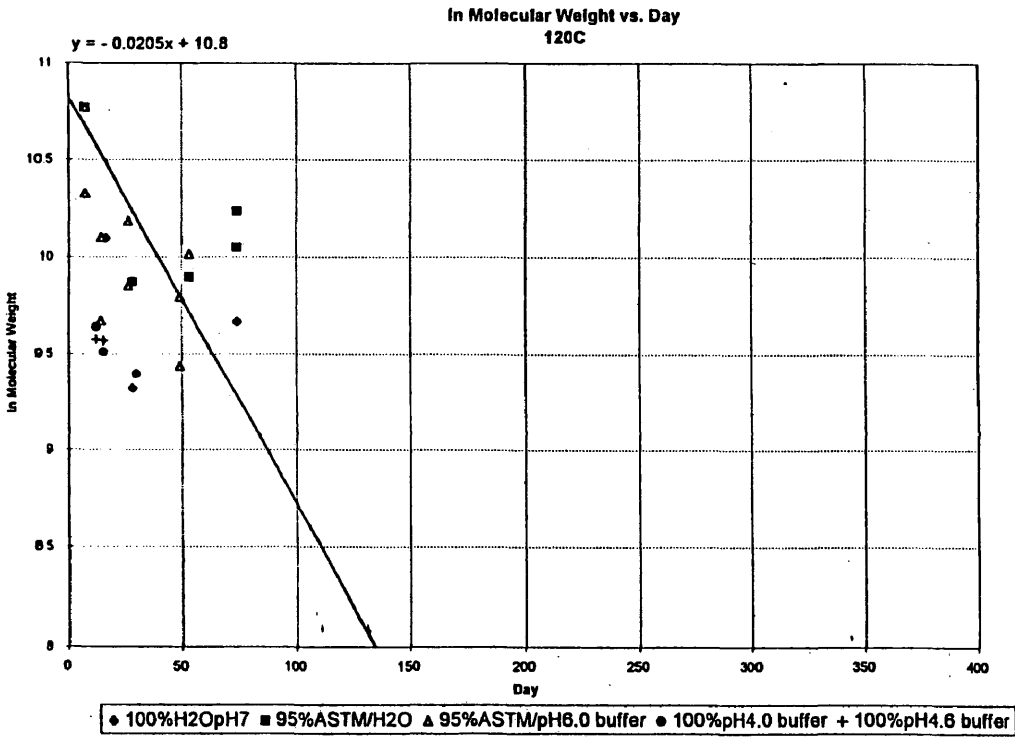


Figure [3.16]

Ln Molecular Weight vs Day 105C 100% Buffer Environments

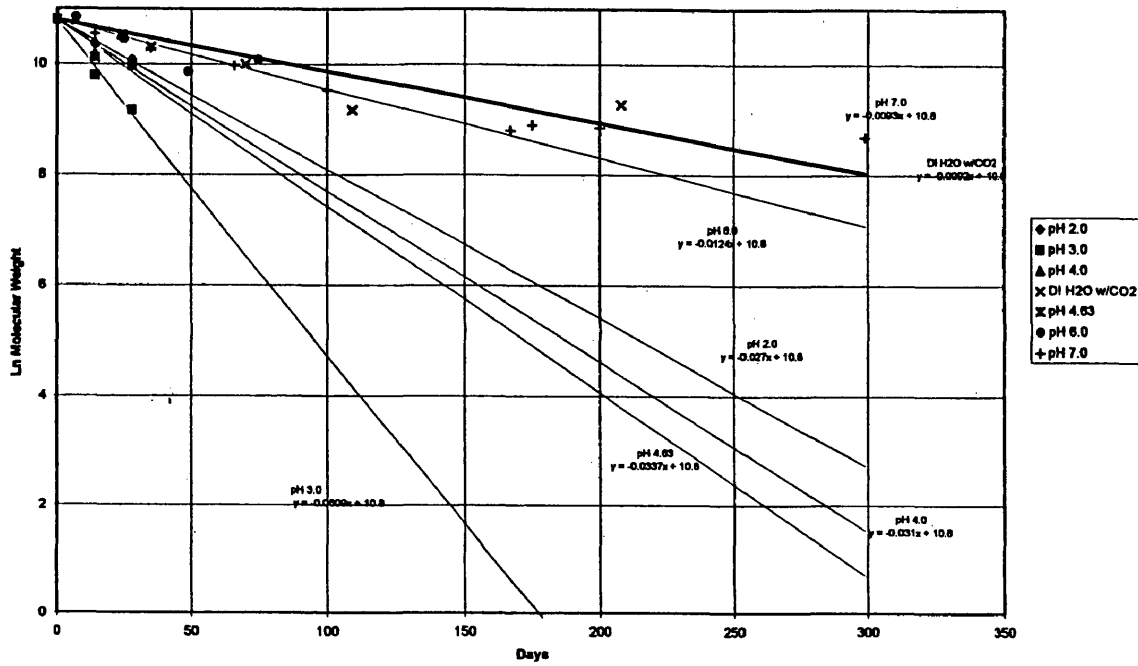


Figure [3.20]

Ln Molecular Weight vs Day at 120C 100% Buffer Environments

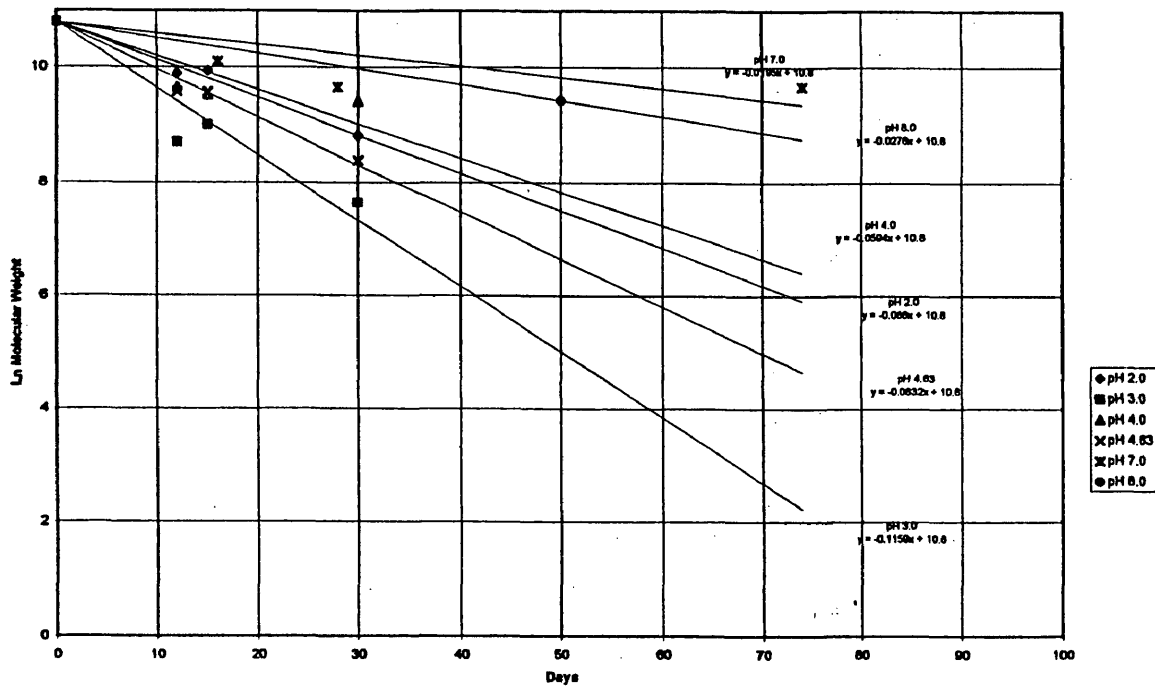


Figure [3.21]

**Extrapolated k(120 -> 105) and Experimental
(from Ln Molecular Weight versus Day plots)
versus pH**

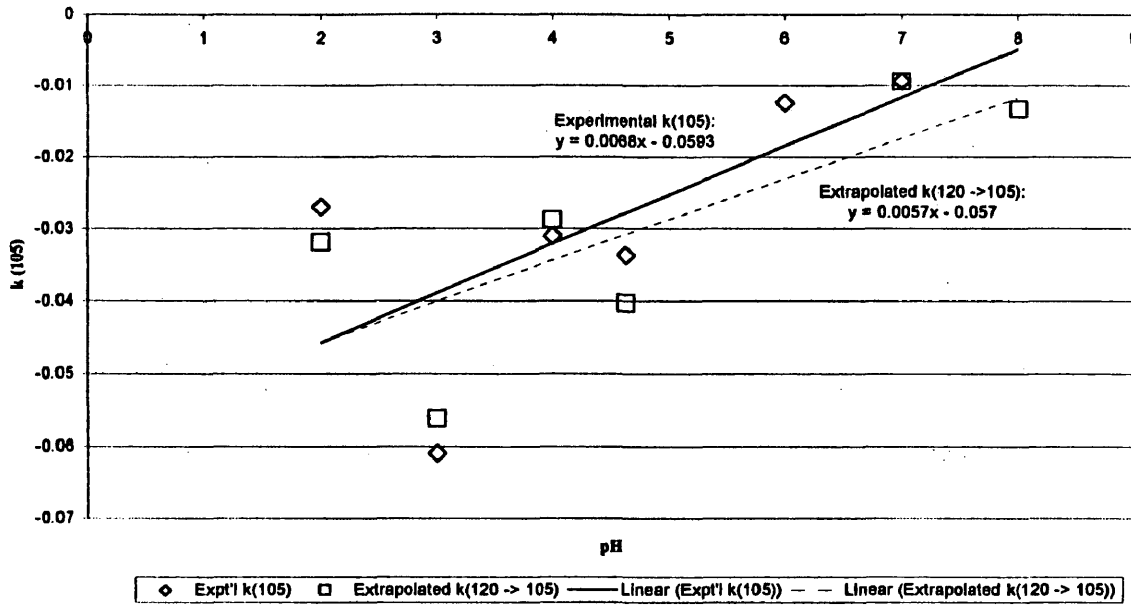
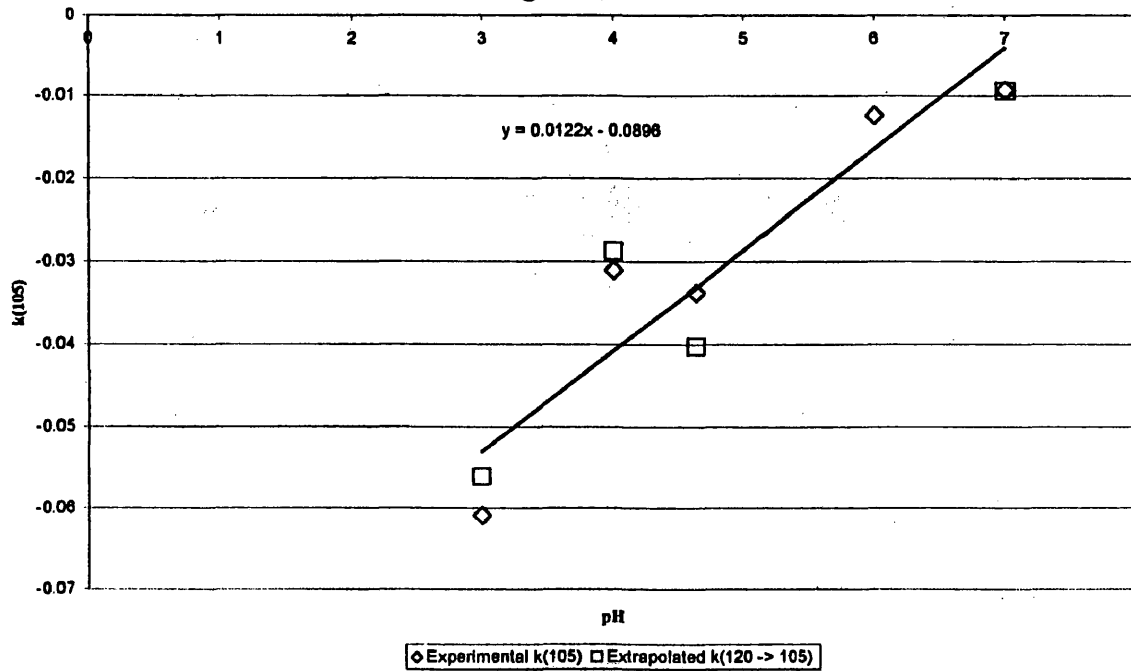


Figure [3.22]

**105C pH Slopes versus pH for Nylon-11
Figure [3.23]**



Sensor C1 left in 95% Oil Pot

Log ϵ'

105°C

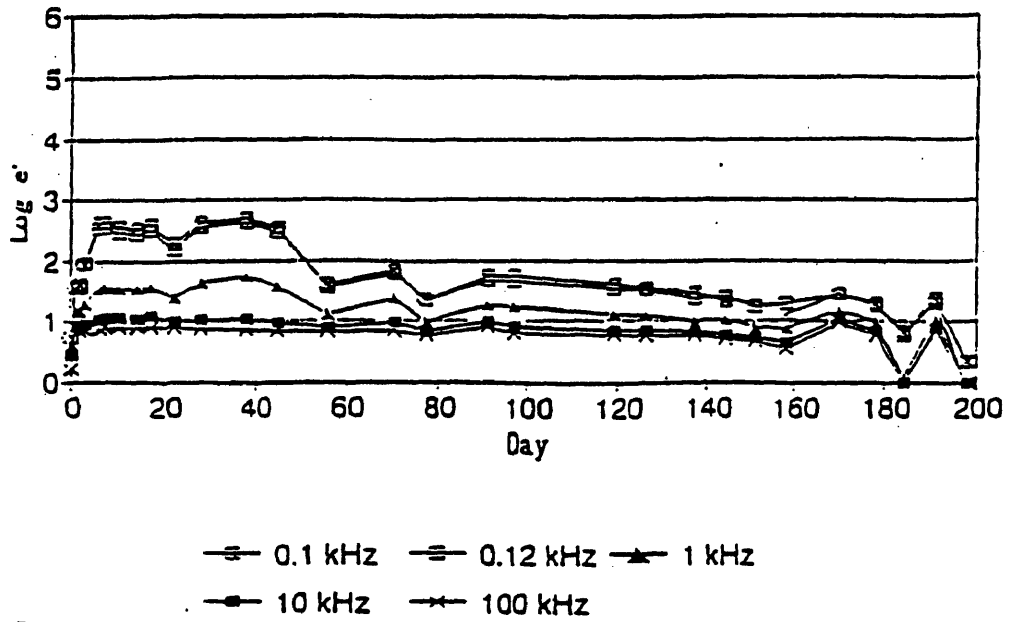


Figure [3.25]

FDEMS data for sensor C1 left, log ϵ'

Sensor C1 left in 95% Oil Pot

Log ($\epsilon'' \cdot \omega$)

105°C

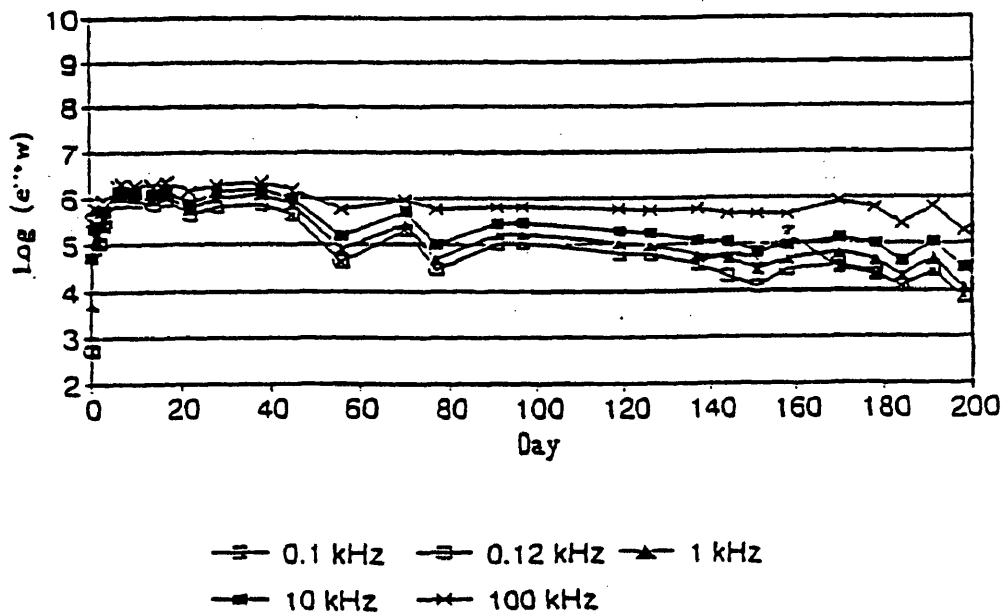


Figure [3.26]

FDEMS data for sensor C1 left, log $\epsilon'' \cdot \omega$

Nylon Sensor in 90C 95% ASTM/5% H2O

Log e''^*w vs Day

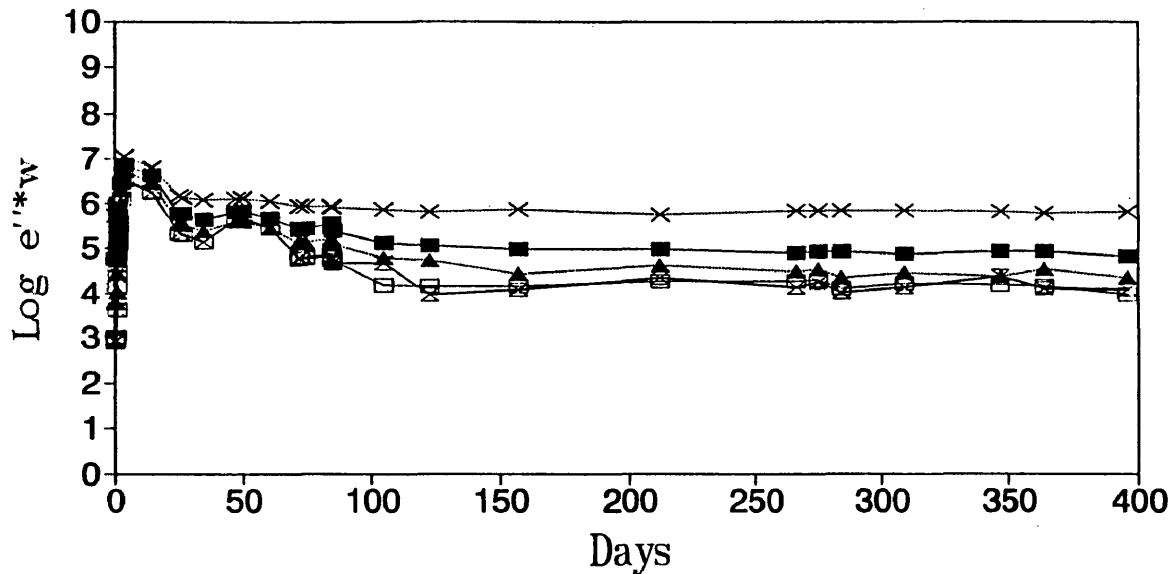


Figure [3.27]

—x— 0.1 kHz —□— 0.12 kHz —▲— 1.0 kHz
 —■— 10 kHz —x— 100 kHz

Nylon Sensor in 90C 95% ASTM/5% H2O

Log e' vs Day

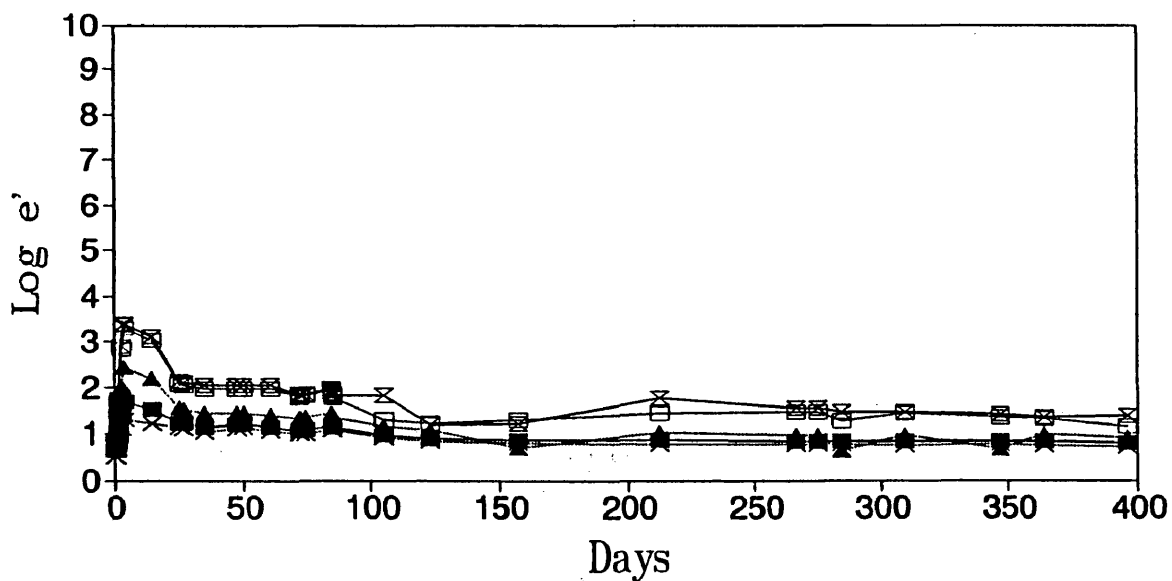


Figure [3.28]

—x— 0.1 kHz —□— 0.12 kHz —▲— 1.0 kHz
 —■— 10 kHz —x— 100 kHz

Nylon Sensor #8 in 90C 5% ASTM/95% H2O

Log e''*w vs Day

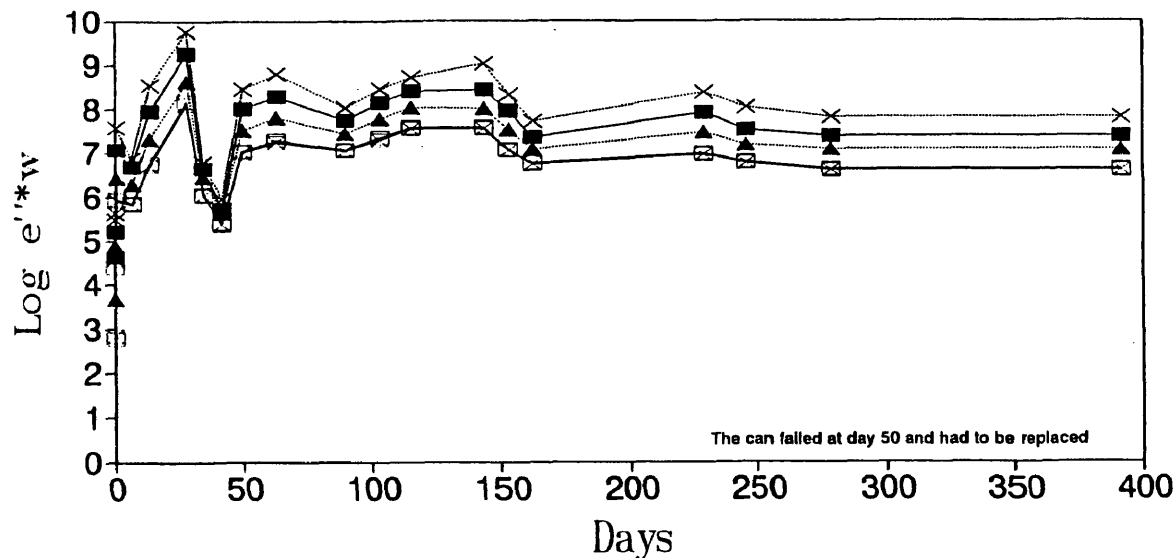


Figure [3.29]

—x— 0.1 kHz —□— 0.12 kHz —▲— 1.0 kHz
 —■— 10 kHz —x— 100 kHz

Nylon Sensor #8 in 90C 5% ASTM/95% H2O

Log e' vs Day

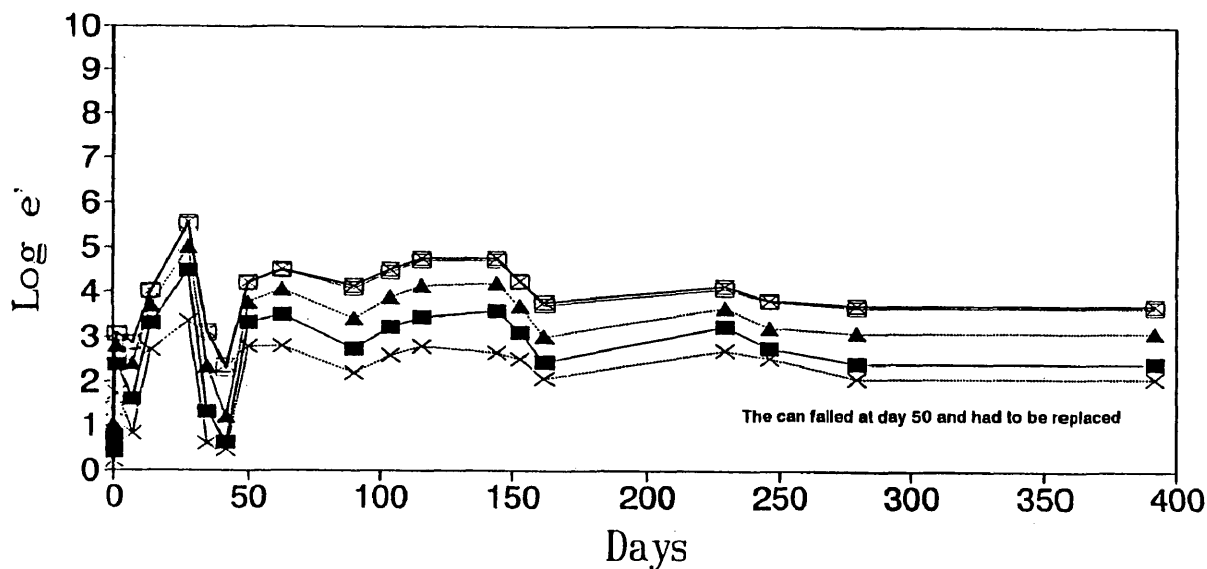


Figure [3.30]

—x— 0.1 kHz —□— 0.12 kHz —▲— 1.0 kHz
 —■— 10 kHz —x— 100 kHz

Nylon Sensor #5 in 90C 100% Buffer
Log e''*w vs Day

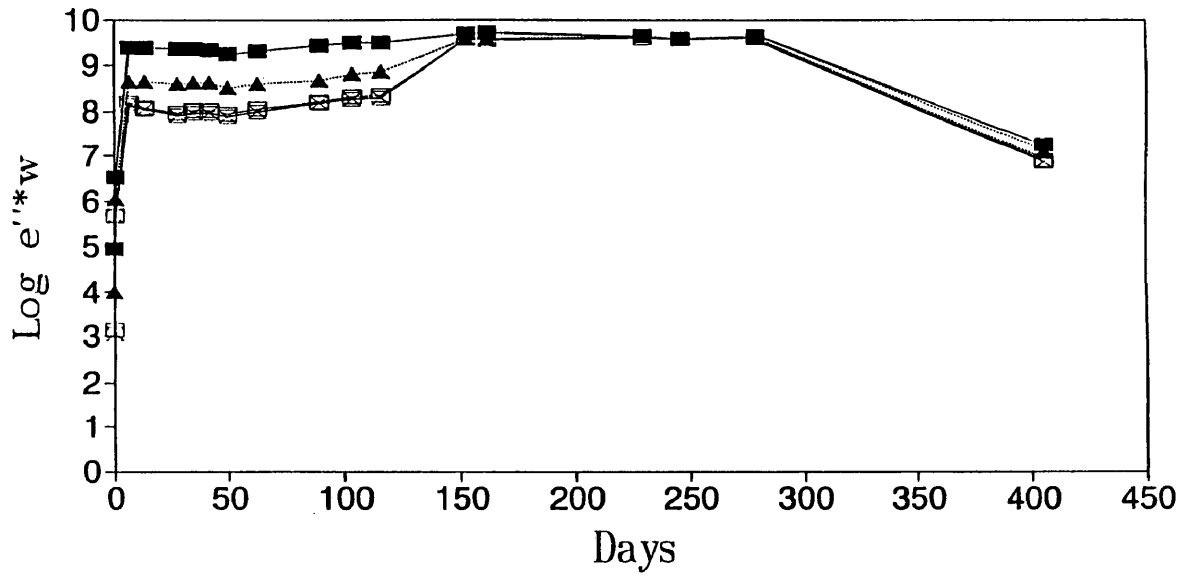


Figure [3.31] —x— 0.1 kHz —□— 0.12 kHz —▲— 1.0 kHz
—■— 10 kHz ——— 100 kHz

Nylon Sensor #5 in 90C 100% Buffer
Log e' vs Day

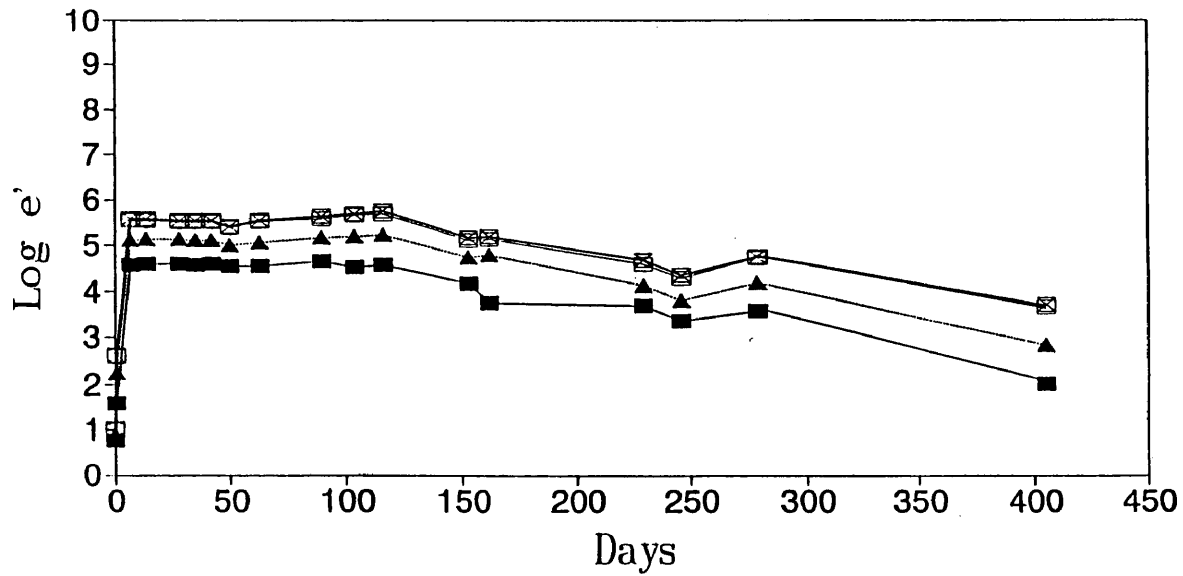


Figure [3.32] —x— 0.1 kHz —□— 0.12 kHz —▲— 1.0 kHz
—■— 10 kHz ——— 100 kHz

Nylon Sensor #1 in 70C 95% ASTM/5% H2O

Log e' vs Day

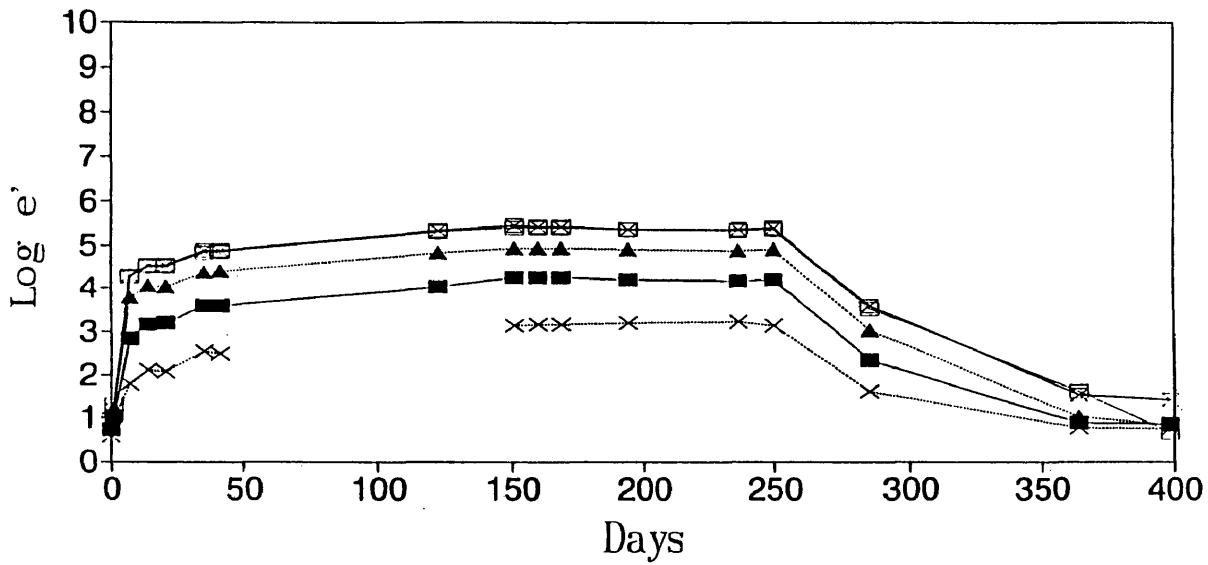


Figure [3.33] —x— 0.1 kHz —□— 0.12 kHz —▲— 1.0 kHz
 —■— 10 kHz —x— 100 kHz

Nylon Sensor #1 in 70C 95% ASTM/5% H2O

Log e''*w vs Day

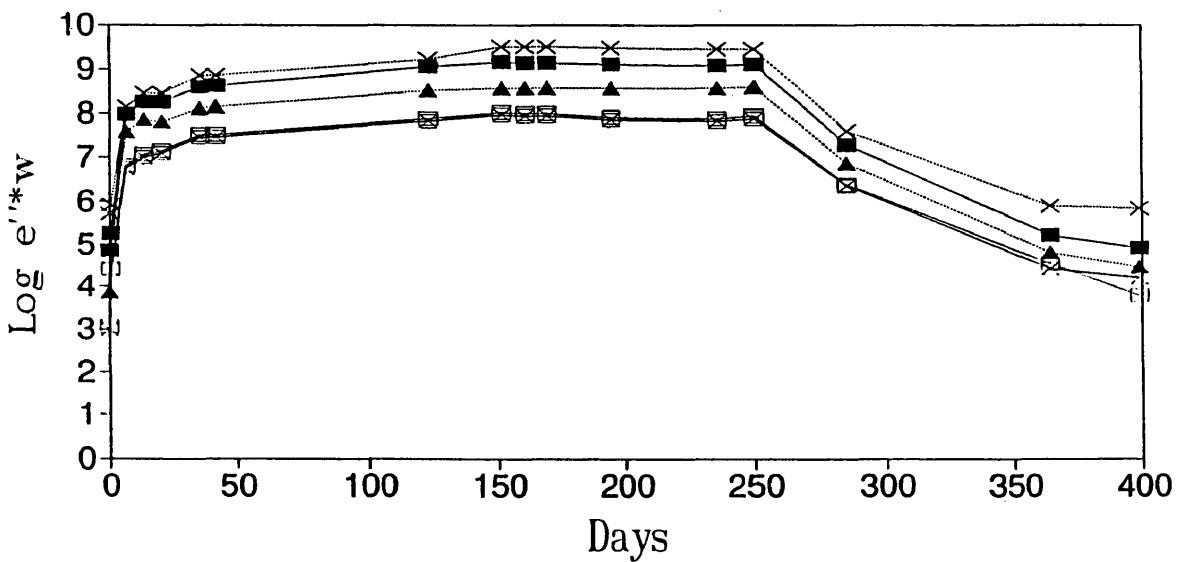
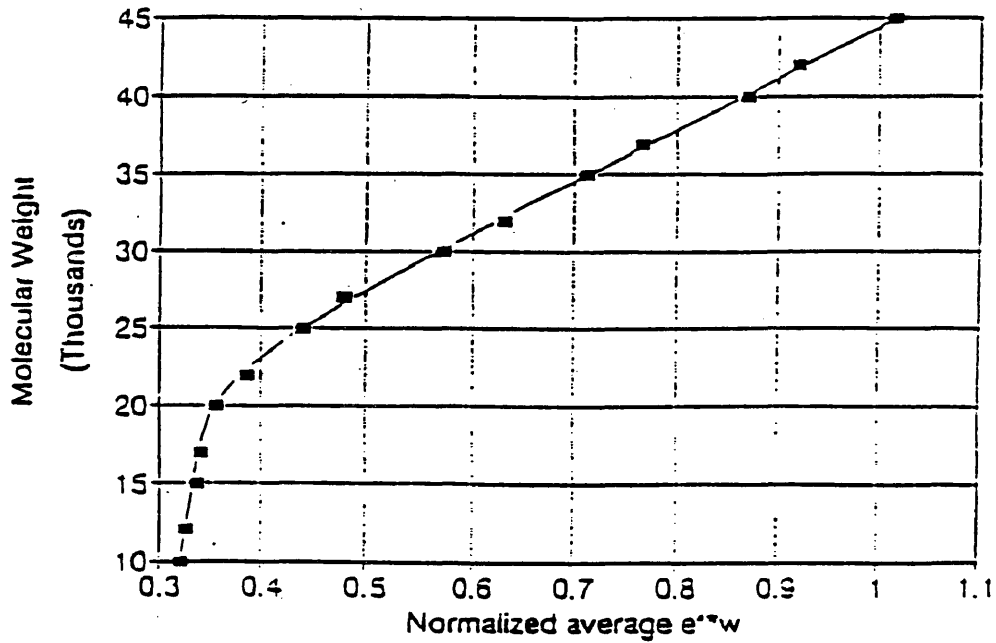


Figure [3.34] —x— 0.1 kHz —□— 0.12 kHz —▲— 1.0 kHz
 —■— 10 kHz —x— 100 kHz

Figure [3.35] 105°C 95% Oil, 5% Water Environment

Correlation

Normalized ϵ''^*w vs Molecular Weight



Molecular weight versus normalized ϵ''^*w

Figure [3.35]

Nylon Sensor in 90C (Dessicator) 95% ASTM Oil with 5% Water
Molecular Weight vs Normalized $e^{**}w$

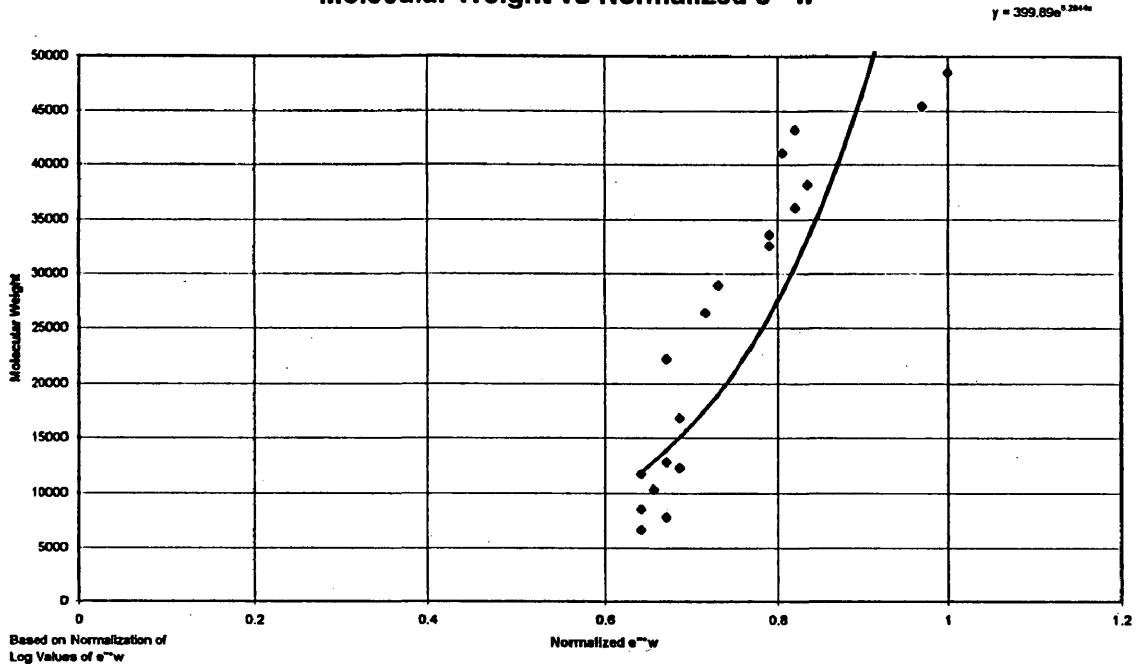


Figure [3.36]

Nylon Sensor #8 in 90C 5% ASTM/95% Water
Molecular Weight vs Normalized $e^{**}w$

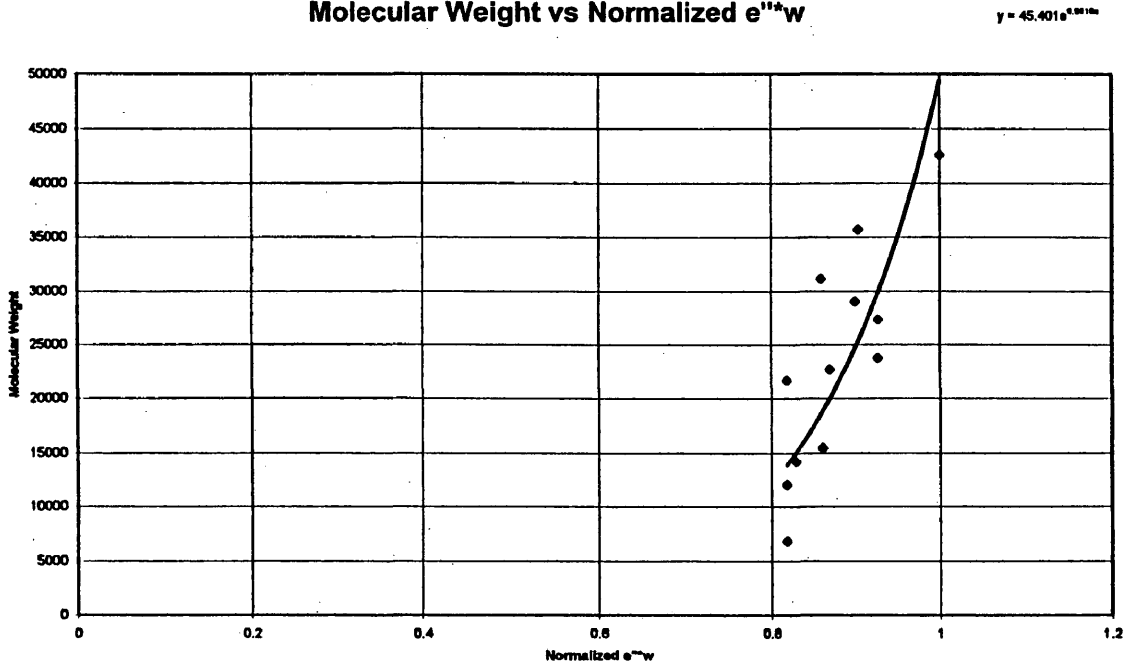


Figure [3.37]

Nylon Sensor #5 in 90C 100% pH 6 Buffer
Molecular Weight vs Normalized $e^{**}w$

$y = 10757e^{1.418x}$

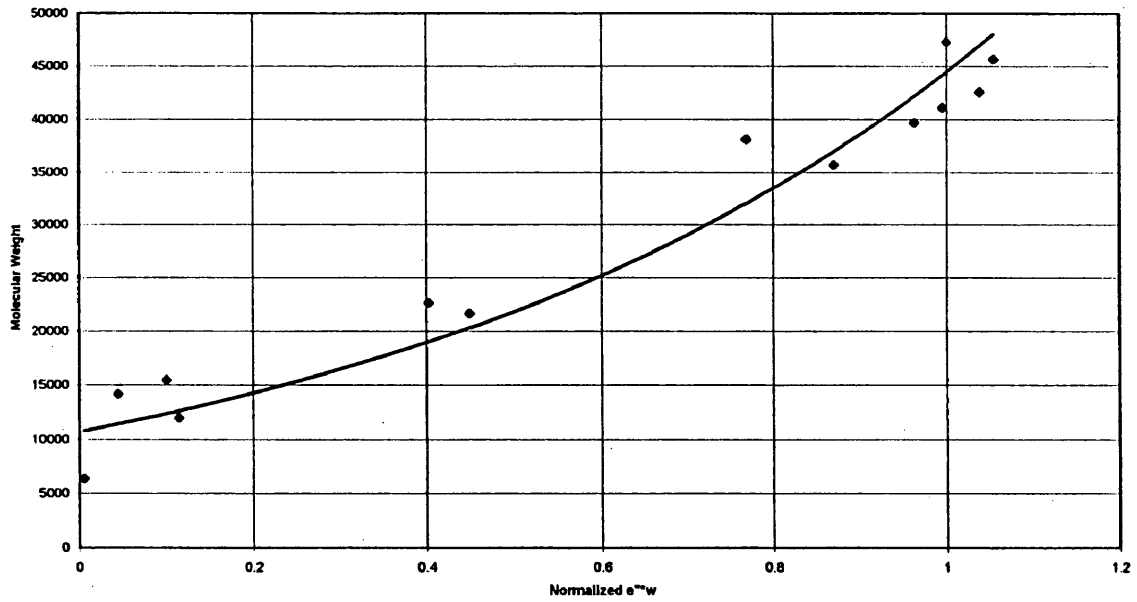


Figure [3.38]

Enthalpy versus Time for Nylon-11 at 105C

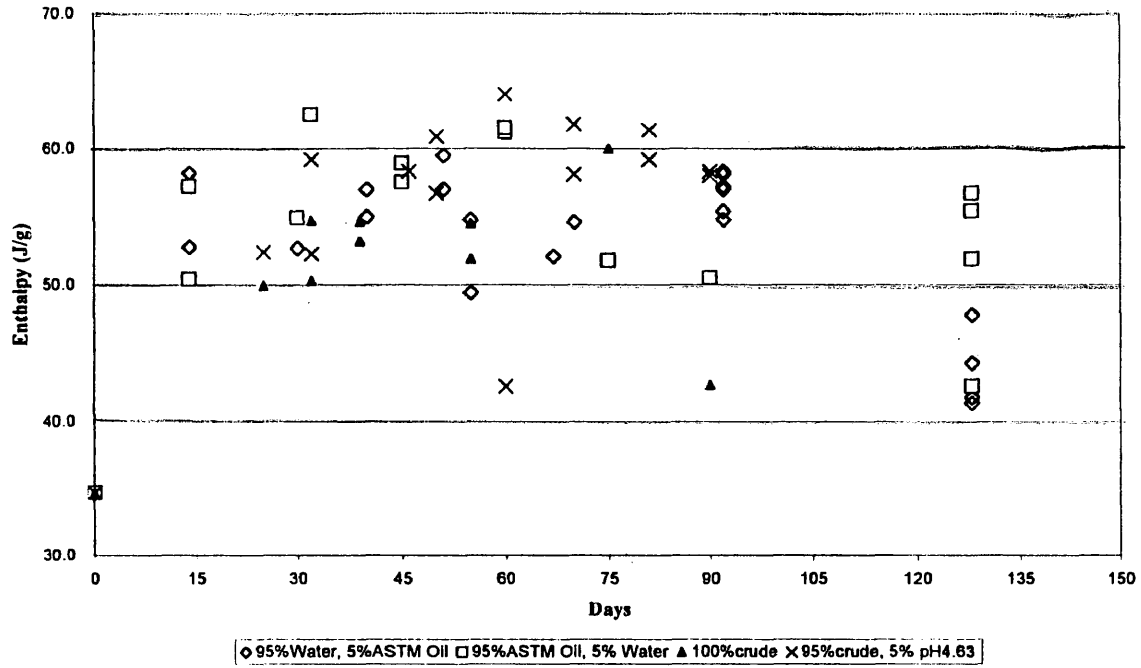
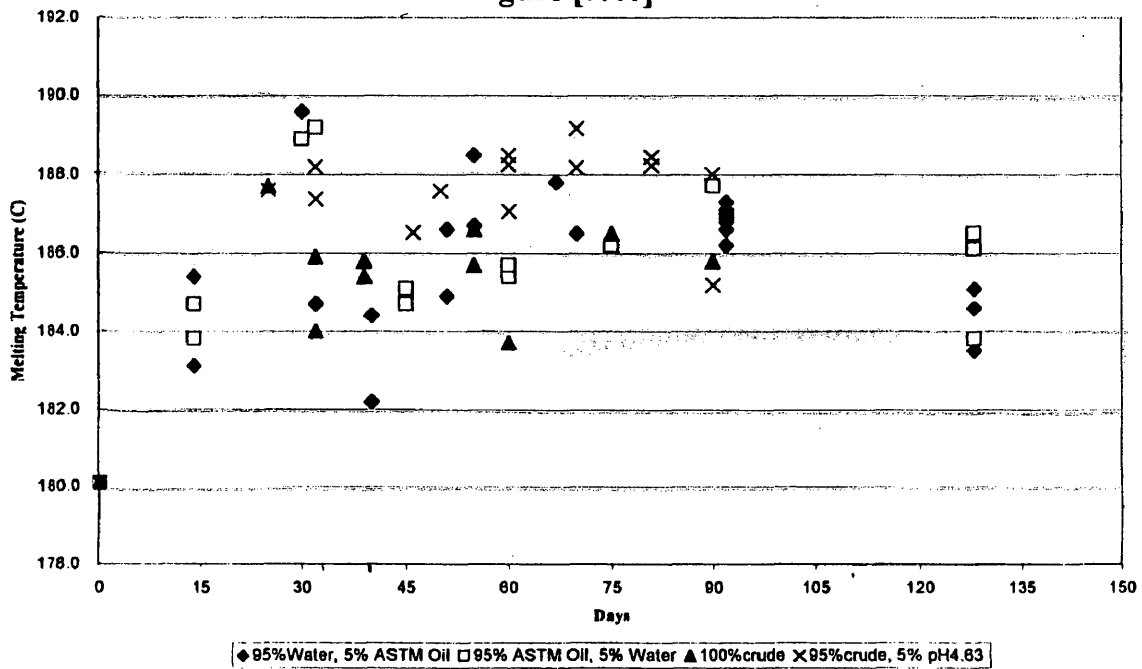


Figure [3.39]

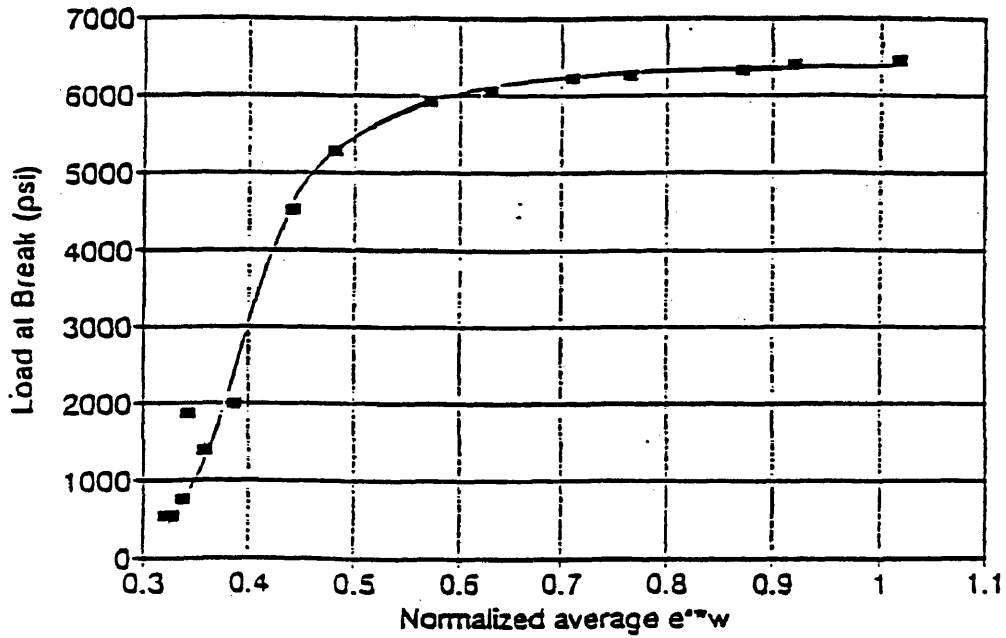
Melting Temperature versus Day for Nylon-11 at 105C

Figure [3.40]



Correlation

Normalized $\epsilon''w$ vs Load at Break



Load at break versus normalized $\epsilon''w$

Figure [3.41]

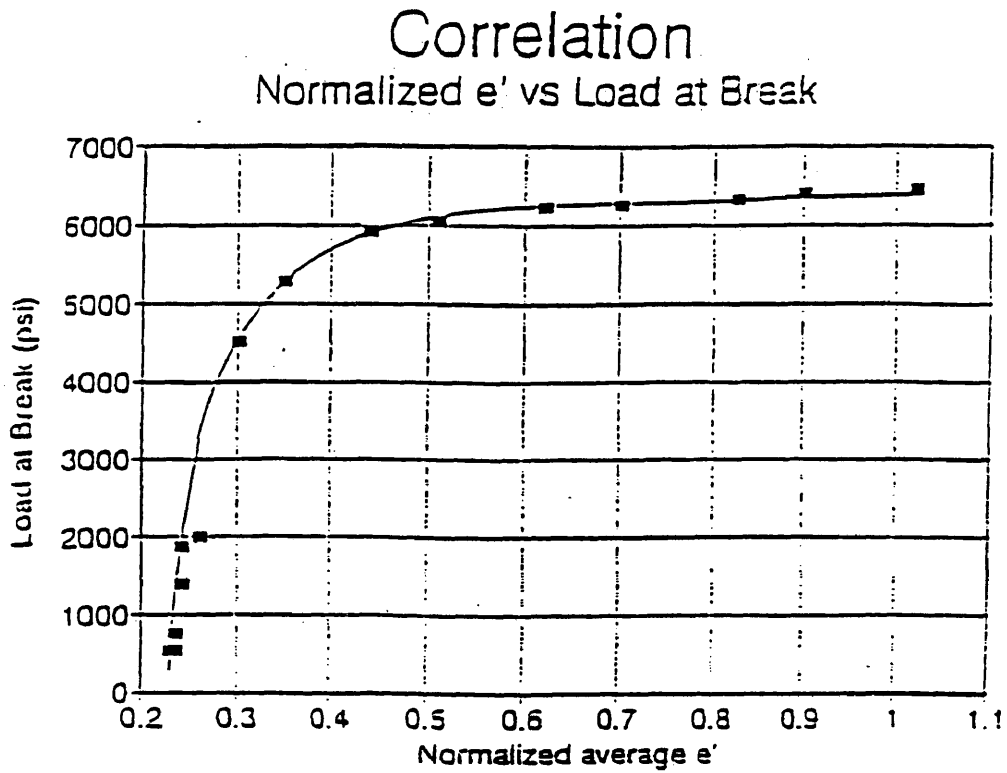


Figure [3.42] Load at break versus normalized ϵ'

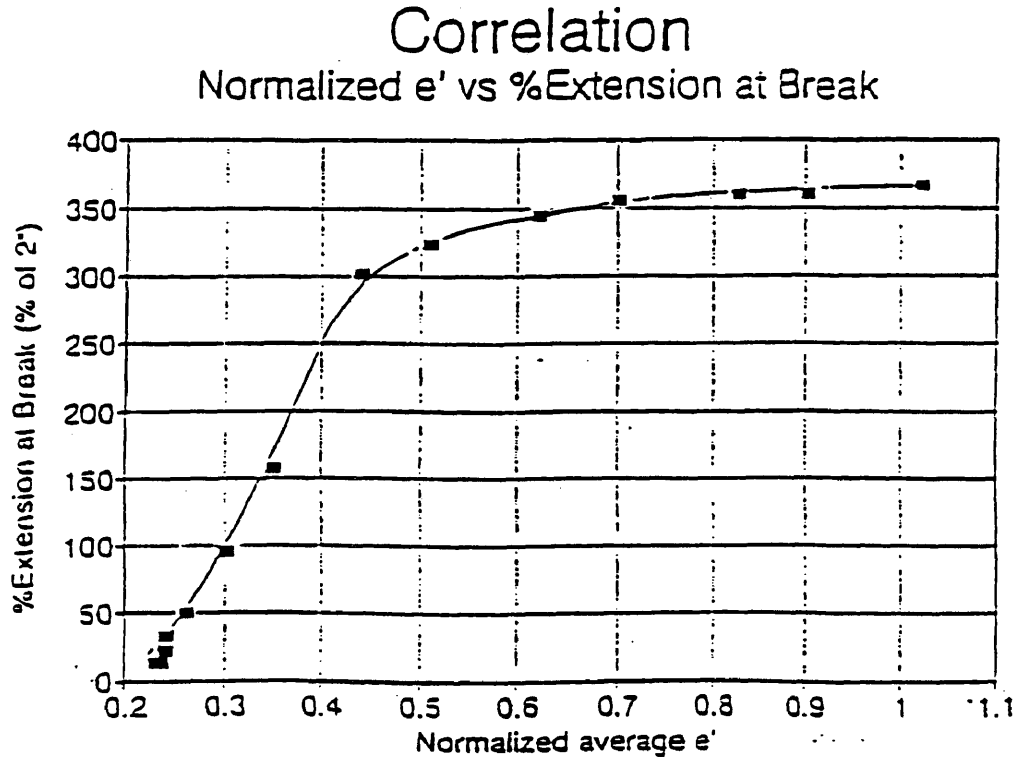
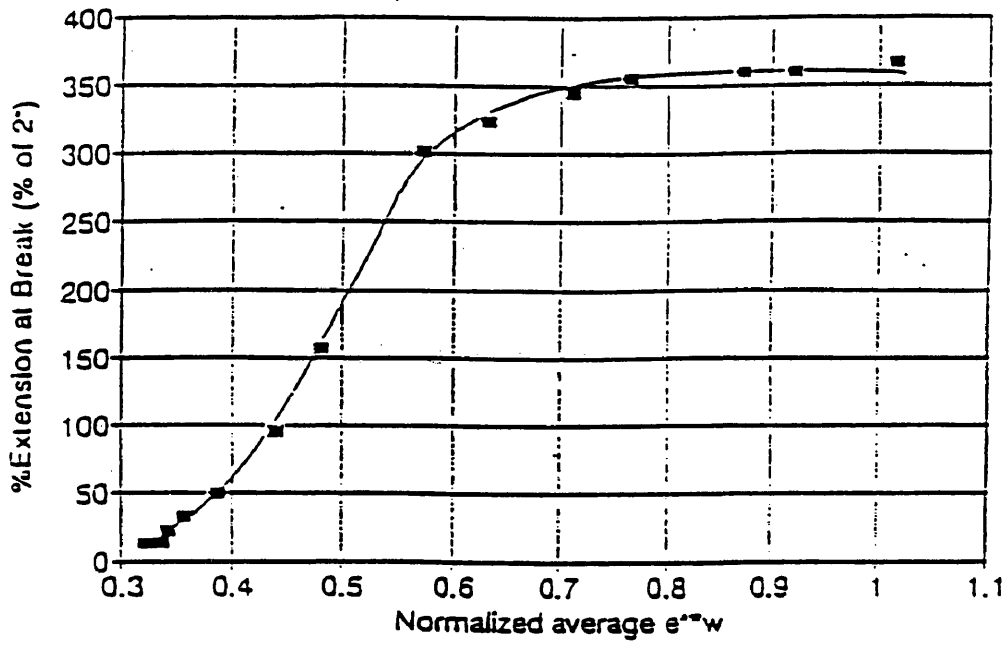


Figure [3.43] % Extension at break versus normalized ϵ'

Correlation

Normalized $\epsilon''w$ vs %Extension at Break



% Extension at break versus normalized

$\epsilon''w$

Figure [3.44]

**Nylon-11 Mechanical Samples
aged in 95%ASTM Oil with 5% pH 4.63 Buffer at 105C**

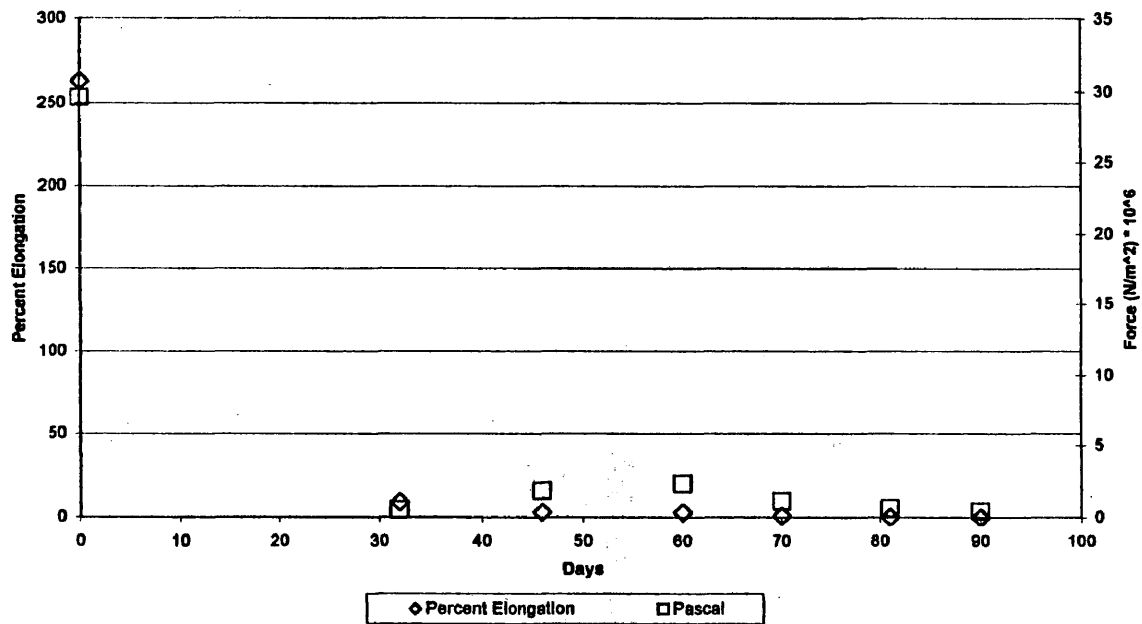


Figure [3.45]

Chapter IV

Poly(vinylidene fluoride) Degradation

A. Introduction

Poly(vinylidene fluoride), or PVDF, is a semicrystalline thermoplastic polymer much like nylon-11. The fluoride group which is a smaller, more symmetrical and more polar group than the amide group in nylons characterizes this polymer. This high amount of polarity and small size causes PVDF to have more crystalline regions than nylon-11. With the higher crystallinity the polymer is stronger and tougher than nylon-11 and is more resistant to harsh environments. For these reasons it is beginning to be used as a replacement for nylon in oil pipes.

PVDF is formed by the radical-initiated addition polymerization of 1,1-difluorethene or (vinylidene fluoride):



This reaction can occur via either emulsion or suspension polymerization.

Two separate phases of study were conducted for PVDF. The first phase monitors the effects of many different aging environments on PVDF. Two types of PVDF were used for this study: Coflexip, or Robit, produced by Atochem and Wellstream produced by Solvay. The second phase, termed the comparative study, investigated the differences between different types of PVDF manufactured for use in flexible pipe. For the purposes of this study four different types of PVDF were used: Robit, or Coflexip, produced by Atochem; Wellstream produced by Solvay; 60512 and 1015 produced by Solvay which are unplasticized

samples of the Wellstream product; and a sample referred to as Elf-Atochem (EA) produced by Elf-Atochem which is a deplasticized sample of the Coflexip mentioned earlier. The unplasticized samples are copolymers of various degrees of fluorinated hydrocarbon chains. This causes the polymer to be less symmetric with more amorphous regions and therefore less apt to crystallize.

Solvay provided an example of the manufacturing specifications of its polymers. The Solvay products are produced by a suspension polymerization resulting in a narrow molecular weight distribution.¹ Occasionally head-to-head addition occurs during polymerization lowering the thermal stability of the polymer. Typical samples of PVDF have approximately 3.5-3.6 mole percent of this type of defect.²

B. Mechanism of Degradation of PVDF

PVDF is enormously stable under most conditions even with the defects mentioned above. Polymers with fluorine substituents are generally more stable to harsh environments than their hydrocarbon counterparts. The greater electronegativity of the fluorine atom contributes to the high bond dissociation energy of the carbon-fluorine bonds on the polymer chain.³ PVDF is resistant to oxidative, thermal and hydrolytic degradation. It has high mechanical strength and resistance to load deformation. The polymer is extremely hydrophobic and hence mostly water insoluble. The water absorption of PVDF is reported to be approximately 0.4%, which is much lower than that of nylon-11.⁴

Degradation of PVDF is possible, however, in certain harsh conditions. These include sulfuric acid, strongly basic amines, and concentrated alkalis and alkaline metals. Hence, care must be employed when adding cleansing agents to the offshore oil pipes as some cleaners contain primary amines.⁵ In the absence of these environments, non-oxidative thermal degradation occurs via the elimination of HF gas, resulting in a conjugated polyene system, or through backbone scission and depropagation to form monomer. The HF gas produced is self-catalyzing, therefore degradation continues as shown in Figure [4.2].⁶

There is an increase in the crystallinity of the polymer due to annealing. In contrast, crosslinking, which can also occur during the degradation, leads to a decrease in crystallinity. Crosslinking is a process by which side groups on a linear polymer, such as PVDF, are initiated to react with one another to form a bond. This links the two linear chains together making a crosslink.

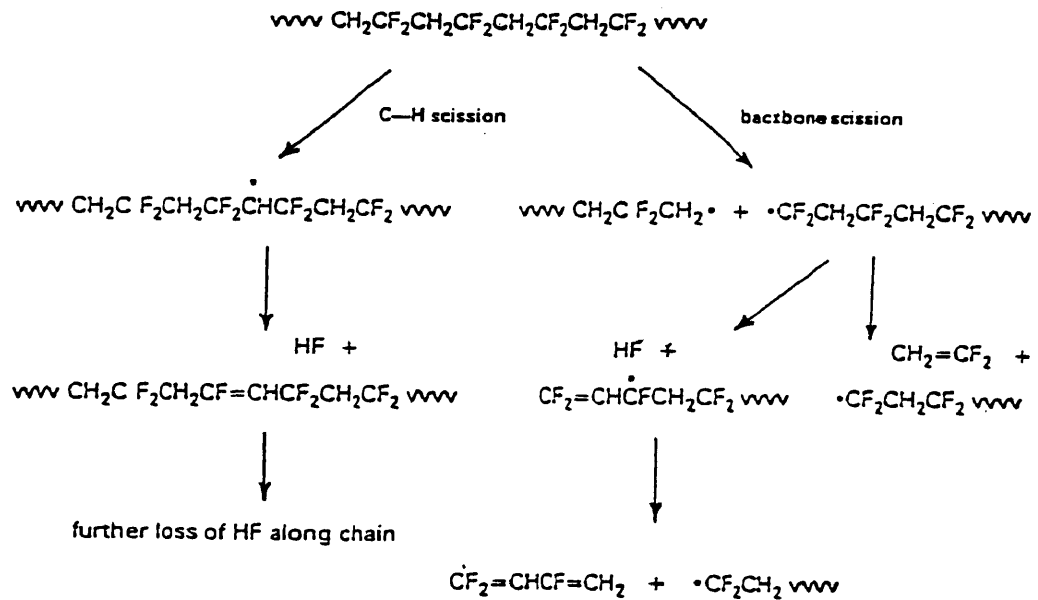


Figure [4.2] Mechanism for the Degradation of PVDF⁷

C. Aging Environments

The aging environments of PVDF emphasize the effects of increased temperature, oil and water exposure, and cleansing agents flushed through the pipes. The environments studied are listed in table [4.1]. Only two environments were used for sensor monitoring. These are labeled with FDEMS (dielectric sensor) in the third column. If the environment was used for aging mechanical testing samples the label MS is in the third column.

130°C	Environment	FDEMS /MS
	10% Ammonium Bisulphate, 90% Water	
	60% Ammonium Bisulphate, 40% Water	
	1000ppm Ethylene Diamine Tetramethylene Phosphonic Acid with Water	
	1000ppm Aniline with Water	
	100% Aniline	FDEMS, MS
	100% Ethylene Glycol	
	10% Tetraethylammonium Chloride, 90% Ethylene Glycol	
	Ethylene Glycol with 1000 ppm Tetraethylammonium Chloride	
	1000ppm Tetraethylammonium Chloride with Water	
	95%ASTM Oil, 5% Water	FDEMS, MS
	Air Oven	

Table [4.1] PVDF Aging Environments

D. Results and Discussion

In the aging environments mentioned above, samples were analyzed for viscosity average molecular weight, DSC, mass, thickness and hardness.

Mechanical testing and dielectric sensing was done on the indicated samples.

Overall the results indicated that the polymer is resistant to many chemical

environments. The flexible PVDF oil pipes frequently maintain temperatures close to the 130°C test temperature used for this study. PVDF has a projected twenty-year lifespan in the field. Any degradation experienced in the first year of study indicates potential grave consequences for long term use of the polymer.

Phase I

Phase I of the PVDF study shows similar behavior in the dielectric measurements during early days as those witnessed in the nylon study. Initially there is an increase in the ionic mobility as the small molecules such as water and aniline infiltrate the polymer. In the 95% ASTM, 5%Water environment a gradual decrease in the $\epsilon''^*\omega$ data is seen over time (Figure [4.3]). This is expected as the polymer slowly degrades. The aniline environment however does not show as a decrease, but rather an increase over time (Figures [4.4] – [4.5]). This is due to the degradation of the polymer and the increased penetration and plasticization by aniline, which has a higher dielectric constant and high molecular mobility. This conclusion is supported by the continued increase in the percent mass of the samples during the aniline study. What appears to be happening is that the polymer is degrading and small polar molecules are diffusing more freely through the now lower molecular weight polymer.

The DSC results show a gradual increase in the T_m of the samples (Figures [4.6] – [4.9]). In the 95% ASTM Oil with 5% Water environments as well as in most of the amine environments there is a slight increase in ΔH over time. This indicates an increase in the percent crystallinity (Figures [4.10] – [4.13]). The

TEAC and ammonium bisulphate environments indicate slightly higher long-term degradation effects. In the 100% aniline environment, however, there is an enormous decrease in the percent crystallinity within the first few days of the study. This decrease takes into account the increase in the percent mass that occurs in the 100% aniline environment. This correction for the plasticization by the aniline, or any other small molecule in the environment, is calculated by multiplying the ΔH values by the percent of the original mass of the polymer at that day. This decrease in percent crystallinity exemplifies the rapid degradation of PVDF by concentrated amounts of aniline. Figures [4.14] – [4.15] specifically show the changes in T_m and ΔH for both Wellstream and Coflexip(Robit) in the 130°C 95% ASTM Oil with 5% Water environment. The change is smaller than the effects of the amine additives and aniline.

Viscosity average molecular weight data verify the results seen in both FDEMS measurements and DSC data. The molecular weight of the PVDF in the 95% ASTM oil, 5% water environment stays relatively constant over the duration of the study indicating little degradation. TEAC and ammonium bisulphate at higher concentrations suggest a modest rate of degradation. The molecular weight of the polymer in the 100% aniline environment, however, rapidly drops and by day 140 is nearly zero (Figure [4.16] and [4.17]). The data suggest possible degradation of the PVDF in the other aging environments, where the rate is significantly slower (Figures [4.18] and [4.19]). Figure [4.20] compares the molecular weights of both Wellstream and Coflexip (Robit) in 95% ASTM oil with 5% water.

Mechanical tests further exemplify the distinctions between the 95%ASTM Oil, 5% Water environment and the 100% aniline environment. The load at break and peak for the oil environment increases while the loads of corresponding samples in the 100% aniline environment decrease (Figures [4.21] – [4.22]). The percent elongation plots indicate a decrease in the oil environment and an increase in the aniline environment (Figures [4.23] – [4.24]). The changes in the mechanical properties appear to occur in the first 40 days of the aging study and then level off. These data correlate to the absorption of small molecules from the aging environment during the first several days. Aniline is infiltrating the polymer and re-plasticizing the material. Therefore the PVDF loses some of its stiffness. The polymer then becomes more susceptible to deformation under load. This could be detrimental in a high pressure confined space such as an oil pipe. Each of the data points on the plots represents an average of three to eight mechanical testing samples for a given day.

Due to its low percentage of water absorption, little solution penetrates the polymer in the 95% ASTM Oil, 5% Water environment. The 100% aniline environment, however, rapidly soaks into the polymer. The results of these processes can be seen by the change in percent mass of the polymer over time (Figures [4.25] – [4.28]). Those environments with a decrease in percent mass experience an evaporation of the plasticizer from solution at the high temperature.

Each of the environments studied indicate significant percent changes in thickness (Figures [4.29] – [4.32]). This could be partially due to curvature of the samples. The samples used for the mass, hardness and thickness testing were of

smaller dimensions than a dielectric sensor and were not imbedded between metal plates as with the dielectric sensors. These conditions contributed to the deformation of the samples, therefore increasing the percent change in thickness not solely due to swelling, but also due to changes in curvature of the sample. Similar changes are seen in the data for the percent change in hardness (Figures [4.33] – [4.34]).

Phase II

The focus of this phase of the study was to monitor differences in the various types of PVDF manufactured for use in flexible pipe construction. Different amounts and types of plasticizer as well as monomer are used in the manufacture of PVDF. This study investigates the changes in physical properties of PVDF with plasticizer {Wellstream and Coflexip(Robit)}, a copolymer without plasticizer (Wellstream 1015 and 60512), and polymer that has been deplasticized {Elf-Atochem(EA)}. Two different aging environments were used: 95%ASTM Oil with 5% Water at 130°C and an air oven at 130°C. Data were taken on the mass, thickness, and hardness, with DSC testing and mechanical tensile testing being done on these samples to analyze the changes in macroscopic properties over time.

Figures [4.35] – [4.36] indicate percent change in the mass of the samples over 200 days of study in the 130°C air oven. As expected, the unplasticized copolymer samples (1015 and 60512) had little to no change in mass as the samples were aged. The other samples experienced weight loss, indicating the

plasticizer evaporated out of the samples. The amount of evaporation of plasticizer is considerably lower for the EA sample than the Wellstream or Coflexip samples. This is because the EA sample was previously deplasticized, meaning some of the plasticizer had already been removed after manufacture of the sample.

Data for the 130°C oil bath (95% ASTM Oil with 5% Water) shows similar results. The unplasticized samples gain weight slightly as small molecules from the fluid environment infiltrate the polymer. The other samples, however, lose mass as more plasticizer diffuses out of the sample than environmental molecules diffuse into the polymer (Figures [4.37] – [4.38]).

The thickness of the polymer increased in the air oven for the samples with lower amounts of plasticizer. This could be due to expansion of the polymer at this high temperature (Figures [4.39] – [4.40]). The samples with plasticizer, however, tended to have a decrease in thickness. This could be due to the plasticizer diffusing out and the molecules becoming more tightly packed together. Similar results are indicated in the oil bath (Figures [4.41] – [4.42]). The unplasticized samples and the copolymers change like they did in the air oven, slightly expanding once exposed to the high temperature. The plasticized samples had a slightly smaller decrease in thickness as in the oil pot as compared to the air oven. This could be due to initial loss of plasticizer when introduced to the 130°C oil environment and a re-plasticization effect due to small molecules simultaneously infiltrating the polymer. Comparing the change in thickness of the Phase II polymers to those in Phase I indicates the PVDF tends to swell

considerably in amine environments. This swelling in aniline and the other additive environments is much more pronounced than the decrease in expansion seen in the oil pot. The polymer is therefore extremely vulnerable to amine additives. This is significant as these types of amine environments are introduced into the pipelines for cleaning and maintenance. It would be valuable to study the unplasticized polymers in the amine environments of Phase I to see if the copolymer was as susceptible to swelling.

It is difficult to ascertain any detailed trends in the hardness measurements of the polymers in either environment (Figures [4.43] – [4.46]). However, looking at all the data there does seem to be an overall increase in hardness in the air oven. The same conclusion cannot be made for the oil bath. Within the standard deviation for the data points, it appears the hardness for the polymer in the oil bath is staying fairly constant after a rapid initial rise. Hardness measurements are more subjective than other forms of physical testing, therefore these data are less definitive. They probably show the initial rise due to the increase in crystallinity.

From DSC data, the melting temperature, T_m , and the change in the enthalpy were determined. The change in the enthalpy is directly related to the change in the crystallinity of a sample as explained in chapter 1. The T_m is indicative of the crystal structure within the polymer. The T_m of the copolymer and deplasticized samples does not vary significantly throughout the aging of the samples (Figures [4.47] – [4.50]). The plasticized samples do show a slight increase in the T_m indicating a reorganization of the crystal structure. The

enthalpy, however, shows a significant increase over time (Figures [4.51] – [4.54]). This indicates the samples are aging and becoming more crystalline. This increase in the percent crystallinity is rapid at 130°C reaching approximately 20% within the first 50 days. Apparently the initial introduction to the high temperature causes significant changes in the amount of crystallinity during the early days of aging, but not in the crystal structure itself.

Mechanical testing was performed on samples of Wellstream PVDF, 60512 (Unplasticized Wellstream) PVDF, and Robit (Coflexip) PVDF. The results of the tests are shown in Figures [4.55] – [4.57]. For each of the samples there is an initial large drop in the elongation at both peak and break. Wellstream PVDF has a drop that is substantially smaller, although it does still drop. For the Wellstream and Robit (Coflexip) samples there is an initial increase in the force required to break the aged samples in comparison to the day 0 samples. The 60512 samples, also, show a significant decrease in the force at peak and break. The day 0 value for 60512 is much higher than for the plasticized polymers. The plasticization effect of the environment may contribute to this drop in the force. After the initial sharp drop for 60512, there is a much slower, gradual decrease in the force similar to the drop seen for the plasticized samples of Wellstream and Robit. Particularly noteworthy is the fact that the percent elongation in 60512 remains over the period of study well above the 7% failure limit while the plasticized samples come very close, approximately 10%, to this failure point.

E. Conclusions

As evidenced by macroscopic measurements such as viscosity average molecular weight testing, mass, hardness, thickness, mechanical tensile testing and DSC testing, PVDF is a very resilient polymer which stands up to many harsh environments. The first phase of study observed the effects of the ASTM oil pot as well as many amine environments of high and low concentration. The only environment which significantly degraded the polymer was the 100% aniline environment. The other environments showed gradual degradation over time, but nothing that brought the mechanical properties of the polymer to failure.

The second phase of the PVDF study investigated the effects of the 130°C air oven and 130°C ASTM oil pot on different types of polymer. These polymers were composed with different amounts of plasticizer. The polymer with the least plasticizer, Wellstream's 60512 and 1015, indicated a plasticization effect shown by the increase in mass when placed in the 95% ASTM oil environment. This is also reflected by the initial decrease in the load at peak and break in the early mechanical tensile tests. The plasticized samples showed an initial decrease in mass and slight increase in the load at peak and break. Overall, the four different types of polymer used had similar properties, and withstood the high temperature environment well with respect to molecular weight degradation. However, the plasticized samples experienced large changes in dimensions, swelling and shrinkage in different environments. All the polymers experienced significant decreases in percent elongation. These aging properties are of concern for long term use and in a constantly changing high pressure temperature environment.

References to Chapter IV

¹ Kalman, M.D., Belcher, J.R., and Plaia, J.R. "Advanced Materials for Flexible Pipe Construction." *Offshore and Arctic Operations*. 1995, PD-Vol 53, p.2.

² Mark, H.F. *et al.* Encyclopedia of Polymer Science and Engineering. 2nd Ed. New York: Wiley & Sons, Inc. 1985, Vol. 11, p.370.

³ Allcock, H.R. and Lampe, R.W. Contemporary Polymer Chemistry. 2nd Ed. New Jersey: Prentice-Hall, Inc., 1990, p.546.

⁴ Mark, H.F. Vol 17, p.537.

⁵ Kalman, M.D. p.9.

⁶ Nguyen, T. Degradation of Poly(vinyl fluoride) and Poly(vinylidene fluoride). JMS-Rev. Macromol. Chem. Physics., 1985, p.268.

⁷ Zulfigar, S., M. Aulfigar, R. Masroor, and A. Munir. "Study of the Thermal Degradation of Polychlorotrifluorethylene, Poly(vinylidene fluoride) and Copolymers of Chlorotrifluorethylene and Vinylidene Fluoride." Polymer Degradation and Stability. 1994, Vol. 43, p.429.

**PVDF in 130C 95% ASTM 5% Water
Wellstream (Sensor WR)**

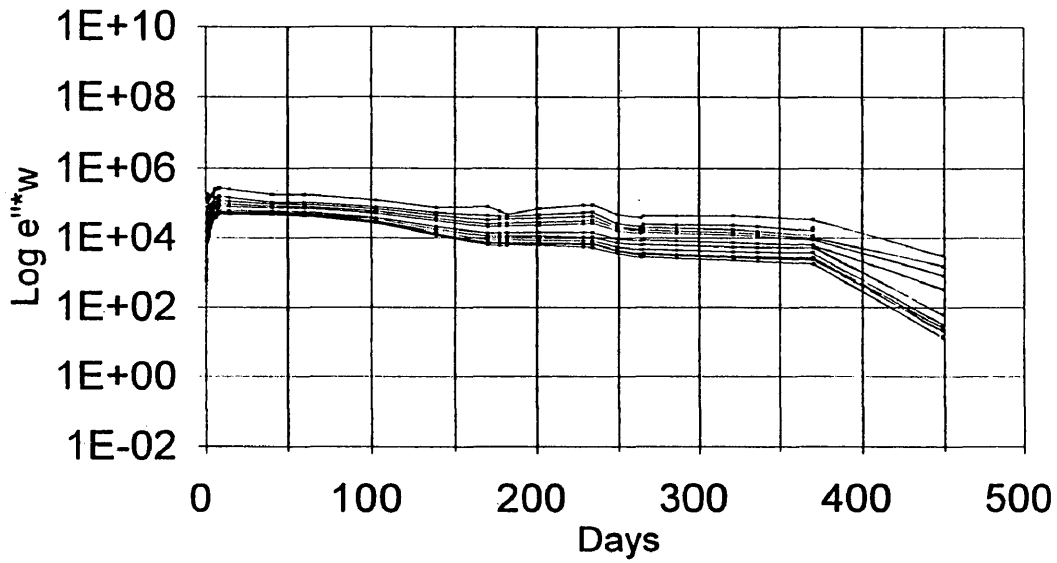


Figure [4.3]

**WS PVDF Sensor in 130C 100% Aniline
Phase I - $\text{Log } e'' \cdot w$ vs Day**

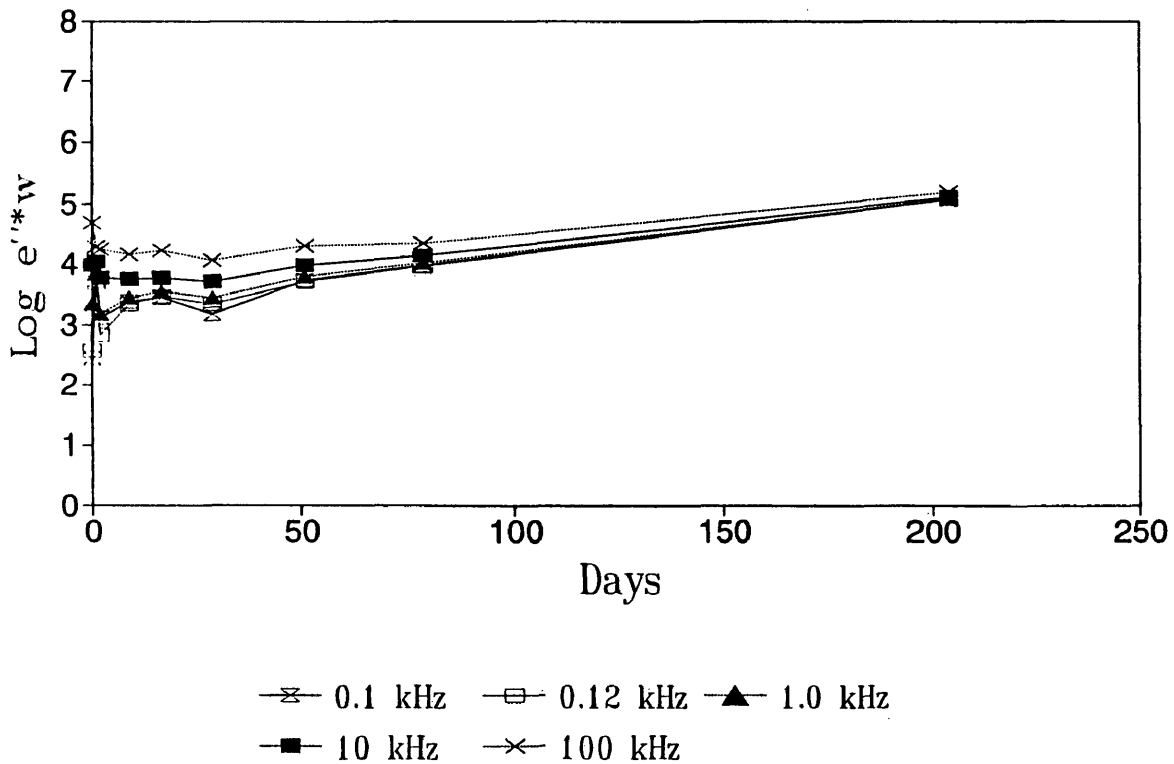


Figure [4.4]

Coflexip PVDF in 130C 100% Aniline
Phase I - Log $\epsilon''w$ vs Day

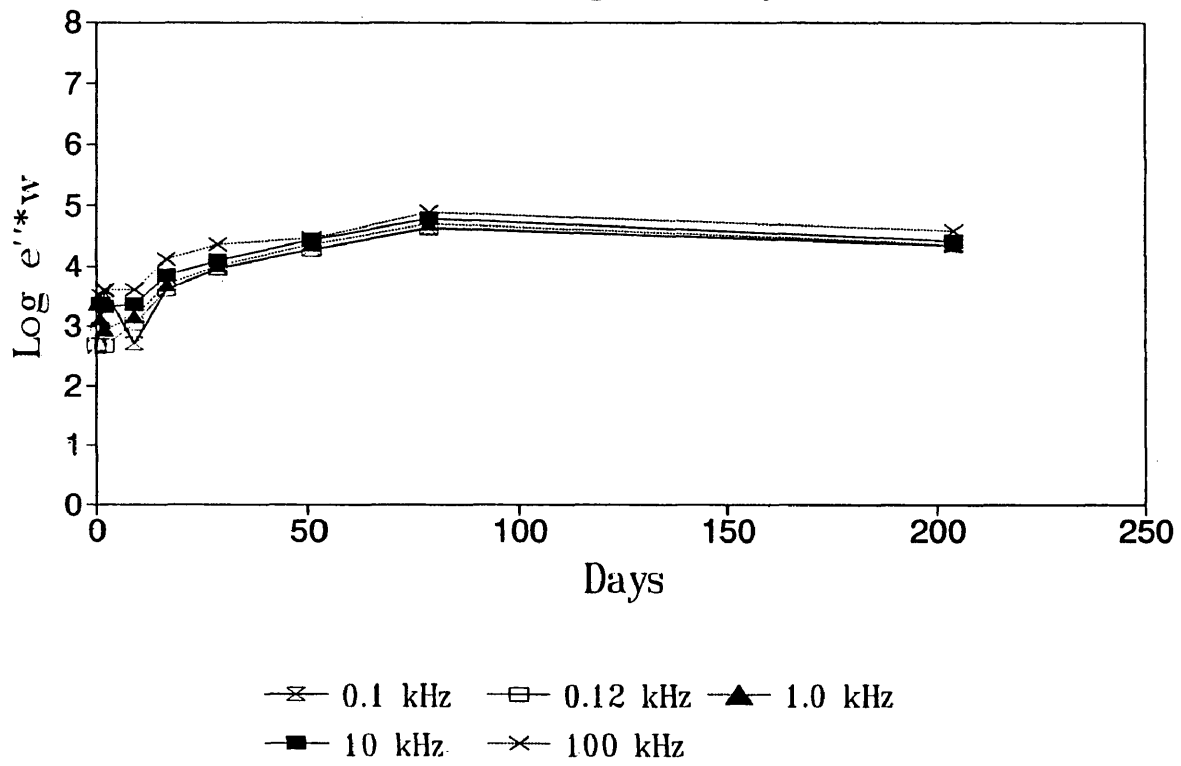
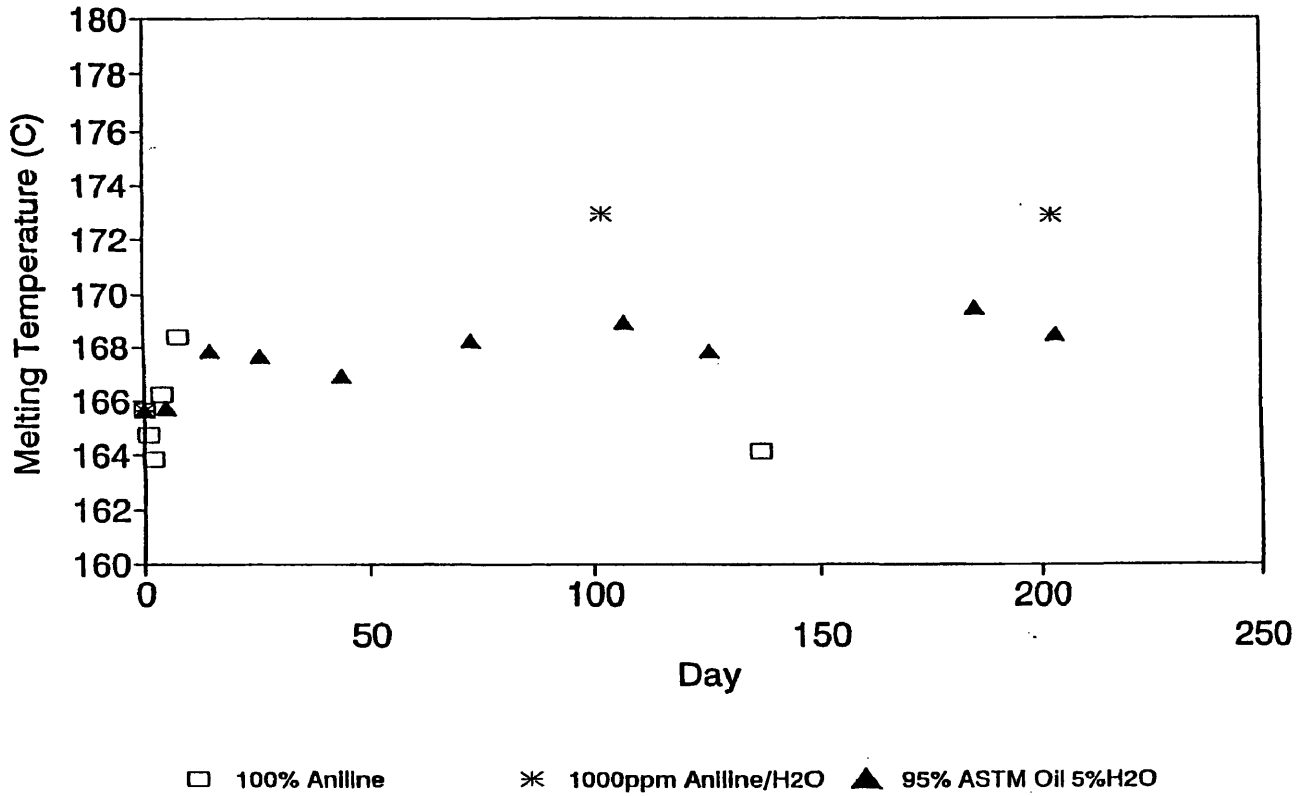


Figure [4.5]

Figure [4.6]

Melting Temperature vs Day Coflexip PVDF in Aniline & Oil at 130C



Melting Temperature vs Day Coflexip PVDF Environments at 130C

Figure [4.7]

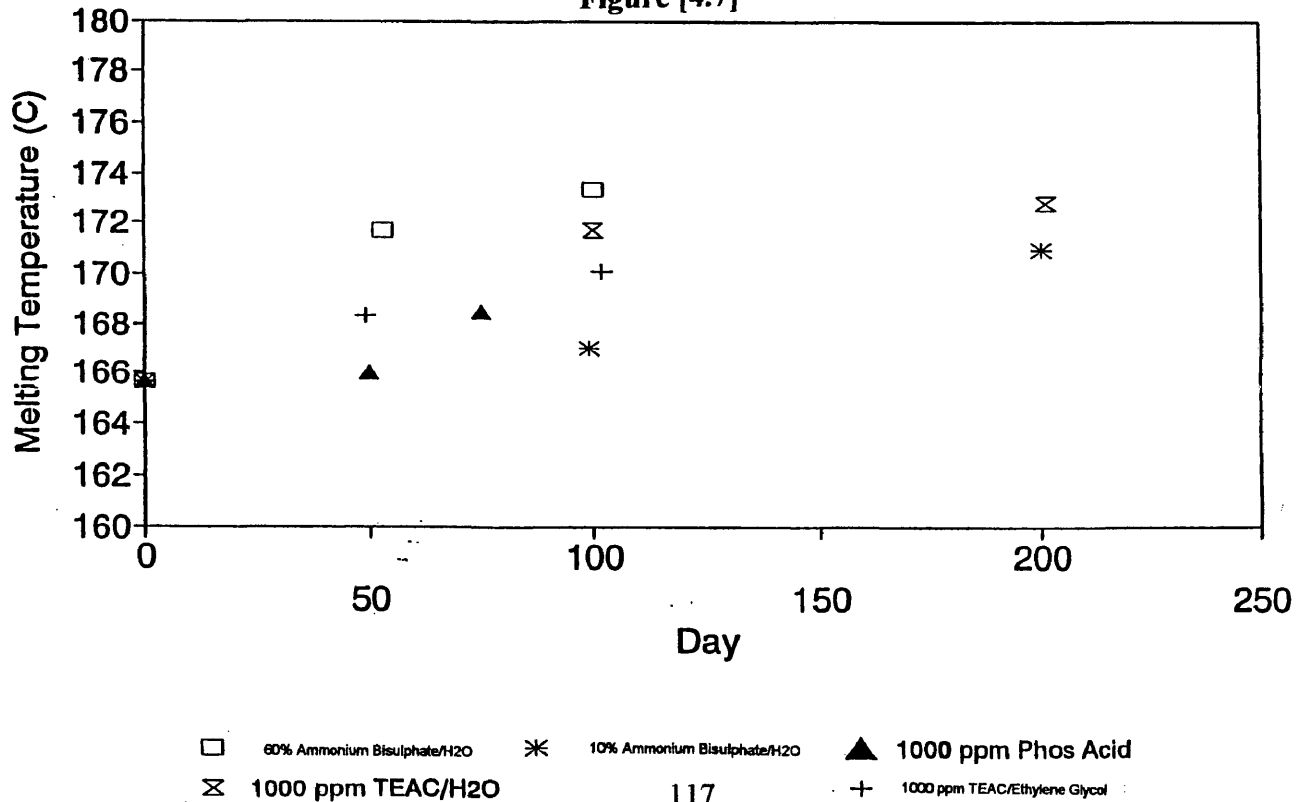
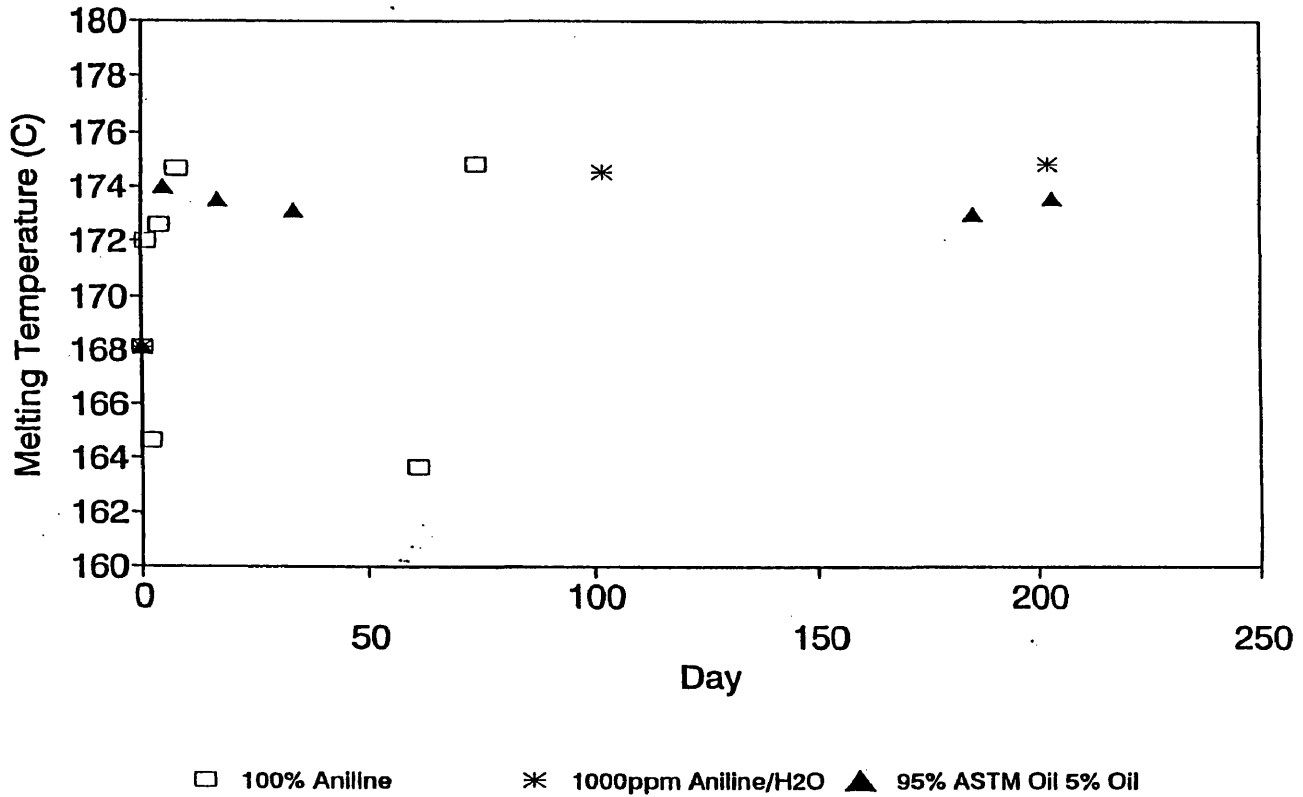


Figure [4.8]

Melting Temperature vs Day Wellstream PVDF in Aniline & Oil at 130



Melting Temperature vs Day Wellstream PVDF Environments 130C

Figure [4.9]

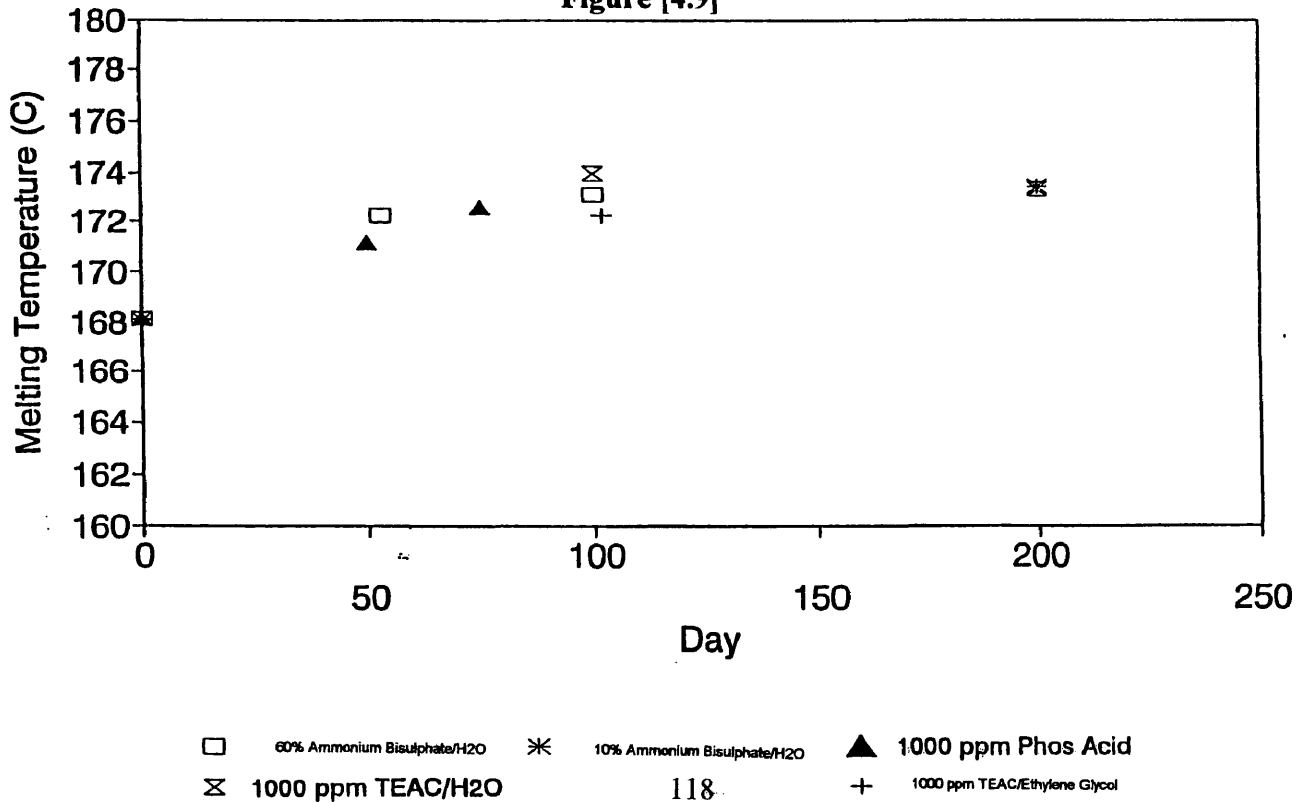
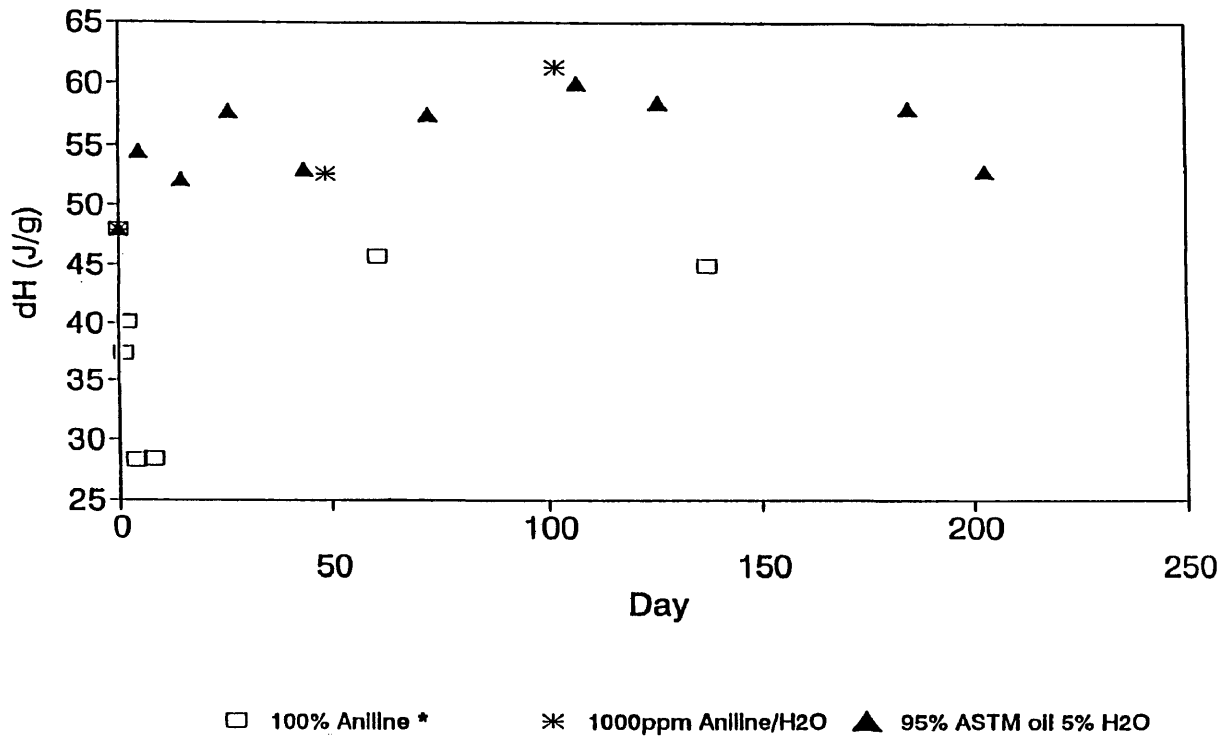


Figure [4.10]
dH vs Day
Coflexip PVDF in Aniline & Oil at 130C



dH vs Day
Coflexip PVDF Environments at 130C

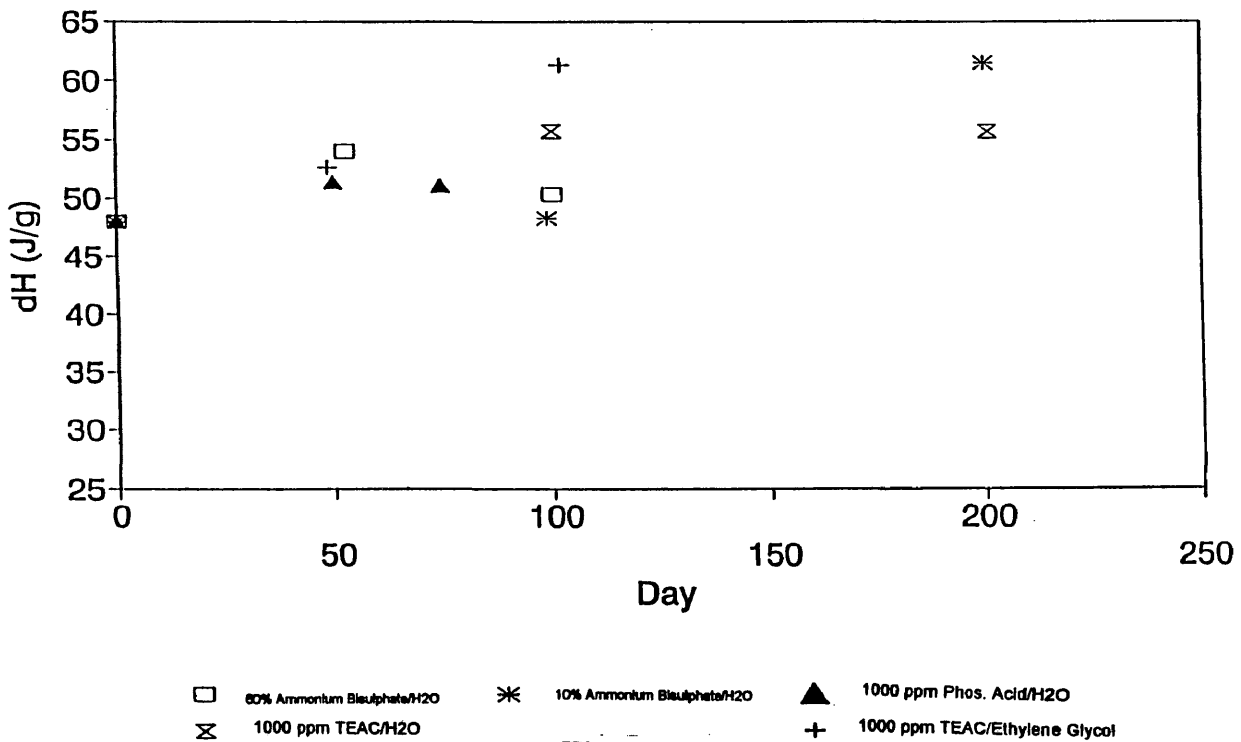
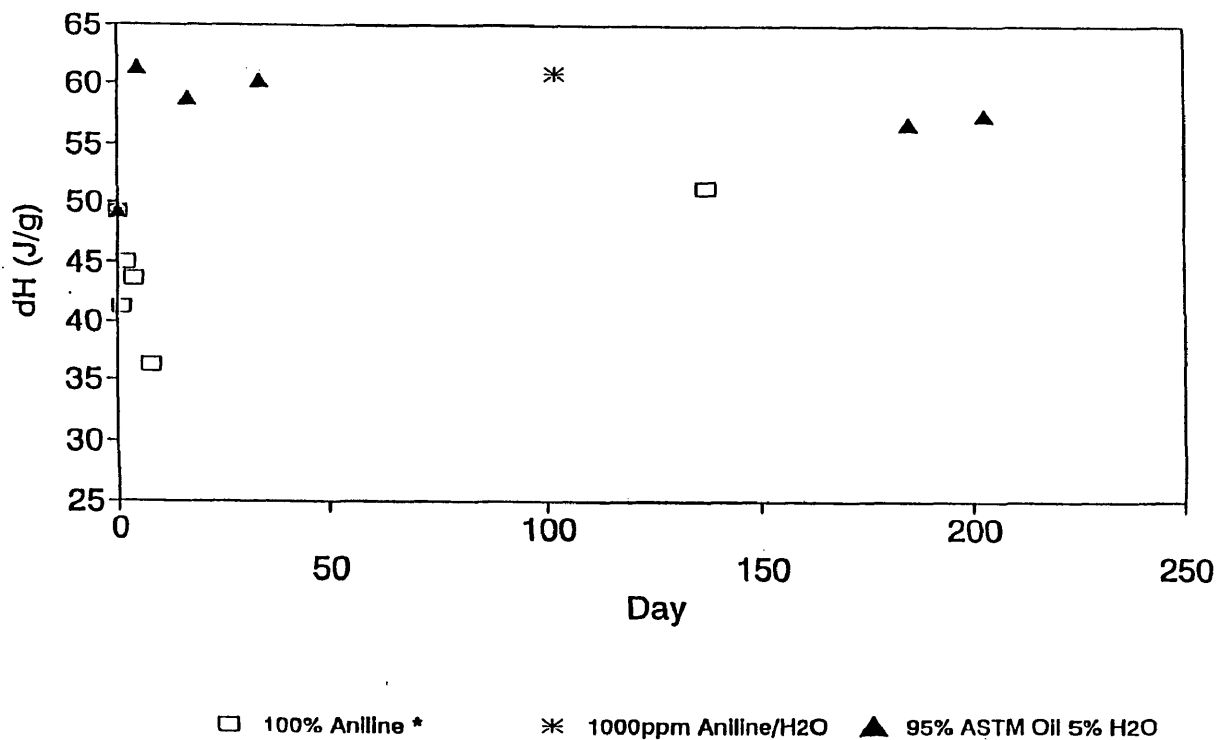


Figure [4.11]

Figure [4.12]
dH vs Day
 Wellstream PVDF in Aniline & Oil at 130



dH vs Day
 Wellstream PVDF Environments at 130C

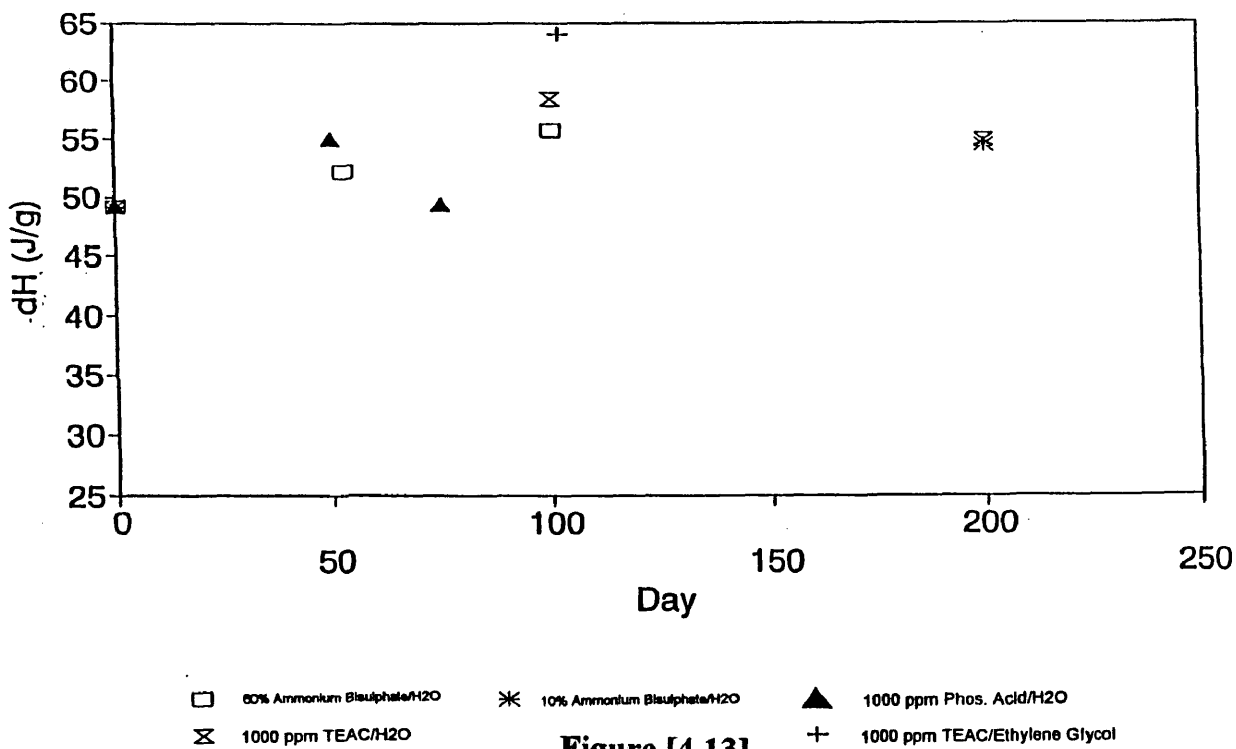


Figure [4.13]

Figure [4.14]

130C 95% ASTM Oil/5% H2O w/CO2

Wellstream PVDF, Melting Temp.

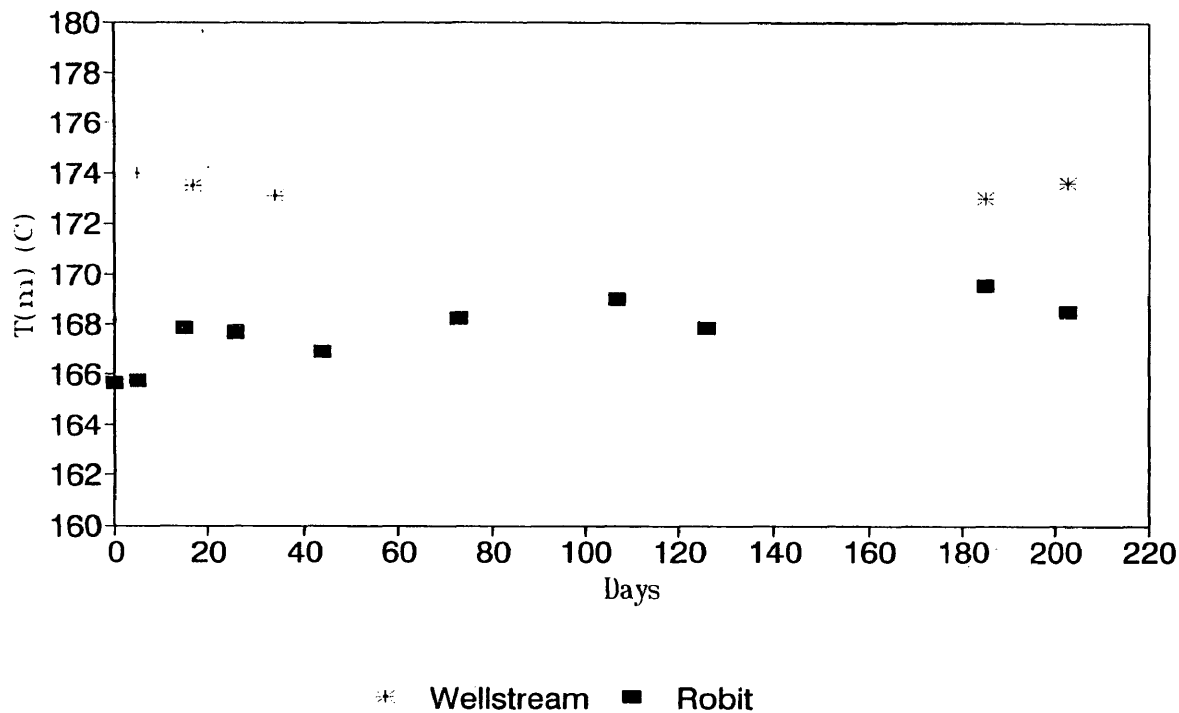


Figure [4.15]

130C 95% ASTM Oil/5% H2O w/CO2

Phase I Enthalpy vs Day

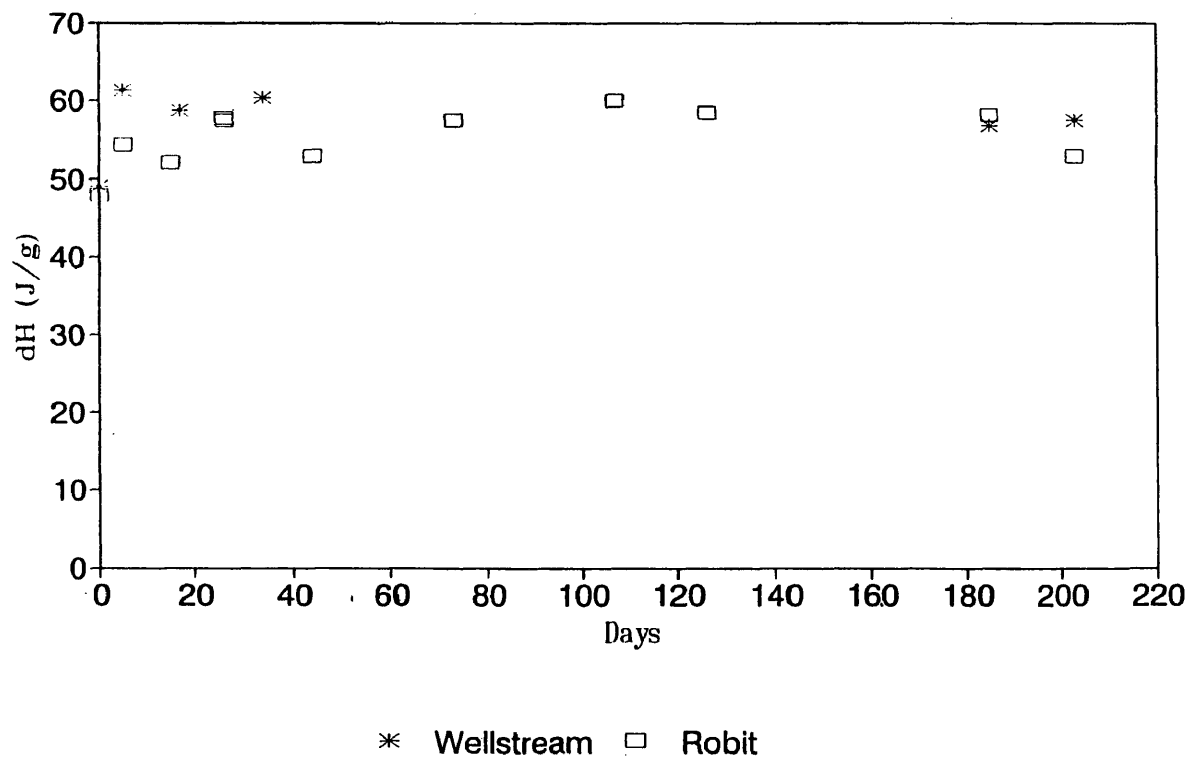


Figure [4.16]

Molecular Weight vs Day Coflexip PVDF in Aniline & Oil at 130C

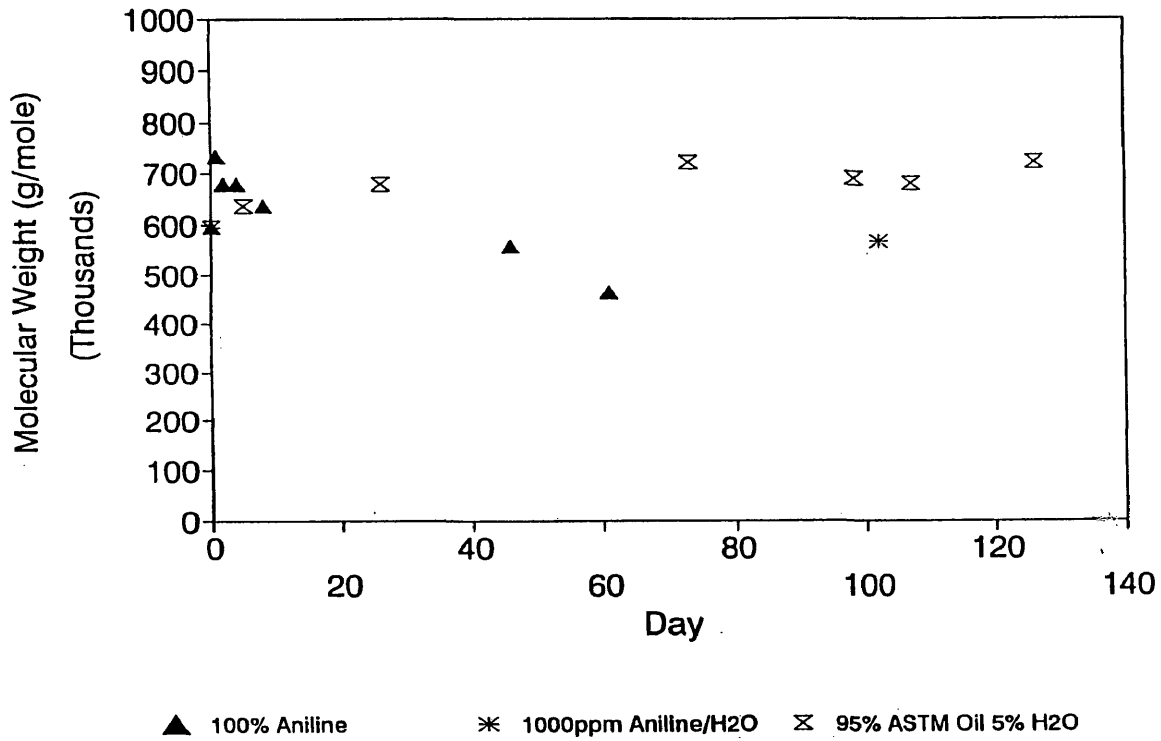


Figure [4.17]

Molecular Weight vs Day Wellstream PVDF in Aniline & Oil at 130

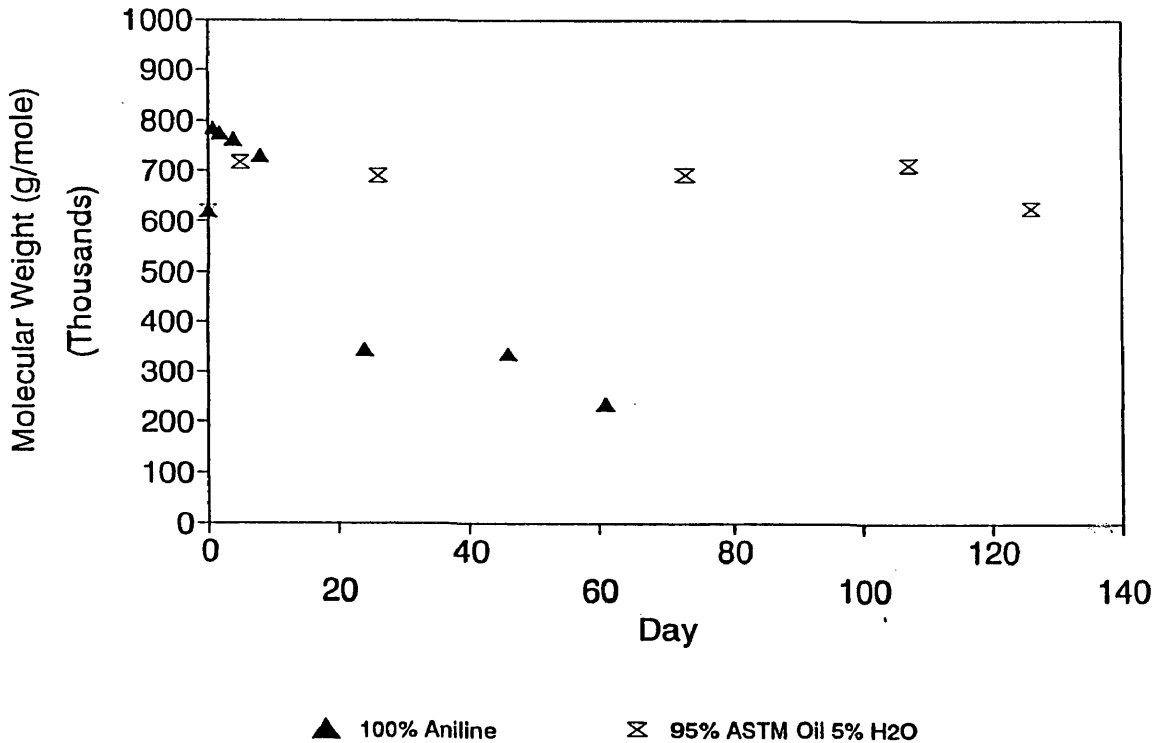


Figure [4.18]

Molecular Weight vs Day Coflexip PVDF Environments at 130C

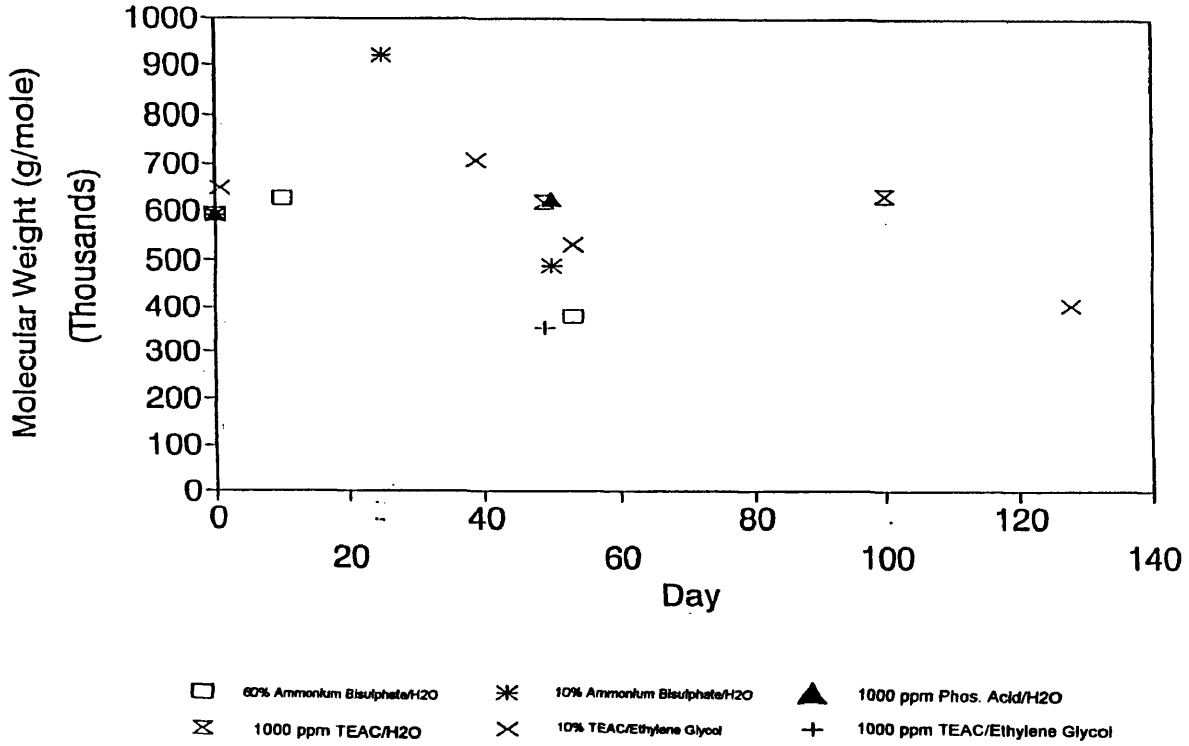
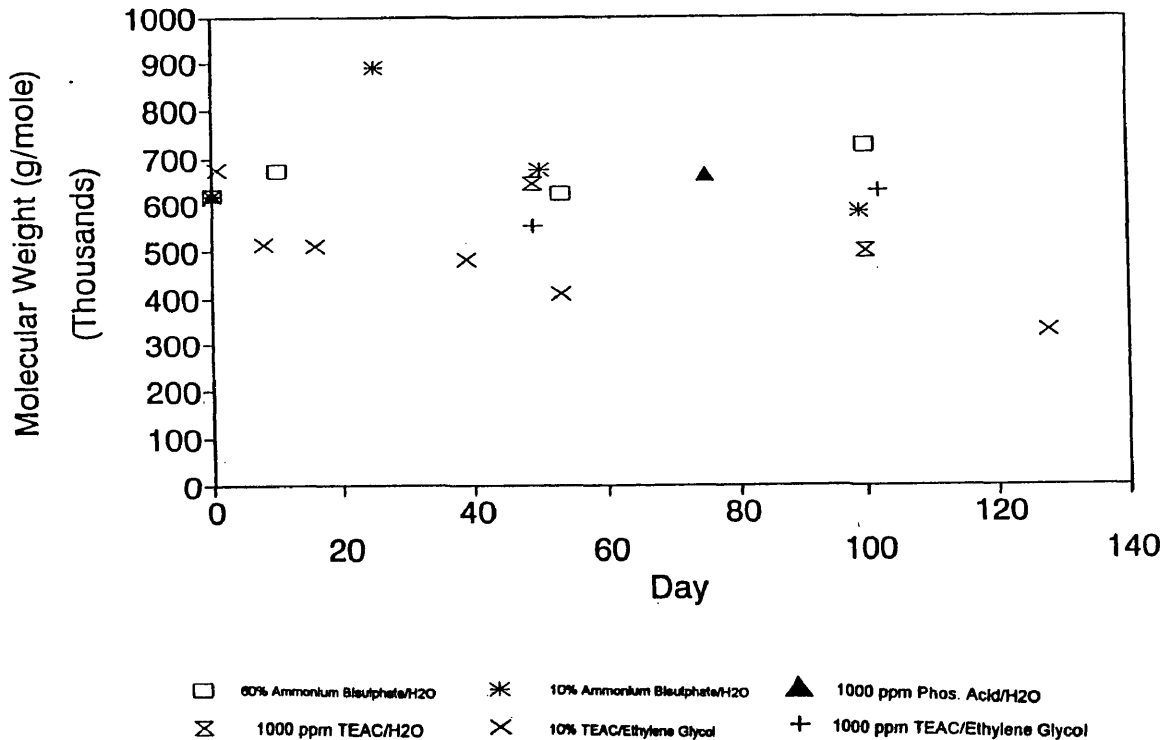


Figure [4.19]

Molecular Weight vs Day Wellstream PVDF Environments at 130C



130C 95% ASTM Oil/5% H2O w/CO2

MW vs Day

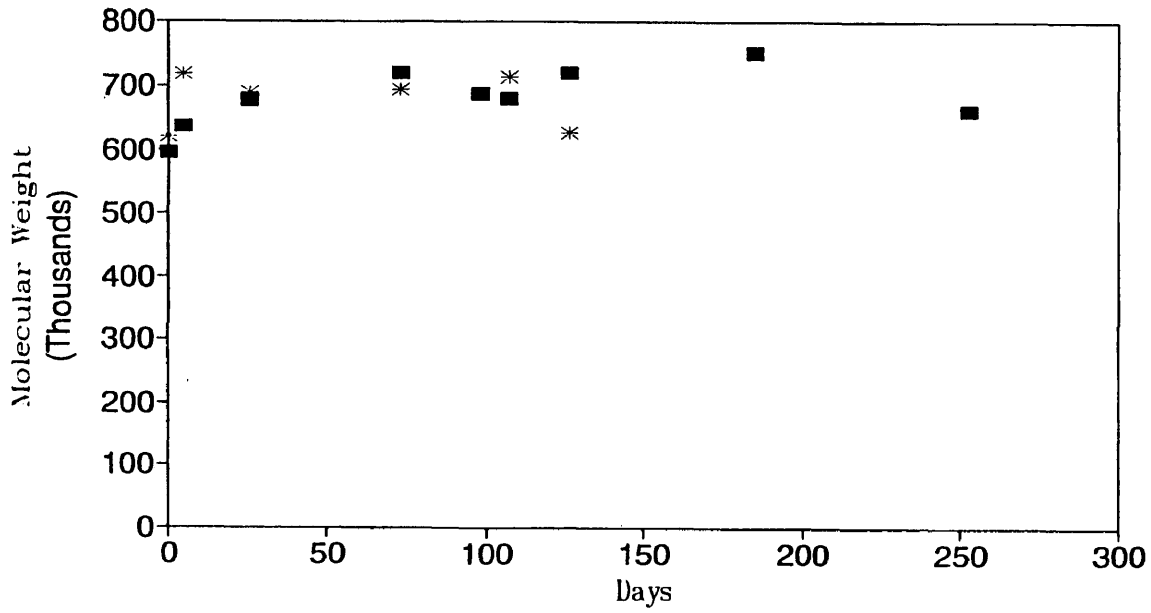


Figure [4.20] * Wellstream ■ Robit

Load vs Day

Coflexip PVDF in 95% ASTM 5% H2O at 130

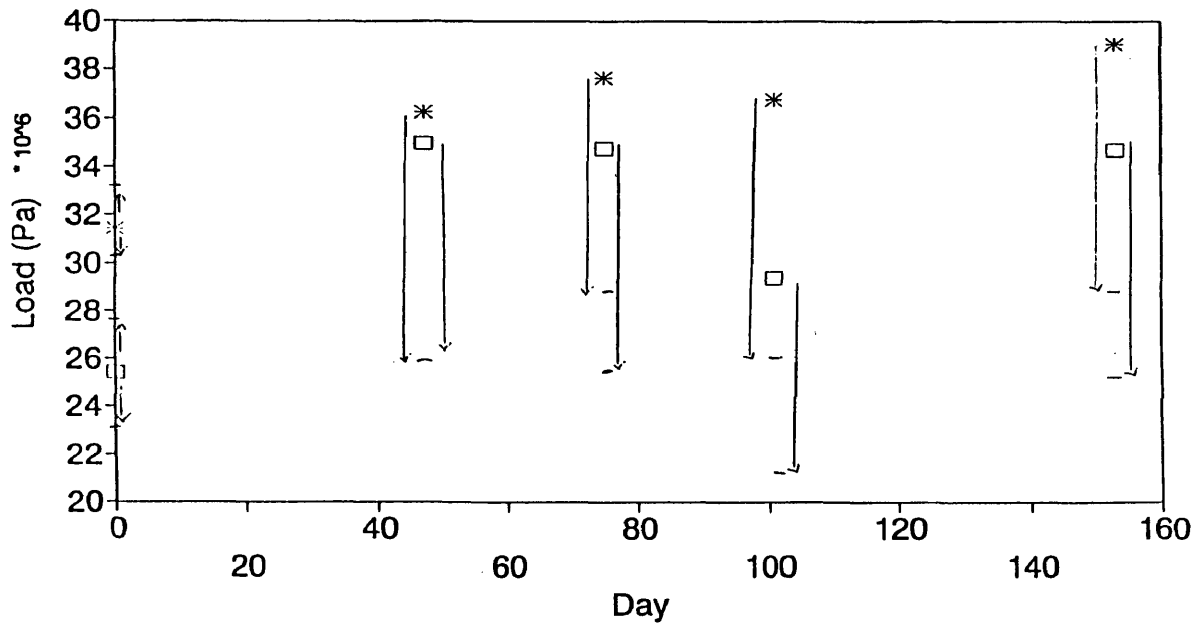


Figure [4.21] □ Load at Break * Load at Peak

Figure [4.22]

Load vs Day Coflexip PVDF in 100% Aniline at 130C

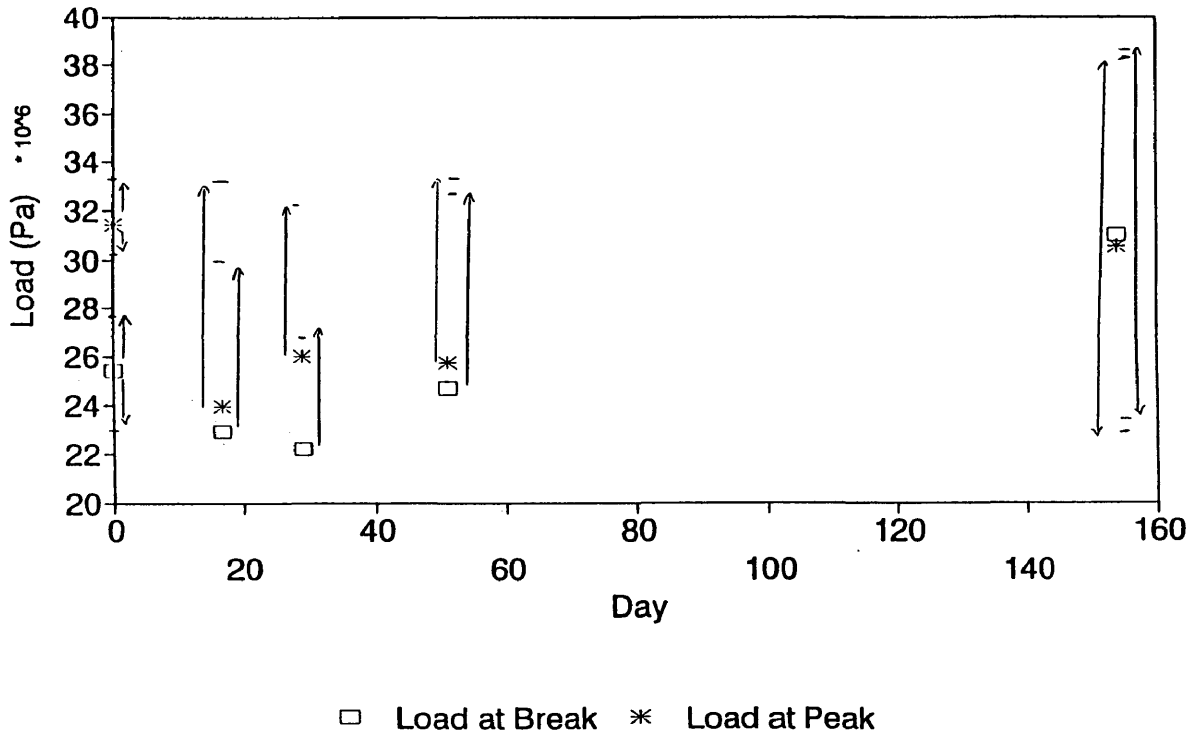
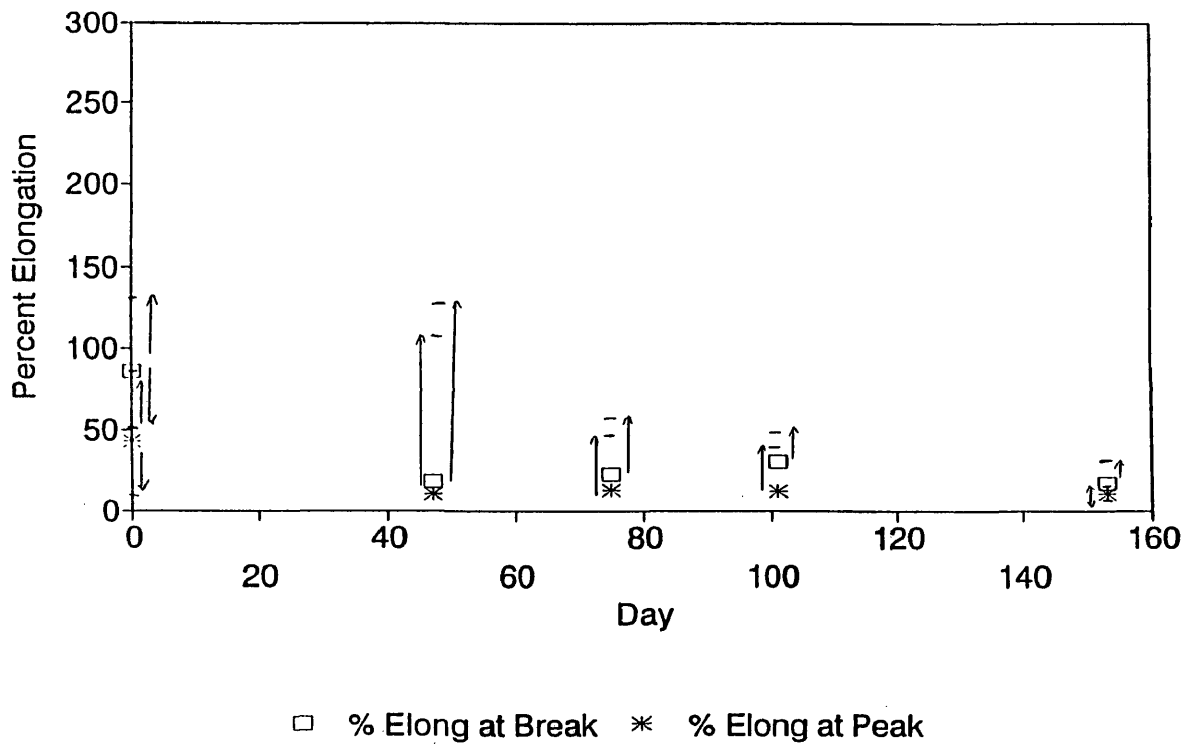


Figure [4.23]

Percent Elongation vs Day Coflexip PVDF in 95% ASTM 5% H₂O at 130



Percent Elongation vs Day Coflexip PVDF in 100% Aniline at 130C

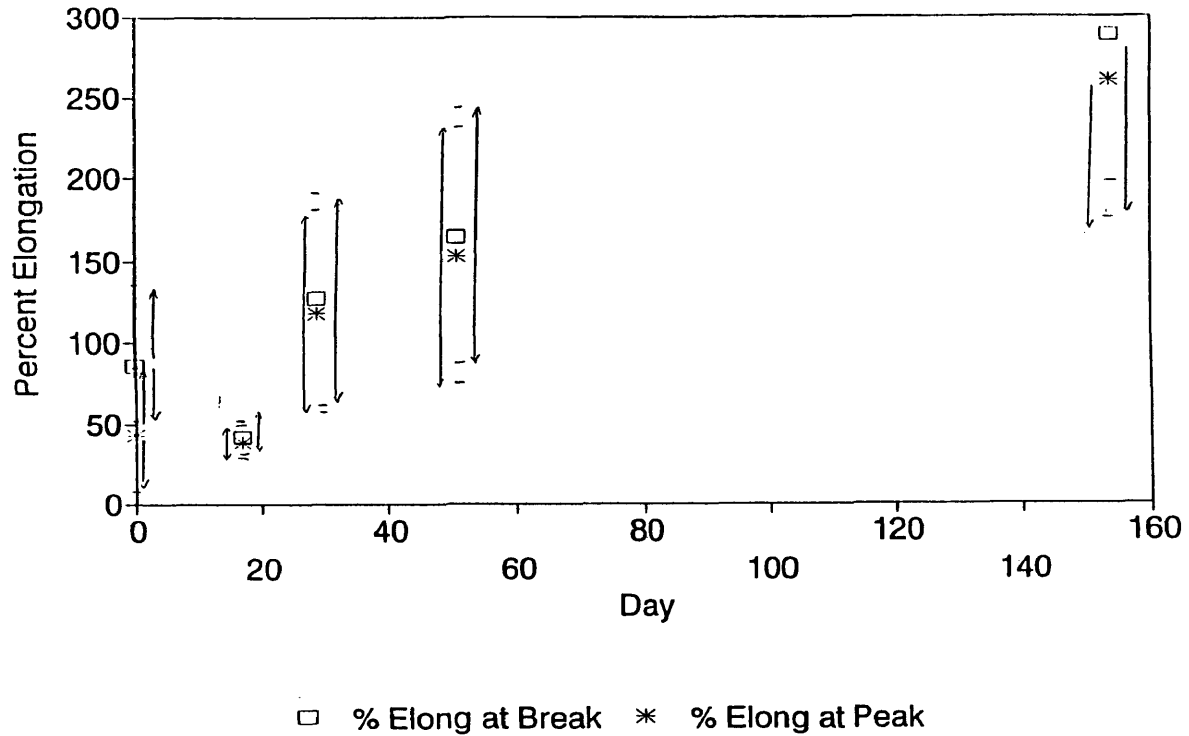


Figure [4.24]

Percent Change in Mass vs Day Coflexip PVDF in Aniline & Oil 130C

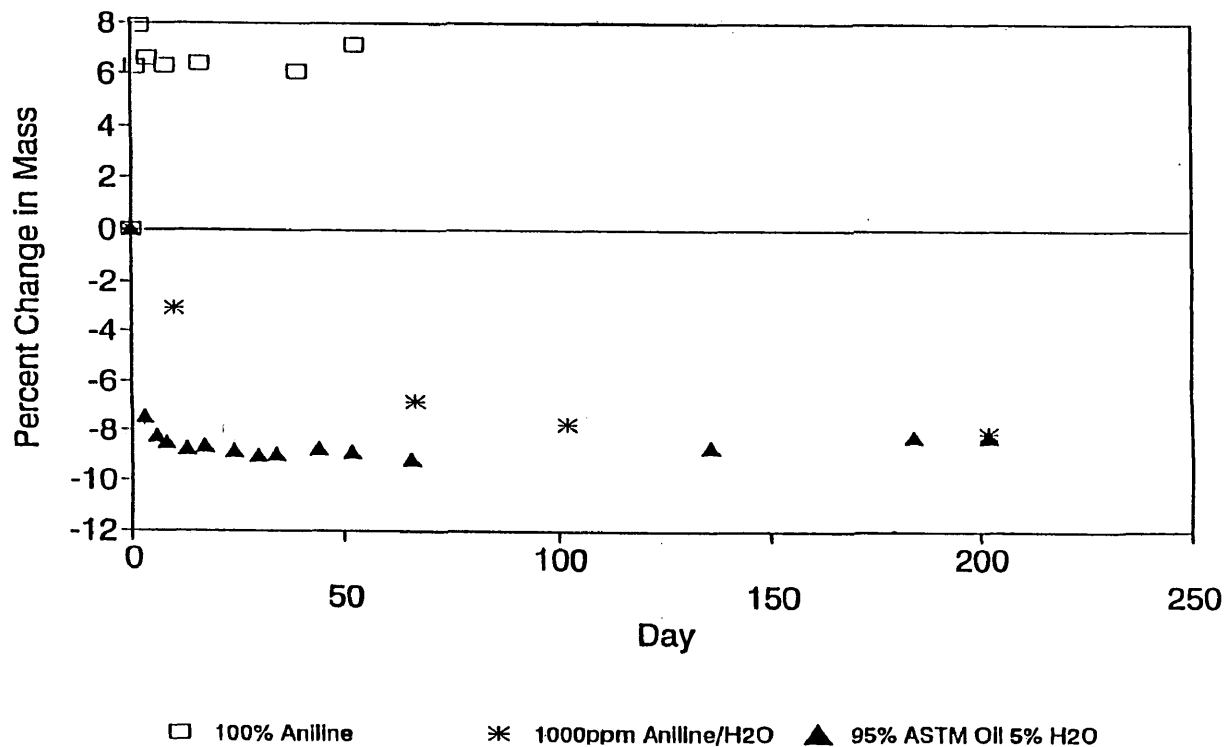
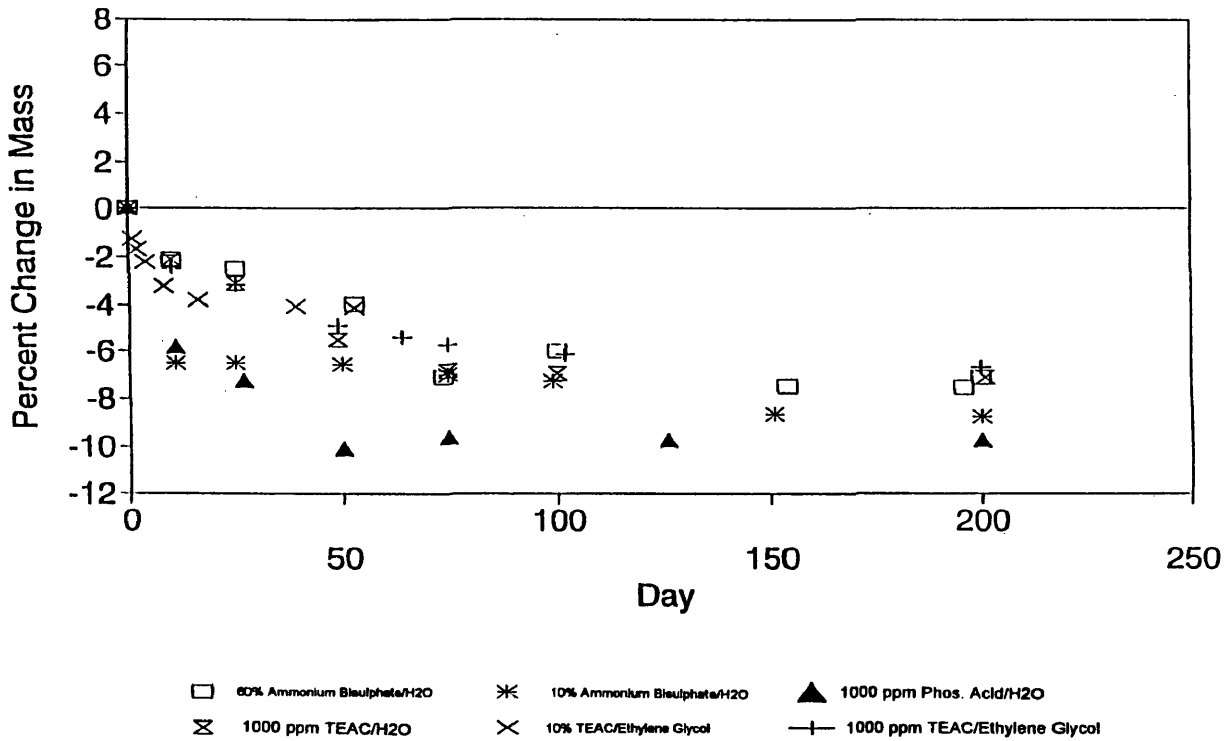


Figure [4.25]

Figure [4.26]

Percent Change in Mass vs Day Coflexip PVDF Environments at 130C



Percent Change in Mass vs Day Wellstream PVDF in Aniline & Oil at 130

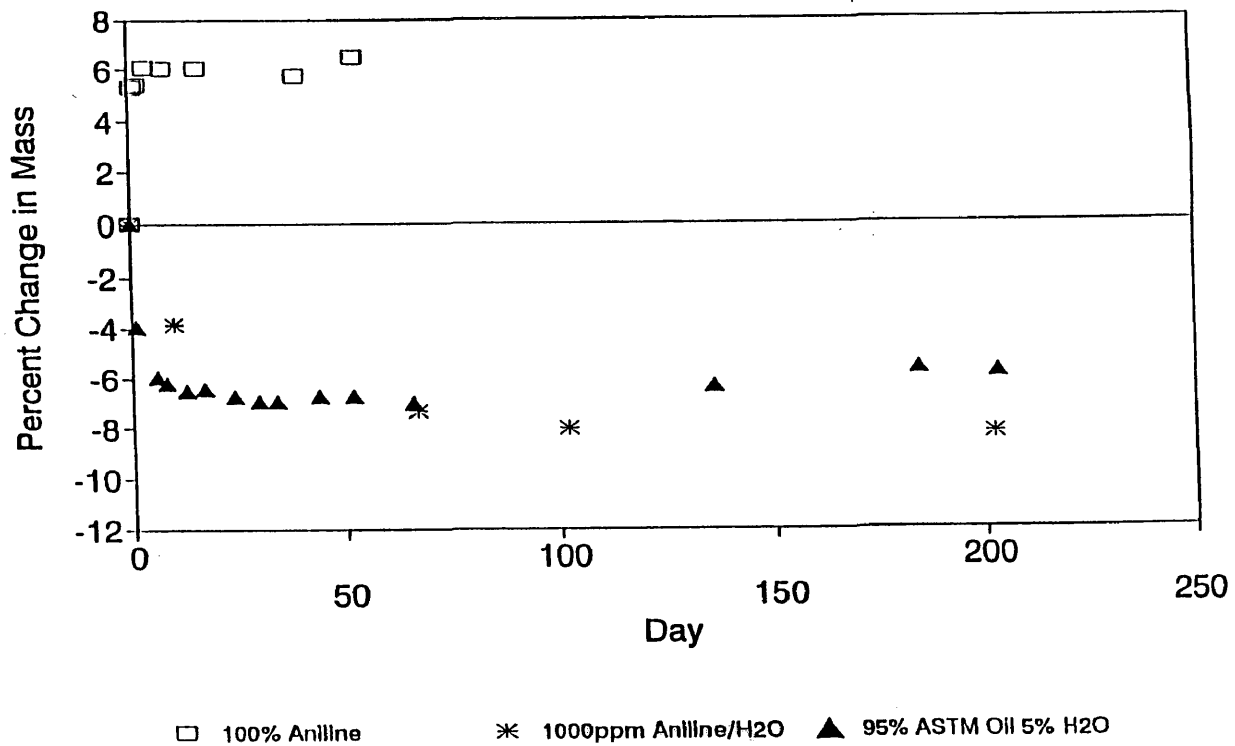


Figure [4.27]

Figure [4.30] Percent Change in Thickness vs Day
Coflexip PVDF Environments at 130C

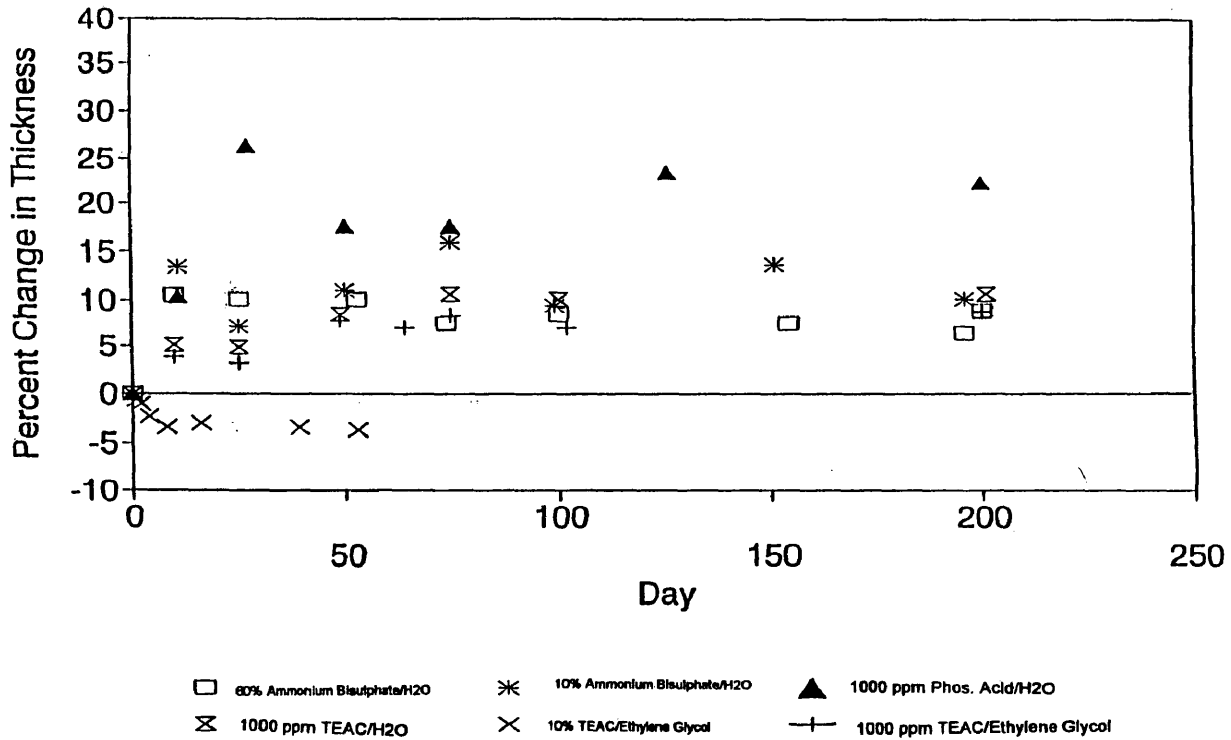


Figure [4.31] Percent Change in Thickness vs Day
Wellstream PVDF in Aniline & Oil at 130

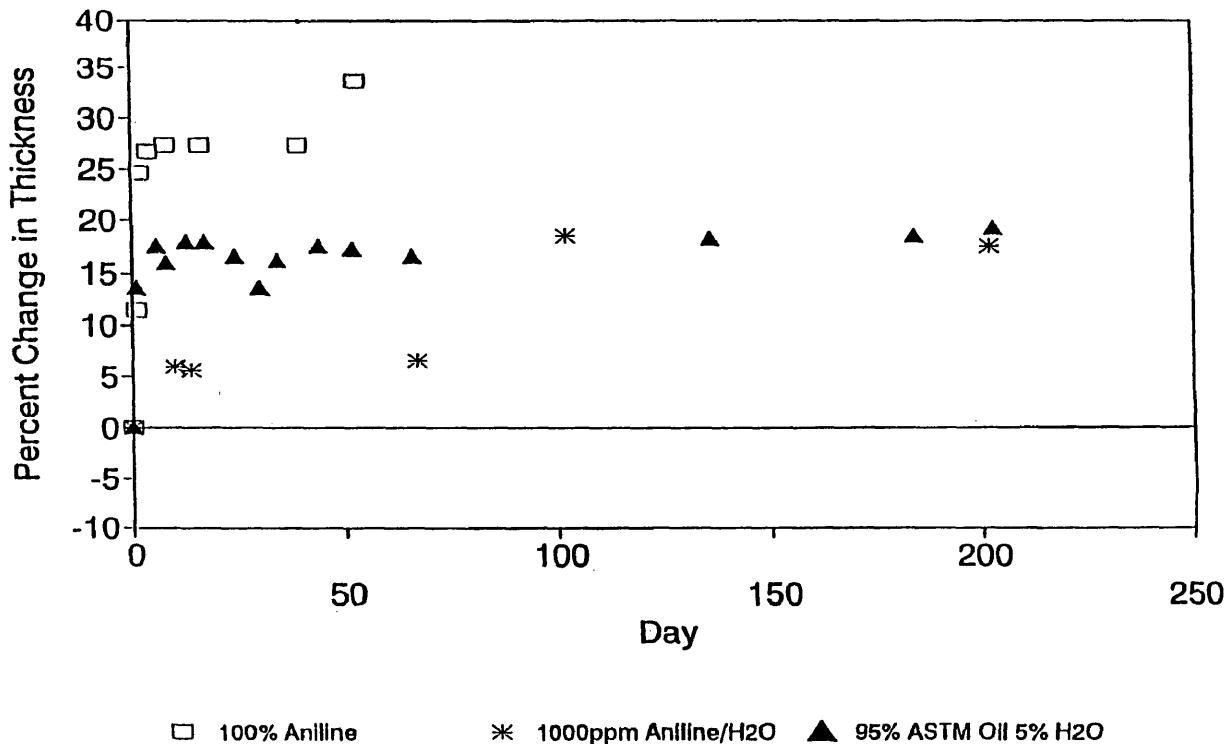


Figure [4.32] Percent Change in Thickness vs Day
Wellstream PVDF Environments at 130C

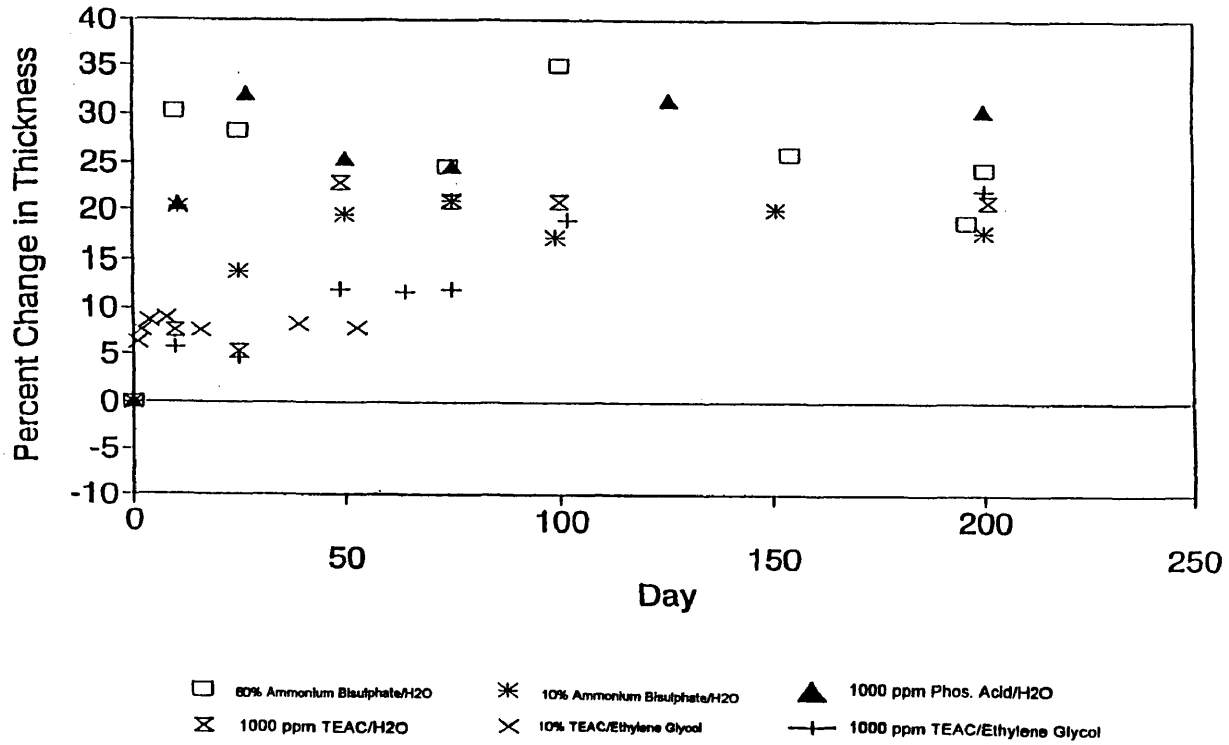
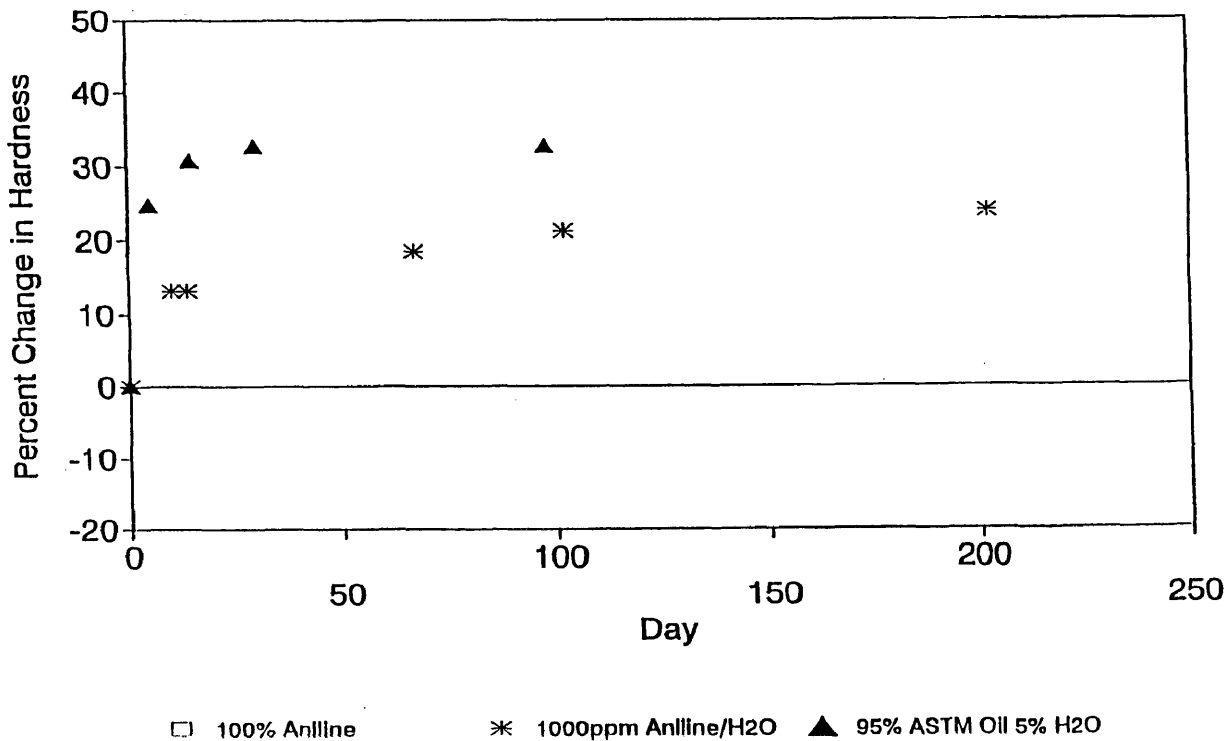


Figure [4.33] Percent Change in Hardness vs Day
Coflexip PVDF in Aniline & Oil at 130C



Percent Change in Hardness vs Day Coflexip PVDF Environments at 130C

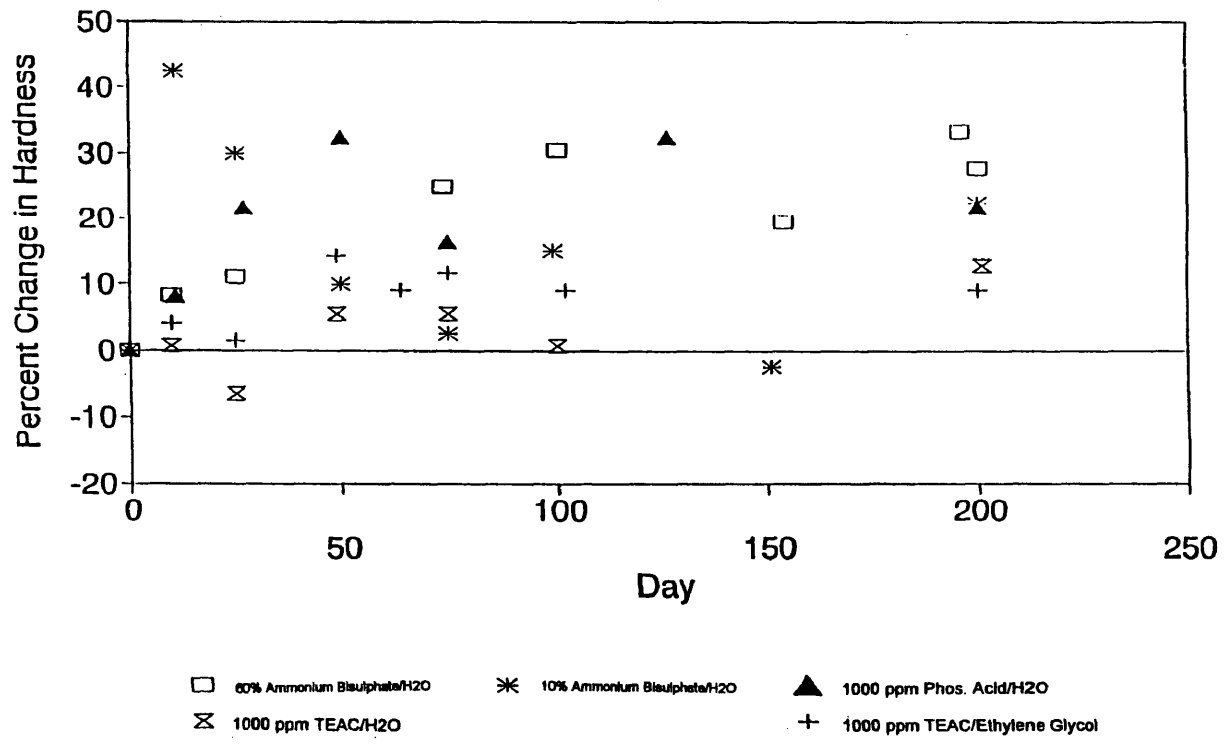
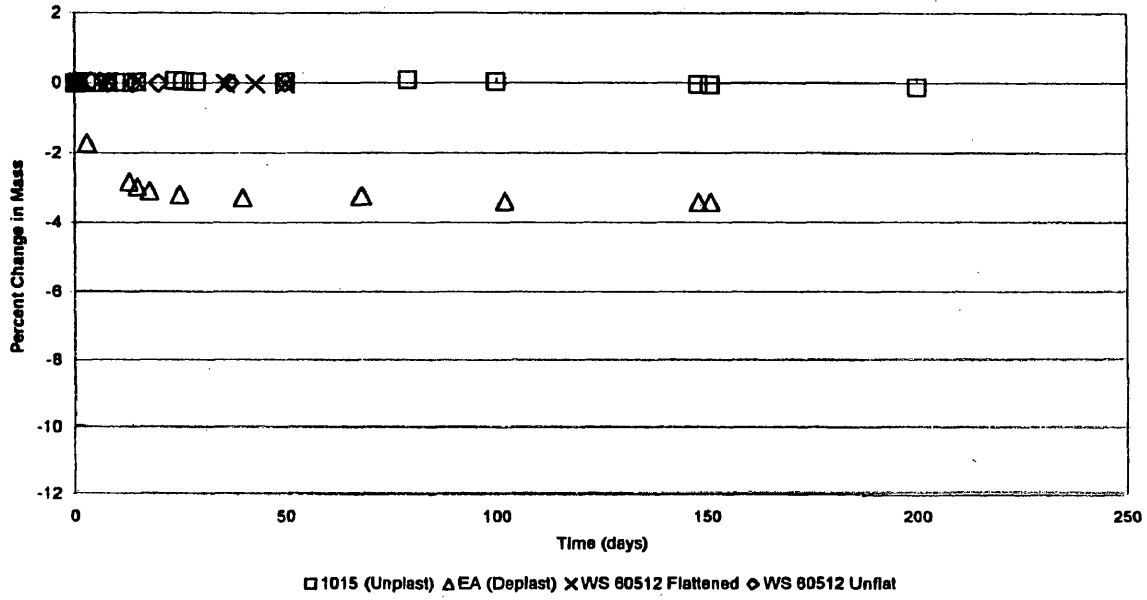


Figure [4.34]

PVDF Phase II In 130C Air Oven
 Non-Plasticized Samples
 Change in Mass vs Day

Figure [4.35]



PVDF Phase II In 130C Air Oven
 Plasticized Samples
 Change in Mass vs Day

Figure [4.36]

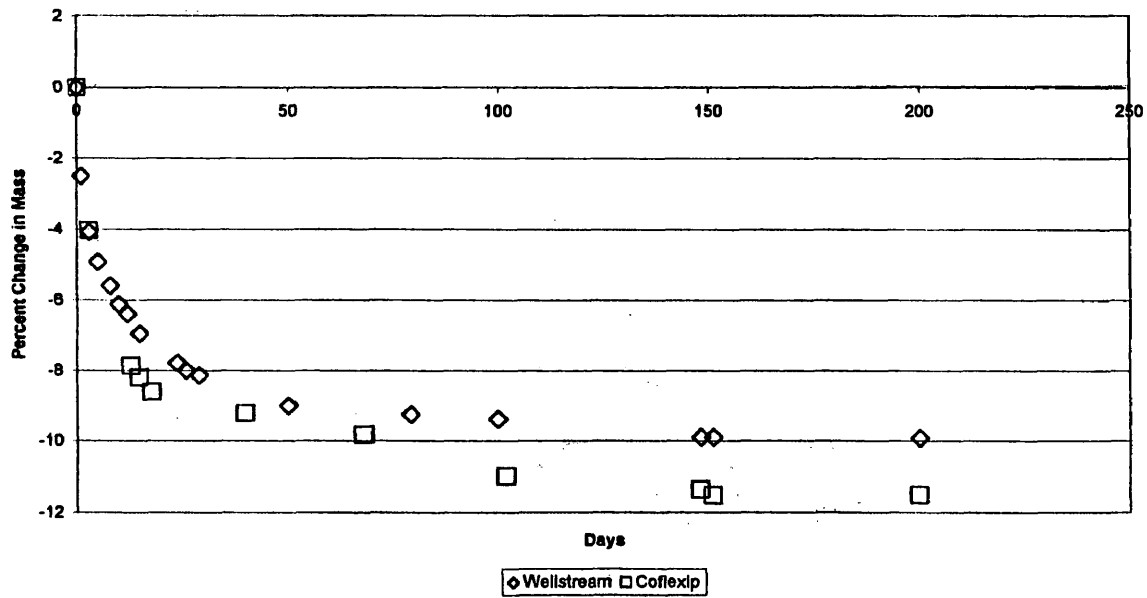


Figure [4.37]

**PVDF Phase II in 130C Oil Pot
Plasticized Samples
Change In Mass vs Day**

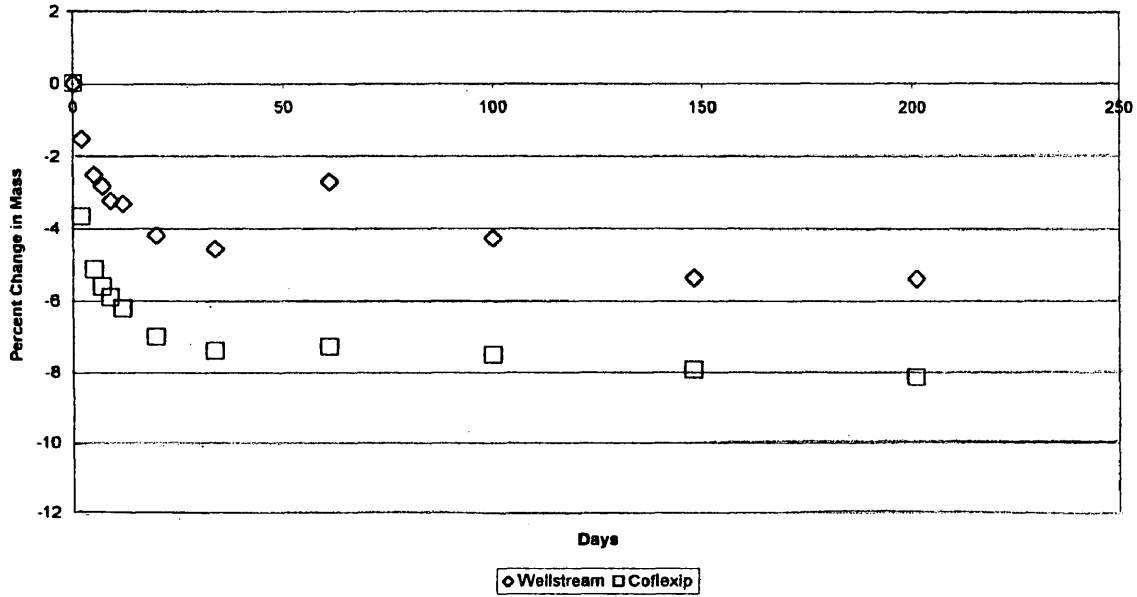
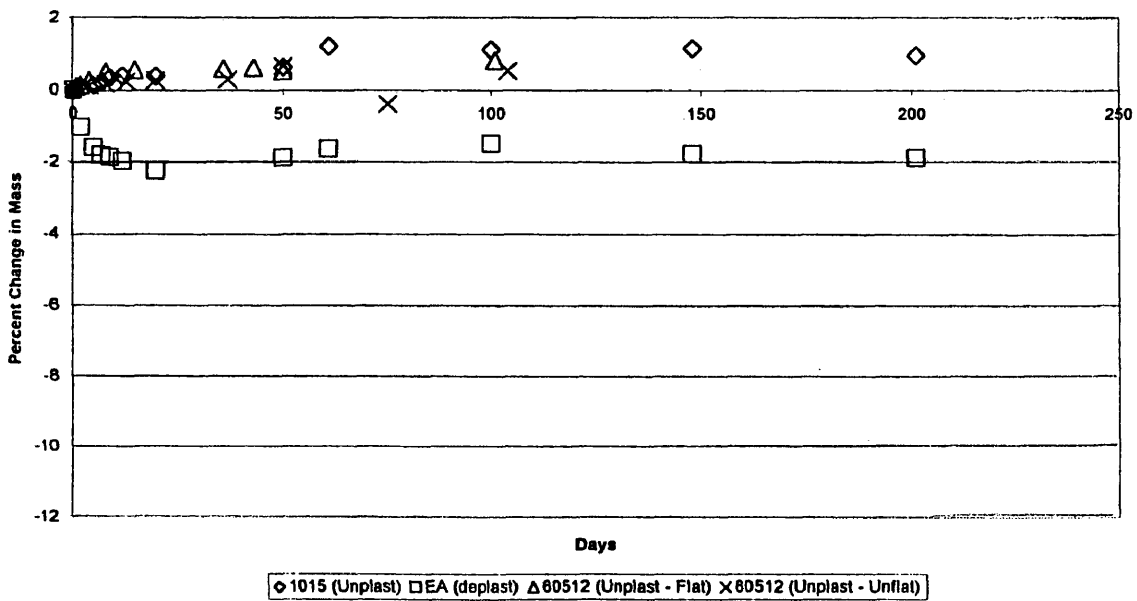
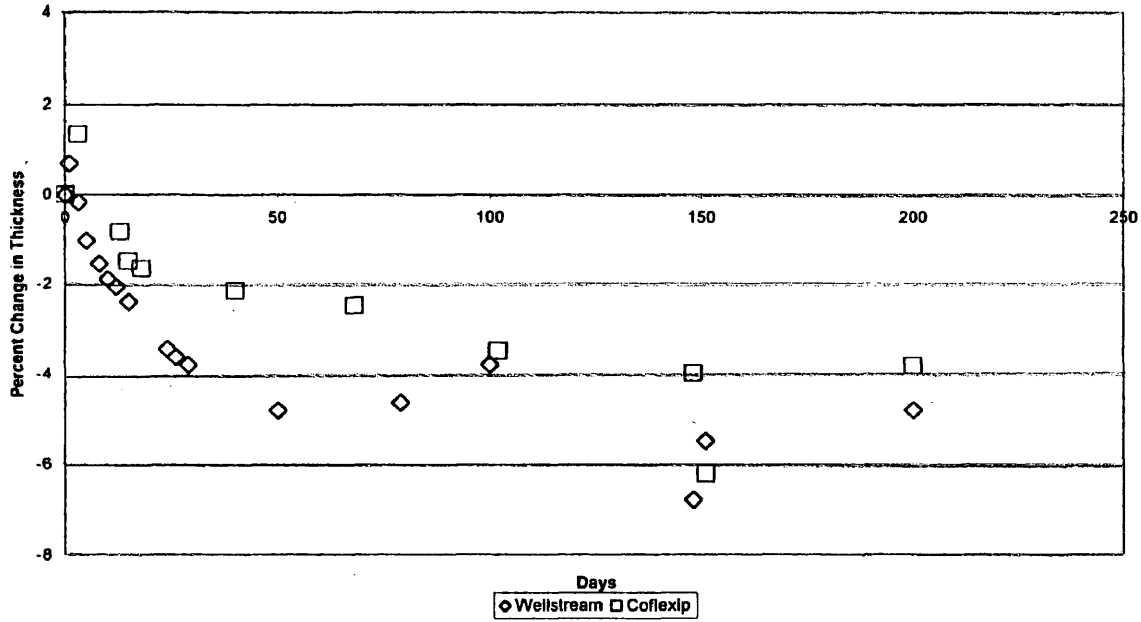


Figure [4.38]

**PVDF Phase II in 130C Oil Pot
Non-Plasticized Samples
Percent Change in Mass vs Day**



**Figure [4.39] PVDF Phase II in 130C Air Oven
Plasticized Samples
Change in Thickness vs Day**



**Figure [4.40] PVDF Phase II in 130C Air Oven
Non-Plasticized Samples
Change in Thickness vs Day**

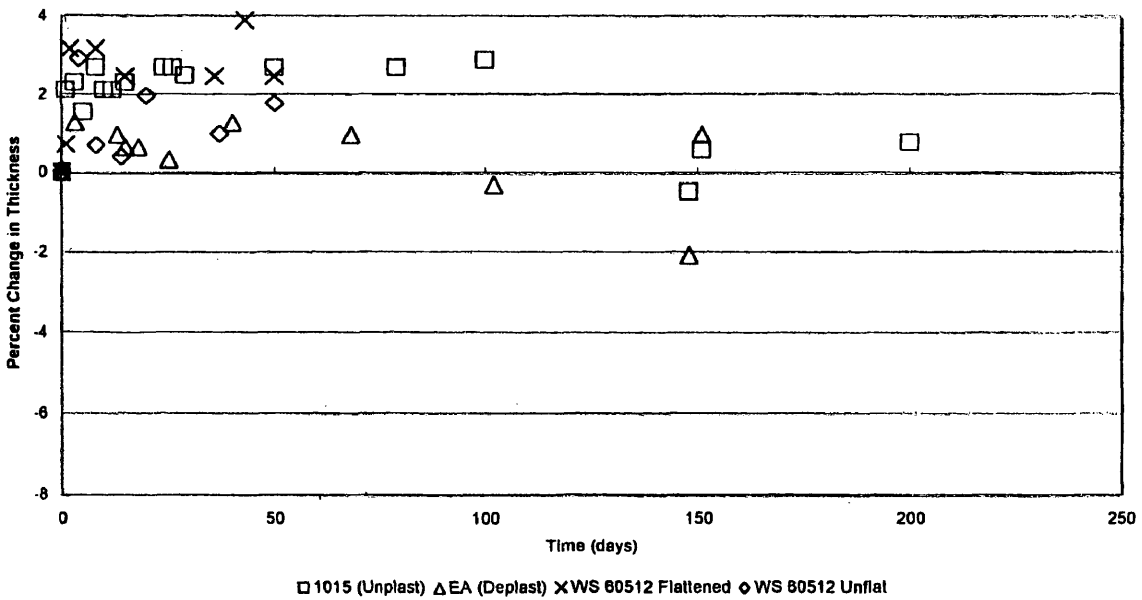


Figure [4.41]

PVDF Phase II In 130C Oil Pot
Plasticized Samples
Percent Change in Thickness vs Day

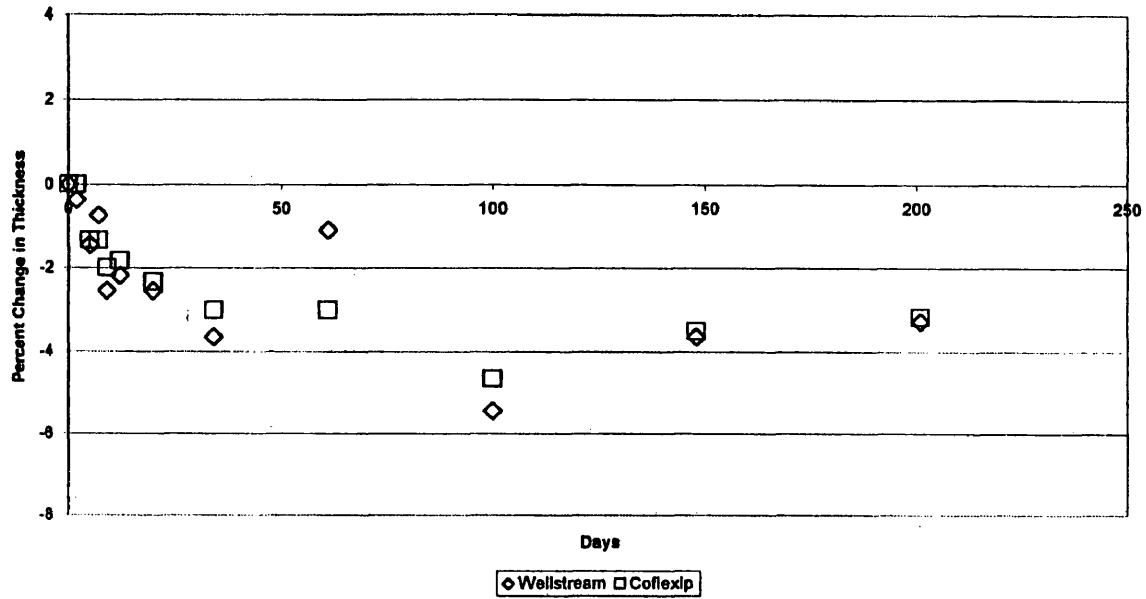


Figure [4.42]

PVDF Phase II In 130C Oil Pot
Non-Plasticized Samples
Percent Change in Thickness vs Day

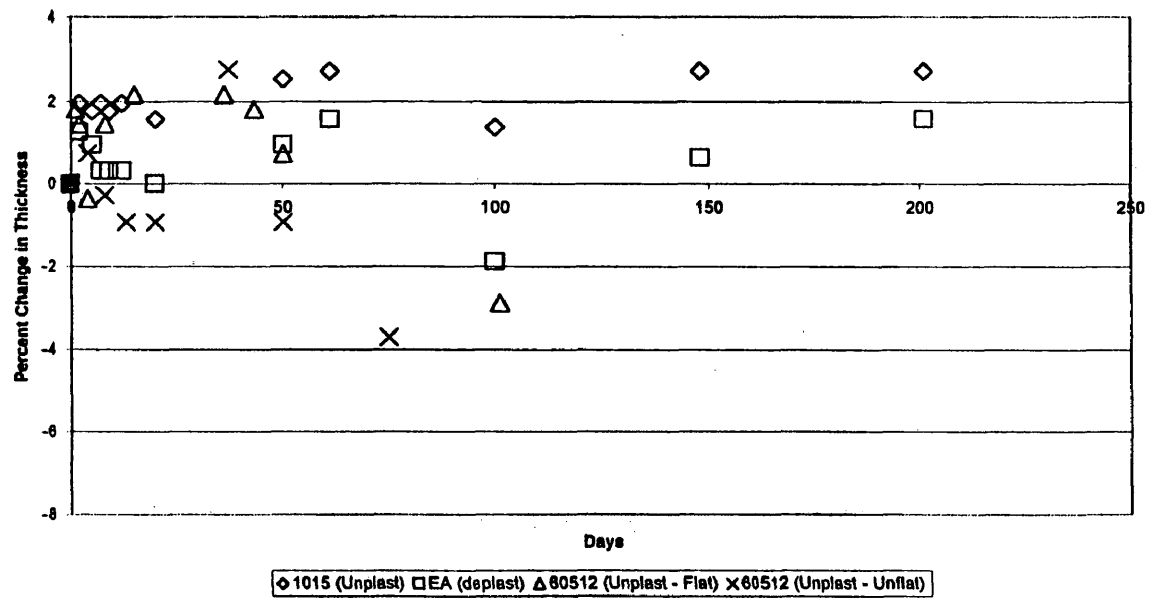
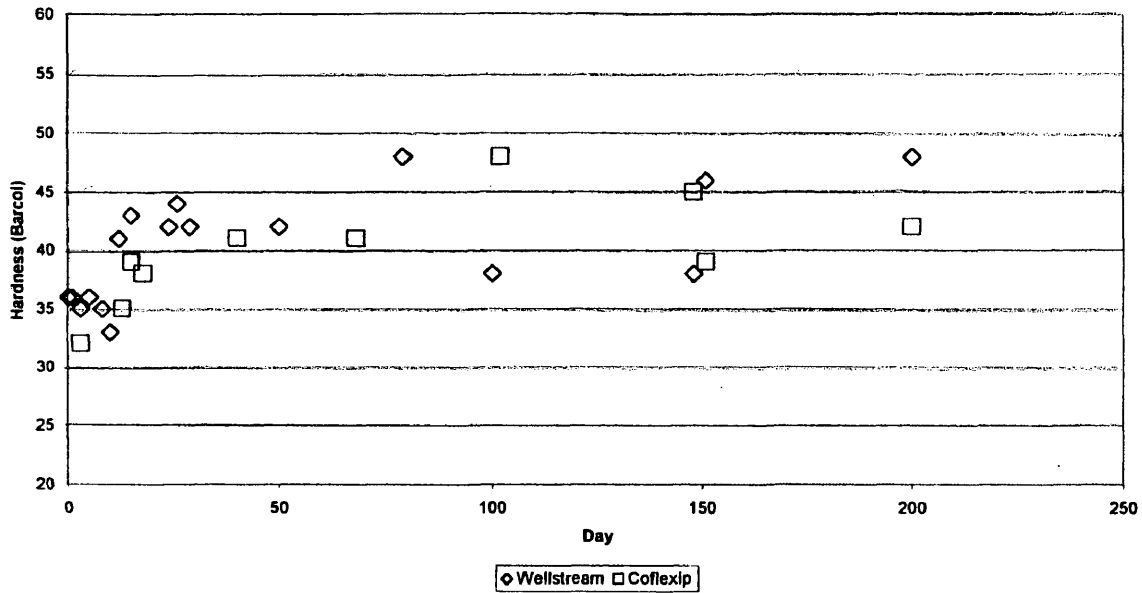


Figure [4.43]

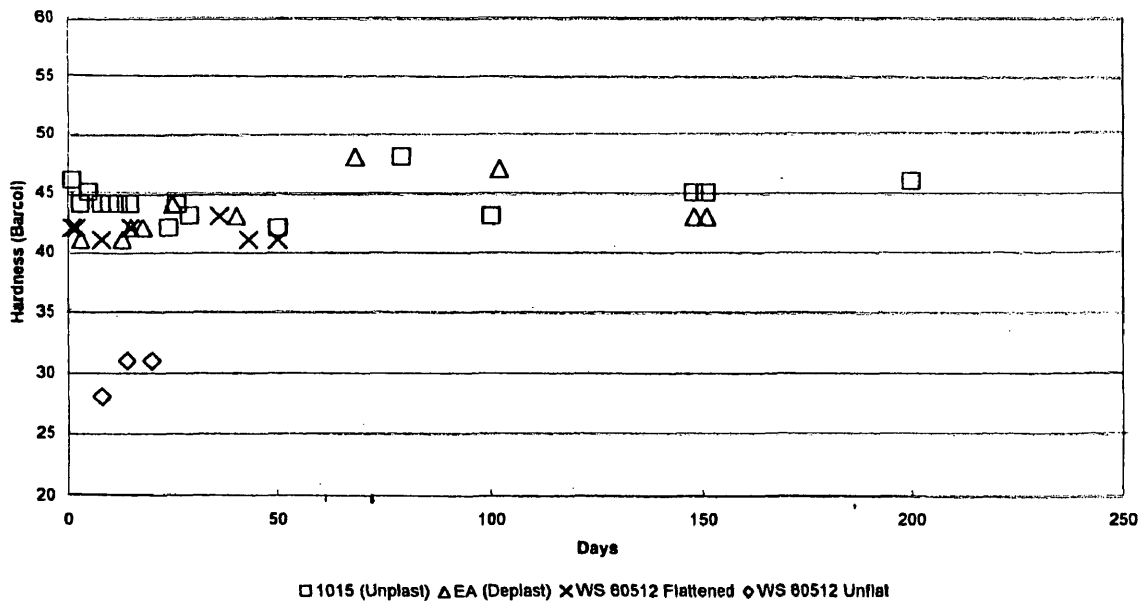
**PVDF Phase II in 130C Air Oven
Plasticized Samples
Hardness vs Day**



Compare Hard Air Unplast

Figure [4.44]

**PVDF Phase II in 130C Air Oven
Non-Plasticized Samples
Hardness vs Day**



**PVDF Phase II in 130C Oil Pot
Plasticized Samples
Hardness vs Day**

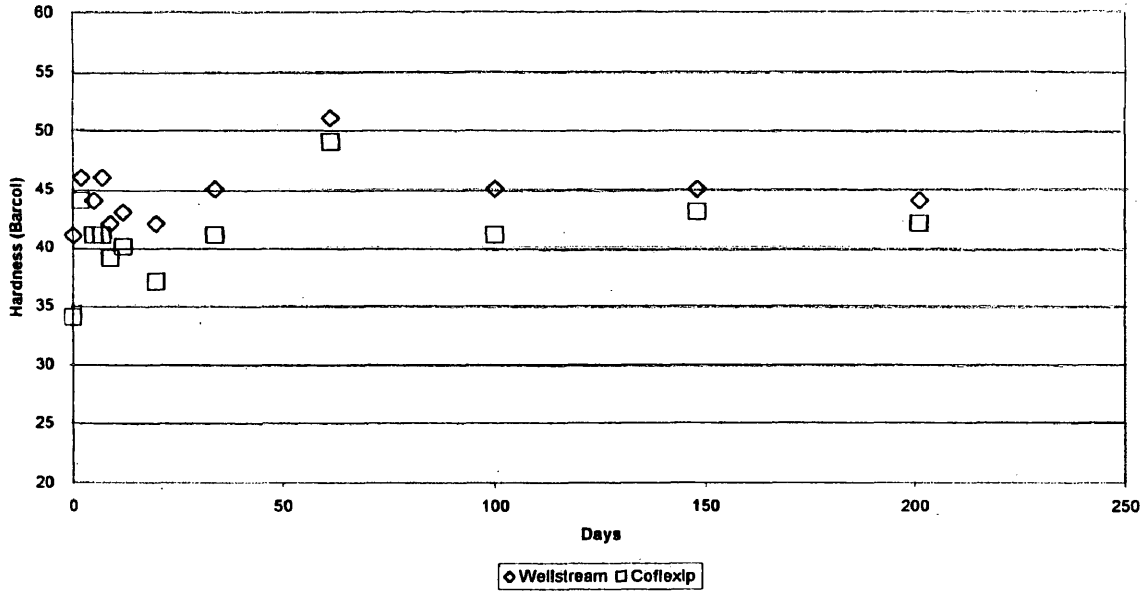


Figure [4.45]

**PVDF Phase II in 130C Oil Pot
Non-Plasticized Samples
Hardness vs Day**

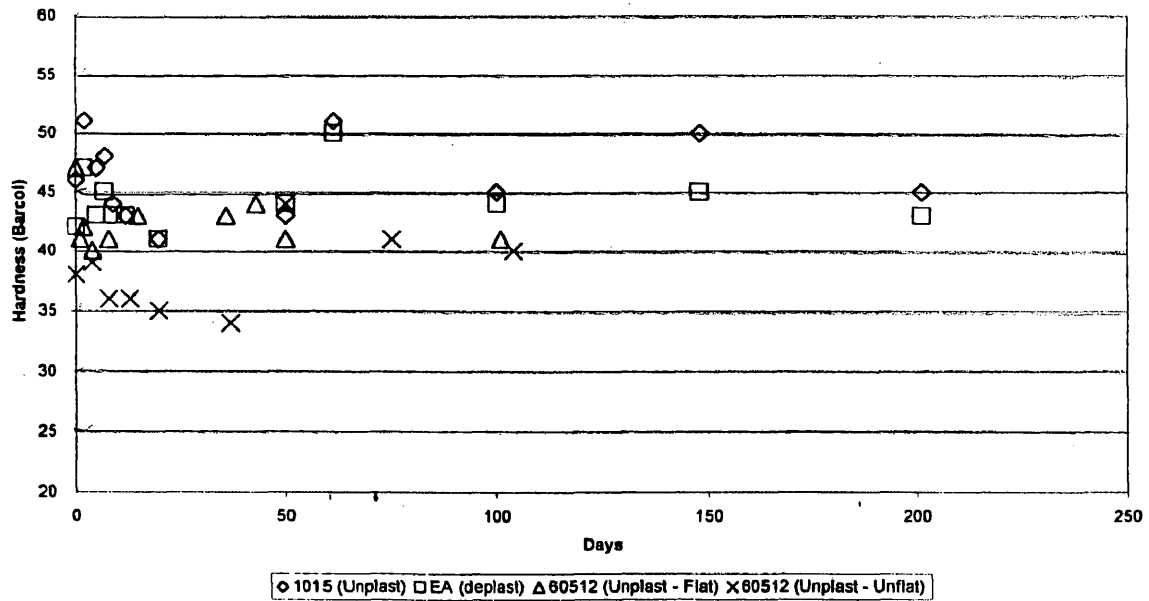


Figure [4.46]

**PVDF Phase II In 130C Air Oven
Plasticized Samples
Melting Temperature vs Day**

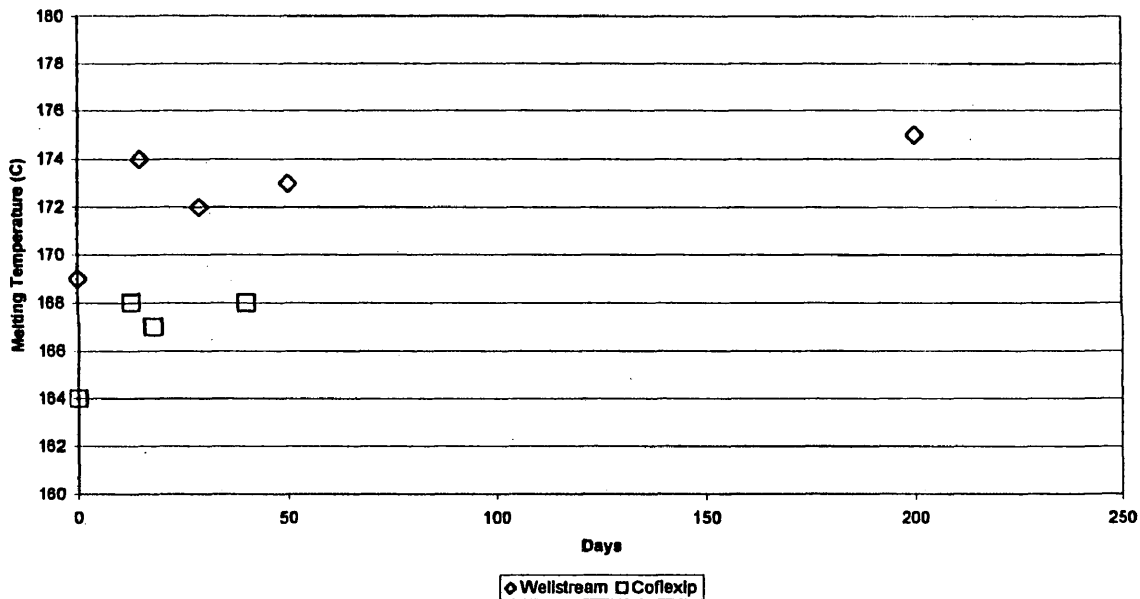


Figure [4.47]

**PVDF Phase II In 130C Air Oven
Non-Plasticized Samples
Melting Temperature vs Day**

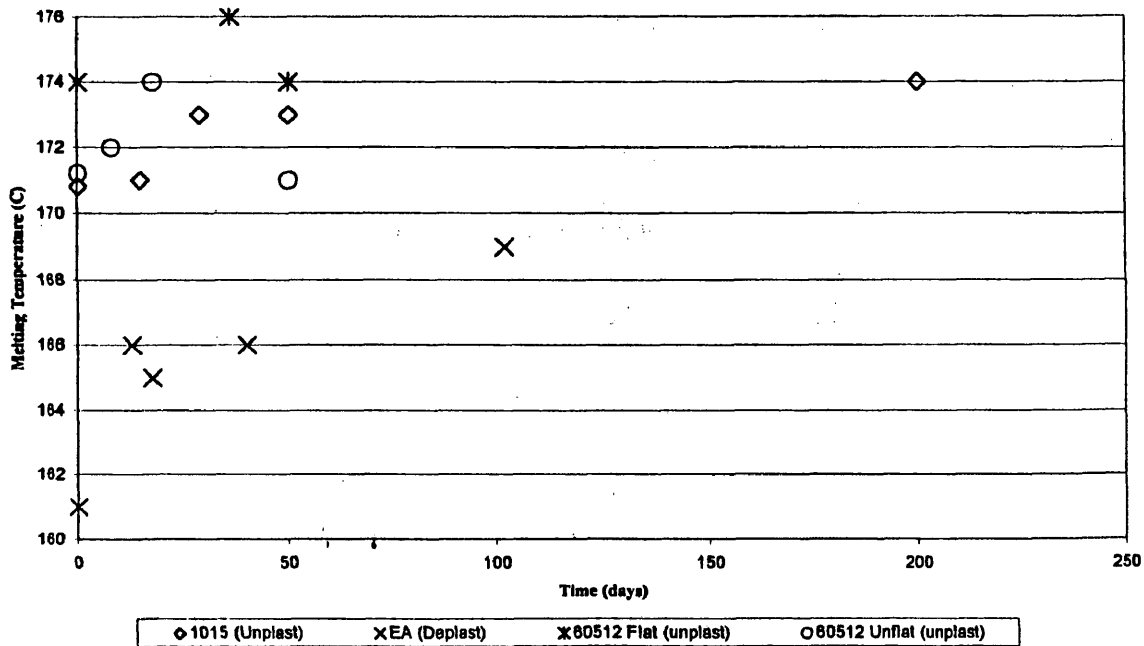


Figure [4.48]

**PVDF Phase II in 130C Oil Pot
Plasticized Samples
Melting Temperature vs Day**

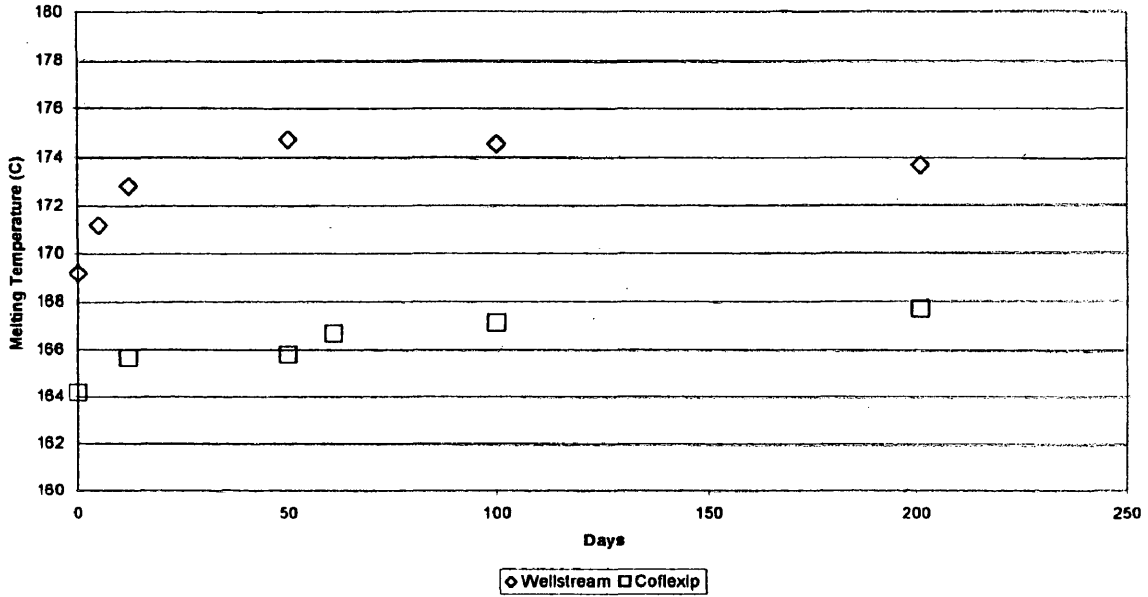


Figure [4.49]

**PVDF Phase II in 130C Oil Pot
Non-Plasticized Samples
Melting Temperature vs Day**

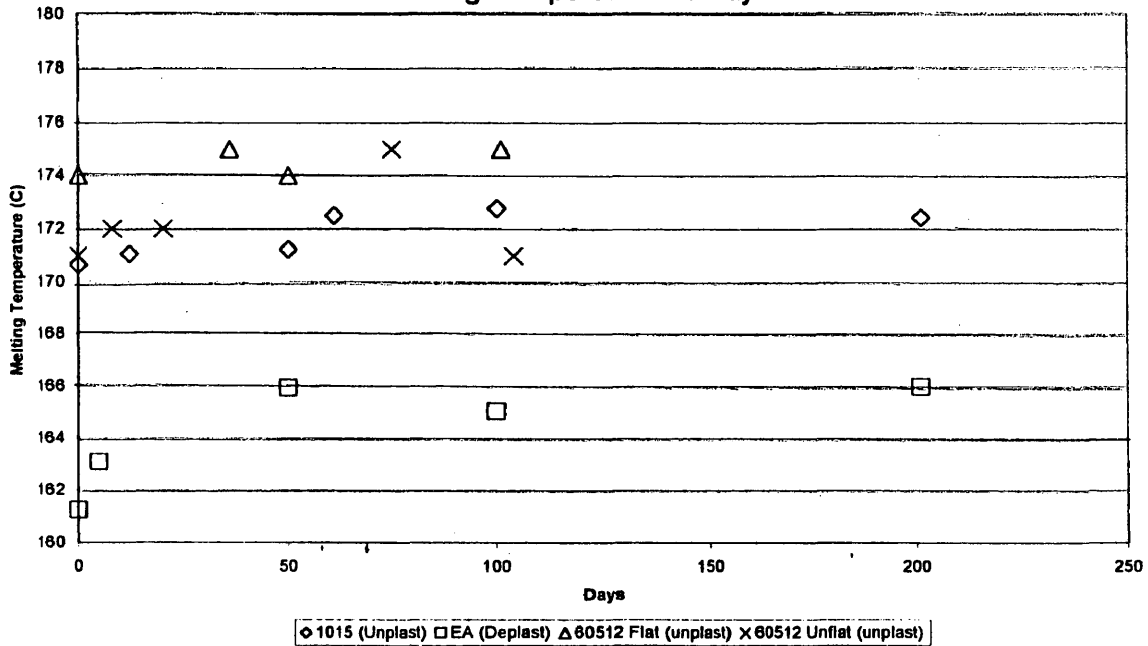


Figure [4.50]

**PVDF Phase II in 130C Air Oven
Plasticized Samples
Enthalpy vs Day**

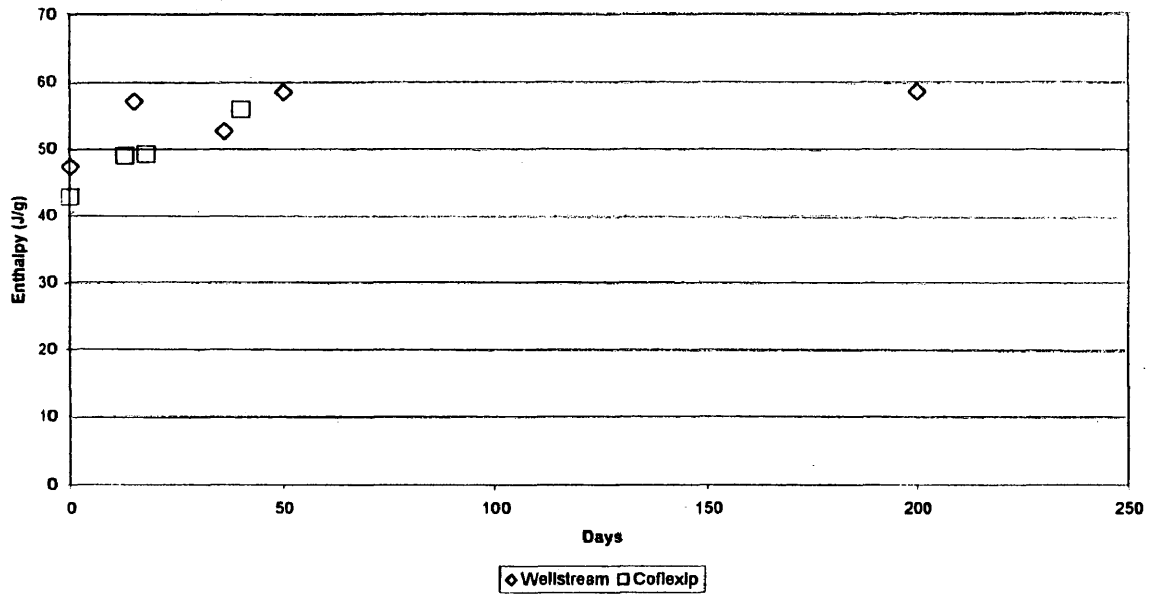


Figure [4.51]

**PVDF Phase II in 130C Air Oven
Non-Plasticized Samples
Enthalpy vs Day**

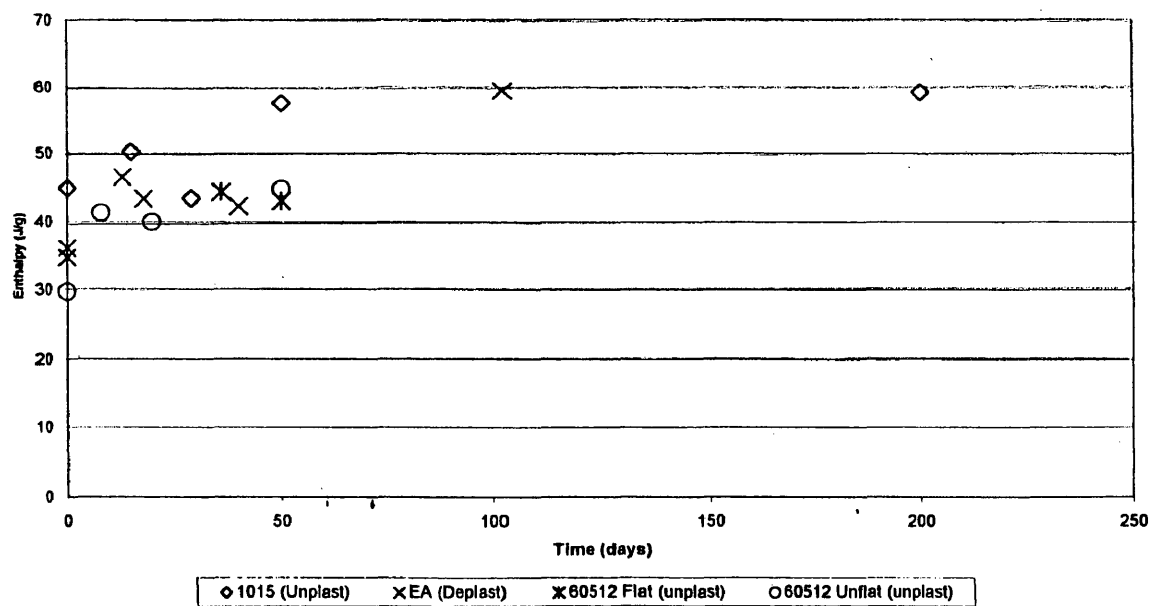


Figure [4.52]

**PVDF Phase II in 130C Oil Pot
Plasticized Samples
dH vs. Day**

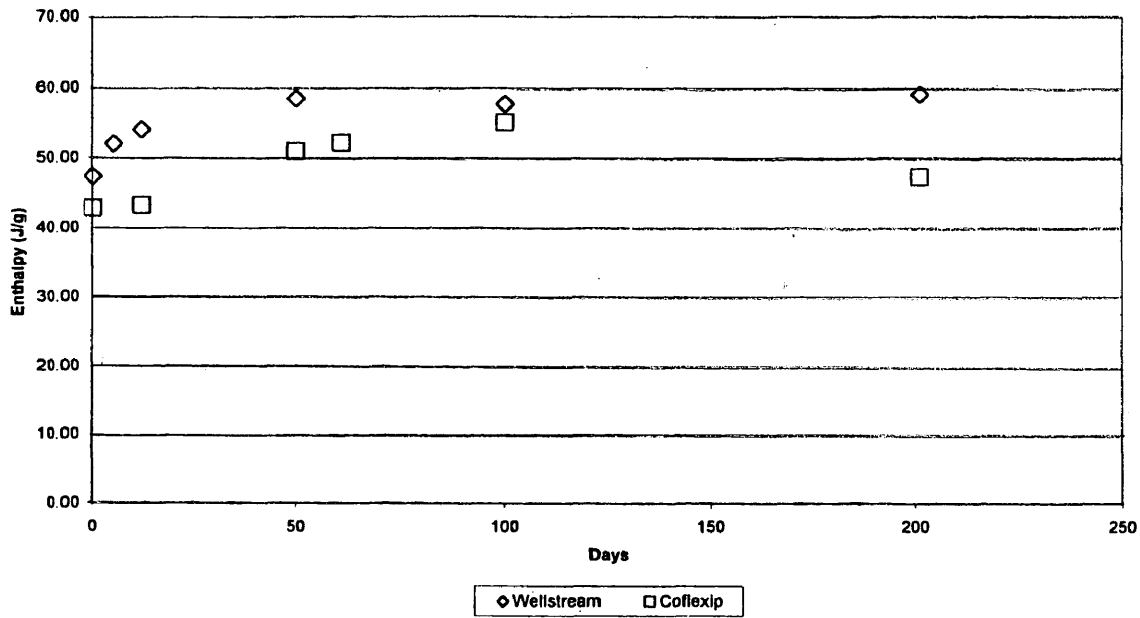


Figure [4.53]

**PVDF Phase II in 130C Oil Pot
Non-plasticized Samples
dH vs Day**

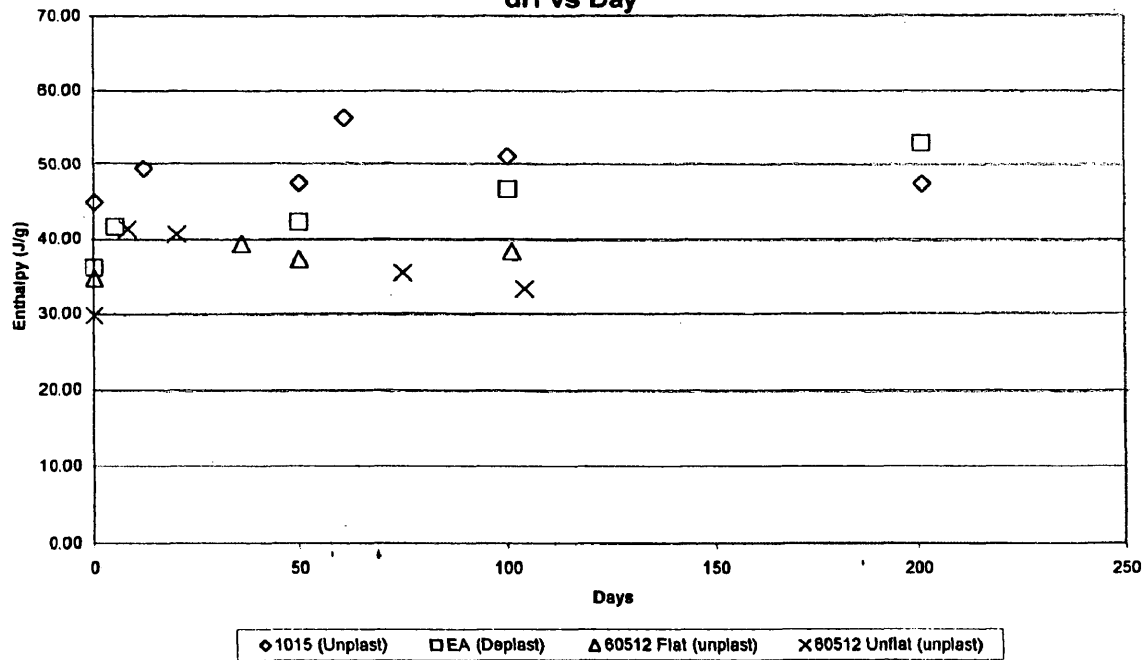


Figure [4.54]

**Mechanical Data vs. Day;
130C Wellstream PVDF
Aged in 95% ASTM Oil with 5% Water**

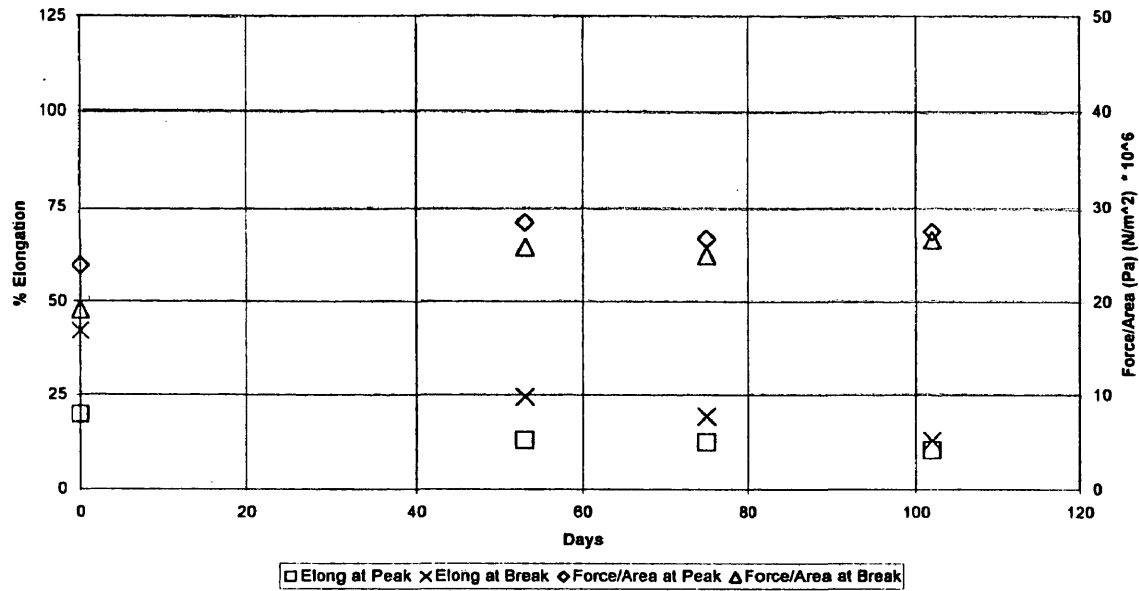


Figure [4.55]

**Mechanical Data vs. Day;
130C Coflexip PVDF
Aged in 95%ASTM Oil with 5% Water**

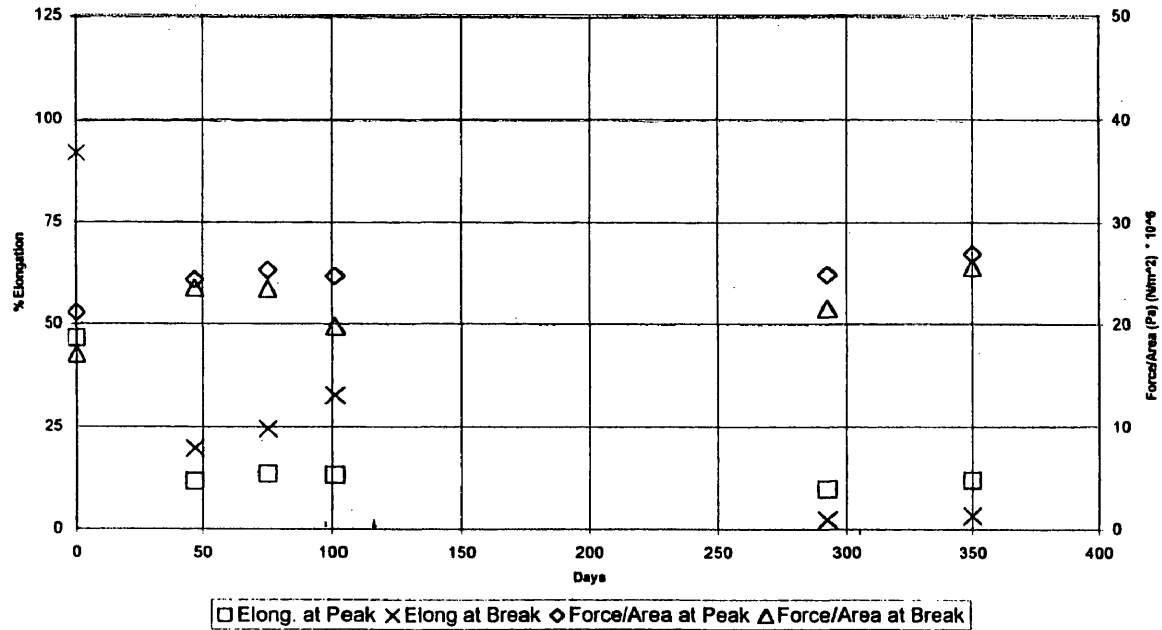
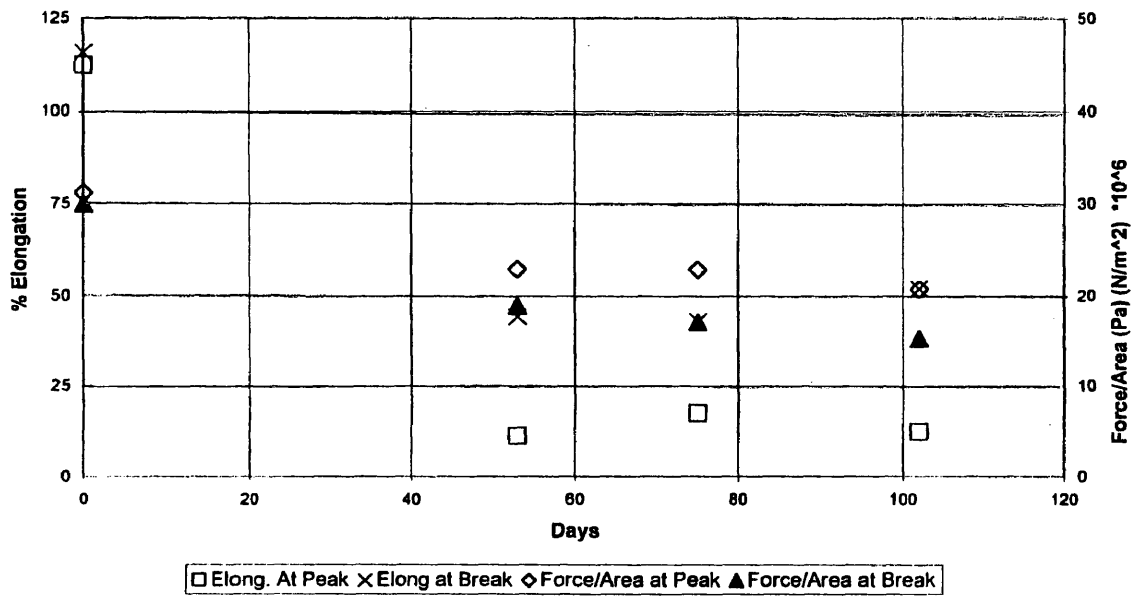


Figure [4.56]

Figure [4.57]

Mechanical Data vs Day;
130C 60512 PVDF
Aged in 95% ASTM oil with 5% Water



Conclusions

In situ FDEMS testing is a viable and proficient method for monitoring changes in polymeric properties. This technique can be used to monitor materials starting with the initial mixtures of monomers, through polymerization or cure, continuing on to observe degradation during use.

The behavior of epoxy resins was observed during isothermal cure. The correlation between the dielectric data and mechanical properties was elucidated. Early during isothermal cure for linear systems changes in the conductivity and viscosity are inversely coupled: the conductivity decreases while the viscosity increases. Branching and crosslinking systems did not follow this trend as shown in the tetrafunctional amine system, DGEBA:mcdea. This system experiences crosslinking from very early in the reaction. Post-cure data indicate the linear systems can become decoupled at some point during the cure. This is thought to be due to branching or entangling experienced by the systems at higher degrees of conversion.

The mechanism for polymeric degradation of nylon-11 is temperature, hydrolysis and pH dependent. As the temperature and concentration of hydrogen ions increase, the rate of degradation also increases. An activation energy of 60kJ/mol was determined for nylon-11. The dielectric and mechanical data were correlated to allow accurate *in situ* monitoring of the polymer's degradation.

Testing has shown that PVDF is a polymer resilient to many harsh environments. Aniline showed the most significant degradation of the polymer.

The other environments showed a small amount of degradation. The environments created in this study were only slightly accelerated in comparison to field conditions. In this case, any degradation seen in the laboratory indicates the potential for serious consequences in the field over long times. The projected 20 year lifespan of this polymer may be an overestimation if further studies continue to indicate slow degradation of the polymer. Comparison of several different types of PVDF revealed little difference in the overall performance of the polymers. Copolymers, however, appeared to be much better with respect to dimensional change and percent elongation. The dielectric measurement will be correlated at a later date to mechanical data allowing service life predictions for this polymer as well.

Intelligent processing and life monitoring can be done on polymeric systems through the use of FDEMS *in situ* testing. This technique can be used in batch operations such as production of epoxy materials commercially as well as in operational environments such as the sub-sea oil pipes. The uses and applications of FDEMS testing are unlimited. With continued investigation and reinforcement of protocols, this technique should become a valuable tool in the continued expansion of uses for polymers.

Bibliography

Allcock, H.R. and Lampe, R.W. Contemporary Polymer Chemistry. 2nd Ed. New Jersey: Prentice-Hall, Inc., 1990.

Anton, A. *Journal of Analytical Chemistry*, 1968, 40, p.1116.

Argiriadi, M.A. "Characterization and Modeling of Amine Epoxide Resins," Masters Thesis, College of William & Mary, 1994.

Carey, F.A. Organic Chemistry. New York: McGraw-Hill Company, 1987.

Chanda, Manas and Salil, R.K., Plastics Technology Handbook, 2nd edition. New York: Marcel Dekker, Inc. 1993.

Chaupt, G.S. and Verdu, J. "Ageing of polyamide 11 in acidic solutions." *Polymer*, 1997, 38, No. 8.

Eloundou, J.P., *et al.* "Microdielectric Study of Epoxy-Amine Systems: Relationships between Kinetics, Dielectric, and Rheological Parameters." Pre-print in *J. of Polymer Sci.*, 1997.

Girard-Reydet, E., *et al.* "Epoxy-Aromatic Diamine Kinetics. 1. Modeling and Influence of Diamine Structure." *Macromolecules*, 28, 7599-7607, 1995.

Gruenwald, G. Plastics. New York: Hanser Publishers, 1993.

Hall, Christopher. Polymer Materials. 2nd ed. New York: John Wiley & Sons, 1989.

Hood, D.K. "Monitoring and Modeling of Infiltration, Polymerization and Degradation Phenomena in Polymeric Systems," Ph.D. Dissertation, College of William & Mary, 1996.

Inoue, M. "Studies on Crystallization of High Polymers by Differential Thermal Analysis." Journal of Polymer Science, Part A. New York: John Wiley & Sons, Inc., 1963.

Kalman, M.D., Belcher, J.R., and Plaia, J.R. "Advanced Materials for Flexible Pipe Construction." *Offshore and Arctic Operations*. PD-Vol 53, 1995. Kranbuehl, David E., "Cure Monitoring," Encyclopedia of Composites. New York: VCH Publishers, 1990.

Kohan, M.I. Nylon Plastics Handbook. New York: Hanser/Gardner Publishers, Inc., 1995.

Kranbuehl, D., *et al*, *Polymer Eng Sci*, **29**, 285, 1989.

Kranbuehl, David E., "Cure Monitoring," Encyclopedia of Composites. New York: VCH Publishers, 1990.

Kranbuehl, D., D. Hood, L. McCullough, H. Aandahl, N. Haralampus and W. Newby. "Frequency Dependent Electromagnetic Sensing (FDEMS) for Life Monitoring of Polymers in Structural Composites During Use." 1995, in press.

Lee, H.; Neville, K. Handbook of Epoxy Resins. New York: McGraw-Hill, 1967.

Lovell, Peter A. "Dilute Solution Viscometry." Comprehensive Polymer Science, Volume 1. New York: Pergamon Press. 1989. p.174.

McNaughton, J.L. and C.T. Mortimer. Differential Scanning Calorimetry. Reprint from "IRS; Physical Chemistry Series 2, 1975, Volume 10." London: Butterworths.

Mark, H.F. *et al*. Encyclopedia of Polymer Science and Engineering. 2nd Ed. Vol 11. New York: Wiley & Sons, Inc., 1985.

Nguyen, T. Degradation of Poly(vinyl fluoride) and Poly(vinylidene fluoride). *JMS-Rev. Macromol. Chem. Physics.*, 1985.

Sanford, W.M. and McCullough, R.L. *Polymer Science, Polymer Physics*, **28**, 973, 1990.

Senturia, S.D., Read, B.E., Williams, G. "Dielectric Analysis of Thermoset Cure." Advances in Polymer Science, Vol 80, Springer-Verlag Publishers, Berlin, Germany, 1986.

Smith, William F. Foundations of Materials Science and Engineering, 2nd ed. New York: McGraw-Hill, Inc., 1993.

Sperling, L.H. Introduction to Physical Polymer Science. 2nd ed. New York: John Wiley & Sons, 1992.

Tipler, Paul A., Physics. New York: Worth Publishers. 1991.

Wang, Y., *et al*, Polymer Mater. Sci. and Eng. 70, 279, 1993.

Welch, Gordon, and Robert Miller. Journal of Polymer Science, Polymer Physics Edition. Vol. 14.

Zulfigar, S., M. Aulfigar, R. Masroor, and A. Munir. "Study of the Thermal Degradation of Polychlorotrifluorethylene, Poly(vinylidene fluoride) and Copolymers of Chlorotrifluorethylene and Vinylidene Fluoride." Polymer Degradation and Stability. Vol 43, 1994.

VITA

Wendy Raquel Mahler

The author was born Wendy Raquel Newby in Sterling, Illinois on January 9, 1970. She graduated from East Chambers High School in Winnie, Texas in May, 1987. In May, 1996, a bachelor of science with high honors in Chemistry from the College of William & Mary in Williamsburg, Virginia was earned. The requirements for the degree of Master of Arts in Chemistry will have been completed at the College of William & Mary in May, 1998.

Currently, the author is a candidate for a Ph.D. in molecular genetics at Emory University Medical Sciences Center in Atlanta, Georgia.